Lawrence Berkeley National Laboratory
Recent Work

Title
TRANSPORT PROCESSES IN HIGH RATE ELECTROLYSIS

Permalink
https://escholarship.org/uc/item/2gj8f8wr

Author
Acosta, Raul Edmundo.

Publication Date
1974-05-01

eScholarship.org Powered by the California Digital Library
University of California

LBL-2242
c.1

TRANSPORT PROCESSES IN HIGH RATE ELECTROLYSIS

Raul Edmundo Acosta
(Ph.D. thesis)

May 1974

Prepared for the U. S. Atomic Energy Commission
under Contract W-7405-ENG-48

For Reference

Not to be taken from this room

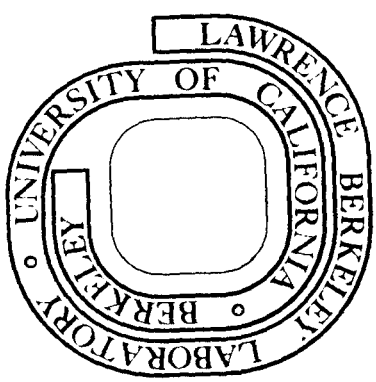

LBL-2242
c.1

DISCLAIMER

This document was prepared as an account of work sponsored by the United States Government. While this document is believed to contain correct information, neither the United States Government nor any agency thereof, nor the Regents of the University of California, nor any of their employees, makes any warranty, express or implied, or assumes any legal responsibility for the accuracy, completeness, or usefulness of any information, apparatus, product, or process disclosed, or represents that its use would not infringe privately owned rights. Reference herein to any specific commercial product, process, or service by its trade name, trademark, manufacturer, or otherwise, does not necessarily constitute or imply its endorsement, recommendation, or favoring by the United States Government or any agency thereof, or the Regents of the University of California. The views and opinions of authors expressed herein do not necessarily state or reflect those of the United States Government or any agency thereof or the Regents of the University of California.

0 0 0 0 4 0 0 5 8 . 2

TRANSPORT PROCESSES IN HIGH RATE ELECTROLYSIS

Contents

0 0 0 0 4 0 0 5 8 . 3

TRANSPORT PROCESSES IN HIGH RATE ELECTROLYSIS

Raul Edmundo Acosta

Inorganic Materials Research Division, Lawrence Berkeley Laboratory and Department of Chemistry; University of California, Berkeley, California 94720

ABSTRACT

Rates of mass transport to planar electrodes imbedded into closely spaced walls (0.2 - 0.5 mm) of flat rectangular channels were determined by the limiting current technique. The nickel electrodes, on which ferric cyanide was reduced to ferrous cyanide, were subdivided into four electrically insulated segments, allowing for the determination of decline of transport rates in the direction of flow. The electrode surfaces were polished to optical smoothness, or provided with well defined roughness patterns. Friction factors were obtained by measurement of pressure drop between four positions in the hydrodynamic entrance region, and four in the mass transport section. The ranges of significant variables and parameters were:

$$220 \leq \text{velocity, cm/sec} \leq 7{,}700$$

$$1{,}300 \leq \text{Reynolds Number} \leq 22{,}000$$

$$2{,}200 \leq \text{Schmidt Number} \leq 3{,}050$$

$$4 \leq \frac{\text{Electrode length}}{\text{duct equiv. diameter}} \geq 28$$

$$0.05 \leq \text{Peak-to-Peak roughness, } \mu > 60 \text{ .}$$

In the laminar regime, on smooth and moderately rough surfaces, the mass transfer coefficients were found to follow the extension to the Graetz-Levêque equation:

$$Sh_{ave} = 1.85 \ (Re \ Sc \ D_h/x)^{1/3} \ .$$

Mass transfer coefficients and friction factors obtained in the hydraulically smooth channel in turbulent flow ($Re > 10^4$) can be correlated by the Chilton-Colburn equation:

$$j_D = St \ Sc^{2/3} = \frac{f}{2} = 0.0395 \ Re^{-0.25}$$

Mass transport rates obtained on roughened surfaces, because of the contribution of the form-drag, show significant departure from those predicted by the Chilton-Colburn analogy; $j_D/(f/2) > 1$ when $Re > 2 - 4 \times 10^3$.

0 0 0 0 4 0 0 5 3 , 4

TABLE OF SYMBOLS

C	Concentration	[g mole cm^{-3}]
D	Diameter	[cm]
D_h	Hydraulic Diameter, $D_h = \frac{4 \text{ (wetted Area)}}{\text{perimeter}}$	[cm]
D	Diffusivity	[cm^2 sec^{-1}]
F	Faraday's Constant	[96,494 Coulomb]
g	Interelectrode Gap	[cm]
g	Gravitationa Constant	[981 cm sec^{-2}]
i	Current Density	[A cm^{-2}]
i_{lim}	Limiting Current Density	[A cm^{-2}]
J	Molar flux with respect to the mass average velocity $\langle v \rangle$, Eq. (2-16)	[g mole cm^{-2} sec^{-1}]
k	Mass Transfer Coefficient, Eq. (3-3)	[cm sec^{-1}]
k'	Mass Transfer Coefficient, Eq. (2-22)	[cm sec^{-1}]
N	Molar Flux, Eq. (2-2a)	[gmole cm^{-2} sec^{-1}]
ΔP	Pressure Drop	[Dyne cm^{-3}]
R	Volumetric Reaction Rate	[gmole cm^{-3} sec^{-1}]
t	Temperature	[°C]
T	Temperature	[°K]
u_i	Mobility of ionic species i	[cm^2 gmole sec^{-1}]
v	Velocity	[cm sec^{-1}]
v_*	Frictional Velocity $v_* = \sqrt{\tau/\rho}$	[cm sec^{-1}]
w	Width of the Channel	[cm]
x	Distance from the mass transfer leading edge	[cm]
z_i	Valence of ionic species i	

Greek Symbols

ε	Roughness, Peak-to-Peak	[μm]
ε_D	Turbulent Diffusivity of Mass	[$cm^2\ sec^{-1}$]
ε_ν	Turbulent Diffusivity of Momentum	[$cm^2\ sec^{-1}$]
μ	Viscosity	[cps]
ν	Kinematic Viscosity	[$cm^2\ sec^{-1}$]
ρ	Density	[$g\ cm^{-3}$]
τ	Momentum Flux	
Φ	Potential Field	[$V\ cm^{-1}$]

Subscripts

ave	Average Quantity
b	Bulk Quantity
δ	Quantity Evaluated at $y = \delta$
k	Belonging to Species "k"
t	Evaluated at Temperature t
w	Evaluated at the Wall
x	In the x Direction
y	In the y Direction

Superscripts

t	Turbulent Quantity
+	Dimensionless Quantity

Other Symbols

-	(Overscore) Time Average
~	(Tilde) Fluctuating Quantity
$\langle\ \rangle$	Mass Average
'	Derivative with Respect to y

0 0 0 0 4 0 0 5 8 3 5

Dimensionless Numbers

f	Friction Factor
Gr	Grashof Number. $Gr = g\alpha\Delta Cx^3/(\nu^2)$
j_D	Chilton-Colburn factor. $j_D = Sh/(Re\ Sc^{1/3})$
Nu	Nusselt Number. $Nu = kx/D$
Pr	Prandtl Number. $Pr = \nu/a$
Ra	Rayleigh Number. $Ra = Gr\ Sc$
Re	Reynolds Number. $Re = Dv/\nu$
Sc	Schmidt Number. $Sc = \nu/D$
Sh	Sherwood Number. $Sh = kx/D$
St	Stanton Number. $St = Sh/(Re\ Sc)$

0 0 0 0 4 0 0 5 8 6

I. INTRODUCTION

Industrial electrochemical processes are characteristically carried out at very modest (low) rates (10^{-2}-1.0 A/cm^2) (see Table I). This necessitates large capital investments, heavy labor charges and large physical size of plants. In recent years, there has been a growing interest in the possibility of increasing the rates at which these processes can be carried out. To date, only one process is operated at current densities of the order of 100 A/cm^2; electrochemical machining (ECM). This process is of interest as a means for shaping very hard metal alloys without introducing mechanical strains in the worked piece.

Since electrolytes are relatively poor conductors, increase of rate, i.e., of current density, results in increasing energy costs in almost direct proportion. Also, for processes that employ electrolyte solutions (as opposed to molten salt electrolysis processes) one of the immediate disadvantages in increasing the current density is the concomitant increase in the amount of heat produced as a result of the ohmic potential drop across the electrodes. Since the conductivity of aqueous electrolytes is of the order of 0.10 (Ω cm)$^{-1}$, a current density of 100 A/cm^2) a 100 to 10,000 increase over the usual rates) would involve a rate of production of heat of 1,400 kcal/min cm^3 of electrolyte contained between the electrodes. When one considers that in conventional cell processes typical distances between electrodes are of the order of a centimeter, the problem of dissipating all the heat produced between the electrodes becomes very serious.

Table I. Typical current densities of industrial electrochemical processes.

	Amp/cm^2
Au plating	0.001
Cu refining	0.01
Cl_2 (diaphragm)	0.1
Mg, Al reduction	1.
ECM	100

0 0 0 0 4 0 0 5 8 7

Two possible avenues are open to solve this problem: (a) improve the conductivity of the working electrolyte by increasing the concentration of the ionic solute, or (b) decrease the distance separating the electrodes. The first possibility is very limited since the solubility of salts used in electrolyte compositions is in general fairly small (at most several molal), and in practical situations the conductivity could not be increased more than two fold. The second possibility gives more latitude since decreasing the electrode separation to fractions of a millimeter is conceivable.

It is this latter solution that forms the object of the present study. A broader application of high rate electrolysis (using closely spaced electrodes) has been hindered by almost complete lack of understanding of the controlling parameters. In particular, in ECM costly trial and error is required to determine the conditions of operation for any new application. Anodic phenomena in ECM are obscured by the interplay of mass transport, electrical and surface effects. Part of the problem in elucidating this situation arises from the lack of understanding of transport processes outside the laminar regime. Our knowledge is mostly empirical or semiempirical, and we have to rely upon correlations to calculate the rates at which these processes will occur for a given set of conditions. Since most experimental work on momentum and mass (or heat) transfer has been carried out using flow channels with an equivalent diameter of 2 cm or more, extrapolation of these results to flows that occur in channels involving one or two orders of magnitude smaller equivalent diameters could lead to serious errors.

To date, no systematic study of mass and momentum transfer rates in channels with equivalent diameters of fractions of a millimeter has been published. The problem of heat transfer in very thin channels has attracted the attention of investigators in the field of nuclear reactor technology. Table II lists reports of work carried out in ducts with equivalent diameters of the order of a millimeter. These are the smallest values of D_h that have been studied to date. The discrepancies in these results are too large to consider the problem settled.

The present work involved measurements of the rates of mass and momentum transfer in channels with equivalent diameters of 0.096 and 0.038 cm, using electrolyte flow rates in the Reynolds number range of 1,300 to 22,000 (200 to 7,700 cm/sec). Since in practical applications electrodes are seldom hydraulically smooth, in addition to optically smooth walls four different degrees of roughness were also employed.

A study of cathodic gas evolution in very narrow gaps (of importance in electrochemical machining) is reported in Appendix IV.

Table II. Heat transfer in thin channels.

Author	Reference Number	Duct Dimensions (g×w), mm	Re	Pr	Medium	Entrance Length	Remarks
Battista and Perkins	1	2.41×2.41	2.1×10^4 to 4.9×10^4	unspecified	Air	100 D_h	--$Nu = 0.021\ Re^{0.8} Pr^{0.14}\left[\frac{T_w}{T_b}\right]^{-0.7}\left[1+\left(\frac{x}{D_h}\right)^{-0.7}\left(\frac{T_w}{T_b}\right)\right]$
Gambill and Bundy	17	1.34 to 1.44×26.92	9×10^3 to 2.7×10^5	unspecified	Water	unspecified	--f values fall within 15% of Moody Chart line for $\frac{\epsilon}{D} = 0.00064$ (roughness was not independently measured). --Nu within 26% of Sieder-Tate $\left[Nu = 0.027\ Re^{0.8} Pr^{0.33}\left(\frac{\mu_b}{\mu_w}\right)^{0.14}\right]$
James et al.	20	3.17 to 254×6.35	3×10^3 to 1×10^5	6.5 to 100	Water, Glycerine-water	67 D_h	--Sieder-Tate does not correlate results. $Nu = \frac{0.104\ Re^{0.0016\ Pr+0.75}\ Pr^{0.4}\left(\frac{\mu_b}{\mu_w}\right)^{213}\ Re^{-0.9}}{e^{0.134\ Pr}\left[2.05 + 1.62\ e^{-g/w}\right]}$
Jergel et al.	21	0.1 to 1.0×10	unspecified	unspecified	Liquid Helium	unspecified	--Nucleate boiling conditions
Perroud and Rebiere	35	1×6	8×10^3 to 2×10^5	unspecified	Gaseous Hydrogen	40 D_h	--Nu within 20% of Ditus-Boelter correlation $[Nu = 0.023\ Re^{0.8} Pr^{0.4}]$
Ricque and Siboul	40	ID 2 and ID 4	1×10^4 to 1.47×10^5	2.5 to 9.2	Water	50 D_h	--f values fall on $\frac{\epsilon}{D} = 2\times10^{-4}$ line for $Re < 6\times10^4$; and on hydraulically smooth line for $Re > 6\times10^4$ (roughness was not independently measured). $Nu = 0.0092\ Re^{0.88} Pr^{0.5}\left[\frac{\mu_b}{\mu_w}\right]^{0.14}$

II. FUNDAMENTALS

The equations describing the processes of mass and momentum transport in closed channels have been established and used by numerous authors to calculate rates of transport. In the case of developed laminar flow the equation for the velocity at any point in the channel is known for a variety of channel cross section configurations.[13a] This makes it possible to predict mass (heat) transfer rates with a satisfactory degree of accuracy. In the case of turbulent transport, however, our imprecise knowledge of the nature of turbulence demands making some assumptions regarding the distribution of the velocity and the mechanism of transport. These assumptions are used to find approximate solutions to the momentum and mass transfer equations.

In this work, no attempt was made at establishing still another semi-empirical equation for the rate of mass and momentum transport for the geometry used in the experimental work.

The fundamental equations describing the transport process, as well as the general approach to their solution, are reviewed below.

For steady state conditions, the concentration and the potential distributions in a dilute solution containing n ionic species are described by the following n + 1 equations:

$$-\nabla \cdot N_k + R_k = 0 \qquad (2\text{-}1)$$

$$\sum_{k=1}^{n} z_k C_k = 0 \qquad (2\text{-}2)$$

where the flux N_k is given[32] by the equation

$$N_k = C_k v - D_k \nabla C_k - z_k u_k F C_k \nabla \phi$$

0 0 0 0 4 0 0 5 8 3 9

Since reactions in an electrochemical system are frequently restricted to the interface electrode-electrolyte, the bulk reaction term R_k is zero and Eq. (2-1) simplifies to:

$$\nabla \cdot N_k \equiv 0 \tag{2-4}$$

The current density in an electrolyte solution is due to the motion of charged species and is given by:

$$i = F \sum_{k=1}^{n} z_k N_k \tag{2-5}$$

The fluid velocity is determined by the solution to the Navier-Stokes equation

$$\rho v \cdot \nabla v = -\nabla p - \mu \nabla^2 v + \rho g \tag{2-6}$$

and the equation of continuity for an incompressible fluid

$$\nabla \cdot v \equiv 0 \tag{2-7}$$

For the reaction of a minor ionic species in a solution containing excess supporting electrolyte the contribution of the ionic migration to the flux can be neglected, so that Eq. (2-3) becomes

$$N_k = -D_k \nabla C_k + v C_k \tag{2-8}$$

and substitution into Eq. (2-4) yields

$$v \cdot \nabla C_k = D_k \nabla^2 C_k \tag{2-9}$$

This is the same equation that describes convective transport in non-electrolytic solutions, consequently many of the results of studies in heat and mass transport can be directly applied to the study of

electrochemical systems that fulfill this condition. Conversely, electrochemical systems sometimes provide the most convenient experimental means for testing these results or for arriving at new ones for systems too complex to analyze.

For the case of laminar flow, the solution to the velocity equation is available in a closed analytical form for the geometry of a circular pipe and in the form of infinite series for a number of other geometries.

In turbulent flow the motion of the fluid is irregular, which in general causes all the intensive variables to fluctuate irregularly in space and time. A simplification that is often used involves the assumption that the same differential equations that describe laminar flow can be applied to turbulent flow, with the proviso that the concentration, velocity, etc, be expressed in the form

$$v = \bar{v} + \tilde{v} \tag{2-10a}$$

$$C = \bar{C} + \tilde{C} \tag{2-10b}$$

where the overscore indicates a time average quantity, and the tilde the superimposed effect of turbulence, a variable in space and time.

By definition, the time average of the fluctuating quantities is identically zero. Substituting the value of v from Eq. (2.10) into Eq. (2.6) one obtains after taking the time average

$$\rho\bar{v}\cdot\nabla\bar{v} = -\nabla p - \mu\nabla^2\bar{v} + \rho g - \nabla\cdot\bar{\tau}^t \tag{2-11}$$

where $\bar{\tau}^t$ is the turbulent momentum flux. The components of $\bar{\tau}^t$, (i.e., $\overline{\bar{\tau}^t_{xx}} = \overline{\rho\tilde{v}_x\tilde{v}_x}$; $\overline{\tau^t_{x,y}} = \overline{\rho\tilde{v}_x\tilde{v}_y}$; etc) are referred to as the Reynolds Stresses.

0 0 0 0 4 8 0 5 8 1 0

Following the definition of Boussinesq[2] for the eddy diffusivity: $\rho\widetilde{\widetilde{vv}} = \mu^t\nabla\bar{v}$, we can express Eq. (2-12) as

$$\rho\bar{v}\cdot\nabla\bar{v} = -\nabla p - (\mu + \mu^t)\,\nabla^2\bar{v} + \rho g \quad . \tag{2-13}$$

Similarly, for component k,

$$\bar{v}\cdot\nabla\bar{C}_k = (D_k + \varepsilon_D)\,\nabla^2\bar{C}_k \tag{2-14}$$

where

$$-\overline{\widetilde{C}_k\widetilde{v}} = \varepsilon_D\nabla C_k \tag{2-15}$$

Sherwood[45] has reviewed the generalized development of semiempirical correlations relating mass (heat) and momentum transfer. Define a molar flux of species k with respect to the mass average velocity $\langle v\rangle$,

$$J_k = N_k - C_k\langle v\rangle \quad . \tag{2-16}$$

We can express the fluxes of momentum and mass as

$$\tau = -(\nu + \varepsilon_\nu)\,\rho\nabla\bar{v} \tag{2-17a}$$

$$J_k = -(D_k + \varepsilon_D)\,\nabla\bar{C}_k \tag{2-17b}$$

The simplest solution, the Reynolds' analogy, is to assume that

$$(\nu + \varepsilon_\nu) = (D + \varepsilon_D) \tag{2-18}$$

and that the mass flux is proportional to the momentum flux

$$J_k = a\tau \tag{2-19}$$

Then,

$$\frac{dC_k}{\rho dv} = \frac{J_k}{\tau} = \frac{J_{k,w}}{\tau_w} \tag{2-20}$$

$$\frac{C_{k_w} - C_k}{\rho\langle v\rangle} = \frac{J_{k,w}}{\tau_w} \tag{2-21}$$

and defining a mass transfer coefficient k'

$$k' = \frac{J_{k,w}}{C_{k_w} - C_b} \tag{2-22}$$

and the friction factor

$$f = \frac{\tau_w}{(1/2)\rho\langle v\rangle^2} \tag{2-23}$$

$$\frac{k'}{\langle v\rangle} = \frac{f}{2} = St \tag{2-24}$$

Most later attacks to the problem have sought to account for the variation of ϵ with position. In order to do this the mean velocity profile and the eddy diffusivity distribution for the turbulent flow have to be described by use of dimensionless variables with the assistance of the "Law of the Wall".[2] These distributions, originally proposed for flows in a smooth circular pipe, have been applied to two-dimensional channels,[4] and to channels of large aspect ratio.[49] The approach is as follows. Define the dimensionless quantities

$$v^+ = \frac{v}{v_*} \quad \text{and} \quad y^+ = \frac{y}{\nu} v_*$$

where y is the distance measured from the wall, and the frictional velocity, v_*, is defined by

$$v_* = \sqrt{\frac{\tau_w}{\rho}}$$

0 0 0 0 4 0 0 5 3 4 1

The velocity profile can then be expressed in dimensionless form as

$$v^+ = f(y^+) \quad .$$

The velocity gradient becomes

$$\frac{dv}{dy} = \frac{\tau_w}{\nu\rho} \frac{dv^+}{dy^+} = \frac{\tau_w}{\nu\rho} f'(y^+) \tag{2-25}$$

Substituting this value in Eq. (2-17a) we obtain

$$\left(1 + \frac{\varepsilon_\nu}{\nu}\right) = \frac{1}{f'(y^+)} \tag{2-26}$$

where it has been assumed that $\tau = \tau_w$ since most of the resistance occurs near the wall.

The velocity distribution can be obtained from Eq. (2-25)

$$v_\delta = \sqrt{\frac{\tau_w}{\rho}} \int_0^\delta f'(y^+)\, dy^+ \tag{2-27}$$

Similarly, for the mass flux, assuming that for $0 \leqslant y \leqslant \delta$, J_k is constant,

$$C_{k,\delta} - C_{k,w} = -\frac{J_k}{v_*} \nu \int_0^\delta \frac{dy^*}{(D_k + \varepsilon_{D,k})} \tag{2-28}$$

$$C_{k,w} - C_{k,\delta} = \frac{J_k}{\sqrt{\frac{\tau_w}{\rho}}} \int_0^\delta \frac{dy^+}{\frac{1}{Sc} + \frac{\varepsilon_{D,k}}{\nu}} \tag{2-29}$$

and assuming that

$$\varepsilon_{D,k} = \varepsilon_\nu$$

$$C_{k,w} - C_{k,\delta} = \frac{J_k}{\sqrt{\frac{\tau_w}{\rho}}} \int_0^\delta \frac{dy^+}{\left(\frac{1}{S_c} + \frac{1}{f'(y^+)} - 1\right)} \qquad (2\text{-}30)$$

At this point a specific value of the function $f(y^+)$ has to be chosen in order to be able to perform the integrations. The earliest and simplest model was that due to Taylor, who pictured a laminar film adjacent to the tube wall, where

$$v^+ = y^+ \quad ,$$

and ε_D, $\varepsilon_\nu = 0$ since the transfer processes are assumed to occur by molecular processes only. Choosing δ empirically as 8.7, and with $f = 0.08\ Re^{-1/4}$

$$\frac{1}{St} = 25\ Re^{1/4}[1 + 1.74\ Re^{-1/8}(Sc - 1)] \qquad (2\text{-}31)$$

Using velocity distributions determined empirically, several formulations have been proposed for the function $f(y^+)$. In order to obtain better agreement with experimental data, these equations divide the region of validity of the law of the wall in one,[38,49,52] two[9] and even three[54a] different ranges of y^+. From these equations the distributions of eddy diffusivity for momentum can be calculated. A complete review of velocity and eddy diffusivity distributions is given by Spalding[49] and by Kitamoto.[22]

0 0 0 0 4 0 0 5 8 4 2

The empirical approach to the problem of momentum and mass transfer has been successful in many instances. The (1/7)-power law of turbulent velocity distribution

$$\frac{v}{v_*} = 8.56\left(\frac{yv_*\rho}{\mu}\right)^{1/7} \tag{2-32}$$

can be used to calculate the average velocity

$$\frac{\langle v\rangle}{v_*} = (0.817)(8.56)\left(\frac{Rv_*\rho}{\mu}\right)^{1/7} \tag{2-33}$$

and from this, the Blasius equation for the friction factor is smooth pipes,

$$f = 0.079\ \mathrm{Re}^{-1/4} \tag{2-34}$$

This equation has been found to represent experimental values of f accurately up to about $\mathrm{Re} = 10^5$.

For mass (heat) transfer Chilton and Colburn[6] in 1934 found that the equation

$$\mathrm{StSc}^{2/3} = \frac{f}{2} \tag{2-35}$$

represented available experimental data rather well. The usefulness of this equation has been recently confirmed among others by Sherwood and Pigford[46] and Hubbard.[16]

Lin, Moulton, and Putnam[29] based their development on von Káramán's approach, but introduced an empirical allowance for eddy diffusion in the region very close to the wall. In the region $0 \leq y^+ \leq 5$, they assume an eddy diffusivity dependence of the form

$$\frac{\varepsilon_D}{\nu} = \left(\frac{y^*}{14.5}\right)^3 \tag{2-36}$$

This dependence on the third power of y^+ has been criticized by some authors[9,11,48] who conclude that the eddy diffusivity must show a dependence on $(y^+)^4$. However, later studies[16,39,47] seem to support the form adopted by Lin et al. Their final result is

$$\frac{1}{St} = \frac{2}{f} + \sqrt{\frac{2}{f}}\,\phi(Sc) \tag{2-37}$$

where $\phi(Sc)$ is a complicated function of the Schmidt number. The limiting result for high Sc is:

$$Sh = 0.05704\ Re\sqrt{\frac{f}{2}}\,Sc^{1/3} \tag{2-38}$$

Equation (2-38) agrees with experimental data with an error of ±10% over the range $0.6 \leqslant Sc \leqslant 3{,}200$.

Table III presents some of the more reliable empirical and semi-empirical equations for the rate of mass transfer in fully developed turbulent flow.

0 0 0 0 4 0 0 5 8 4 3

Table III. Fully developed mass transfer. Turbulent regime.

Authors	Equation	Remarks
Chilton-Colburn[6]	$Sh = \frac{f}{2} ReSc^{1/3}$	Empirical
Deissler[9]	$Sh = 0.0789 \sqrt{f}\, ReSc^{1/4}$	$\varepsilon \sim (y^+)^4$
Levich[27]	$Sh \sim Re \sqrt{f}\, Sc^{1/4}$	$\varepsilon \sim (y^+)^4$
	$Sh \sim Re \sqrt{f}\, Sc^{1/3}$	$\varepsilon \sim (y^+)^3$
Lin, Moulton and Putnam[29]	$Sh = 0.05704 \sqrt{\frac{f}{2}}\, ReSc^{1/3}$	$\varepsilon \sim (y^+)^3$
Vieth, Porter, and Sherwood[54]	$Sh = 4.586 \left[\frac{v_{max}}{\langle v \rangle}\right] \frac{f}{2} ReSc^{1/3}$	semi-empirical
Spalding[50]	$Sh = 0.053\, f\, ReSc^{1/3}$	semi-empirical

III. EXPERIMENTAL METHOD AND APPARATUS

The experimental method employed in this study for the determination of mass transfer coefficients involved the measurement of limiting currents in the cathodic reduction of ferricyanide ion on nickel electrodes.

Friction factor coefficients were determined from pressure drop measurements in the same flow channel used for the mass transfer experiments.

A. Limiting Current Method

When an electric current is caused to flow across two electrodes connected by an electrolyte, two or more reactions occur at the interfaces between the electrodes and the electrolyte: oxidation at the anode and reduction at the cathode.

For cases when the reaction at the electrode is "fast" (small charge transfer and/or reaction and crystallization overpotential), the rate may be limited by the slow supply of the reactant to the electrode interface. Under these conditions, further increase of the applied potential will not result in increased passage of current until such a potential is reached when another reaction becomes feasible. If one constructs a plot of current passing through the electrode against the applied potential, the above mentioned limitation in reaction rate will be manifested by the appearance of a flat section in the curve, the limiting current plateau.

Since the reaction rate at the limiting current is determined by the rate of transfer of the reacting ionic species, i, the value of the limiting current for a given set of conditions gives us a direct measurement of the maximum rate of mass transfer of species i for those

0 0 0 0 4 0 0 5 8 4 4

conditions. Variations leading to a change in the magnitude of this rate will be reflected in corresponding changes in the limiting current value (see Fig. III-1). Accordingly, the measurement of limiting current values as a function of Reynolds Number, Schmidt Number, etc, provides a means for the determination of the dependence of mass transfer rates on those parameters.

At the limiting current the rate of transport of the reactant to the interface is smaller than the rate at which it can potentially be consumed by the charge transfer reaction. As a result, at the interface the concentration of this species approaches zero.

Since

$$N_i = \frac{i}{nF} \quad , \tag{3.1}$$

defining a mass transfer coefficient k as

$$N_i = k(C_b - C_o) \tag{3.2}$$

$$k = \frac{i}{(C_b - C_o)\ nF} \tag{3.3}$$

and at the limiting current

$$k = \frac{i_{lim}}{C_b(nF)} \tag{3.4}$$

from which it is possible to evaluate the coefficients and exponents of functional relations of the type

$$Sh = \phi(Re, Sc, x/D_h, Ra, Gr, \text{ etc}) \tag{3.5}$$

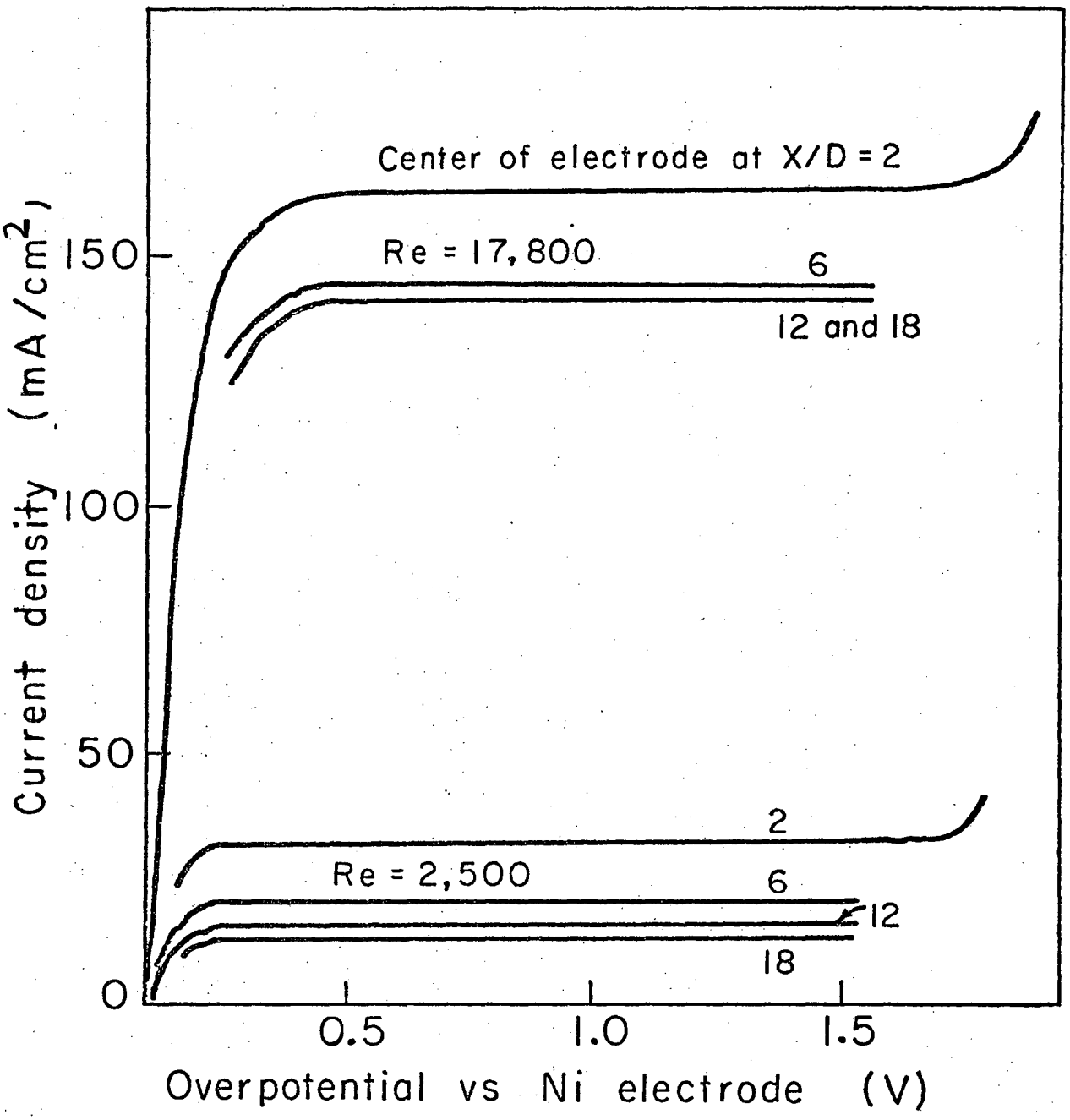

Fig. III-1. Effect of Reynolds number and distance downstream of the leading edge on the value of the limiting current.

Several assumptions are implicit in the above definition of the mass transfer coefficient. The first assumption is that the reaction is limited only at the electrode under consideration, and not at the counter electrode. That is, the conditions of operation must be such that it is precisely the reaction under consideration that is giving us the potential invariant limiting plateau, not the reaction at the other electrode.

The second assumption is that the limiting current is due entirely to the electrochemical reaction that is being considered; side reactions will introduce errors.

The third assumption is that the contribution of the electric field to the ionic mass flux (i.e., migration) is negligible. The complete flux equation written for any component $\underline{i}$ is:[32]

$$N_i = -D_i \nabla C_i - z_i u_i F C_i \nabla \phi + C_i v \qquad (3.6)$$

The definition of a mass transfer coefficient given in Eq. (3.2) should be valid for any species regardless of whether it is ionic or electrically neutral. For this to be true it is necessary that the second term, that due to the potential field acting on the species $\underline{i}$, be zero. For the case of electrically charged species this effect can be very large if the contribution of the reacting species $\underline{i}$ to the conductivity of the electrolyte is large. In order to make the migration effect negligible, the concentration of species $\underline{i}$ (assuming similar mobilities for all species) relative to the total ionic concentration must be small. This is achieved by flooding the electrolyte with a large excess of an "indifferent" electrolyte.

The fourth assumption is that the mass transfer coefficient is independent of the magnitude of the bulk concentration of component i.

Measurement of limiting currents is an experimental technique that has been quite widely employed in mass transfer studies.[3,12,16,29,44,51,53,56] Its relative simplicity and flexibility make the limiting current method a powerful tool in experimental studies of forced and free convection, as well as in pure diffusion studies. However, its inherent limitations have been either overlooked or treated lightly. A recent review of the advantages and limitations of this method by Selman[44] should help place this method within the proper framework as an experimental tool.

The important criteria for selection of an electrolyte suitable for limiting current studies are:

1) It should give a long plateau, i.e., the potential at which a consecutive reaction occurs should be very different from that of the reaction of interest.

2) Its preparation and analysis should be simple.

3) The solubility of the reacting species should not be too small.

Two main types of reactions are usable in limiting current measurements.

a) Deposition of the reacting species at the cathode (e.g., Cu from $CuSO_4$ deposited on copper electrodes, gold, silver, cadmium on mercury).

b) Oxidation (at the anode) or reduction (at the cathode) of a species in solution to give a soluble species at the interface (e.g., a redox couple, oxygen-OH, iodine-triodide).

0 0 0 0 4 0 0 5 8 4 5

These two types of reactions have inherent advantages as well as disadvantages. A wise choice of the reaction will greatly simplify the experimental procedure and provide greater precision in the determination of the true limiting currents.

Deposition reactions in general produce large density gradients between the interface and the bulk of the solution. This makes them particularly suitable for the study of mass transfer under free convection[12,56] and in the mixed regime of forced and free convection.[51]

One very important disadvantage of deposition reactions is the fact that near the limiting current the metal tends to form a rough deposit. In this respect experiments using deposition reactions present the same problem as experiments using soluble walls, i.e., the surface changes as the experiment progresses.[32] In forced convection studies this may alter the hydrodynamic characteristics of the flow past the surface, limiting the usefulness of this method to situations where the runs are of a short duration, or to those conditions where the change in roughness is not appreciable or important. One way of avoiding the problem of rough deposits inherent in the use of the copper sulfate bath is to use addition agents, e.g., gelatin. In this case, however, the physical properties of the solution at the interface become very difficult to evaluate.

Redox reactions in which both the reacting and the product species are in solution have the advantage of not altering the nature of the electrode surface. However, the fact that at the interface an oxidized ion appears for each reduced ion being transformed, and vice versa, results in very small densification coefficients which renders redox

redox reactions not well suited for the study of free convection effects.[3]

In forced convection studies, redox reactions would seem to be the ideal choice. In fact, the ferri-ferrocyanide system has been used extensively for this purpose[8,12,16,48,53] over the past twenty years.

The Potassium Ferricyanide-Potassium Ferrocyanide System.

In this system, the net reactions at the electrodes are:

Cathode:

$$Fe(CN)_6^{\equiv} + e^- \rightarrow Fe(CN)_6^{\equiv\equiv}$$

Anode:

$$Fe(CN)_6^{\equiv\equiv} \rightarrow Fe(CN)_6^{\equiv} + e^-$$

Since the value of the standard electrode potential for this couple is $V^o = 0.36$ volt, for the cathodic reduction of ferricyanide in the presence of a large excess of NaOH one has a very convenient large potential span available before hydrogen evolution is possible. On the other hand, the difference between the standard potential for oxidation of ferrous cyanide and that for OH^- to oxygen is rather small ($V^o_{OH^-,O_2} = 0.40$); therefore, the oxidation reaction offers a less convenient vehicle for mass transfer studies.

Limitations to the use of this system are:

a) Slow decomposition of the solution,

b) sensitivity of the electrodes to "poisoning" by cyanide ion,

c) short plateaus for oxidation of ferrocyanide ion,

d) overlap of the potential for reduction of ferricyanide ion and dissolved oxygen.

0 0 0 0 4 0 0 5 8 4 6

a) Ferricyanide is a strong oxidizing agent; it oxidizes organic materials very quickly. However, polymeric materials are only attacked very slowly; rubber gaskets that were used in the experimental equipment underwent a very slow attack that became evident only after several weeks of standing in contact with the solution. In addition to the above, the ferrocyanide ion has been reported to undergo spontaneous oxidation.[12,25] When exposed to light the ferrocyanide ion decomposes according to

$$Fe(CN)_6^{\equiv} + H_2O \overset{\text{light}}{\rightleftharpoons} [Fe(CN)_5 \cdot H_2O]^{\equiv} + CN^-$$

$$CN^- + H_2O \rightleftharpoons HCN + OH^-$$

Ferricyanide ion, in addition to undergoing such decomposition, may undergo hydrolysis in alkaline solutions[24] according to:

$$2Fe(CN)_6^{\equiv} + 6OH^- \rightleftharpoons 2Fe(OH)_3 + 12CN^-$$

In order to prevent the effect of light on the solution it must be kept in the dark. To minimize the effects of spontaneous degradation of the ferricyanide ion, the solution may have to be discarded after only a few days of use.

b) The sensitivity of the electrodes to poisoning has been a recurrent source of chagrin in studies conducted in this laboratory.[12] Some experimenters have reported no difficulty whatsoever using this system, but out experience indicates that reliable results are obtained only through very careful handling and continuous checking of the state of the electrodes.

c) The inconvenience of a short plateau for the oxidation of ferrocyanide is easily offset by measuring only the cathodic limiting current. Using anode surfaces that are much larger than the cathode surface ensures that the limiting current for the ferrocyanide is never attained. Another method, a simpler one, is the use of a ferrocyanide ion concentration larger than that of ferricyanide ion. Since the diffusion coefficient of ferricyanide is approximately 20% less than that of ferrocyanide, electrolyte compositions containing proportionately larger concentrations of ferrocyanide ion will ensure that the anodic limiting current will not be reached.

d) The occurrence of other reactions simultaneous with the discharge of ferricyanide ion will lead to increased currents and skewed, or non-discernible, limiting current plateaus. One possible simultaneous reaction is the reduction of dissolved oxygen. This reaction can occur at potentials of -0.3 to -0.6 volts (on a stainless steel electrode [28]). Since this potential region overlaps the potential region for reduction of ferricyanide ion, the solution must be thoroughly purged with an inert gas, e.g. nitrogen, in order to remove any dissolved oxygen.

B. Determination of Friction Factor

The friction factors for the channels used were calculated from pressure drop measurements made during the course of the mass transfer experiments. This pressure drop was calculated from pressure drop measurements at four points in the channel spanning the length of the mass transfer section. The channel was provided with eight pressure taps, five upstream of the mass transfer section, two in the mass transfer section, and one downstream from the mass transfer section

0 0 0 0 4 0 0 5 8 7

(see Section III-D). The absolute values of the static pressure, when plotted as a function of position, gave a line that becomes essentially straight for the four positions spanning the electrodes. This was taken as an indication that the entrance length provided was sufficient to allow for a fully developed flow at the mass transfer region (Fig. III-2).

The flow rate used for calculating the f value defined below was that given by the magnetic flow meter. This was also the value used for the calculation of the Reynolds number used for plotting the mass transfer results.

The friction coefficient was then calculated according to the equation

$$f = \frac{1}{4} \frac{D_h(\Delta P/L)}{\left(\frac{1}{2}\rho v^2\right)}$$

Inaccuracies in the pressure drop measurements were mainly due to disturbances of the flow caused by the presence of the pressure taps. Even though measurement of static pressure gradients during flow in smooth ducts and pipes is usually made through piezometer holes on the walls, due to the extremely small hydraulic diameter of the present system, the presence of holes in the walls is bound to disturb the flow. The error introduced by this disturbance is difficult to estimate. Nevertheless, since we were interested in pressure differences only, and since the opening of the piezometric holes appeared to be the same when inspected through a microscope, it is reasonable to believe that any error introduced by the hole itself would be substantially the same at each measuring station, and consequently would cancel out when the difference between two readings was taken.

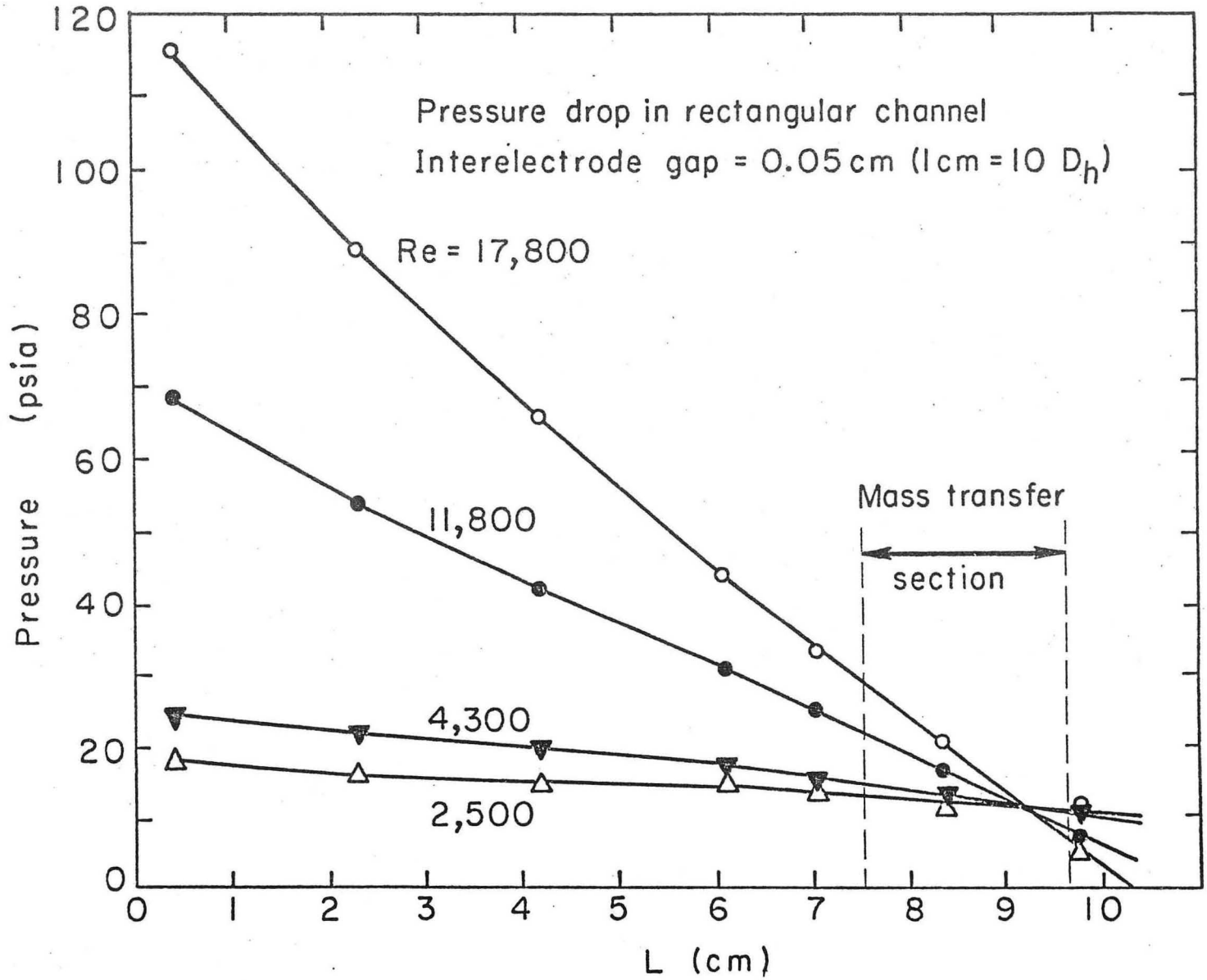

Fig. III-2. Absolute pressure as a function of axial distance in Cell I.

0 0 0 3 4 0 0 5 8 . 8

At the smallest flow rates used in this work the pressure differences being measured were very small. For these measurements a differential U-tube manometer was employed, using chloroform in contact with the electrolyte for the manometer fluid. Since the pressure taps were of capillary dimensions, at the smallest flow rates the response time of the system was very long, which lead to uncertainty as to when a steady value had been obtained. The accuracy of these measurements was low.

For the measurement of the friction factor for the rough channels still another uncertainty was introduced: The roughness at the mouth of the piezometric hole could not be controlled to be the same for all the holes. Since the turbulence created by the rough edge will depend strongly on the local characteristics, the assumption that the errors introduced by the presence of the hole cancel upon taking the difference between two readings is difficult to justify. A possible solution to this problem might have been to leave a smooth area around each of the piezometric holes. However, the effect that the upstream and downstream roughness would have had on the pressure value would still have been unknown, and no positive advantage would have been derived with this artifice.

C. Electrolyte Properties

The electrolyte used in this study was an aqueous solution of potassium ferricyanide and potassium ferrocyanide, with a relatively high concentration of NaOH as a supporting electrolyte. The approximate concentration of the solution was:

$K_3Fe(CN)_6$	0.04 M
$K_4Fe(CN)_6$	0.20 M
NaOH	2.0 M

The solution was prepared in a polyethylene tank by dissolving the weighed amounts of reagent-grade chemicals in a measured amount of water that had been treated in a commercial deionizing system and afterwards distilled in an all glass still.

The relevant physical properties of the solution were viscosity, diffusivity, density and concentration of ferricyanide ion.

Concentration of each of the components was determined from samples taken daily from the tank immediately after completion of a series of experiments. At the initiation of this study, samples had been taken before and after a series of experiments. However, since it was found that the concentration of the components did not change in a detectable manner during the course of a run, in later stages of this study the concentrations were checked only after the completion of the run.

The concentration of ferricyanide ion was determined by the iodometric method using sodium thiosulfate to titrate the amount of iodine liberated during reduction of ferricyanide.[24]

Ferrocyanide ion concentration was determined potentiometrically by measuring the equivalence point when titrating with potassium permanganate in an acidified solution.[23]

Hydroxide concentration was determined by titration with 1 N hydrochloric acid using phenolphtalein as indicator.

0 0 0 0 4 0 0 5 8 4 9

The density of the solution was measured using a 25 c.c. calibrated pycnometer. It was also calculated from the measured concentrations using a polynomial equation derived by Boeffard[3] for this solution. Agreement of the measured values and those calculated was always within 0.5%.

The viscosity and diffusion coefficient of the solution were respectively calculated from a polynomial equation given by Boeffard[3] and from the equation given by Gordon et al.[13] In using the latter, a correction for ionic strength was included.

Since some of the experimental runs could not be conducted at the temperature of 25°C, correction for temperature effects was made by using a relationship of the form

$$\mu_t = \mu_{25}[1 + \alpha(25 - t)]$$

The value for the temperature coefficient, α, was estimated from values of the viscosity of water vs temperature obtained from.[18] Although this method of correction is not exact, the deviations are of necessity small, since the concentration of the components was not very large and the deviation of the temperature from the standard value of 25°C was always small (never larger than ±2.5°C).

The equations used and the confidence limits given by the original sources are:

$$\rho(g/cm^3) = 0.99702 + 0.04423\ C_{NaOH} + 0.17118\ C_{Ferri} + 0.23119\ C_{Ferro} - 0.00133\ C_{NaOH}^2 - 0.00787\ C_{NaOH}\ C_{Ferri} - 0.00978\ C_{NaOH}\ C_{Ferro}$$

Standard deviation = 0.0005

$$\mu_{cps} = 0.96714 + 0.09622\ C_{NaOH} - 0.20528\ C_{Ferri} + 0.090255\ C_{Ferro} + 0.05404\ C^2_{NaOH} + 0.53303\ C^2_{Ferri} + 0.43505\ C^2_{Ferro} + 0.23546\ C_{NaOH}\ C_{Ferri} + 0.302585\ C_{NaOH}\ C_{Ferro} + 0.99923\ C_{Ferro} C_{Ferri}$$

Standard Deviation = 0.0046

$$\frac{D\mu}{T} = (0.234 + 0.0014\Gamma)\ 10^{-9}\ \frac{cm^2\ poise}{sec\ °K}$$

Standard deviation = 0.005.

D. Experimental Cells

Limiting currents and friction factor coefficients measured in the present experimental study were determined in experimental cells I and II. The description below applies directly to cell I, cell II being a replica of cell I, except that it was of smaller dimensions. The exact dimensions of the two cells are given at the end of this section. Appendix I contains details of the design.

Experimental cell I contained a rectangular cross section flow channel 0.05 cm deep, and with an aspect ratio width/height of 30 (40 and 20 for some experiments). The mass transfer sections were formed by facing rectangular pieces of nickel imbedded in the two widest walls of the channel. The surface of the nickel electrode was flush with the wall of the channel and occupied its entire width. See Figs. III-3 and III-4.

The total length of the channel was 10.6 cm. The leading edge of the electrode was located 7.8 cm from the entrance to the channel, providing for a hydrodynamic entrance length equal to 80 D_h. This rather long entrance length was required to assure a fully developed velocity

0 0 0 0 4 0 0 5 8 0

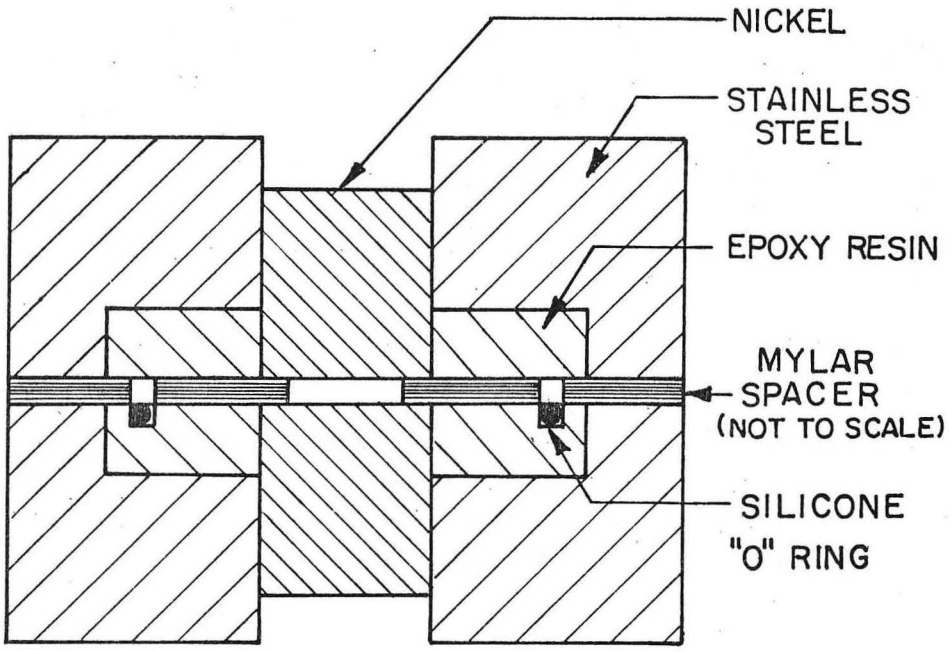

FLOW CHANNEL CROSS-SECTION

XBL 742-5642

Fig. III-3. Cross section of the flow channel.

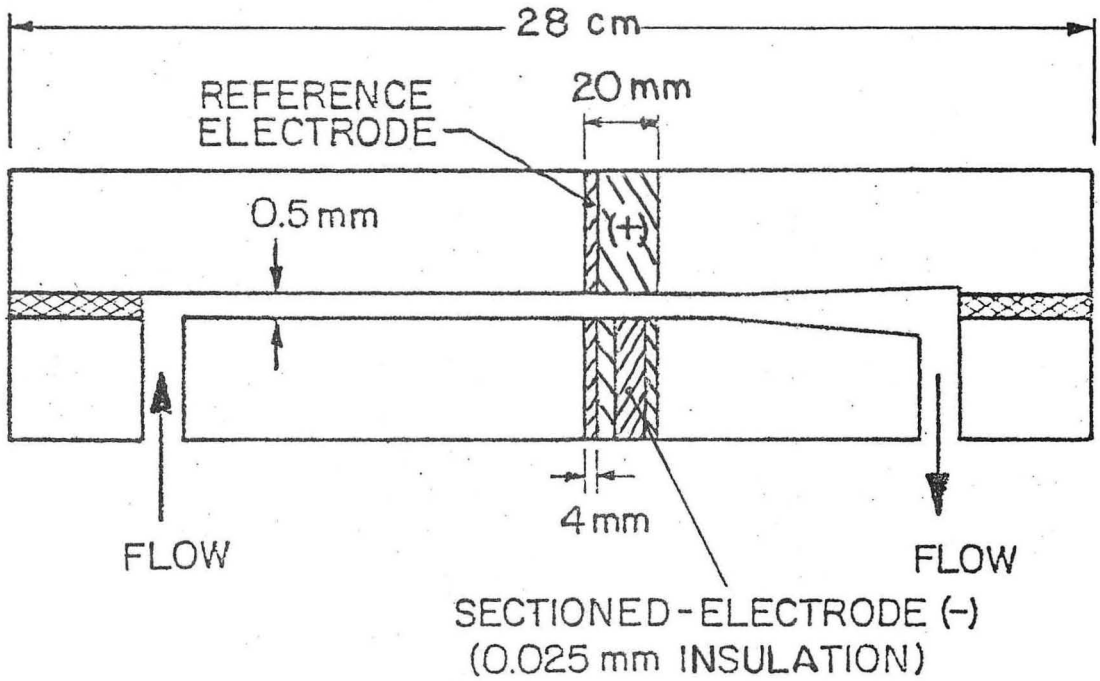

Fig. III-4. Schematic diagram of Cell I. Not to scale.

0 0 0 0 4 0 0 5 8 1

profile at the beginning of the mass transfer region. Even though shorter entrance lengths have been employed in earlier mass transfer experiments,[8,16,51] the concensus of more recent hydrodynamic experiments fixes the length necessary to insure a fully developed velocity profile at 75 D_h.[5,7] In any case, the pressure drop measurements conducted for the determination of the friction factor coefficient verified that a fully developed velocity profile existed at the leading edge of the electrode.

As mentioned above, the two electrodes were located on opposite walls of the channel. The one on the top was connected as the anode and the one at the bottom of the channel as the cathode. The cathode was composed of four sections (hereafter named sections I, II, III and IV) electrically insulated from each other by strips of epoxy resin 25μ in thickness. The length of these four sections in the axial (flow) direction was approximately 4, 4, 8 and 4 D_h respectively (Fig. III-5). This sectioned cathode permitted the determination of the mass transfer coefficient (and hence Sh) as a function of the distance from the leading edge of the mass transfer section. Since the limiting current measured is obtained over the entire length of the individual section, the values of i_{lim} provide <u>average mass transfer coefficients</u> over that individual section. The assignment of this value to any specific point can of course represent only a approximation. For ease in understanding, in this section we refer to this average mass transfer coefficient as if it were assigned to a point halfway along the length of the electrode section. Correction for a non-linear dependence of the mass transfer

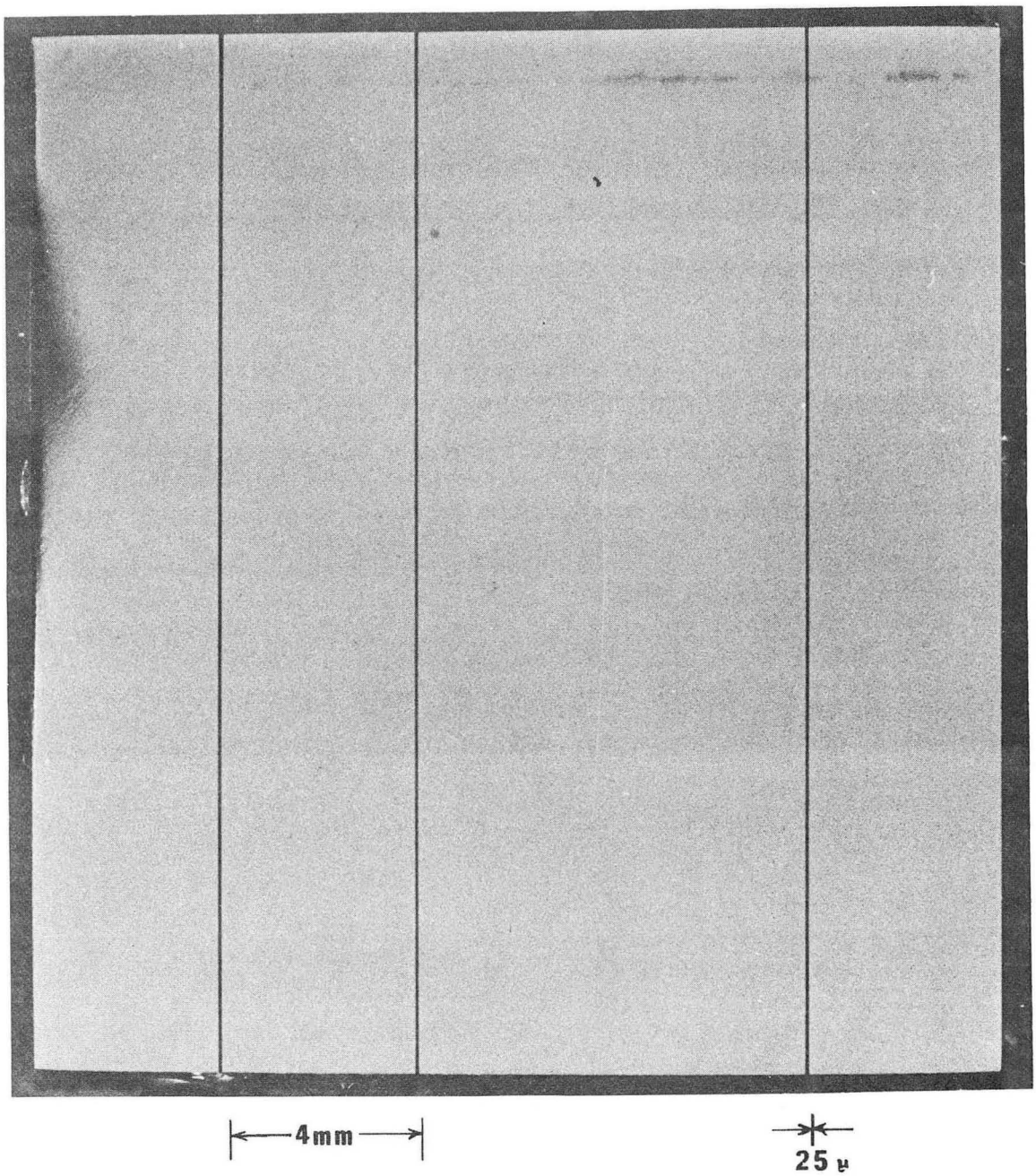

XBB 719-4162

Fig. III-5. Sectioned cathode, Cell I.

0 0 0 0 4 0 0 5 8 2

coefficient on the distance from the leading edge has the effect of moving these points closer to the leading edge, see Section IV-A.

By a simple scheme, the four cathode sections allowed the assignment of eight points in the curve of k (or Sh) vs x/D_h: with the four sections active (electrically connected to the power source), the points obtained corresponded to positions at x/D_h values of approximately 2, 6, 12 and 18. When section I was disconnected the points obtained corresponded to x/D_h values of 2, 8 and 14. With only sections III and IV active, the x/D_h values were 4 and 10, while section IV alone gave again the average mass transfer coefficient for an x/D_h value of 2.

It must be kept in mind that by this scheme of successively disconnecting the upstream sections of the cathode the hydrodynamic entrance length was in effect increased by values of 4, 8 and 16 D_h. Since the limiting current values obtained for the position x/D_h equal to 2 were in very good agreement we have a further assurance that the hydrodynamic velocity profile was fully developed at the leading edge of section I.

As stated above, the values of the mass transfer coefficient at point $x/D_h = 2$ agree within a narrow limit. The small scatter of the values was due to the small variations in the actual length of the electrode sections I, II and IV (see table of values at the end of this section). However, there was no apparent trend in this scatter that would point to hydrodynamically different conditions at each of the sections. Indeed, when Section IV was influenced by disturbances at the exit of the channel, this condition was dramatically reflected by substantially different values of k for $x/D_h = 2$ than those obtained

with Sections I and II. These effects are described in Appendix III.

The electrode facing the cathode had the same overall length and consisted of only two sections, 4 and 16 D_h in length (Fig. III-6). The first section (4 D_h) was used as the reference electrode to measure the cathode potential, while the large section was connected as the anode of the electrolytic cell. These two sections were also insulated from each other by an epoxy resin strip 25μ thick. To verify that the value of the limiting current at the cathode was not affected by the smaller size of the anode, the two sections were shorted (i.e., the whole electrode served as the anode) while the upstream supply pipe was used as the reference electrode. As was to be expected, due to the much higher concentration of ferrocyanide ion employed (see Section III-A), the limiting currents obtained were independent of the size of the anode.

In addition to facilities for measuring mass transfer coefficients, the flow channel cell was provided with eight pressure taps located on the center line of the wall containing the anode. These pressure taps allowed the measurement of pressure drop in the flow direction. The location of these pressure taps measured from the entrance of the channel is given at the end of this section (see page 38).

The friction factor coefficients reported are those obtained from pressure drops determined across taps 5, 6, 7 and 8 spanning the length of the electrode (see Section IV). As mentioned before, the pressure taps in the region of developing flow served to verify the flow was fully developed at the point where the mass transfer region begins.

0 0 0 0 4 0 0 5 8 3

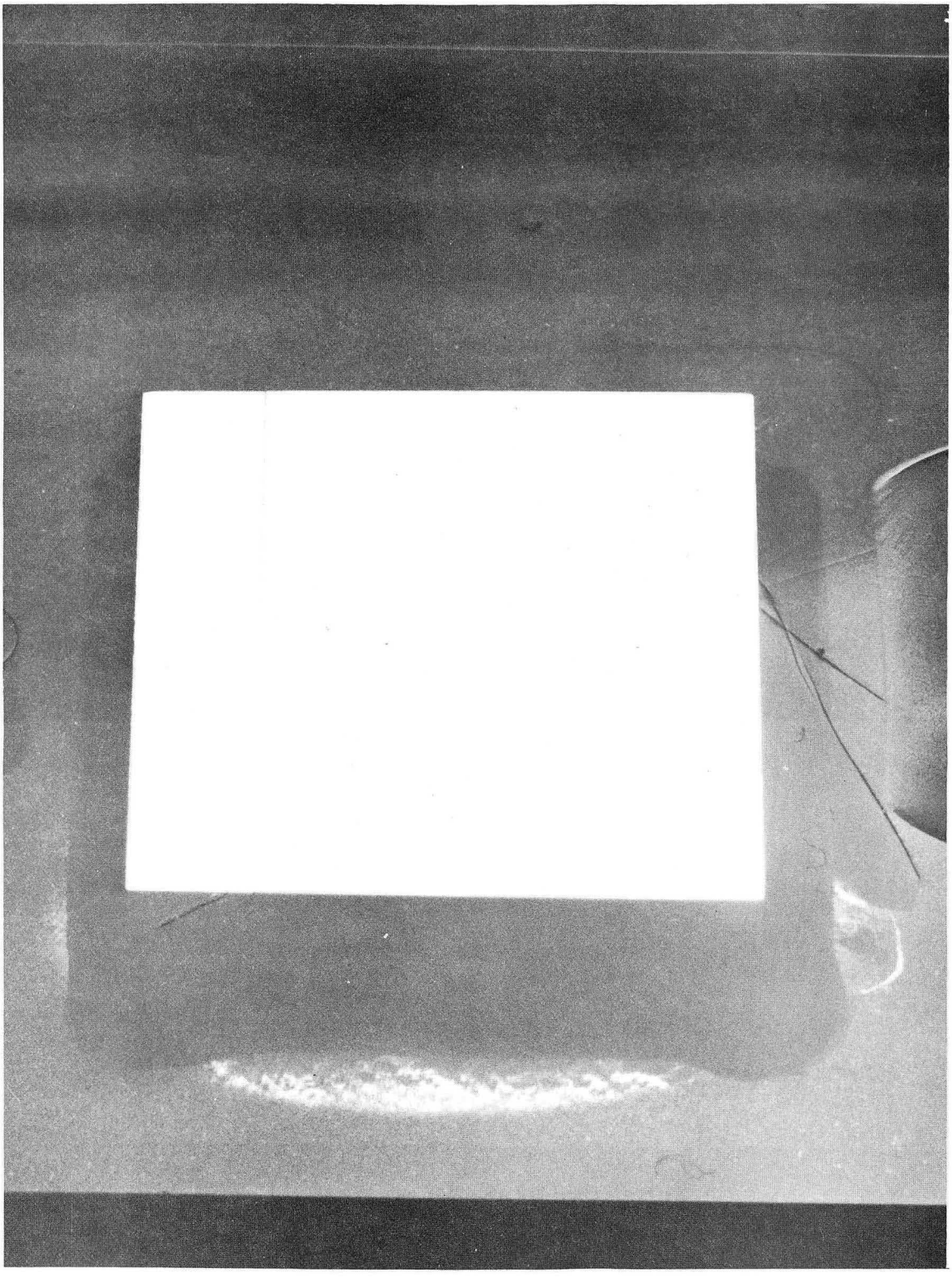

XBB 727-2729

Fig. III-6. Sectioned anode, Cell I.

Table IV. Dimensions of the experimental cells (cm).

	Cell I	Cell II
Total Length	10.40	5.644
Entrance Length	7.80	3.735
Length After Electrodes	0.55	0.920
Width	1.00 (1.5, 2.0)	1.00
Height (Electrode Separation)*	0.05080	0.01877
Cathode Dimensions**		
Section I	0.39056	0.19680
Section II	0.40029	0.19745
Section III	0.79956	0.39795
Section IV	0.39828	0.19680
Hydraulic Diameter	0.09530	0.03689
	(0.09692, 0.09904)	
Aspect Ratio	20(30,40)	53.2
Pressure Tap Locations**		
#1	0.70	1.1350
#2	2.6136	2.1669
#3	4.5240	2.6390
#4	6.4236	3.1398
#5	7.3824	3.6381
#6	8.7332	4.1432
#7	9.5346	4.5455
#8	10.1371	4.9310

*Determined by measuring the thickness of the Mylar spacer with a micrometer. This dimension was rechecked after the cell had been assembled using a micrometer depth gauge.
**These dimensions were determined with an X-Y travelling measuring microscope built at LBL. The X-Y readings are digitally displayed with a resolution of 0.5 and 1μ in the X and Y directions respectively.

E. Roughness, Types and Measurement

The mass transfer coefficient and the friction factor were determined for four types of roughness, in addition to those for hydraulically smooth walls. Three of these roughnesses were of a random distribution nature, while the fourth was geometrically well defined.

Hydraulically smooth channel. Because of the small gap between electrodes and the resulting extreme thinness of the mass transfer boundary layer, it was necessary to polish the cell to optical smoothness to obtain hydraulically smooth surfaces.

Roughness I. This was obtained by sandblasting the surface with a fine abrasive (27μ mesh).

Roughness II. The surface of the cell walls was ground with a fine aluminum oxide wheel. The travel of the grinding wheel was in the axial direction of the cell always; hence, the roughness obtained was not strictly random. However, analysis of the roughness using the Surfanalyzer (see below) showed the roughness to be random in a microscopic sense.

Roughness III. The surface of the cell was sandblasted using a coarse abrasive (mesh size 36).

Roughness IV. The surface was inscribed with "V" grooves running perpendicular to the flow direction. For Cell I these grooves were 0.005 in. wide at the base, 0.002 in. deep at the apex of the triangle and with a separation of 0.015 in. between axis of the triangles (Three times the width of the base). For Cell II, the corresponding dimensions were 0.003, 0.001 and 0.010 in. respectively. These configurations were arbitrarily chosen. This type of roughness is

not normally present in rough electrodes. It was studied only as an extreme case of the effect of roughness on the transfer coefficients.

The four types of roughness, as well as the smooth surface, were evaluated in a surfanalizer profilometer.* This instrument permits the determination of the surface roughness, surface profile and roughness average** through the electronic analysis of the vertical displacement of a stylus travelling over the surface. Sample traces of the profilometer reading, as well as the relevant values of the roughness for both cells are given in Figs. III-7a and III-7b.

F. Test Facility and Instrumentation

An overall view of the test facility is shown in Fig. III-8, while Fig. III-9 provides a simplified diagram of the system.

The basic features of the facility are best described by referring to Fig. III-9.

Due to the very wide range of pumping pressures needed to run the experiments with the very small channel gaps used, two separate pumping systems were required. The first one consisted of a regenerative

---

*Model 21-1330-20 with Surfanalyzer 150 Drive. Gould Inc., El Monte, CA. The diamond stylus used (#21-3100-00407) had a tip radius of 0.0001 in., it excerted a maximum vertical force of 50 mg, and its maximum vertical displacement was 0.004 in.

**The Roughness Average is the arithmetic average of the deviations from a base line over a specified sampling length (the cut-off length). The cut-off length used here was 0.030 in.

0 0 0 0 4 0 0 5 8 4

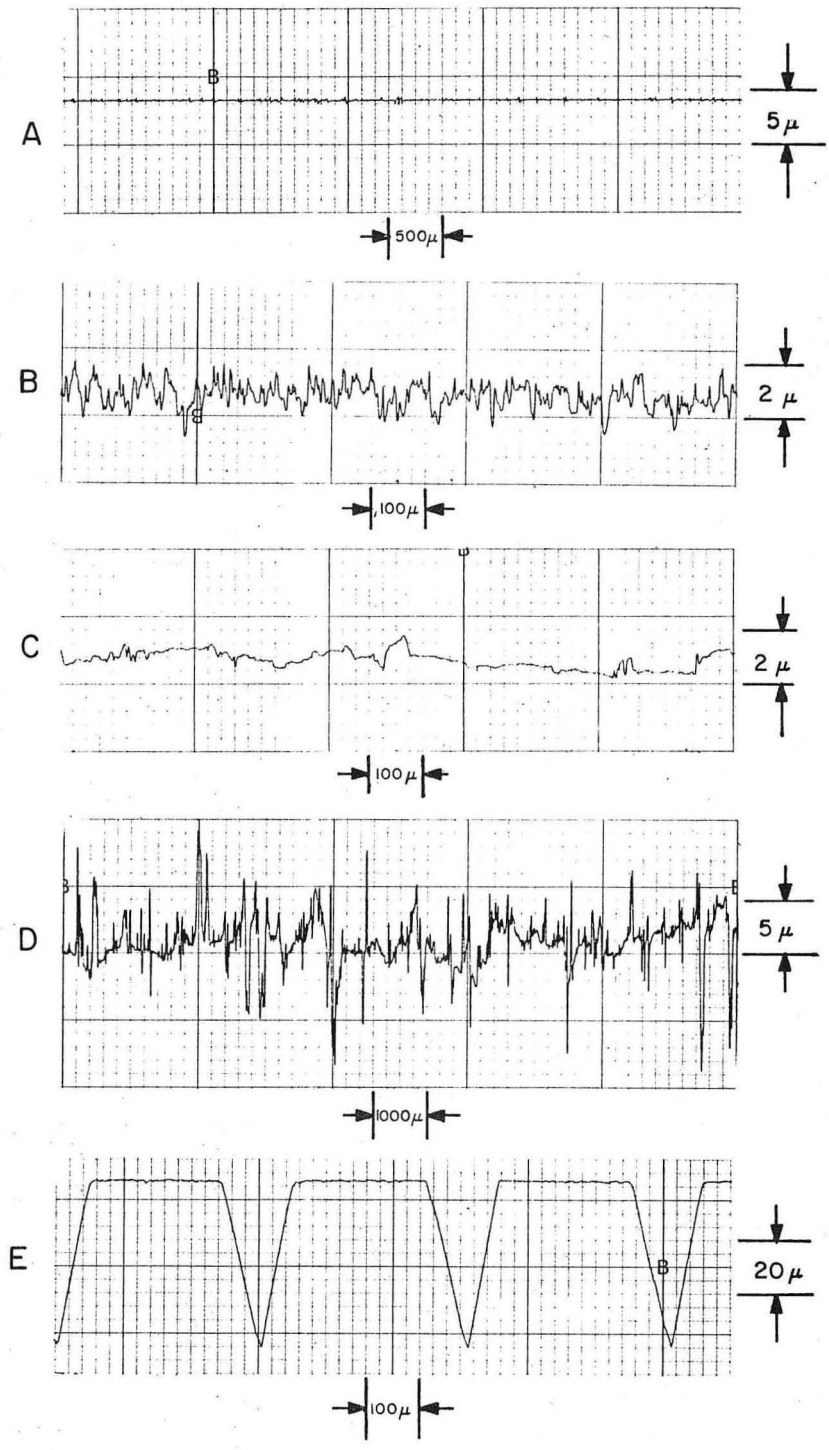

Fig. III-7a. Profilometer traces, Cell I.

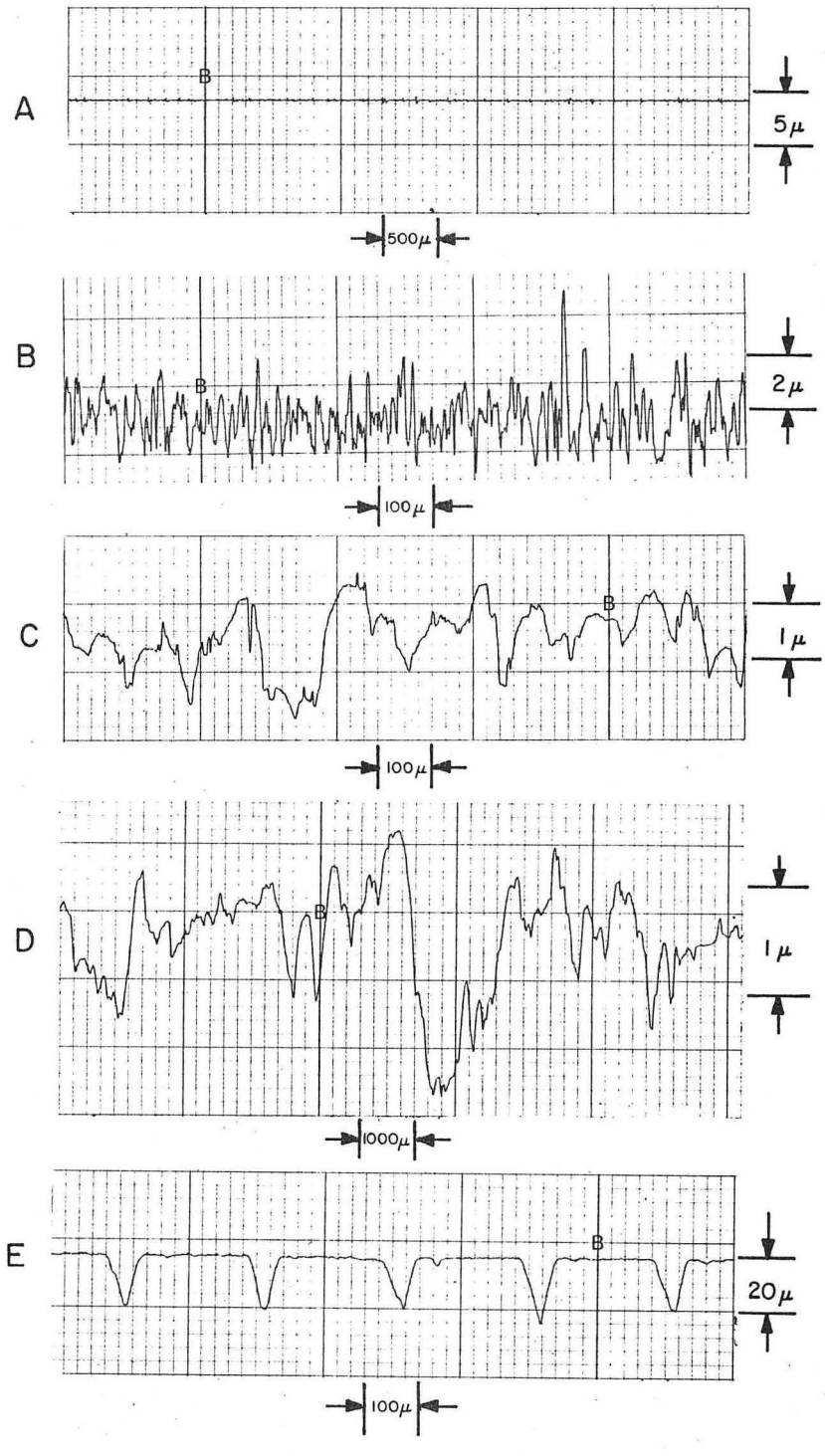

XBL 743-2479

Fig. III-7b. Profilometer traces, Cell II.

0 0 0 0 4 0 0 5 8 5

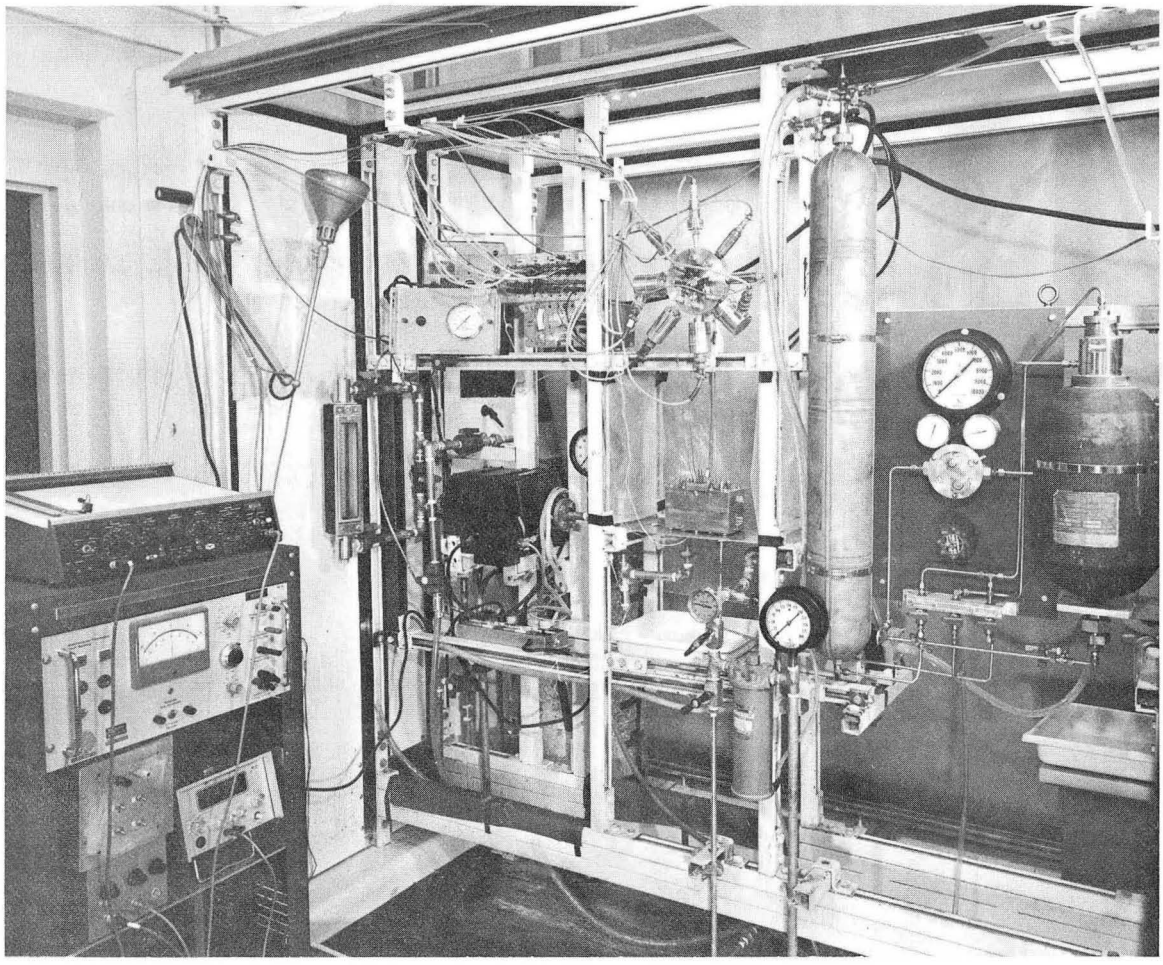

XBB 732-995

Fig. III-8. Overall view of the test facility.

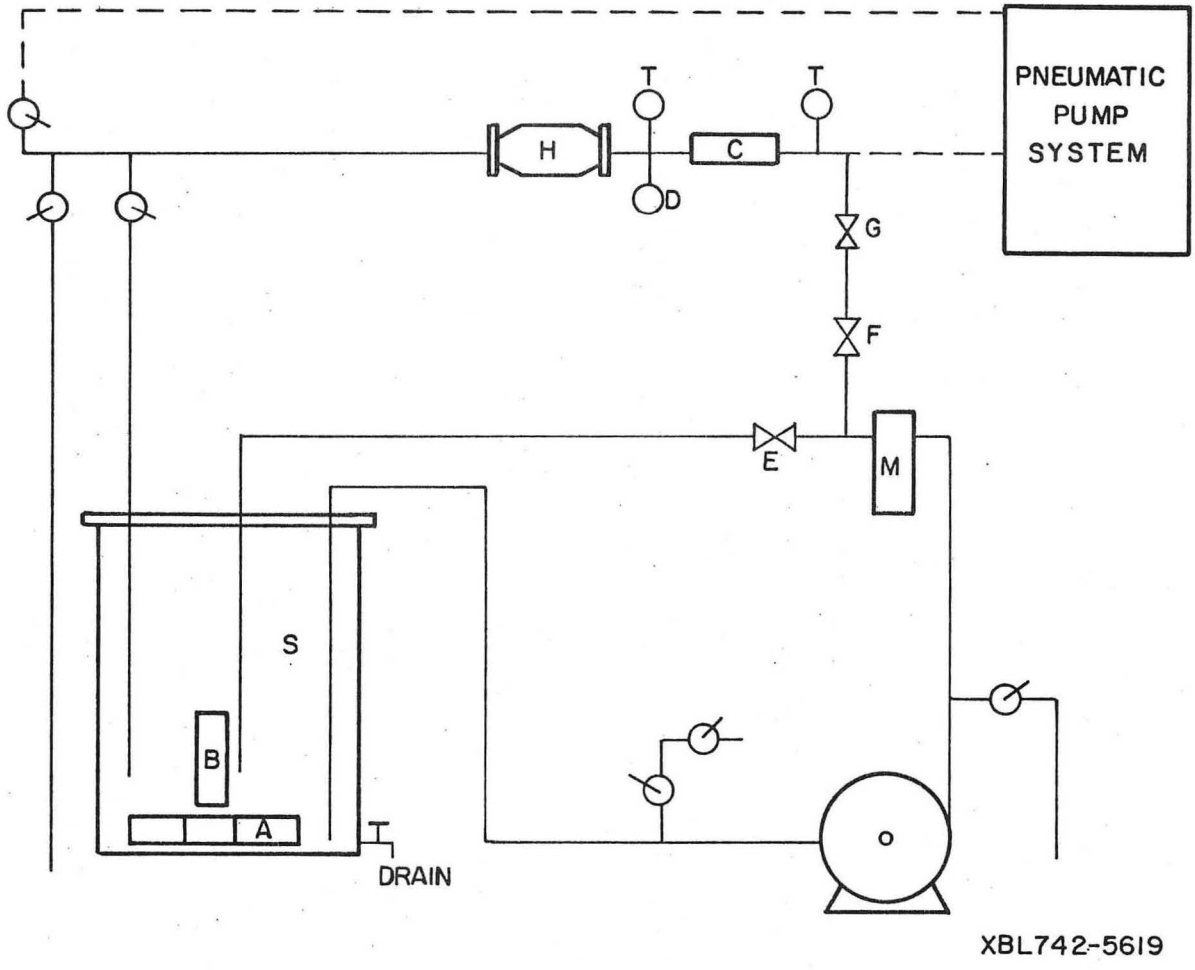

Fig. III-9. Schematic diagram of the test facility.

A. Cooling coil
B. Heater
C. Experimental cell
D. Thermistor
E. Needle valve
F. Needle valve
G. Needle Valve
H. Magnetic flow meter
M. Cartridge filter
S. Polyethylene holding tank
T. Bimetallic thermometers

0 0 0 0 4 0 0 3 8 6

centrifugal turbine pump* with a maximum head of 130 psi (302 ft of water) and a rated constant delivery of 3.5 GPM. The second pumping system consisted of a pneumatic pump, custom-built for this application, capable of delivering 2.5 gal of solution at a maximum pressure of 3600 psi at the exit of the pump. The test facility will first be described with the mechanical pump in use; the important differences when the pneumatic pump was used will be described later.

The flow circuit was built of schedule 40, 1/2 in. stainless steel pipe. The flow circuit consisted of a feed line to the experimental cell and a bypass line to control the flow. Both lines emptied into a holding tank made of polyethylene wrapped with aluminum foil to prevent decomposition of the solution (see Section III-A).

The output of the pump was continuously passed through a cartridge filter.**

The fraction of the flow passing through the experimental cell was determined by the opening of needle values E for the bypass and F and G for the cell.

The flow rate through the cell was measured by means of a magnetic flow meter† located downstream of the cell, H. The signal from the magnetic flow meter was displayed on the dial of the instrument and

---

*Model 5 SC 2129HC. Roy E. Roth Company, Rock Island, Illinois.

**Model 1B1-2278F1. Cuno Engineering Corporation, Meridian, Conn. Polypropylene cartridges with a rated pore size of 5μ were used.

†Model 346 921516 with signal converter Model 460-1, Brooks Instruments Division, Hatfield, Penn.

and alternatively, for greater accuracy, by a digital voltmeter.

The electrolyte solution was maintained at the working temperature of 25°C by means of a temperature control system formed with heating and cooling elements. These were immersed in the solution contained in the holding tank. The cooler consisted of a coil, A, formed with 20 ft of thin walled 1/4 in. nickel tubing through which house cooling water at approximately 15°C was continuously circulated. The heater, B, consisted of four electric immersion heaters, each with a rated power of 500 watts, whose output was determined by a proportional controller C. The sensing unit of the proportional controller* was a thermistor, D, located in a well just downstream of the experimental cell. By means of this control system, the temperature of the solution could be maintained at 25±0.5°C. The actual temperature variation during the course of a potential scan (see page 54) never exceeded 0.1°C.

The temperature of the electrolyte was independently checked by means of two axially located bimetallic thermometers placed 1 ft upstream and 1 ft downstream from the experimental cell. The stem of the thermometers extended 3 in. into the flow.

The pressure taps from the experimental cell were connected through 1/8 in. stainless steel tubing to a pressure manifold made of stainless steel.(Fig. III-10). The pressure at each of the piezometric stations was measured by means of a strain gauge pressure transducer** connected to the

---

*Model 70-115. RFL Industries, Boonton, N. J.

**Models 254; 187; 2201; 185; 206-SA. Teledyne Taber, Inc., North Tonawanda, N. Y.
Models AP-64F-50; GP-46F-100-8455; GP-54F-500; GP-46F-500. Transducers Inc., Santa Fe Springs, CA.

0 0 0 0 4 0 0 5 8 7

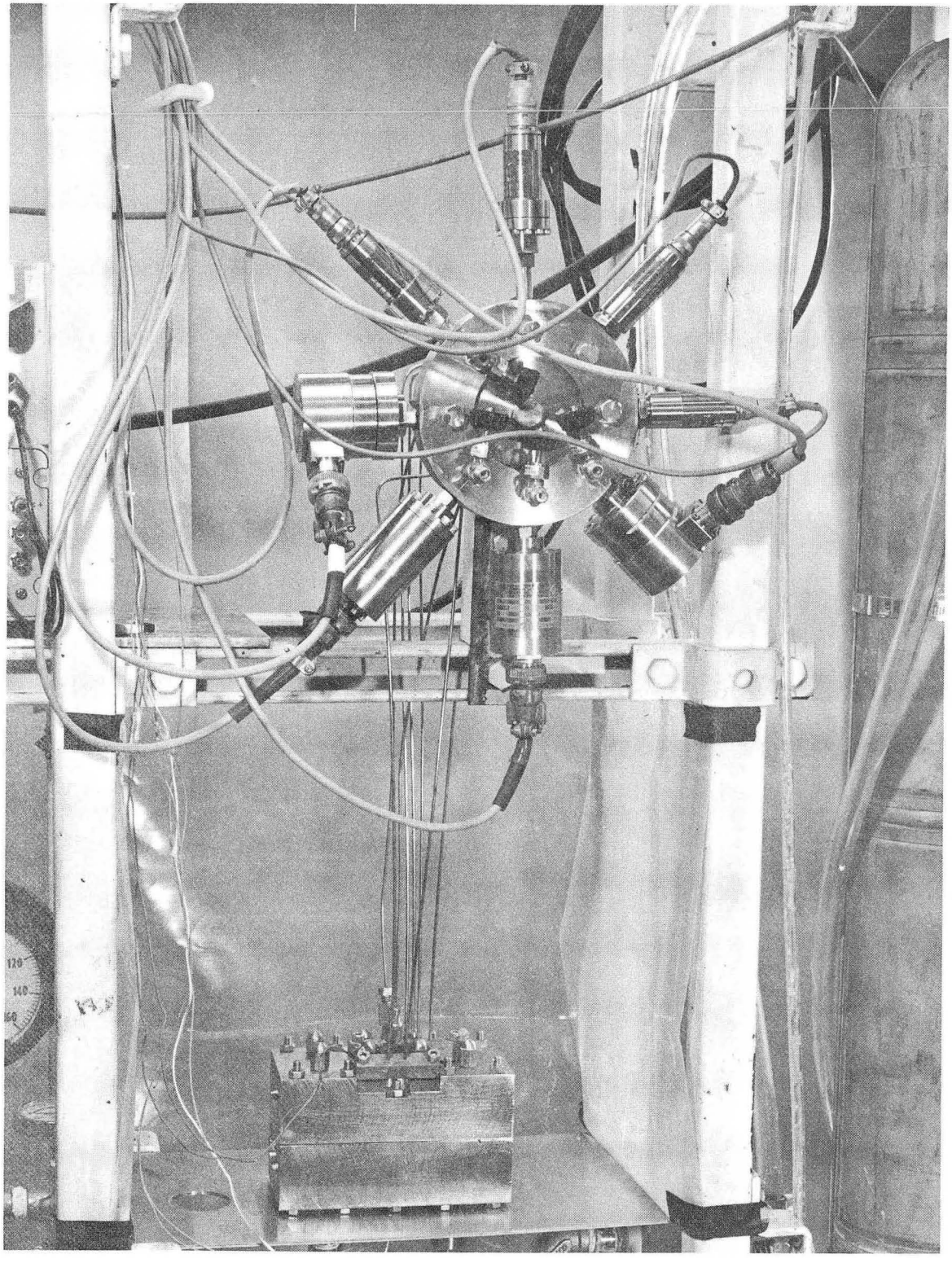

XBB 732-996

Fig. III-10. Cell II pressure taps connected to pressure manifold. The pressure transducers used for the measurements are installed in place in the pressure manifold.

pressure manifold. The output signals of the pressure transducers were successively displayed by a digital voltmeter and were recorded by the experimenter.

Alternatively, for the very small pressure differences at the lowest Reynolds numbers in Cell I, two adjacent piezometric taps were connected to a glass U-tube manometer. The measuring fluid in the manometer was chloroform, and the readings were visually determined by the experimenter using a scale built into the manometer and recorded by hand.

Electric current was supplied to the electrolysis cell by means of a potentiostat,* with a maximum controlled potential of 2 volts and a maximum current of 3 amp.

The cathodic current from the potentiostat passed through a shunt box equipped with four on-off switches that permitted disconnecting the sections of the cathode as required by the scheme of measurement (see Section III-D). The current to the individual cathode sections passed through four precision resistors R1, R2, R3 and R4.** By measuring the voltage drop across these resistors the current flowing through each of the individual cathode sections was determined. The voltage drop across any of the measuring resistors R1 through R4 was displayed as the "y" signal in an X-Y recorder.† The potential

---

*Wenking Potentiostat. Model 78-TS-3. G. E. Bank Elektronik, West Germany.

**The values of the R1, R2, R3 and R4 resistors were 16.66, 16.66, 10.00 and 16.66 mΩ respectively. These small resistances were necessitated in order to maintain the potential at the electrode sections uniform within 1.3 mV for the largest difference in total current between electrode sections.

†Model 7001 A. Hewlett-Packard, San Diego, CA.

0 0 0 0 4 0 0 5 8 . 8

between the common cathode lead and the reference electrode constituting the "x" signal simultaneously fed to it. In this manner, cathodic potential-current curves could be traced and the limiting current determined. By means of a low-resistance four-position switch the current passing through any of the four cathode sections could be selected as the "y" signal being displayed.

A wiring diagram of the electrical connections needed for measurement of the limiting current curves is shown in Fig. III-11.

Pneumatic Pump Facility. For the largest Reynolds numbers studied when using Cell II, the pressure drop through the flow channel demanded that a pumping system capable of delivering the solution at pressures up to 3,000 psi be employed. The only mechanical pumps capable of delivering this head are those of the reciprocating action type. Since reciprocating action pumps give a pulsating flow, they were considered undesirable for the present application. For this reason a pneumatic pump was designed and built for use in this range of pressure heads.

A schematic diagram of the pneumatic pump is given in Fig. III-12. The pneumatic pump consisted a hydraulic accumulator* used as a flow separator, and a pressure regulator to fix the delivery pressure of the pump. The inside of the cast iron accumulator sheel was nickel plated to avoid contamination of the working electrolyte, while the bladder was of a Butyl rubber composition that resists oxidation by this solution. The pneumatic pump was connected to the cell by means of 0.035 in. wall thickness 1/4 in. stainless steel 304 tubing.

*Model A4842-200. Greer Hydraulics, Inc., Los Angles, CA.

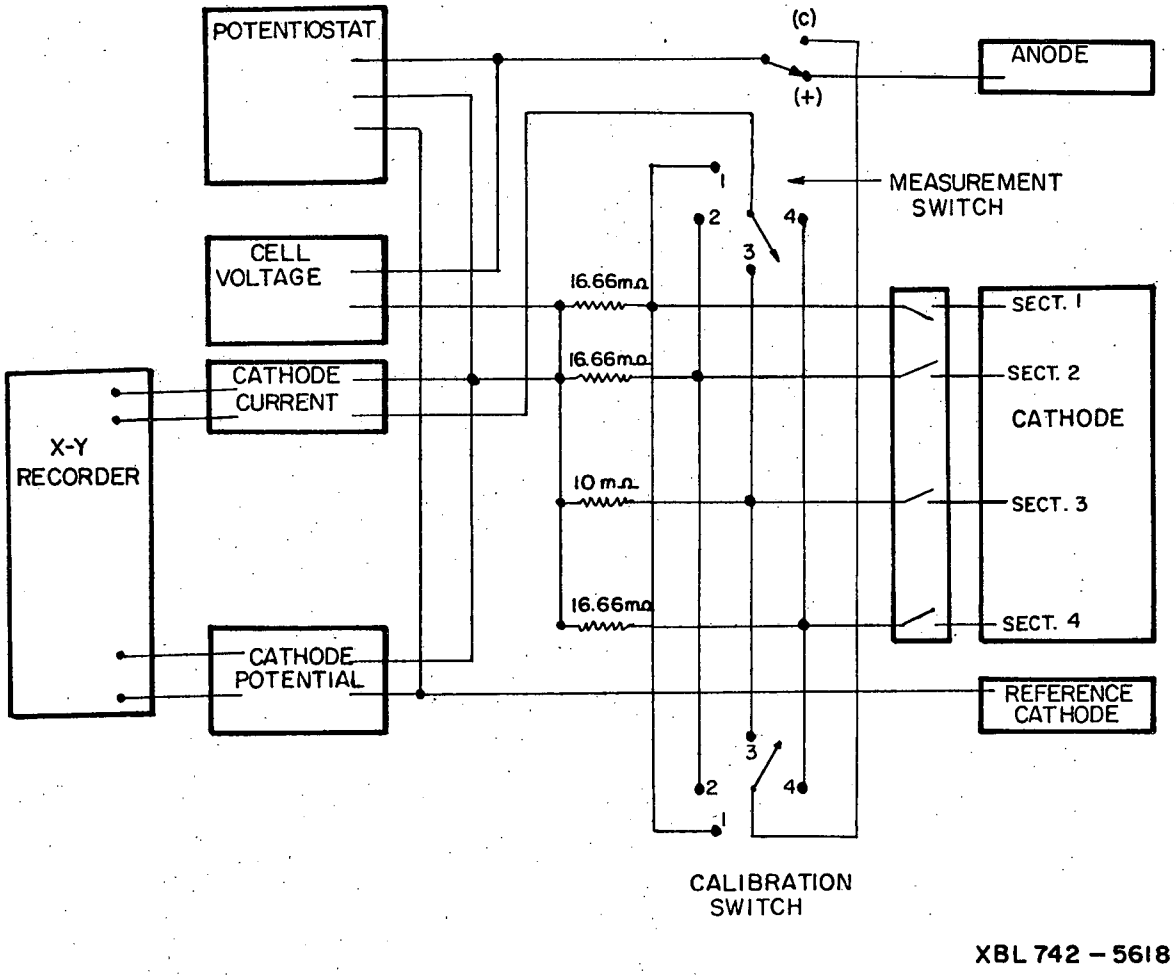

Fig. III-11. Wiring diagram. Electrical connection of the cell for measurement of limiting current curves.

0 0 0 0 4 0 0 5 8 5 9

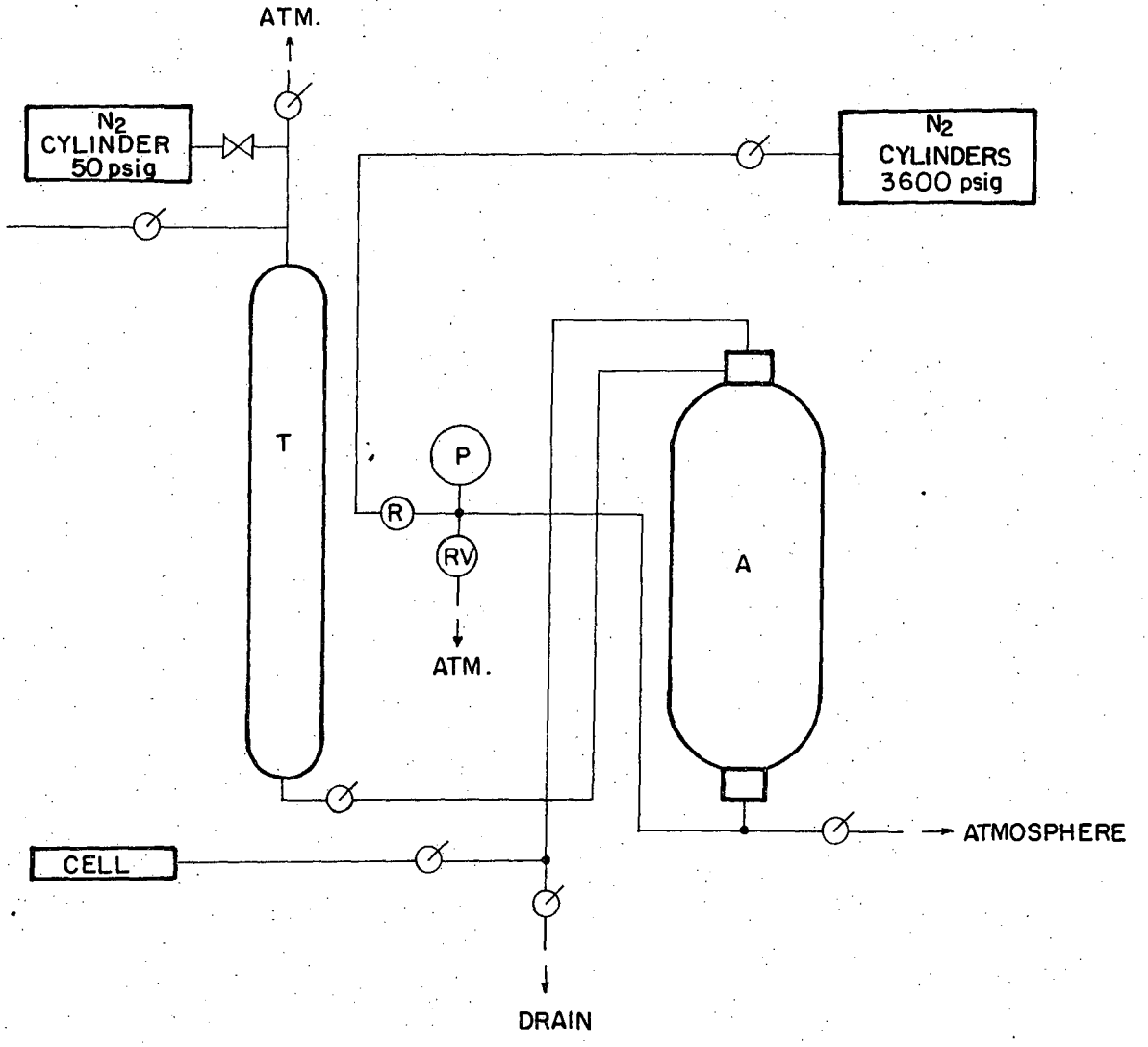

PNEUMATIC SYSTEM DIAGRAM

XBL742-5643

Fig. III-12. Schematic diagram of the pneumatic system.
A. Hydraulic accumulator used as flow separator
P. Manometer (Bourdon type)
R. Pressure regulator
RV. Relief valve
T. Stainless steel holding tank

High pressure fittings* and gate valves** were used in this line.

In operation the solution was pumped into the shell while the bladder was vented to the atmosphere. Once the shell was full, nitrogen gas at the pressure needed to obtain the required Reynolds Number in the cell was fed into the bladder through a pressure regulator.† When the valve controlling the flow of the solution was opened, the constant pressure that the nitrogen exerted on the butyl bladder forced the exit of the solution at a steady rate. In this manner, pulse-free flow could be delivered to the cell. A disadvantage of this system is that the duration of the runs was limited by the capacity of the accumulator (2.5 gallons), coupled with the fact that once the pneumatic pump had been emptied it took approximately 10 min to bleed the nitrogen gas from the bladder and refill the shell with solution.

When using the pneumatic pump the temperature control system could not be employed. These runs were performed at room temperature, quite constant at approximately 22°C. Also, since the pressure drop through a filtering medium would have been prohibitive for these runs, the solution was passed unfiltered through the cell for several runs, and then filtered in the low pressure system before returning it to the pneumatic system.

---

*Swage-Lock, Crawford Fitting Co., Cleveland, Ohio.

**Hoke Inc., Creeskill, N. J.

†GD-80, Victor Controls, Sacramento, CA.

0 0 0 0 4 0 0 5 8 . 0

G. Procedures

1. Operation

Previous to starting a run nitrogen gas was bubbled through the electrolyte solution contained in the holding tank for a period of 30 min to 1 hr. The nitrogen purging was continued throughout the duration of the experimental run.

A typical run was conducted in the following manner:

1) The disassambled cell was washed using deionized water and a cotton wad impregnated with Teepol* soap. After rinsing with distilled water and acetone it was allowed to dry. For the experiments using the roughened electrode surfaces it was found necessary to follow the soap wash by a quick scrubbing using a cotton wad impregnated with dilute sulfuric acid. This quickly removed the tarnish that appeared on the electrode after it had been polarized a number of times. The value of limiting currents obtained in successive runs gradually declined when tarnished electrodes were used. The problem of electrode poisoning was also noticed when using the smooth electrodes, but in that case simple washing with Teepol soap and treatment by cathodic hydrogen evolution (see below) was found sufficient to restore the activity of the electrode. A similar problem when using the ferri-ferrocyanide system with rough electrodes has been reported by Dawson and Trass.[8]

2) The cell was assembled using the appropriate Mylar spacer.

3) The cell was connected in place in the flow circuit.

---

*Trade Mark, Shell Oil Company.

4) Electrical connections to the cell were made.

5) The piezometric openings were connected to the appropriate pressure transducers installed in the pressure manifold.

6) The mechanical pump was started with the bypass valve fully open and the cell valves totally closed.

7) The temperature control was activated by turning on the proportional controller and opening the cooling water valve.

8) The cell valves were then slowly opened and the air trapped in the cell was allowed to be carried off by the electrolyte. Once no more air bubbles were visible in a transparent section of Tygon tubing located downstream of the cell, current was passed through the electrodes. Often the first current vs potential curve would show a steep slant instead of a plateau. In these cases, the potential of the electrode was maintained in the region where hydrogen gas was evolved at the electrode--above one volt against a Ni electrode immersed in the same solution--for a period of 2 to 3 min. This was invariably sufficient to give a flat plateau in subsequent potential scans.

9) Once a flat plateau had been obtained, the flow was adjusted to give the required Reynolds Number in the cell and the temperature was allowed to stabilize. Then the potential was scanned at a rate of approximately 10 mV/sec. For runs in which the pneumatic pump was used the potential scan had to be made as quickly as possible since the duration of the run was limited by the capacity of the pump (see Section E). In these cases, the current vs potential curves showed a peak before the limiting current plateau was reached. However, the value of the limiting

0 0 0 0 4 0 0 5 8 5 1

current plateau was the same for curves obtained using a slower potential scan rate at the same Reynolds Number. This transient effect has been analyzed by Selman.[44]

10) When the current plateau was reached for a given electrode section, the current signal to the X-Y recorder was switched to the next section. This switching permitted obtaining as many as four current plateaus (for the four sections of the electrode) within the same potential scan. This expedient was possible due to the very wide plateau that is obtained in the reduction of ferricyanide ion (cf Section A). Periodically it was confirmed that this artifice did not give false values of the limiting current for each of the cathode sections. This was done by obtaining the limiting currents at a given Reynolds Number both by switching the signal from one electrode to another within the same potential scan and by performing a potential scan for each individual electrode section.

11) Once the value of the limiting current had been obtained for the eight x/D_h values (see Section D), the process was repeated at the same Reynolds Number.

12) The value of the pressure at each of the piezometric stations was read from the pressure transducers output and recorded.

13) Next the flow was adjusted to another value of the Reynolds Number, the temperature of the electrolyte was allowed to stabilize, and steps 9 through 12 repeated at this new Reynolds Number value.

14) After determination of the limiting current value for five different Reynolds Numbers the Reynolds Number was adjusted to the value first used with a "fresh" cell. Then the limiting current was determined

again for the four cathode sections. If these values differed by more than 5% from those first obtained, the previous experiments were discarded and the cell disassambled, washed, and scrubbed with sulfuric acid when necessary.

15) At the end of an experimental run and while the solution was still being circulated through the flow system, a sample of the electrolyte was collected from the holding tank. The composition determined from this sample (cf Section C) was used to calculate the mass transfer coefficients corresponding to the limiting currents obtained in that experimental run.

16) The cell valve was closed (the total flow going through the bypass) and the pump stopped. The nitrogen gas purge was shut off, and the temperature control system turned off. The bypass valve was closed, and the pump rinsed using deionized water. The next day, before the solution was circulated through the flow system, the pump was started for a couple of seconds while diverting the effluent to the drain in order to alter the concentration of the solution as little as possible.

2. Data Reduction

As explained in Section D, the current flow through each individual cathode section was measured as a potential drop across a precision resistor. This potential drop was the "y" signal fed to the X-Y recorder, while the cathodic potential with respect to the reference electrode was the x signal. At a given Reynolds Number the cathode potential was scanned until the limiting current plateau was reached. These curves were afterwards read, and the value of the limiting current in terms of

0 0 0 0 4 0 0 5 8 2

millivolt potential drop recorded, together with the conditions of temperature, concentration, and magnetic flow meter reading. From these data the necessary values of Sherwood Number and j_d factor were to be calculated. The calculations needed are all simple and straight-forward. However, because of the large number of Reynolds Numbers studied, and the number of experiments repeated under the same conditions, the calculations proved to be long and tedious. Consequently, use was made of a digital computer to handle the bookkeeping. A program in FORTRAN language was written for this purpose. The input needed for this program was: temperature and volumetric flow rate, concentration of the three solutes in the electrolyte, interelectrode spacing and channel width. The output of the program gave: the value of the density, viscosity and diffusivity of the solution corrected to the temperature of the experiment, the Reynolds and Schmidt Numbers, the value of the limiting current density, Sherwood and $Sh/Sc^{1/3}$ for each of the cathode sections, the average Sherwood Number and j_d factor, and the values reached by Sh and j_d at the last electrode (the "infinity" values of these quantities).

The output signal of the pressure transducers was recorded as a voltage value in mV. From calibration curves for each of the pressure transducers the equivalent values of pressure were read, and the pressure drop calculated. From these ΔP values the friction factor coefficient was calculated as a function of the Reynolds Number.

H. Estimates of Experimental Errors

The purpose of this section is to present an estimate of errors in the values of f and k determined in these experiments.

In general, the approximate total error expected in a number Q calculated from factors $x_1, x_2, \ldots x_n$ is given by[58]

$$\Delta Q = \left|\frac{\partial Q}{\partial x_1}\right| \Delta x_1 + \left|\frac{\partial Q}{\partial x_2}\right| \Delta x_2 + \ldots \left|\frac{\partial Q}{\partial x_i}\right| \Delta x_i$$

where Δx_i is the error associated with an experimentally measured quantity x_i.

Two types of error appear: random errors in the experimental measurements and constant errors arising from inaccuracies in the values of some of the constant parameters used in the calculations, such as the value of the resistors used to measure the individual section currents, the dimensions of the electrode sections, the dimensions of the channel, distance between pressure taps, etc. The latter were in general small.

Interpretation of Limiting Current Measurements. The conditions for validity of limiting current measurements have been reviewed by Selman.[44] He concludes that correct interpretation of these measurements requires: (a) well defined limiting current plateaus, (b) knowledge of the contribution of ionic migration, (c) proper consideration of changing (increasing) surface roughness (for deposition reactions), and (d) slow approach to the limiting current (under chronogalvanostatic or chronopotentiostatic control). In the interpretation of i_L data ionic diffusivities, not molecular diffusivities, must be used

0 0 0 0 4 0 0 5 8 3

in the calculation of mass transfer coefficients.

In the present experiments the first four conditions were met: (a) the ferri-ferrocyanide system gives long and well defined plateaus (see Fig. III-1); (b) the migrational contribution was negligible since the electrolyte was flooded with a large excess of sodium hydroxide; (c) redox reactions to not alter the nature of the surface; (d) to fulfill the condition of quasistatic approach to the limiting current the scan of the potential was very slow (approximately 10 mV/sec). Only when using the pneumatic pump was a faster potential scan employed, because of the limited volumetric capacity of the pump. In these runs a small peak appeared before the limiting current plateau was reached. Control experiments run using a slower potential scan revealed that the value of the plateau was not affected by this transient effect.

In the calculation of the mass transfer coefficient, effective ionic diffusivities were used.[13]

A major source of inaccuracy in the determination of the limiting current values was noise in the signal recorded. In order to keep the potential of the cathode sections as uniform as possible, the value of the resistors used to measure the current was very small (see Section III-F).* As a consequence, the potential drops recorded were of the order of 0.025 mV at the lowest flow rates employed. In certain runs superimposed on this signal was background noise with an amplitude of up to 0.25 mV. Since the oscillations caused by the

*The resistors employed were precision resistors. No variation with time was noticed in the value of the resistance. The individual values could be determined to within 0.01%.

noise were very regular, the value assigned to the limiting current was read at the center of the fluctuating value. A maximum error of 1% may be assigned to the current value read in this manner.

For measurements in the hydrodynamic transition region fluctuations due to hydrodynamic effects were noticed (see Appendix III). In the worst cases (Fig. AIII-1) these oscillations had amplitudes in the range of approximately 10% of the current being measured. Assignment of the limiting current value for these cases could be in error by up to 5%.

Errors associated with the recording equipment were much smaller than those above. Upon reaching the plateau the value of the current does not change, and the manufacturer's specification for steady state measurements in the lowest potential range used is 0.2%.

Rate of Flow. As explained in Section III-G, the rate of flow through the cell was adjusted by the relative opening of the bypass and cell valves. This gave rise to some fluctuations in the flow through the cell, particularly at the lowest flow rates. Volumetric calibration of the flow meter showed that at the lowest flow rates variations of up to 2% were present. At higher flow rates the variations were smaller (0.5% maximum).

0 0 0 0 4 0 0 5 8 3 4

Composition. Errors in the determination of the total electrolyte composition affect the value of the physical properties of the electrolyte (density, viscosity and diffusivity). Errors incurred due to uncertainties in overall composition were small, since the controlling component, the concentration of NaOH (2.0 M) could be determined very accurately (±0.05%). On the other hand, the calculated mass transfer coefficient is inversely proportional to the concentration of ferricyanide ion. The later could not be determined with an accuracy better than ±1%.

Temperature. The temperature control system was capable of maintaining the electrolyte temperature constant at 25±0.5°C. During the short time needed for a potential scan the temperature never varied by more than ±0.1°C. This could cause an uncertainty in the interpretation of the limiting current of approximately ±0.3%.

Pressure Drop Measurements. Two sources of error were associated with these measurements. The relatively large diameter of the pressure tap hole and the distance between taps. In the absence of detailed description of the disturbance created by the presence of the pressure taps, conservatively an error limit of ±2% was assigned to this source.* The error associated with the measurement of the distance between

*For Cell II, in the hydrodynamic transition region this error may have been much larger, see Section IV-B.

pressure taps is negligible; it was determined with a measuring microscope (Section III-D). The maximum error associated with this measurement was 0.0006 and 0.0012% for Cell I and Cell II, respectively.

Dimensions of the Channel. The dimensions of the channel cross section were determined by the size of the cut-out in the Mylar spacer (see Appendix I). Since Mylar becomes brittle when immersed in the caustic electrolyte solution, the spacer had to be replaced every time that the cell was disassambled. All the spacers used with each of the cells were cut from the same Mylar sheets. The thickness of the Mylar sheets was randomly checked with a micrometer and found to be uniform. The maximum error associated with the thickness (interelectrode gap) was 0.5 and 1.5% for Cell I and Cell II respectively. This error was constant and did not produce scatter of the data. The width of the channel was determined by the jig used to cut the spacer. It was estimated that the width could vary by as much as ±0.01 cm. The maximum error associated with the uncertain knowledge of the width is ±1%.

Length of Electrode Sections. The value of the electrode length was determined with a measuring microscope (see Section III-D). The maximum error associated with this measurement is ±0.0025%. This error was constant and did not introduce scatter in the data. However,

0 0 0 0 4 0 0 5 8 5 5

since electrode Sections I, II and IV were used to determine the first point in the Sh vs x/D_h curve (refer to the scheme of measurements, Section III-D), some scatter must be expected in the data corresponding to this point. The small scatter observed did not show any definite trend that could be attributed to the use of different electrodes.

Table V gives the estimated error limits for the experimentally determined quantities, while Table VI gives the error associated with the calculated quantities.

Table V. Error limits of experimentally determined quantities.

Quantity	Error of Measurement
I_{lim} (due to fluctuations in the trace of the X-Y recorder)	±1.0%
Volumetric Flow Readings	±0.5%
Concentration of Ferricyanide	±1.0%
Temperature of Electrolyte	±0.4%
Pressure Transducer Readings	±2.0%
Channel Width	±1.0%
Channel Height	±0.5%
Cathode Width (same as channel width)	±1.0%
Cathode Length	Negligible (0.0025%)

0 0 0 0 4 0 0 5 8 6

Table VI. Maximum expected error in calculated results.

Calculated Quantity	Expected Relative Error
Cross Sectional Area of Channel	±1.5%
Equivalent Diameter	±0.5%
Cathode Area (Smooth)	±1.0%
Limiting Current Density	±2.0%
Diffusion Coefficient	±0.3%
Kinematic Viscosity	±0.2%
Linear Velocity of Electrolyte	±2.0%
Mass Transfer Coefficient	±3.0%
Schmidt Number	±0.5%
j_D Factor	±3.0%
Sherwood Number	±3.0%
Reynolds Number	±2.5%
Friction Factor	±6.5%

IV. PRESENTATION AND ANALYSIS OF THE RESULTS FOR SMOOTH CELLS

A. Cell I, Smooth

1. Effect of the Channel Corners

Most of the experimental data on mass transfer coefficients in laminar as well as in turbulent flow have been obtained using cylindrical ducts. The few experimental efforts involving rectangular channels may be questioned for the following reasons: (1) the aspect ratio of the channel used was very close to one and hence the effect of secondary hydrodynamic currents at the corners of the channel may have been very important, (2) in experiments using the electrochemical technique the electrodes were made narrower than the channel[16,22,30] to avoid the effect of secondary hydrodynamic currents, but no account was taken of the enhanced rates of mass and charge transfer at the edges of the electrode. The former arises from the edges being exposed to fresh solution with a higher reactant concentration; this is unimportant at the limiting current if the thickness of the mass transfer boundary layer, δ_M, is much smaller than the electrode width. The latter results from the electrode field effect which, below the limiting current, causes high current densities at the edges; this can interfere with obtaining a good plateau as the limiting current is approached, even when δ_M << electrode width.

To solve this problem, Hickman and Tobias[51] and Landau and Tobias[26] employed electrically insulated "buffer" electrodes along the longitudinal edges of the working electrode. These buffer electrodes, polarized to the same potential as the central working electrode, "absorbed" any effects of secondary flows at the corners during limiting current measurements.

0 0 0 0 4 0 0 5 8 7

In the present work an alternative solution was used for this problem: The cathode extended across the full width of the channel, but the aspect ratios employed were very large (20, 30 and 40 for Cell I; 56 for Cell II). Comparison of the values of the mass transfer coefficient for the three different aspect ratios used with Cell I are presented in Figs. IV-1 and IV-2 in the form of the j_D factor vs Reynolds Number. For Fig. IV-1, the mass transfer coefficient used was the average obtained from the mass transfer rates measured for the four cathode sections. Figure IV-2 presents equivalent results using the mass transfer coefficient determined for the last electrode section (Section IV) when the entire electrode was polarized. From both figures it appears that for these large aspect ratios the value of the mass transfer rate is independent of the aspect ratio employed. The values present a scatter of 5%, but no trend with aspect ratio is discernible.

For laminar flows it is possible to calculate the effect that the side walls will have on the velocity profile,[13a] and hence on the mass transfer coefficient. This calculation indicates that the effect will extend to a distance approximately equal to the interelectrode separation. This prediction is consistent with the experimental results of Rousar et al.[41] where the variation of the mass flux in the tranverse direction was measured using one single aspect ratio.

For the case of turbulent flow such calculation is not possible. However, determinations by Nikuradse of isovelocity lines[42] indicate that in turbulent flows the corner effect is also restricted to a distance smaller than the width of the narrower walls.

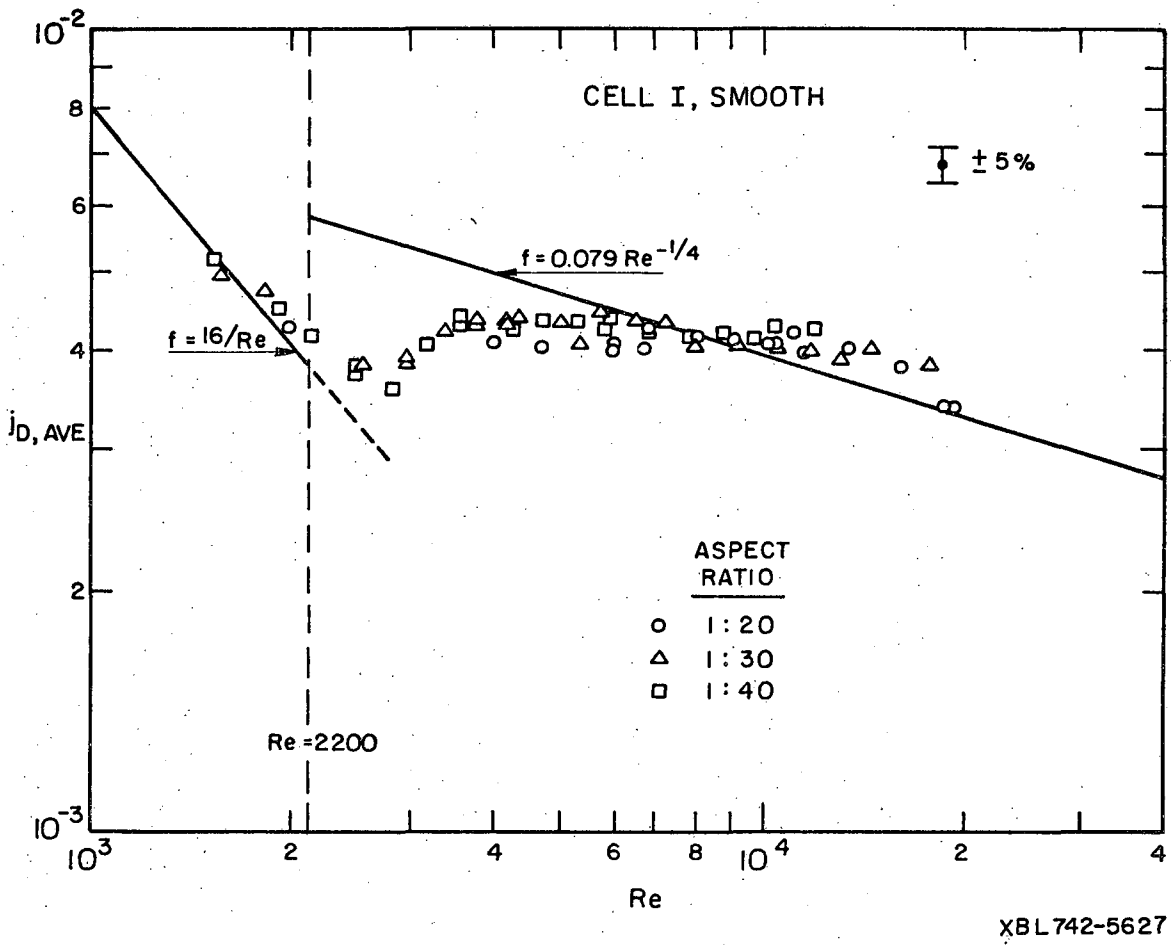

Fig. VI-1. Effect of aspect ratio on the mass transfer coefficient, Cell I. The k value employed to calculate j_D was the average value for the four cathode sections. Sc = 2,000-3,200.

0 0 0 0 4 0 0 5 8 . 8

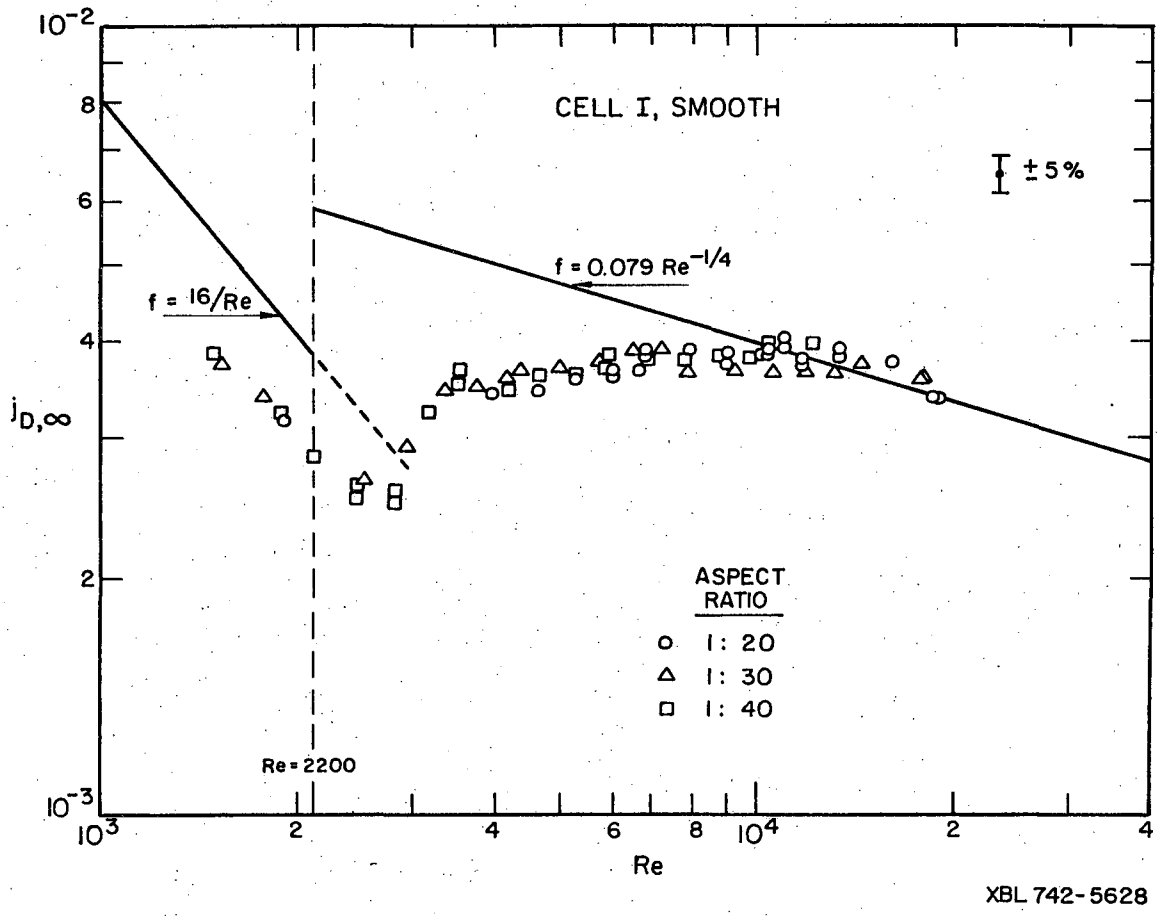

Fig. IV-2. Effect of the aspect ratio on the mass transfer coefficient, Cell I. The k for the last cathode section was employed to calculate the value of j_D. Sc = 2,000-3,200.

According to these considerations, for the three aspect ratios used with Cell I the corner effect would affect 10, 6.6 and 5% respectively of the total electrode width. In the case of the laminar regime the corner effect produces a gradual diminution of the mass flux from the value in the core of the flow to a minimum value at the corner where the velocity reaches a zero value. This, together with the very narrow width affected, leads to a very small decrease in the total value of the mass flux across the width of the electrode.

For the turbulent regime the case is more complicated and only conjectures can be made. The region of the corner will be affected by eddies from the secondary currents, where the fluid flows out of the corner along the bisectrix and returns sweeping along the walls.[15] In this case one would expect a non-monotonic decrease of the mass flux towards the corner and a small variation in the value of the total mass flux. Experimental verification of the variation in mass flux across the walls is not available at present. Picket and Stanmore[36] report a 1.5% difference in overall current density between one central and two lateral strip electrodes in a rectangular channel of aspect ratio 1:6. However, their electrodes did not cover the full width of the channel (the channel was 3 cm wide, and the strip electrodes extended to 0.097 cm from the side walls). Isothermal lines determined by Ibragimov et al.[19] for a square duct indicate a non-monotonic variation of heat flux across the walls.

0 0 0 0 4 0 0 5 8 9

2. Dependence of the Mass Transfer Coefficient on the Distance from the Mass Transfer Section Leading Edge

As explained on page 33, the mass transfer coefficients determined are, in effect, average mass transfer coefficients over a given electrode section, and assignment of this value to any specific point represents only an approximation. For the case of mass transfer in the laminar regime the theoretical solution to the problem dicates the manner in which these average mass transfer coefficients have to be assigned. The extension of the classic Graetz-Lavêque problem to parallel plate channels given by Newman[31] is:

$$Sh = 1.2325\ (ReScD_h/x)^{1/3}$$

and by integration, the average Sherwood number over a section of length L is

$$Sh_{ave} = 1.8488\ (ReScD_h/L)^{1/3}$$

From these equations we can calculate the value of the distance x that would give a local mass transfer coefficient equal to the average mass transfer coefficient for a section of length L comprised between $x = x_a$ and $x = x_b$

$$x = \left[\frac{(2/3)\cdot L}{x_b^{2/3} - x_a^{2/3}}\right]^3$$

Mass transfer in the turbulent regime is characterized by very short entrance lengths and a very fast approach to an asymptotic, fully developed, value of the mass transfer coefficient. van Shaw, Reiss and Hanratty[53] experimentally determined the value of the entrance length. They find

that for $5{,}000 \leqslant Re \leqslant 75{,}000$ their experimental results may be closely represented by

$$Sh_{ave} = 0.276\ Re^{0.58}(ScD_h/L)^{1/3}$$

in the region $0.0177 \leqslant L/D_h \leqslant 0.178$. Their experimental points seem to indicate that this dependence on $L^{-1/3}$ extends to L values from 2 D_h to 0.2 D_h for the Reynolds Number range indicated. Wasan et al.[55] developed an equation showing a similar dependence of Sh on L.

In the present experimental work the smallest electrodes were too long to allow the determination of the value of the entrance length. Furthermore, the fact that for the largest Reynolds Numbers employed only part of the leading electrode was in the developing region gave greater uncertainty to the value of x assigned to a given section average mass transfer coefficient.

Figure IV-3 presents the experimental results in the form of the ratio Sh/Sh_L vs x/D_h. The value of x assigned to the Sherwood number of each section was calculated according to the considerations above. The Sherwood number calculated for the electrode farthest downstream (electrode Section IV when the four sections were polarized) was used for the value of Sh_L.

It should be noticed that all the data fall on smooth lines. As explained on page 35, by the scheme of measurement some of the intermediate points in the curve were obtained with longer values of the entrance length. If the hydrodynamic conditions had been different for each value of the entrance length one would have expected the experimental points to oscillate around a smooth line. The fact that this was not the case

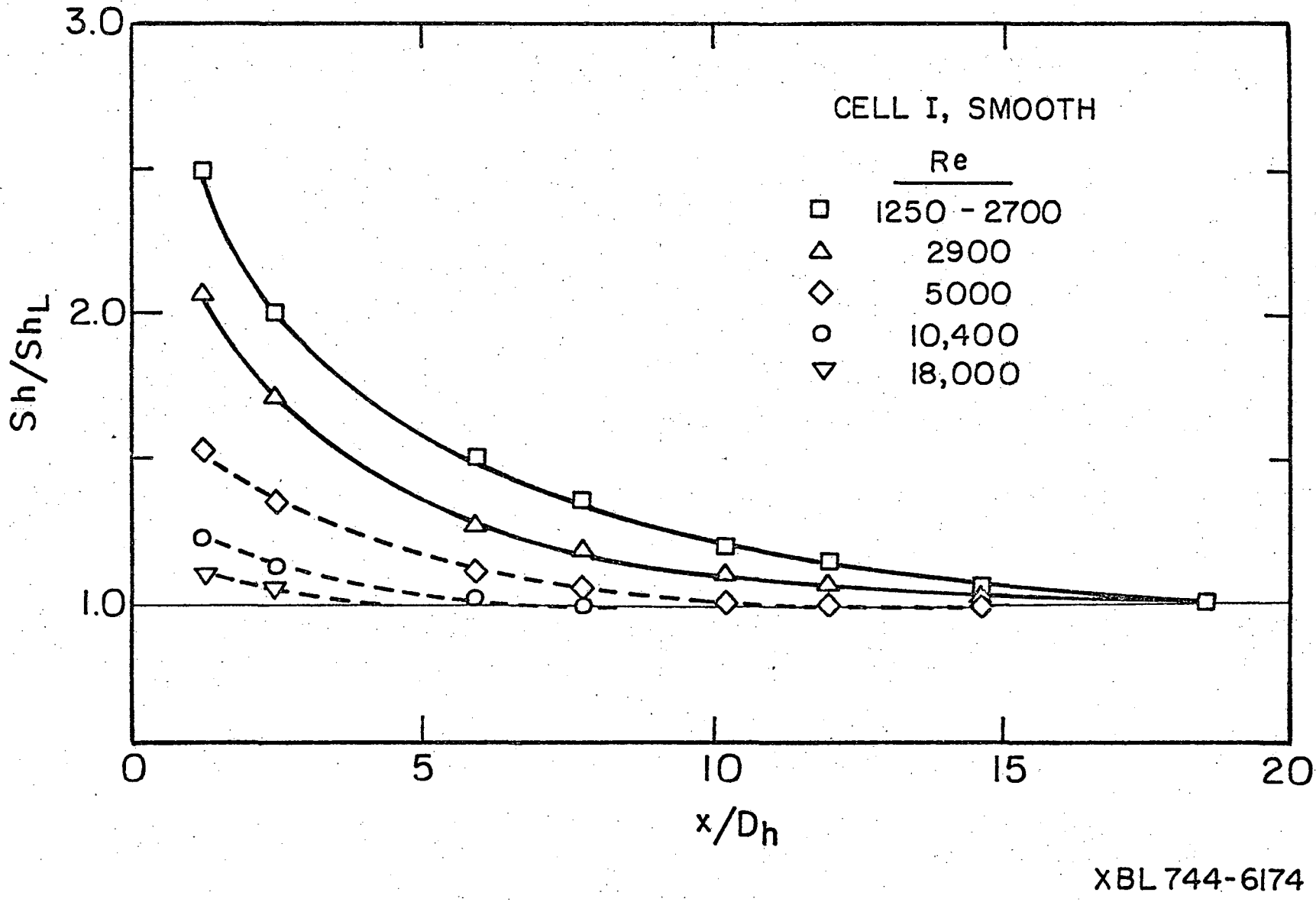

Fig. III-3. Dependence of the mass transfer coefficient on the distance from the mass transfer section leading edge. Sh_L is the value calculated using the k value obtained for electrode Section IV when the four sections were polarized.

0 0 0 4 0 0 5 8 7 0

gives assurance that the flow was already fully developed at the location of the first electrode section.

From this figure it can be seen that the data corresponding to $Re < 2,700$ all fall on the same line, as was to be expected from the unique solution for the purely laminar regime. Beyond this value of Re (at $Re \geq 2,900$) the data fall on separate lines for each Reynolds number studied. The displacement of these curves from the position of the laminar results agrees with the trend predicted by Spalding's calculations [49] and with the experimental results of van Shaw et al.[53]

As explained above, the limitations presented by the relatively large size of the leading electrodes do not allow one to draw definite conclusions regarding the value of the entrance length in the turbulent regime. This is further illustrated in Fig. IV-4, where the uncertainty limits in the assignment of the proper value of x/D_h is indicated for the Sh/Sh_L vs x/D_h curves for $Re \geq 5,000$. The entrance effect indicated by these data seems to extend to $x/D_h = 6$. This entrance length value is larger than those reported [53] for tubes. Picket and Stanmore [36] have also reported longer entrance lengths in rectangular channels.

3. Laminar Results

As mentioned in Section IV-A-2, the extension of the Graetz-Levêque problem gives the solution to the laminar mass transfer in parallel plate channels. A test to the validity of the present results is the agreement with this solution. Figure IV-5 presents the values of the local Sherwood number plotted against the dimensionless group $(ReScD_h/x)^{1/3}$. For $1,500 \leq Re \leq 2,700$ the spread of the data around the straight line with slope 1.2325 is only ±1%. At Re>2,900 the departure from

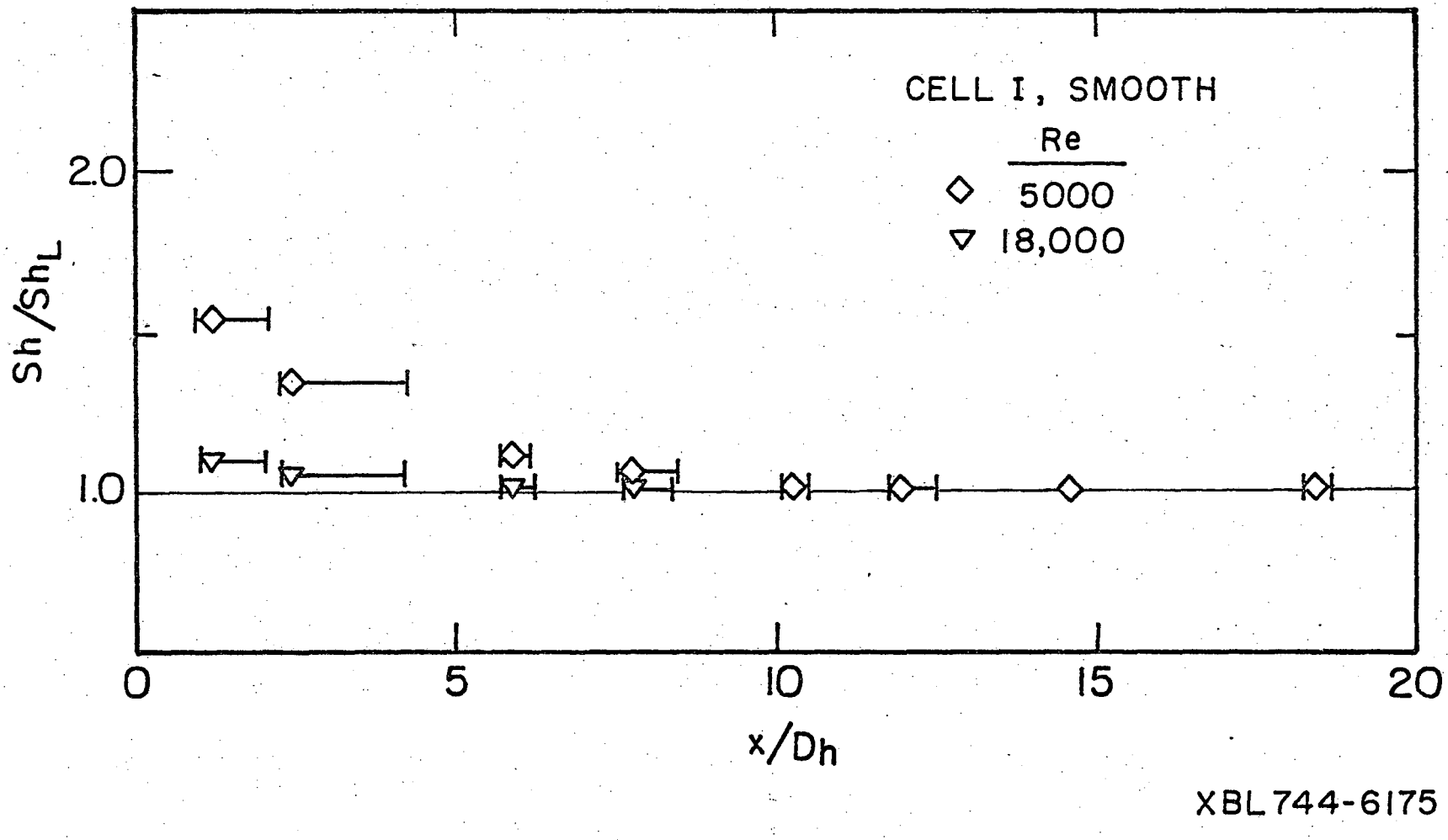

Fig. IV-4. Uncertainty limits in the assignment of the proper value of x/D_h for a given Sherwood Number.

0 0 0 0 2 0 0 5 8 7 1

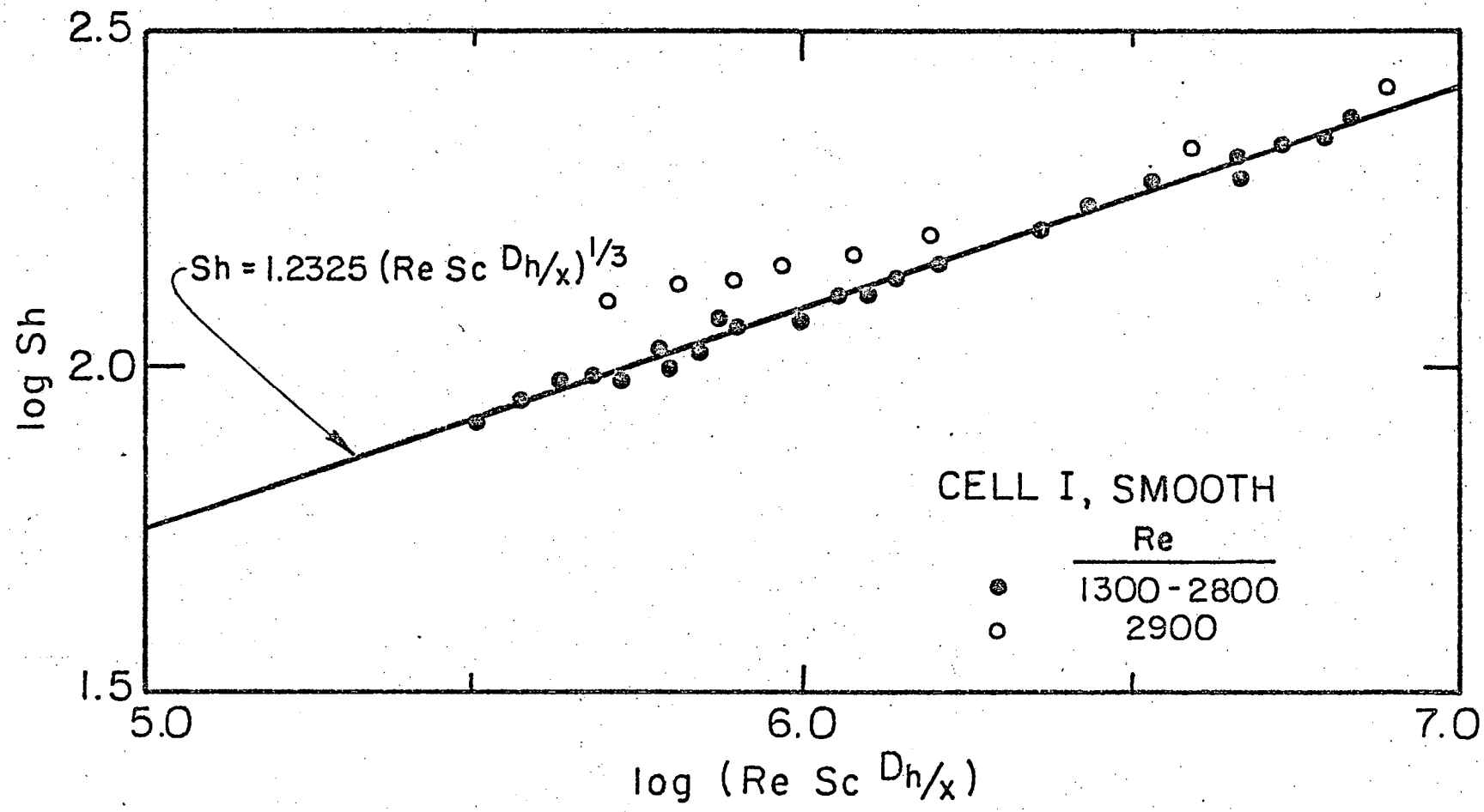

XBL7311-6621

Fig. IV-5. Comparison of experimental local Sherwood Number with the extension to the Graetz-Leveque solution given by Ref. 31. Sc - 2,600-3,200

this line is noticeable, particularly at larger values of x (low values of the abscissa).

4. Turbulent Regime

One of the objectives of the present study was to test the applicability of mass transfer correlations that were obtained using systems with larger equivalent diameters. A complete review of correlations proposed in the past is beyond the scope of the present work. These correlations can be grouped into two categories: empirical and semiempirical. Comparison of the mass transfer data available in the literature is difficult due to the fact that the data spread over a very wide range of values. This spread has been attributed to the formation of minute roughness on the surfaces[4], since the technique employed in many of the experiments was the dissolution of solid walls. This explanation is appealing, since for systems with a high Schmidt number the mass transfer boundary layer is very thin. On the other hand, semiempirical correlations differ mainly in the predicted effect of the Schmidt number on the transfer rate. This discrepancy is due to the different models employed to evaluate the eddy diffusivity in the region very close to the wall, the all-important region for thin mass transfer boundary layers.

Hubbard[16] made a thorough review of turbulent mass transfer correlations, both empirical and semiempirical, and compared them to the simpler Chilton-Colburn correlation. He points out that given our scant knowledge of turbulence in closed channels the development of semi-empirical correlations has reached the point of minimum return. Hubbard reported friction factors measured in the same rectangular channel in which he had obtained mass transfer coefficients. However,

his experimental equipment provided only 45 hydraulic diameters for the entrance length, and the friction factors were calculated from pressure drops measured across only two pressure taps which spanned the length of his mass transfer region. The f values that he obtained differed by up to 20% from those reported by Whan.*[57] Comparing his experimental results with the Chilton-Colburn correlation, Hubbard concluded that this correlation is probably adequate for most design purposes.

The results of the present study for $Re > 2,700$ are plotted in Fig. IV-6 in the form of the Colburn j_D factor vs Reynolds number.** The j_D dimensionless group was chosen since it includes the value $Sc^{1/3}$; this dependence of the Sherwood number on the Schmidt number is proposed in the most reliable empirical and semi-empirical correlations.[6,29,50,54] Two regions are distinguishable in this plot: a transition regime in the region $2,700 \leq Re \leq 5,400$, followed by the turbulent region at $Re > 5,400$. The transition regime is characterized by a fairly sharp increase in j_D with Re, and extends to rather high values of Re. In the turbulent region the j_D factor decreases with increasing Re.

Using the value of the friction factors determined (see below) from the pressure drop measurements performed using the same experimental channel, the group $Sh_{ave}/Sc^{1/3}$ is plotted against $Re\, f$ in Fig. IV-7 and against $Re\, f$

---

*Whan reported experimental pressure drops obtained using an entrance length of 77 D_h, since other values that he had obtained with shorter entrance lengths showed considerable scatter and deviation from linearity.

**The points shown in Fig. IV-7 are average values of the data obtained using three different aspect ratios shown in Fig. IV-1.

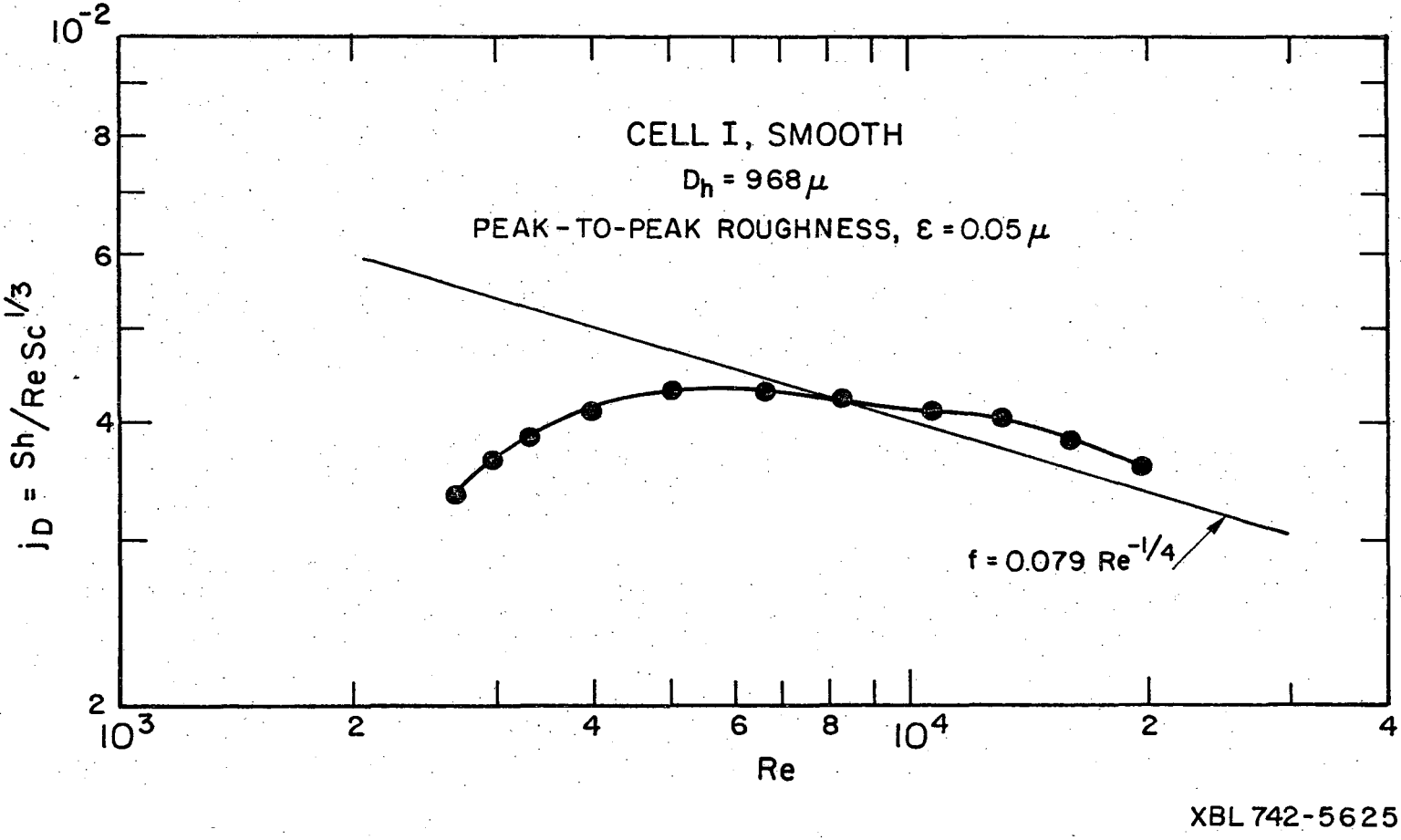

Fig. IV-6. j_D factor for Cell I, smooth. Sc = 2,00-3,200.

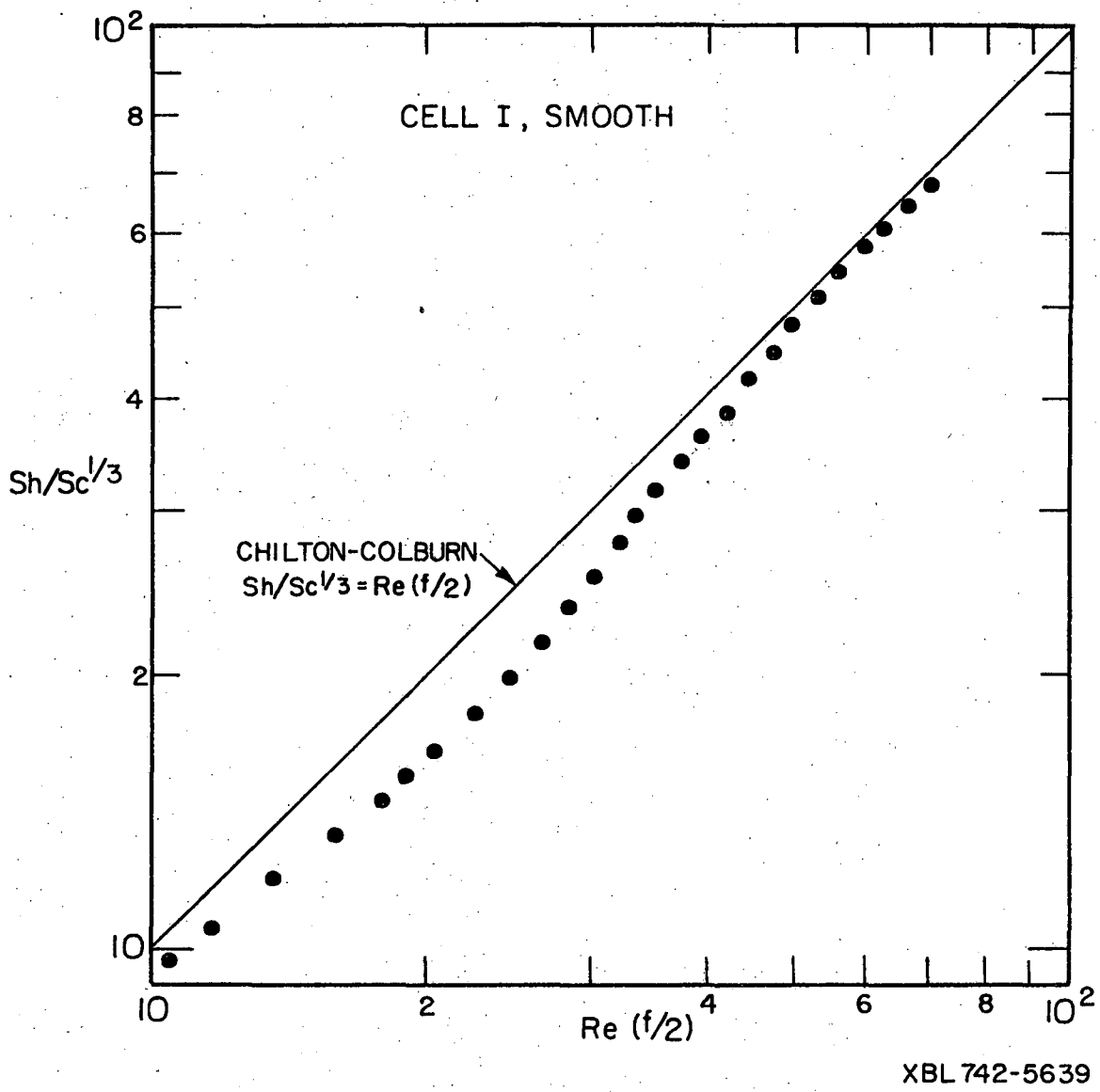

Fig. IV-7. Comparison of the mass transfer and friction factors experimentally determined using Cell I, smooth, with the Chilton-Colburn[6] correlation. Sc = 2,000-3,200.

0 0 0 0 4 0 0 5 8 7 3

in Fig. IV-8. The dependence on the first power of f is implicit in the Chilton-Colburn correlation, and is also shown in the correlation of Vieth, Porter, and Sherwood.[54] A dependence on the square root of f is shown by the semi-empirical correlations of Deissler,[9] Levich,[27] and Lin et al.[29]

5. Friction Factors

The friction factors calculated for the entire Reynolds number range are presented in Fig. IV-9) in the form f vs Re.

At Reynolds numbers less than 2,700 the results follow a distinct linear relationship with a negative slope of -1. This is the type of dependence that is predicted by the Hagen Poiseuille solution for smooth tubes: $f = 16/Re$. However, for this rectangular channel the coefficient is larger. A similar behavior has been observed by Patel and Head[34] using a large aspect ratio (1:48) parallel plate channel.

In the Reynolds number range from 2,700 to 5,000 the value of the friction factor rises rapidly following a trend that has been reported for smooth pipes and channels. The range over which this transition region extends is longer than that commonly reported for pipes, and the approach to a linear (fully turbulent) behavior is rather slow. Similar behavior has been reported by Patel and Head.[34]

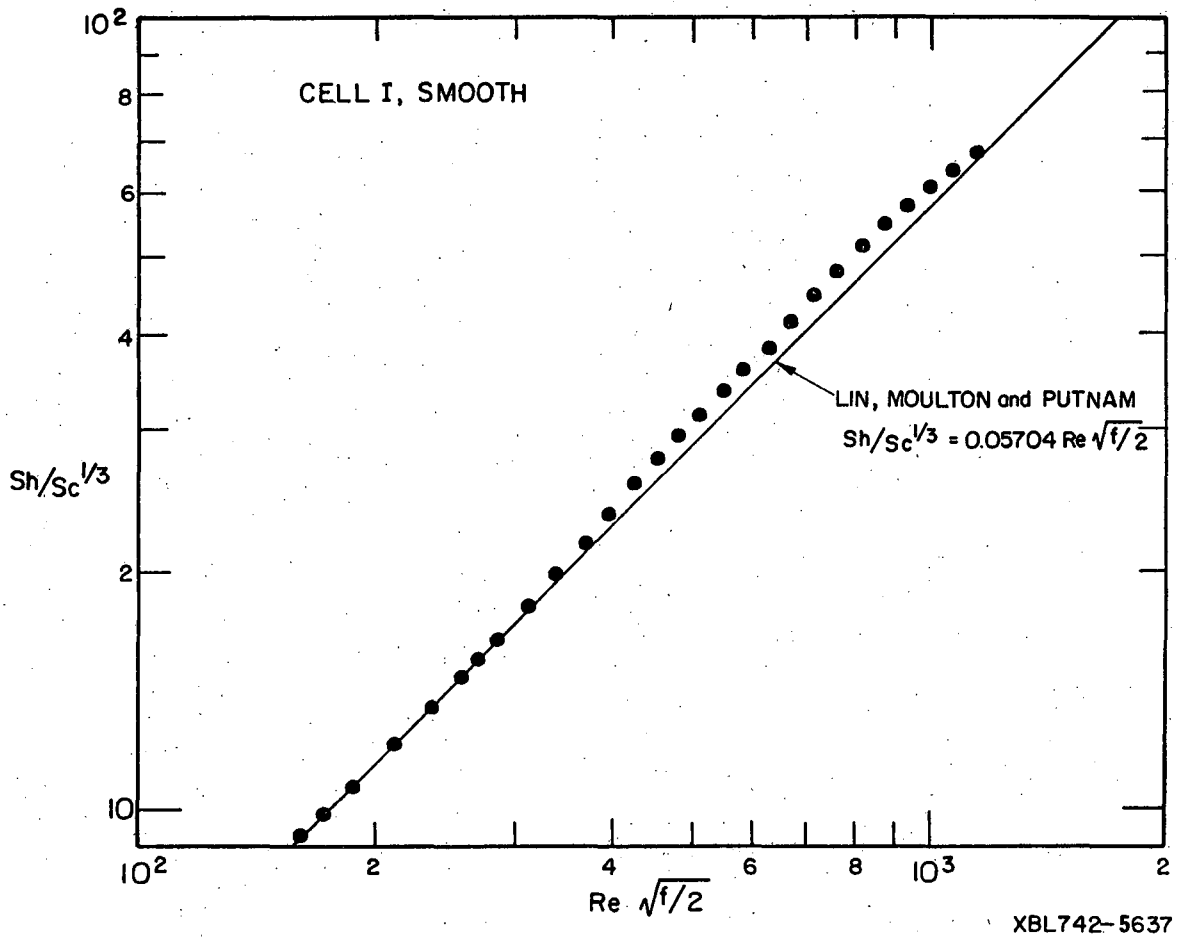

Fig. IV-8. Comparison of the mass transfer and friction factors experimentally determined using Cell I, smooth, with the correlation of Lin et al.[29] Sc = 2,000-3,200.

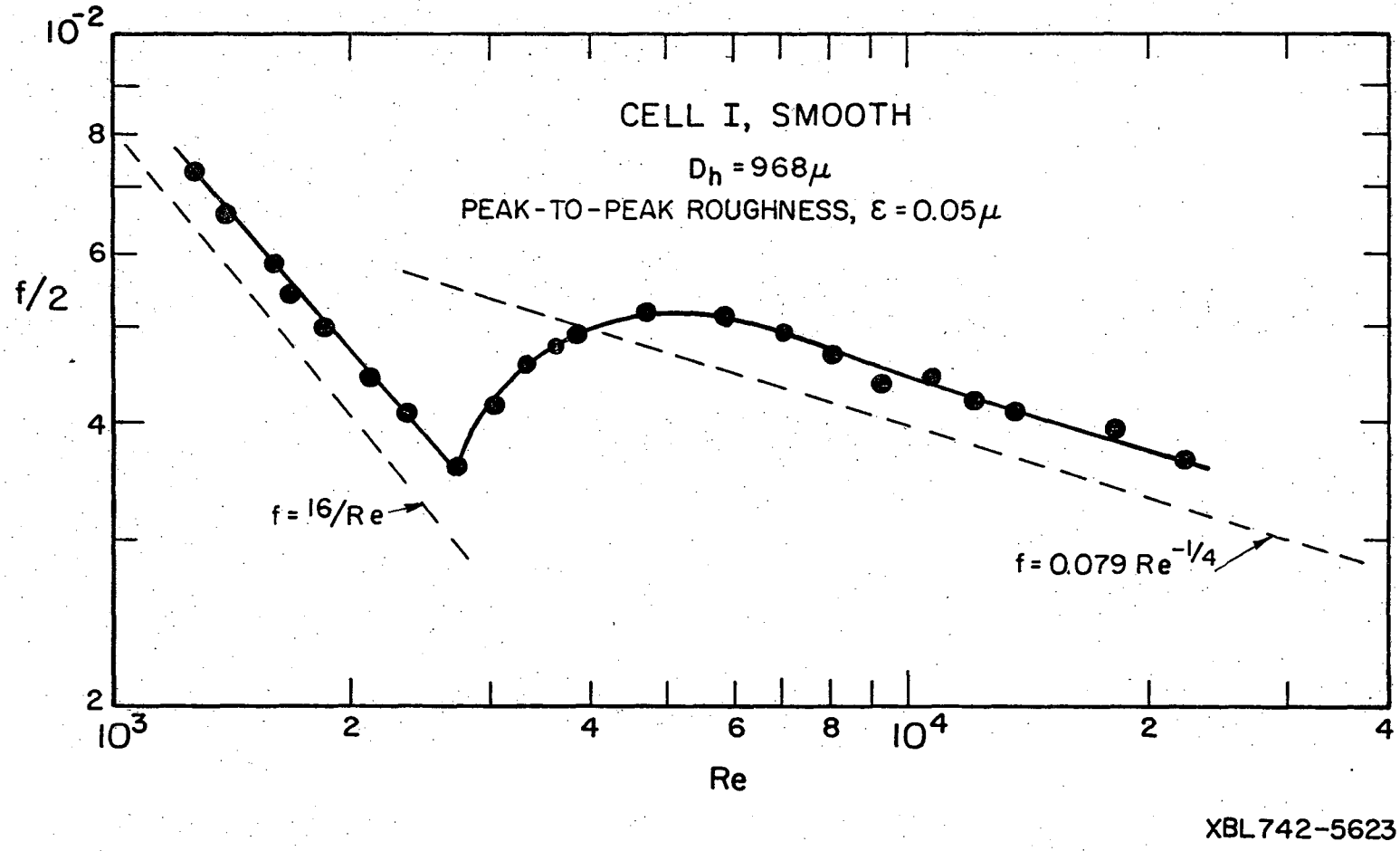

Fig. IV-9. Experimental friction factors for Cell I, smooth.

4 7 8 5 0 0 4 0 0 0

At values of Re larger than 5,000 the dependence of f on Re appears to be linear, following a line parallel to the well known Blasius equation for smooth pipes. Again, the value of the coefficient is larger than for round ducts. This may be due to the effect of the channel corners, since an extra amount of momentum energy will be dissipated in the secondary currents. A similar result has been reported by Hartnett, Koh and McComas.[14]

6. $j_D/(f/2)$ Ratio

Of importance for the present problem is the value of the ratio $j_D/(f/2)$. Since the pressure drop for a given Reynolds number is proportional to D_h^{-3} the expenditure of pumping power when operating electrochemical cells with closely spaced electrodes becomes a very important consideration. The magnitude of the problem is indicated in Table VII, where the pressure drops calculated for hydraulically smooth channels is presented. For many conditions, one will want to operate in a regime where maximum mass transfer (or heat dissipation) is achieved with a minimum pressure drop. Figure IV-10 gives the ratio $j_D/(f/2)$ for the Reynolds number range studied. Even though the Chilton-Colburn correlation ($j_D = f/2$) could not be expected to apply in this Reynolds number range, the value of one for this ratio gives us a measure of the actual gain achieved when operating with rough electrodes, as will be presented later (Section V-f).

B. Presentation of Results for Cell II, Smooth

Figures IV-11 to IV-18 present the results for Cell II, smooth, in the same order as used for the presentation of the results for Cell I in Section A above. In the case of Cell II, the effect of the channel corners was not studied, since the aspect ratio (1:56) was even larger

Table VII. Pressure drop for hydraulically smooth channels.

	Interelectrode Gap = 0.05 cm			Interelectrode Gap = 0.02 cm		
Reynolds No.	Velocity m/sec	Pressure Drop atm/cm	δ mass transf. cm	Velocity m/sec	Pressure Drop atm/cm	δ mass transf. cm
200	0.2	3.2×10^{-4}		0.5	4.9×10^{-3}	
1,000	1.0	1.6×10^{-3}		2.5	2.5×10^{-2}	
2,000	2.0	3.2×10^{-3}		5.0	4.9×10^{-2}	
10,000	10.0	1.5×10^{-1}	2.0×10^{-4}	25.0	2.3	8.1×10^{-5}
20,000	20.0	4.9×10^{-1}	1.1×10^{-4}	50.0	7.7	4.6×10^{-5}
100,000	100.0	8.2	3.2×10^{-5}	250.0	1.3×10^{2}	1.3×10^{-5}

XBL728-3760

This report was done with support from the United States Atomic Energy Commission under Contract No. W-7405-eng-48. To request copies of this report, write to: Technical Information Division, Lawrence Berkeley Laboratory, University of California, Berkeley, California 94720

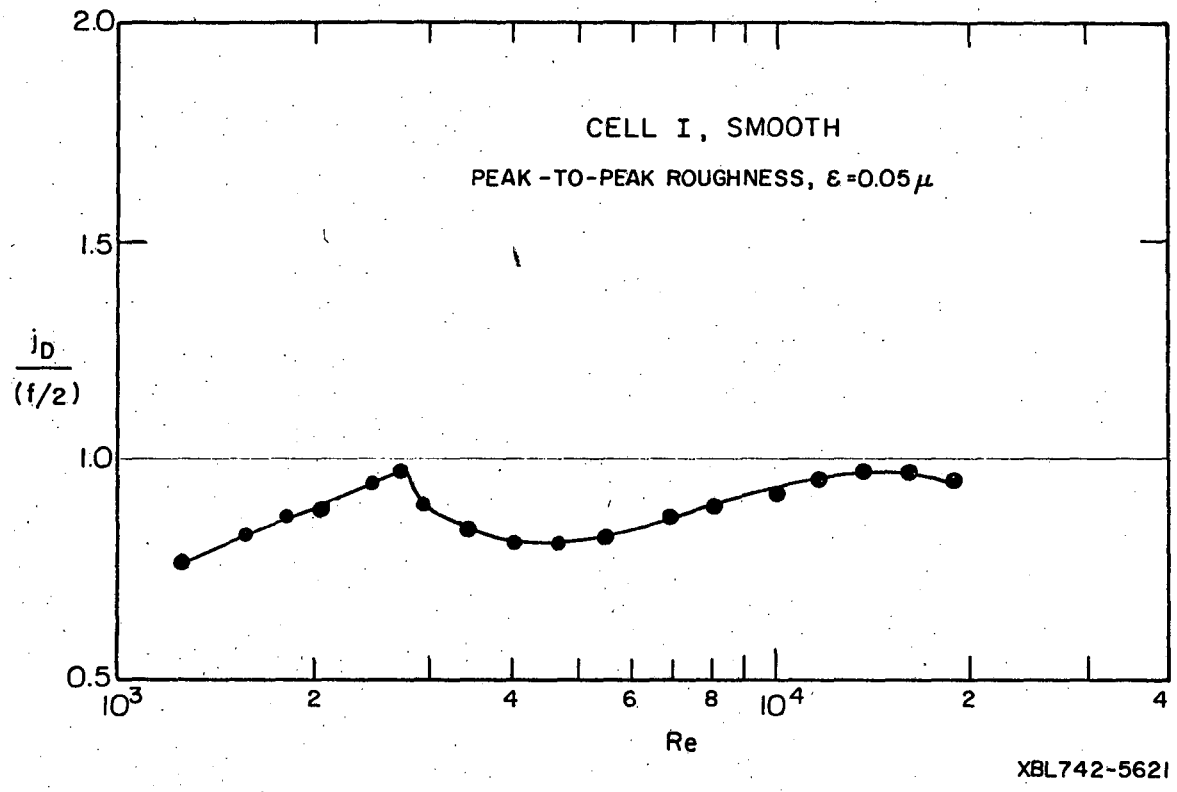

Fig. IV-10. Ratio of mass to momentum transfer coefficient expressed as $j_D/(f/2)$ for cell I, smooth. Sc = 2,000-3,200.

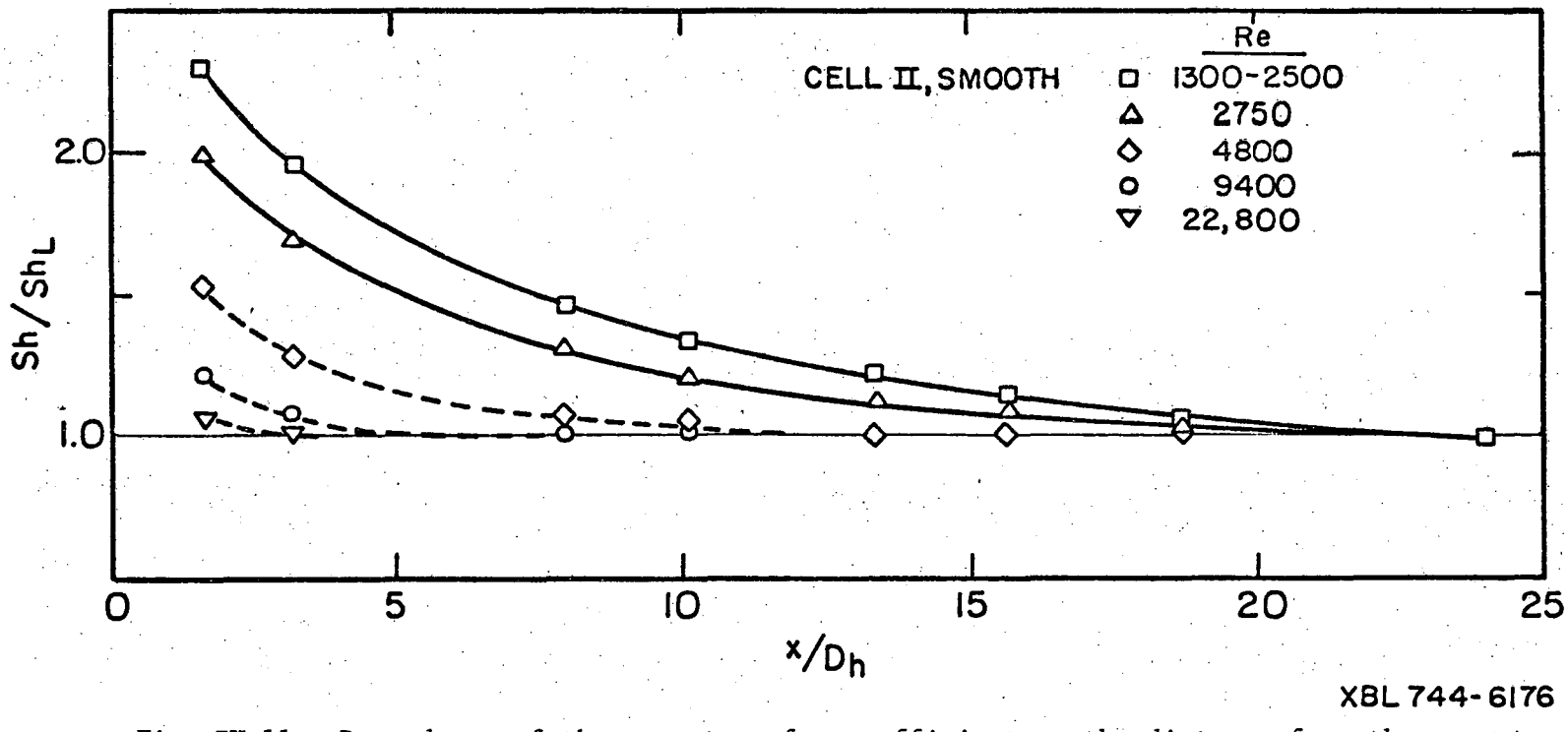

Fig. IV-11. Dependence of the mass transfer coefficient on the distance from the mass transfer section leading edge. Sh_L is the value calculated using the k value obtained for electrode section IV when the four sections were polarized.

0 0 0 5 0 8 9 6 9

than those used with Cell I, and as it has already been pointed out in Section A, at these large aspect ratios the corner effect is negligible.

The remarks to the result of Cell I smooth (Section A) apply in general to the results for Cell II smooth.

Figure IV-12 indicates a departure from the laminar behavior at a value of Re=2,750. This value is lower than that corresponding to Cell I smooth (Re = 2,900). No special significance is attached to this departure at a lower Reynolds number, since both cells are polished to the same degree of smoothness but the ratio of their equivalent diameters was equal to 2.7. The values of the Sherwood number at Re = 2,750 are indicated in Fig. IV-15.

Attention is called to the region $2{,}500 \leqslant Re \leqslant 4{,}000$ in Fig. IV-17. In this range of Reynolds numbers the values of f obtained were not as reproducible as those for larger, and smaller, Reynolds numbers. A similar problem was observed when using Cell II with roughened walls (see Fig. V-19). Recall that for Cell II the ratio of the diameter of the pressure tap holes to the channel gap was equal to 0.8. In this region of hydrodynamic transition, the (relative) large size of the holes, plus any small differences in the shape of their opening, must have created disturbances that were substantially different from one pressure tap to the other. The value of ΔP, and hence f, evidenced this condition. This explanation is substantiated by the observation that the mass transfer coefficient--measured on the opposite wall of the channel--did not show unusual behavior in the same Reynolds number range (see Fig. IV-14).

The odd values of f for $2{,}500 \leqslant Re \leqslant 4{,}000$ are reflected in Figs. IV-15, IV-16 and IV-18.

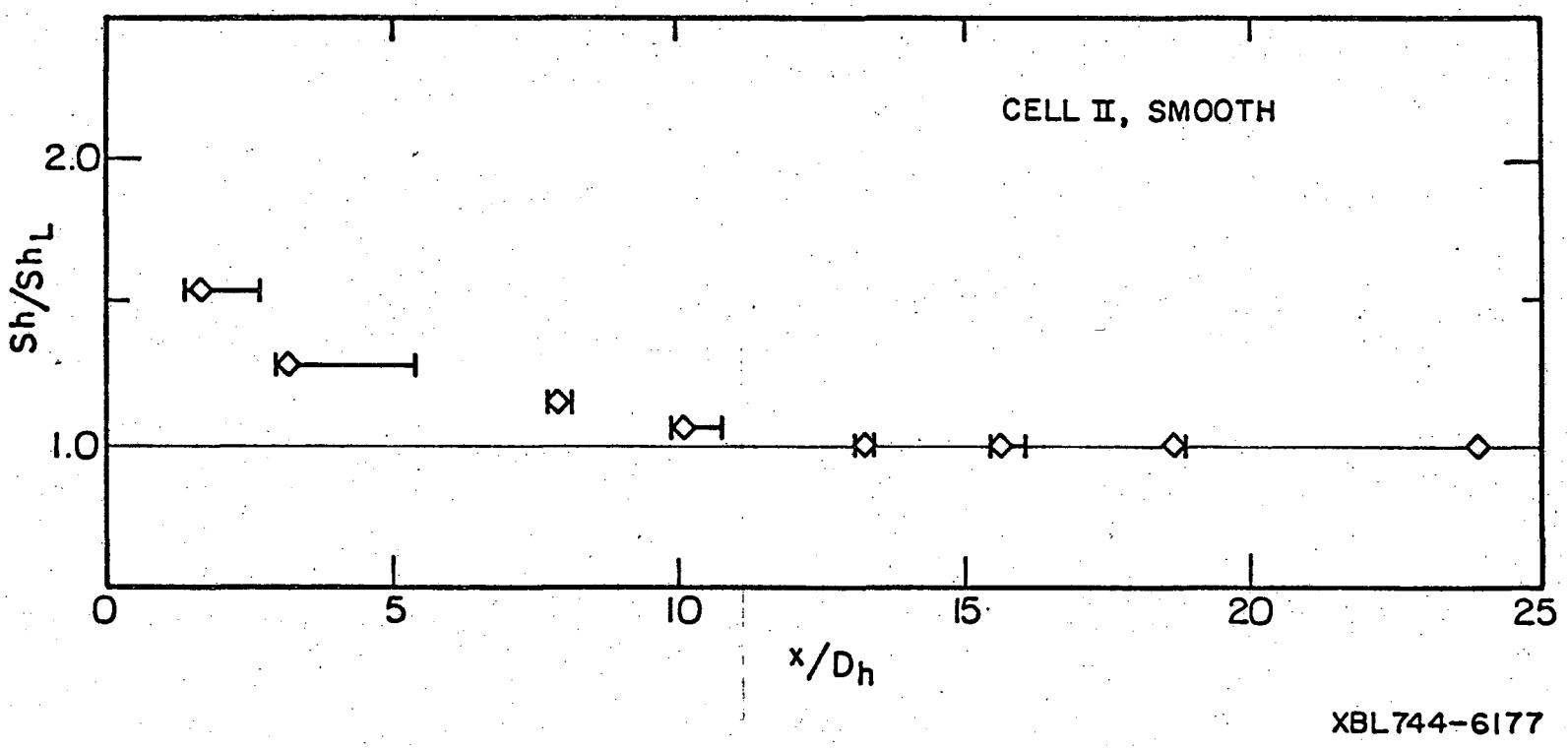

Fig. IV-12. Uncertainty limits in the assignment of the proper value of x/D_h for a given Sherwood Number. Re = 4,800.

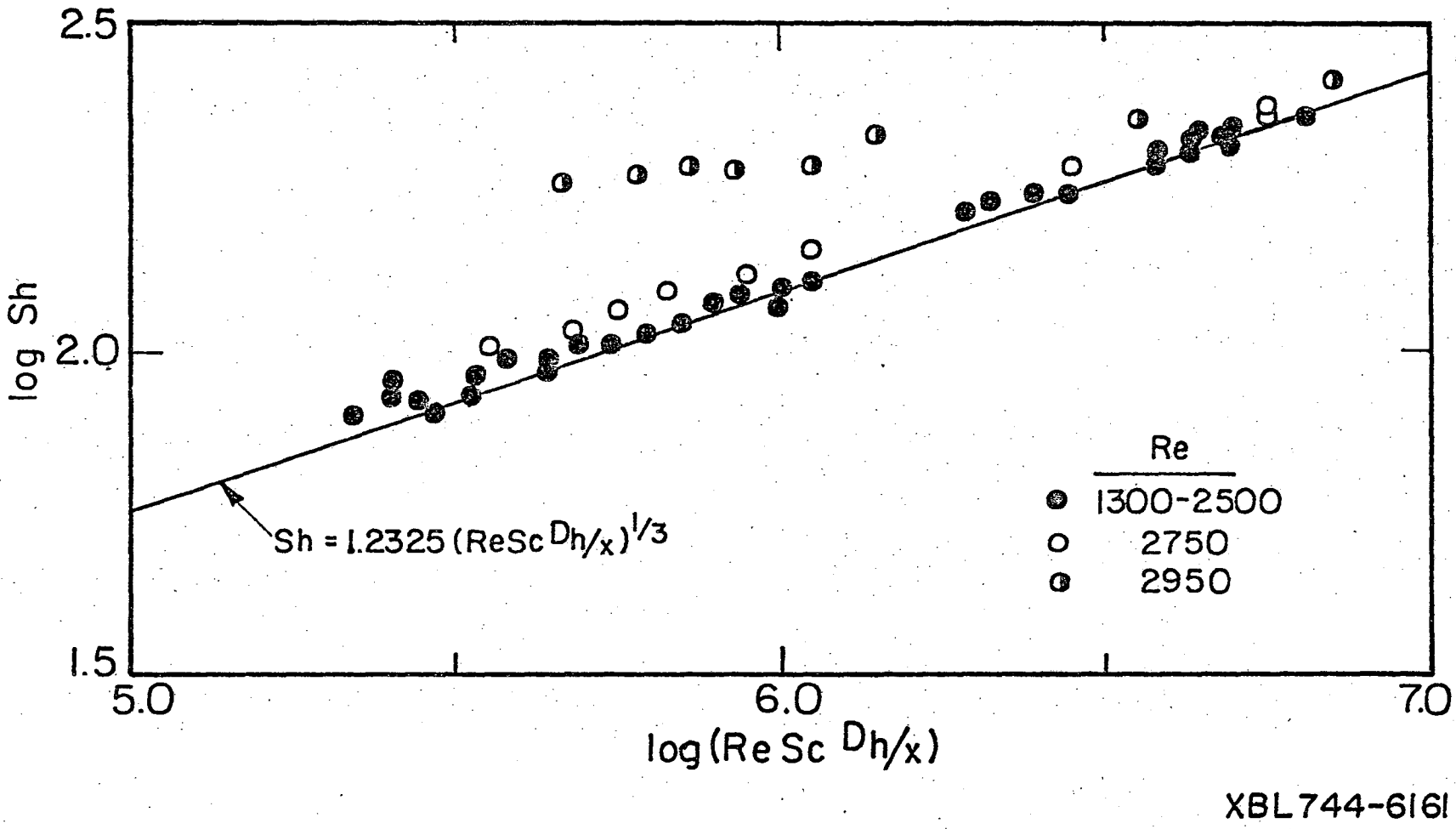

Fig. IV-13. Comparison of the experimental local Sherwood Number with the extension of the Graetz-Leveque solution given in Reference 31. Sc = 3,150.

0 0 0 0 4 0 0 5 8 7 8

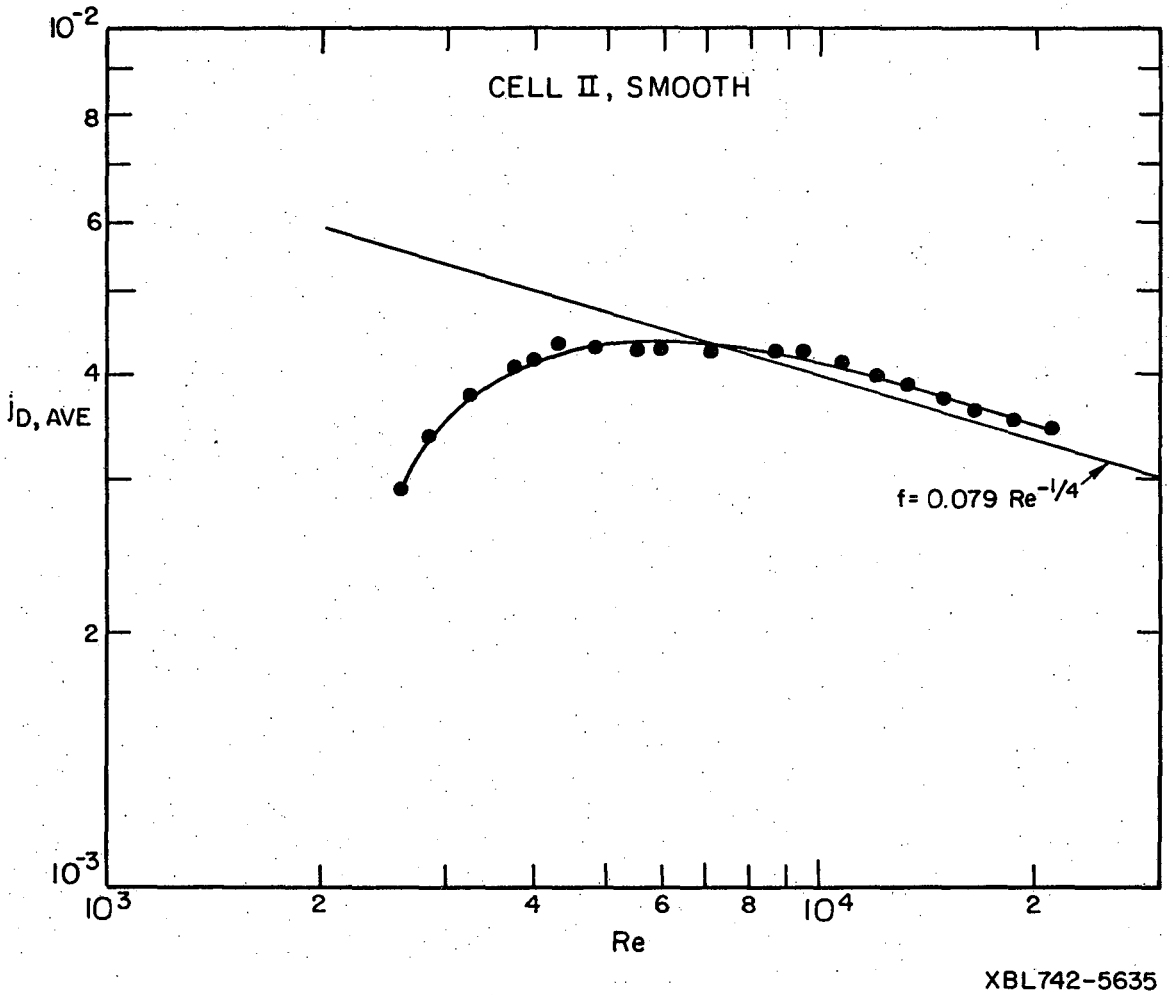

Fig. IV-14. j_D factor for Cell II, smooth. Sc = 3,100-3,500.

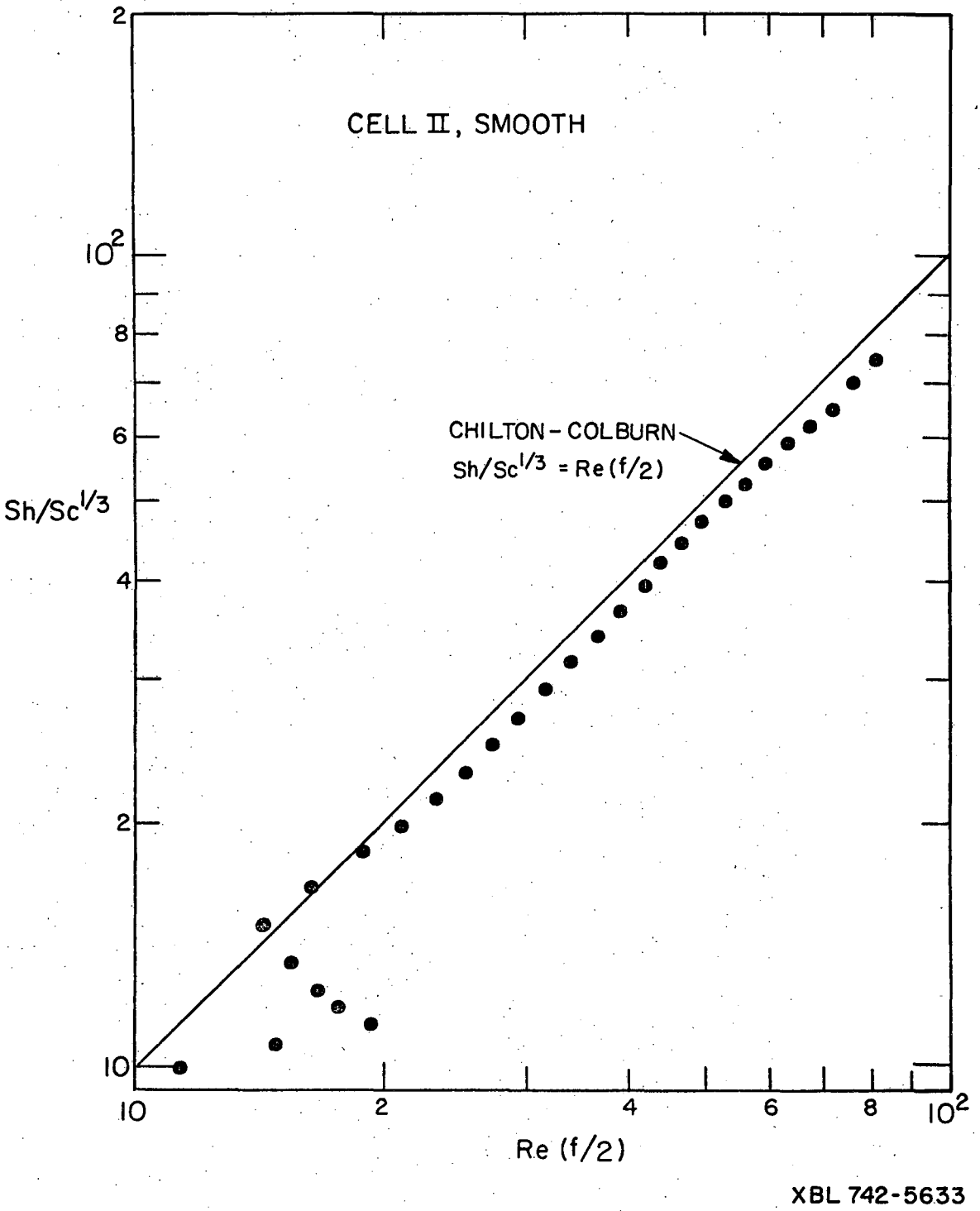

Fig. IV-15. Comparison of the mass transfer coefficients and friction factors experimentally determined using Cell II, smooth, with the correlation of Chilton and Colburn.[6] Sc = 3,100-3,500.

0 0 0 0 4 0 0 5 8 7 9

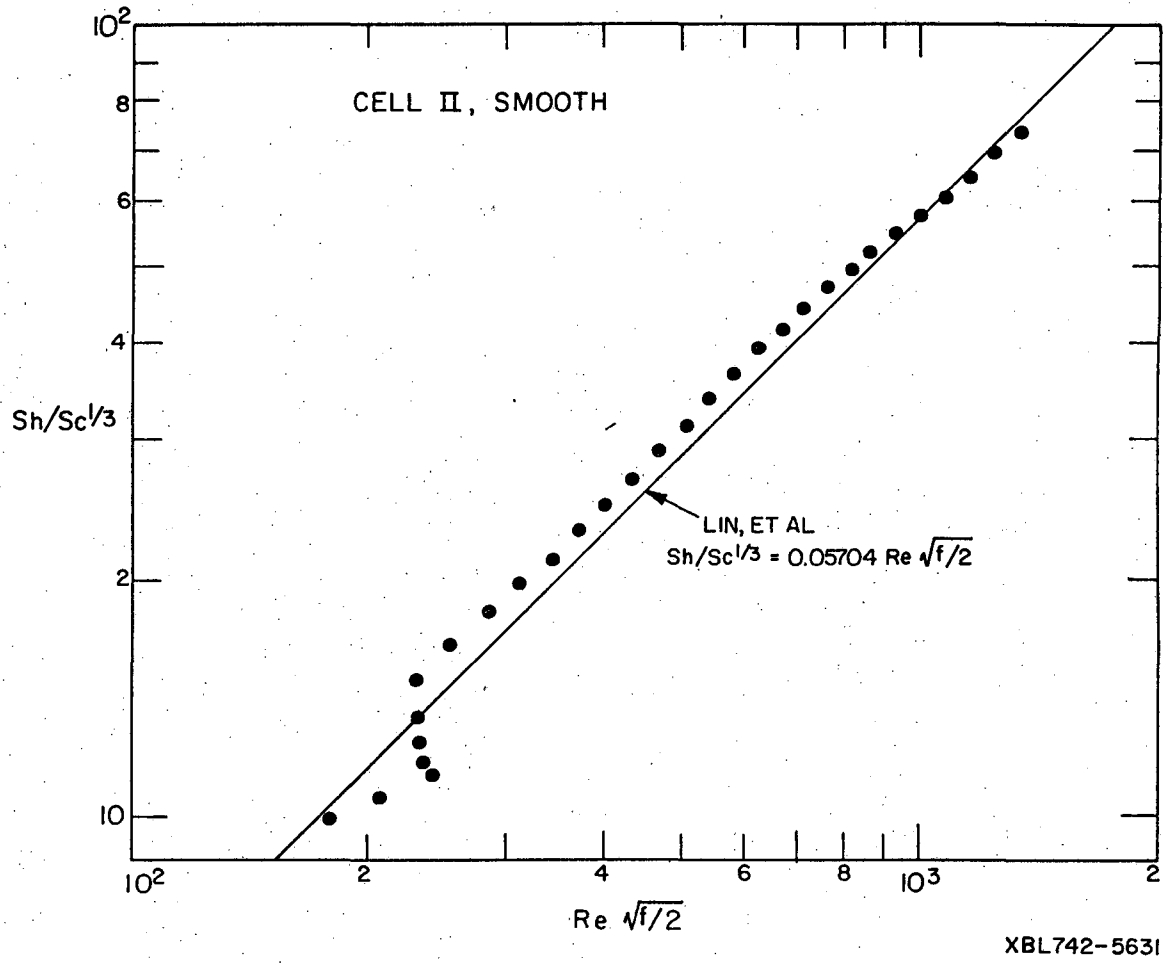

Fig. IV-16. Comparison of the mass transfer coefficients and Friction factors experimentally determined using Cell II, smooth, with the correlation of Lin et al.[29] Sc = 3,100-3,500.

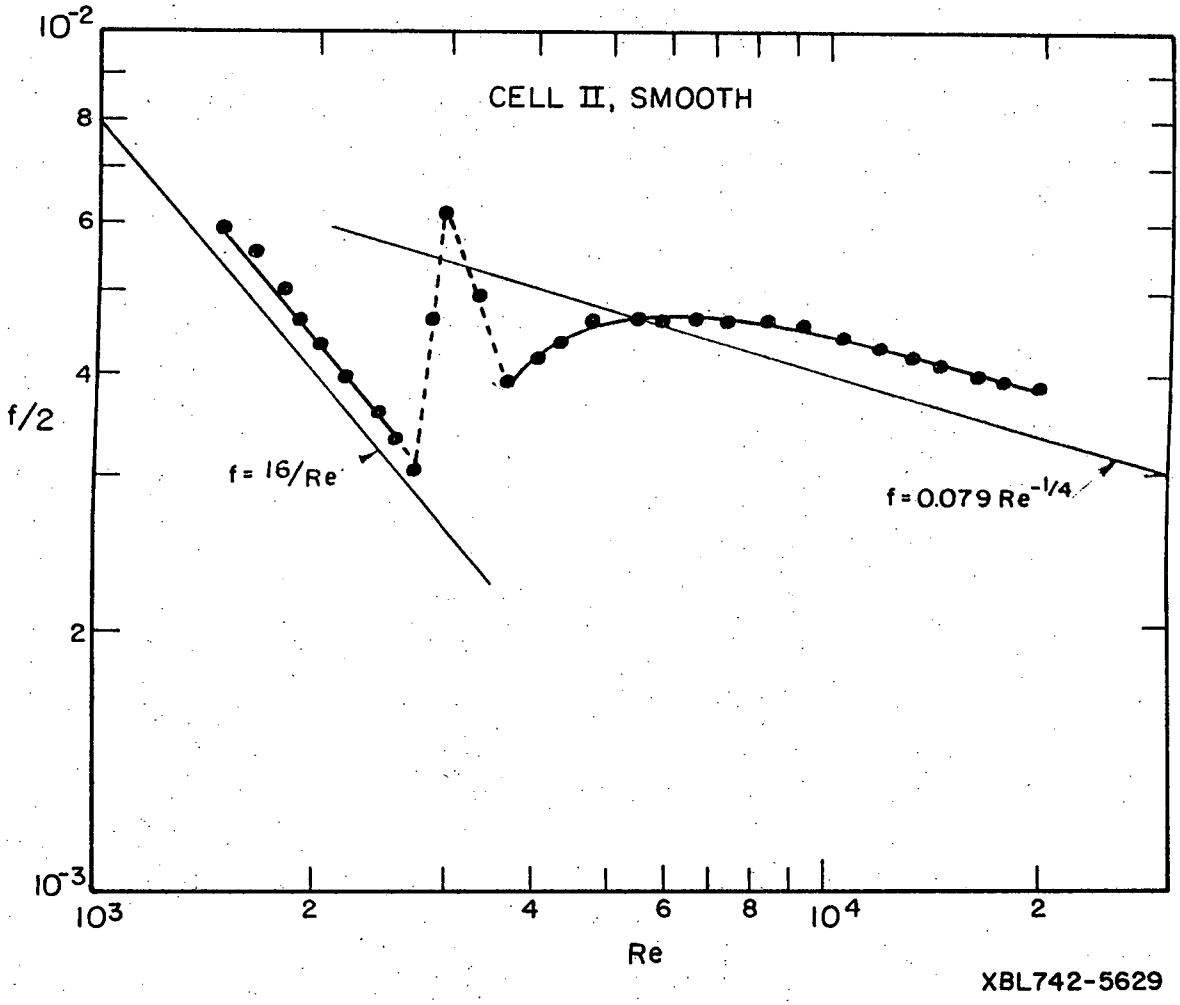

Fig. IV-17. Experimental friction factors for Cell II, smooth.

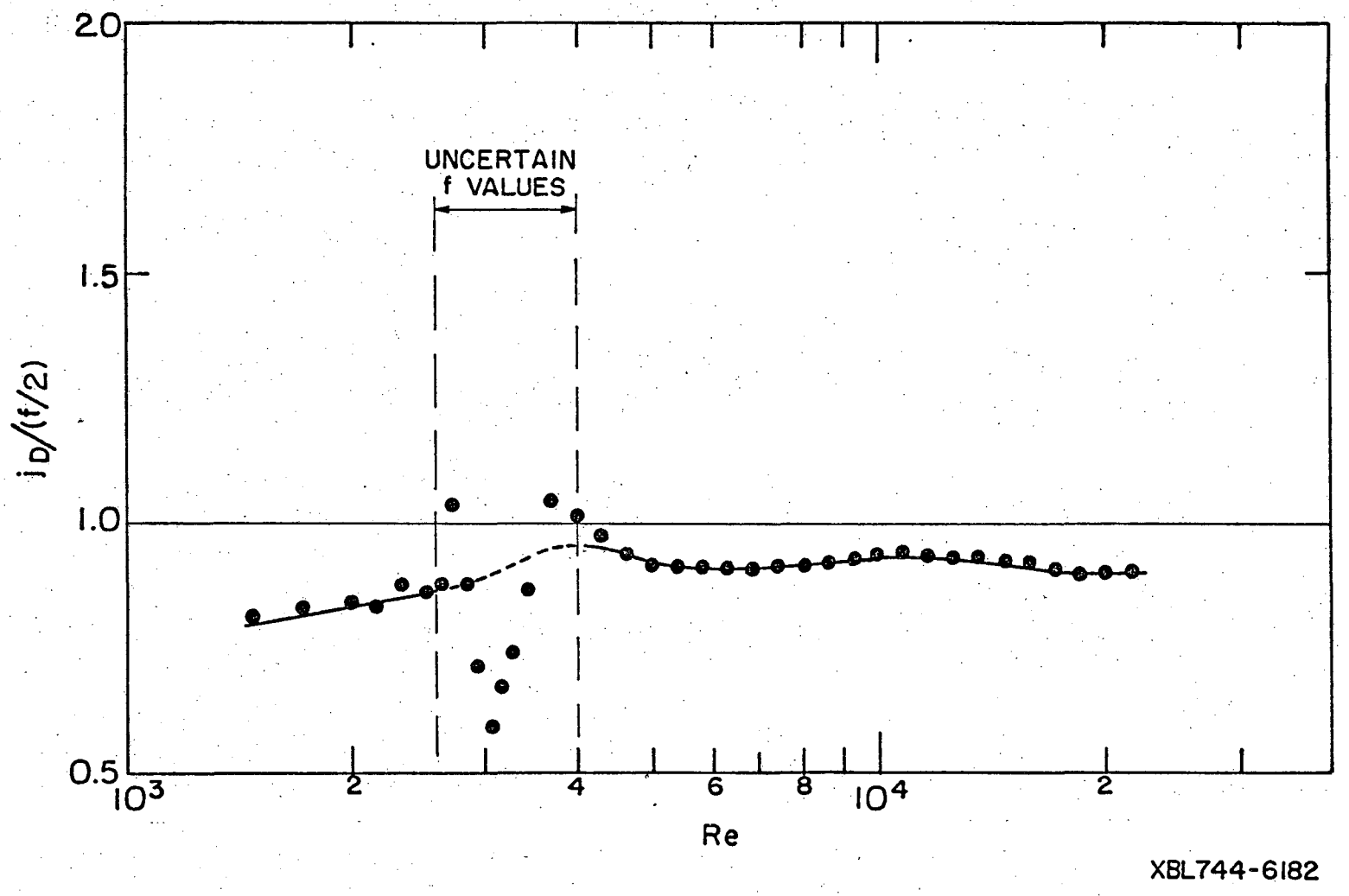

Fig. IV-18. Ratio of mass to momentum transfer coefficient expressed as $j_D/(f/2)$ for Cell II, smooth. Sc = 3,100-3,500.

0 0 0 0 4 0 5 8 8 0

V. PRESENTATION AND ANALYSIS OF THE RESULTS FOR ROUGH CELLS

A. Results for Cell I, Rough

As explained in the introduction, in practical applications the electrodes are seldom hydraulically smooth, and it was therefore of interest to study the effect that various types of roughness have on the mass transfer coefficient, the friction factor, and the ratio $j_D/(f/2)$.

The literature on the subject of roughness effects on mass transfer is practically non-existing. Levich[27] has reviewed this question at some length. Ross and Badhwar,[37a] and Dawson and Trass[8] have presented a more systematic approach to the determination of the effect that different degrees of roughness will have on the mass transfer coefficient.

One of the most difficult problems in dealing with the subject is the characterization of the roughness. The practice prevalent today in friction factor studies is the following: friction factors are determined at very high Reynolds numbers (Nikuradse's "Fully Rough Region") where the friction factor becomes independent of Re and depends solely on the value of the relative roughness. Then, by comparison with the f values obtained by Nikuradse using sand roughened pipes, an "equivalent sand roughness value" is assigned to the roughness in question. The argument for this procedure seems ponderous. In many cases the measured size of the roughness elements, even when sand grains are used, bears no relationship to the value obtained by the equivalent sand roughness determination. Also, the values of f obtained at intermediate Reynolds numbers may differ substantially for the same value of the equivalent sand roughness.

0 0 0 0 4 0 0 5 8 0 1

Even if this method of roughness characterization were effective for momentum transfer studies, there is no valid reason to expect that it would work equally well for the case of mass or heat transfer. Already for smooth surfaces the analogy between the three processes has been found to break down when the Schmidt (Prandtl) number is substantially different from 1. For rough surfaces the applicability of the turbulent eddy diffusivity has never been extensively examined. Kline et al.[23a] point out that the turbulence mechanism for flow adjacent to rough surfaces may be entirely different from that for flow along smooth walls. Townes et al.[51a] from measurements of the cross-correlation of the fluctuating components of velocity in sand-roughened pipes concluded that for fully developed turbulent flow the smooth pipe flow model is not valid.

An in-depth study for the characterization of the rough surfaces used in the present experiments was not possible within the scope of this work. The type of roughness and the method employed to obtain it, as well as the peak-to-peak and the arithmetic average values given by a stylus surface profilometer, are specified in Section III-E.

1. Effect of Channel Corners

Although the secondary currents formed at the corners of a rectangular channel will be affected by the degree and type of roughness of the wall, it is the non-uniformity of the roughness that will exert a decisive influence on the secondary currents.[15] Since the value of the roughness was uniform across the width of the channel (Section III-E), and since for the smooth channels it was found that at these very large aspect ratios the corner effect was not distinguishable, it was considered unnecessary to perform a whole set of experiments using different aspect ratios. Only

two aspect ratios, 1:20 and 1:30, were used with Cell I, rough.* The ranges of Reynolds numbers covered in this manner overlapped in the range $7{,}000 \leqslant Re \leqslant 10{,}000$. No effect of the aspect ratio was discernible.

2. Dependence of the Mass Transfer Coefficient on the Distance from the Mass Transfer Leading Edge

The individual section average mass transfer coefficients were assigned to specific x/D_h values assuming that the dependence on $x^{-1/3}$ that applies to mass transfer in smooth electrodes (Section IV-A-2) also applies to rough surfaces. To date, no studies have been conducted on the effect of wall roughness on the length of the mass transfer entrance length.

As explained in Chapter IV, the length of the electrode sections used in this study did not allow an exact determination of the value of the entrence length at high Reynolds number. However, qualitative conclusions can be drawn from the present experiments. The results are presented in Figs. V-1 to V-4. Comparing these curves with those for a smooth channel presented in Fig. IV-3 the following conclusions can be drawn: increasing the roughness of the mass transfer section leads to a departure from the laminar results at a lower Reynolds number, while at large values of Re the entrance length becomes shorter.

The first conclusion agrees with what would be expected from hydrodynamic considerations: the Reynolds number region of stability of

*This was done for convenience in the experimental procedure. The magnitude of the flow through the cell was determined by the opening of the cell valves relative to that of the bypass. When the cell flow was a very small fraction of the total flow it fluctuated and tended to drift to a different value. A larger aspect ratio (larger volumetric flow) alleviated this condition. Also, in this way it was avoided to use the magnetic flow meter in its lowest range, where its accuracy was lowest.

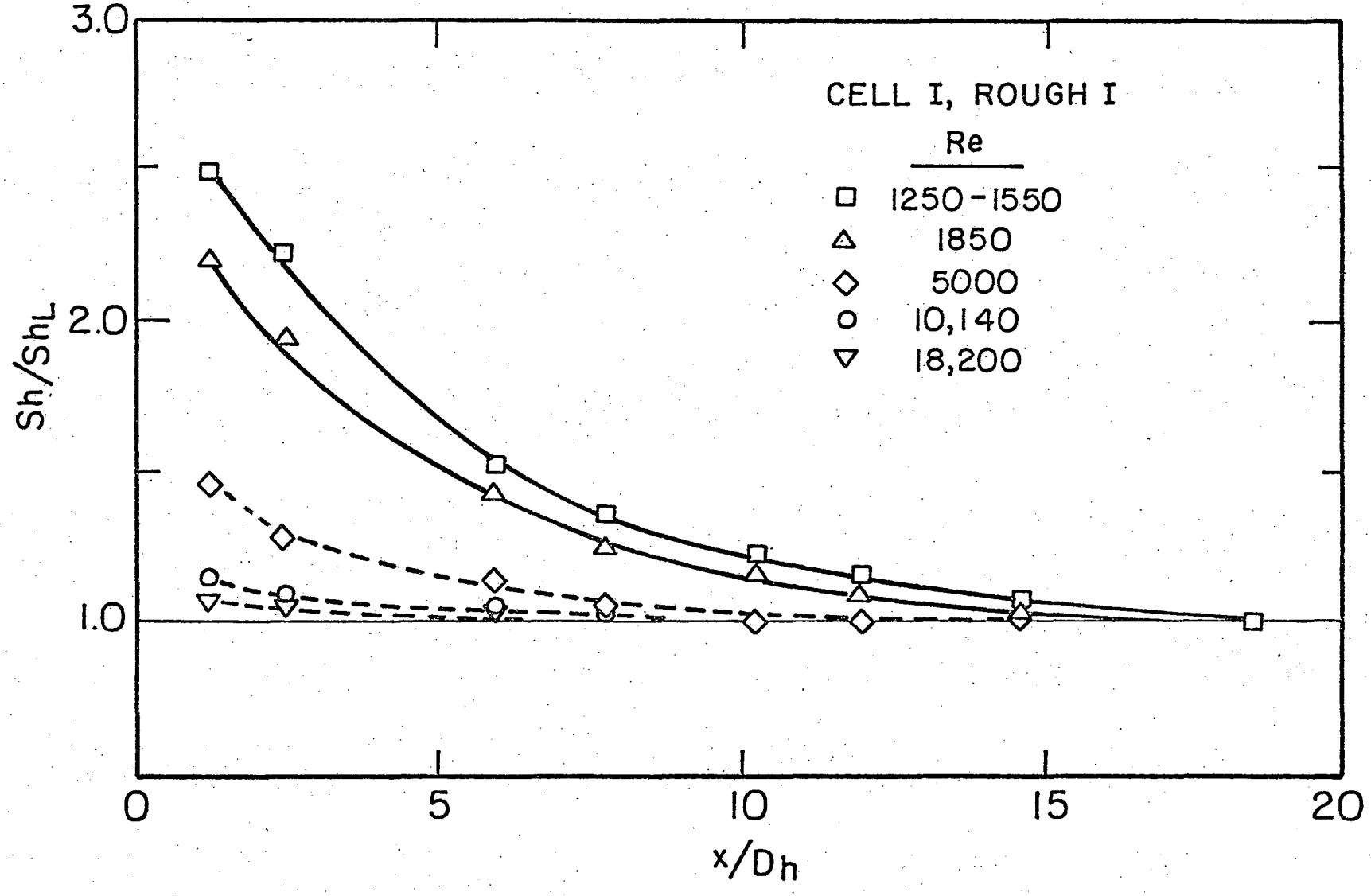

XBL744-6173

Fig. V-1. Dependence of the mass transfer coefficient on the distance from the mass transfer leading edge for Cell I, Rough I. Sh_L is the value calculated using the k value determined for electrode section IV when the four sections were polarized.

0 0 0 0 0 0 0 0 0 0 2

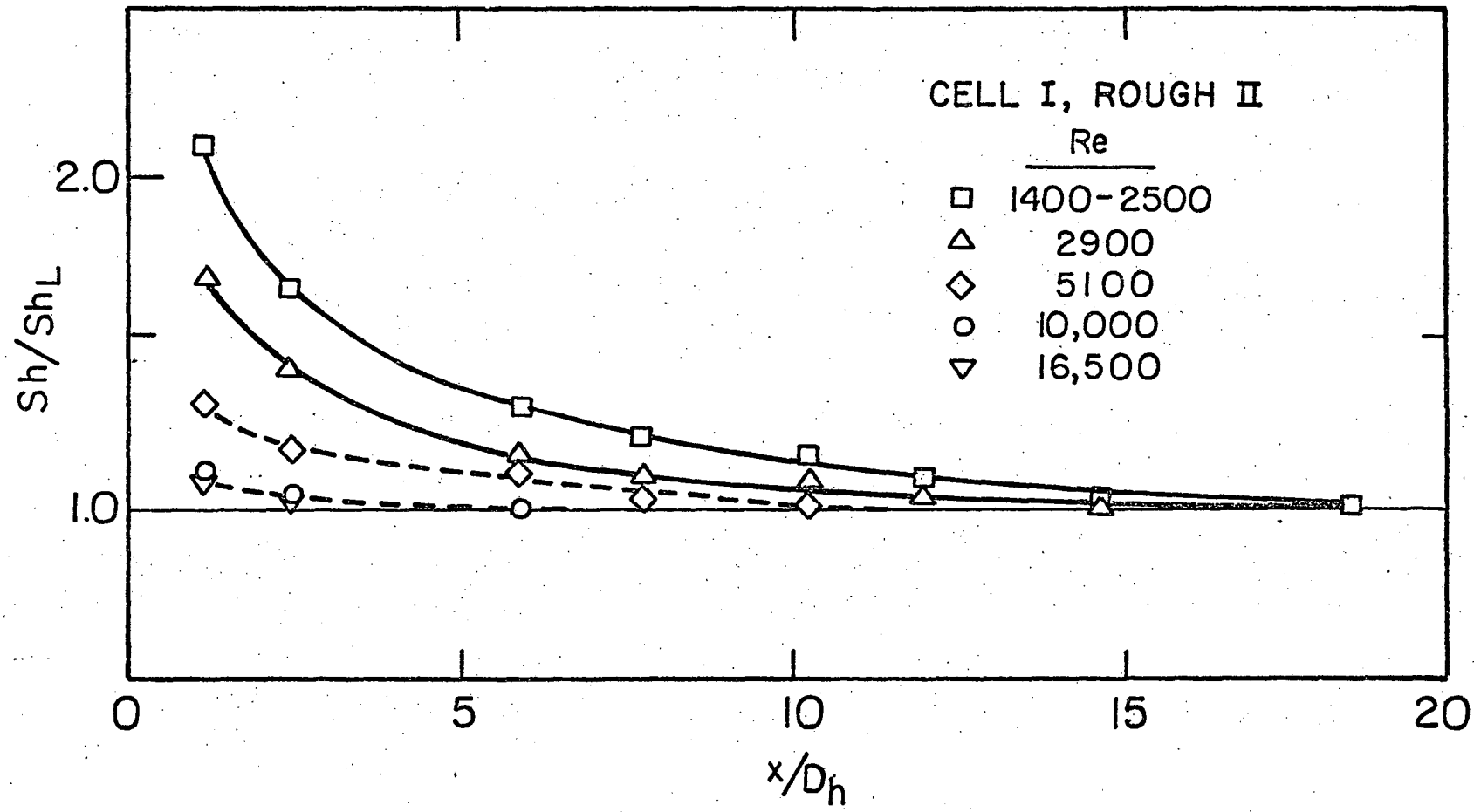

XBL 744-6172

Fig. V-2. Dependence of the mass transfer coefficient on the distance from the mass transfer leading edge for Cell I, Rough II. Sh_L is the value calculated using the k value determined for electrode section IV when the four sections were polarized.

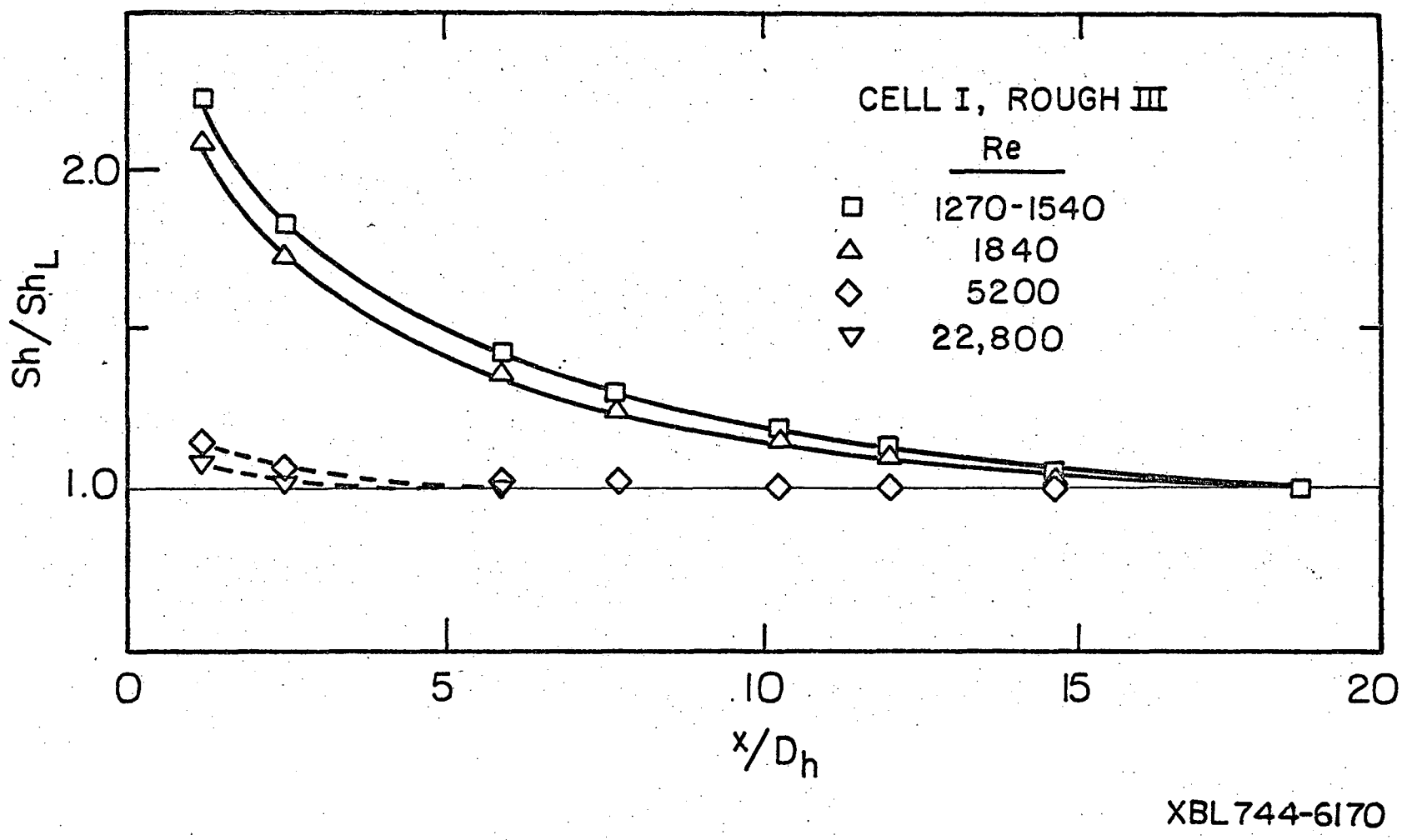

Fig. V-3. Dependence of the mass transfer coefficient of the distance from the mass transfer leading edge for Cell I, Rough III. Sh_L is the value calculated using the k value determined for electrode section IV when the four sections were polarized.

0 0 0 0 4 0 5 3 3

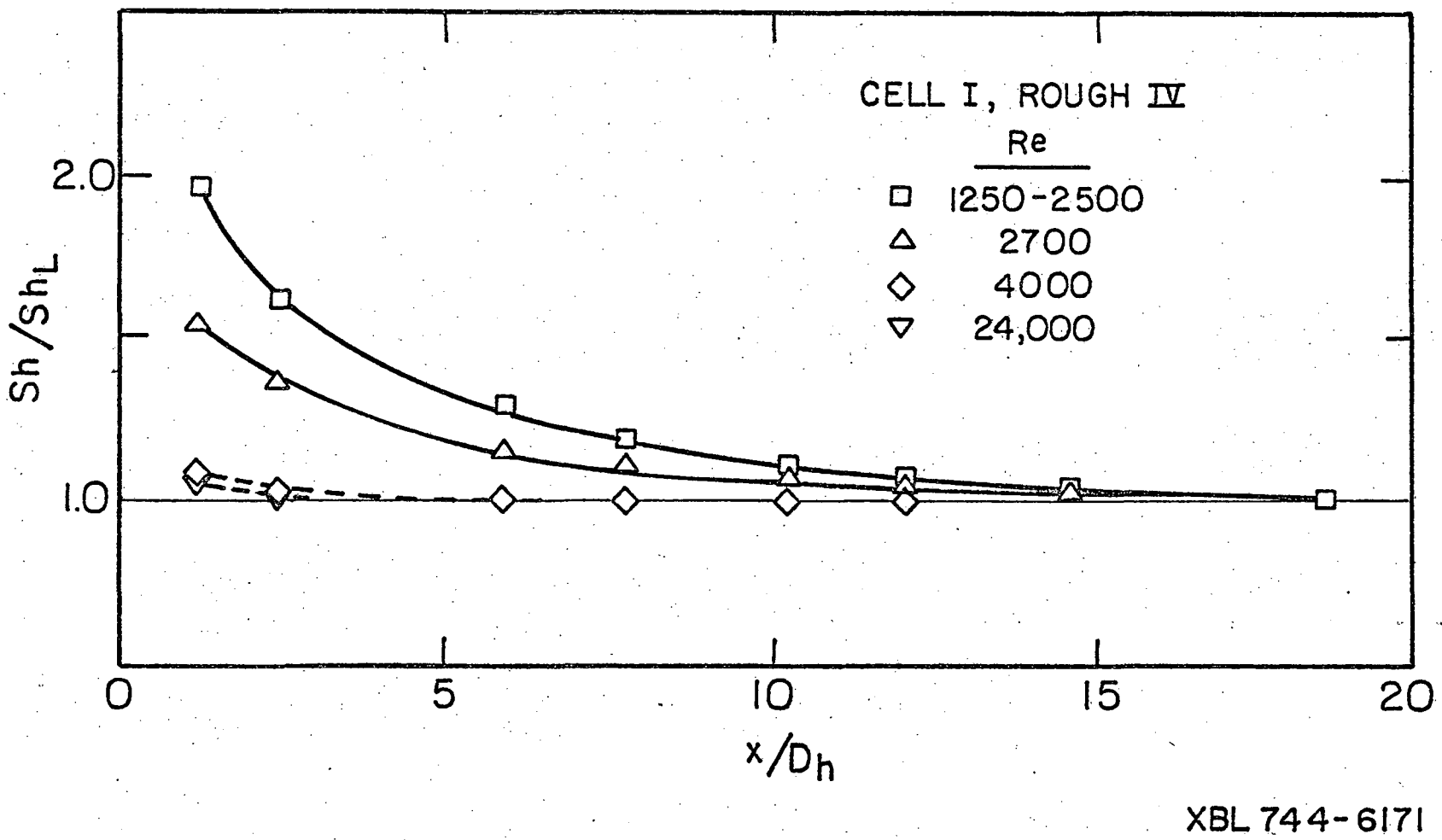

Fig. V-4. Dependence of the mass transfer coefficient on the distance from the mass transfer leading edge for Cell I, Rough IV. Sh_L is the value calculated using the k value determined for electrode section IV when the four sections were polarized.

0 0 0 0 4 0 0 5 8 0 4

a laminar flow decreases with turbulence induced by the roughness of the wall.

The second conclusion can also be substantiated by hydrodynamic considerations. In boundary layer flow the presence of "boundary layer trippers" leads to an early development of the fully developed boundary layer thickness. Similarly one will expect that disturbances present at the point where the mass transfer boundary layer begins will lead to its reaching the fully developed value faster, thereby shortening the entrance length.

3. Laminar Results

At low Reynolds numbers, as long as the flow remains laminar, the mechanism of mass transfer will not be affected by the roughness of the walls. Figures V-5a-d show the values of the local Sherwood number plotted against the dimensionless group $(ReScD_h/x)^{1/3}$. For each of the roughness values studied the departure of the data from the straight line with slope 1.2325 becomes evident at lower Reynolds numbers than for the smooth channel. The lowest value of Re at which departure from the Graetz-Levêque solution was observed is indicated in each case.

4. Turbulent Regime

For rough surfaces the need to determine the relationship between the mass transfer and the momentum transfer coefficient is even more evident than for smooth channels. As explained in the beginning of the present chapter, the literature on the subject is very scant. No claim of generality is intended for the present results. As explained above, the transport process depends on type and degree of roughness, and there is no reliable method available to specify it. The rationale for including

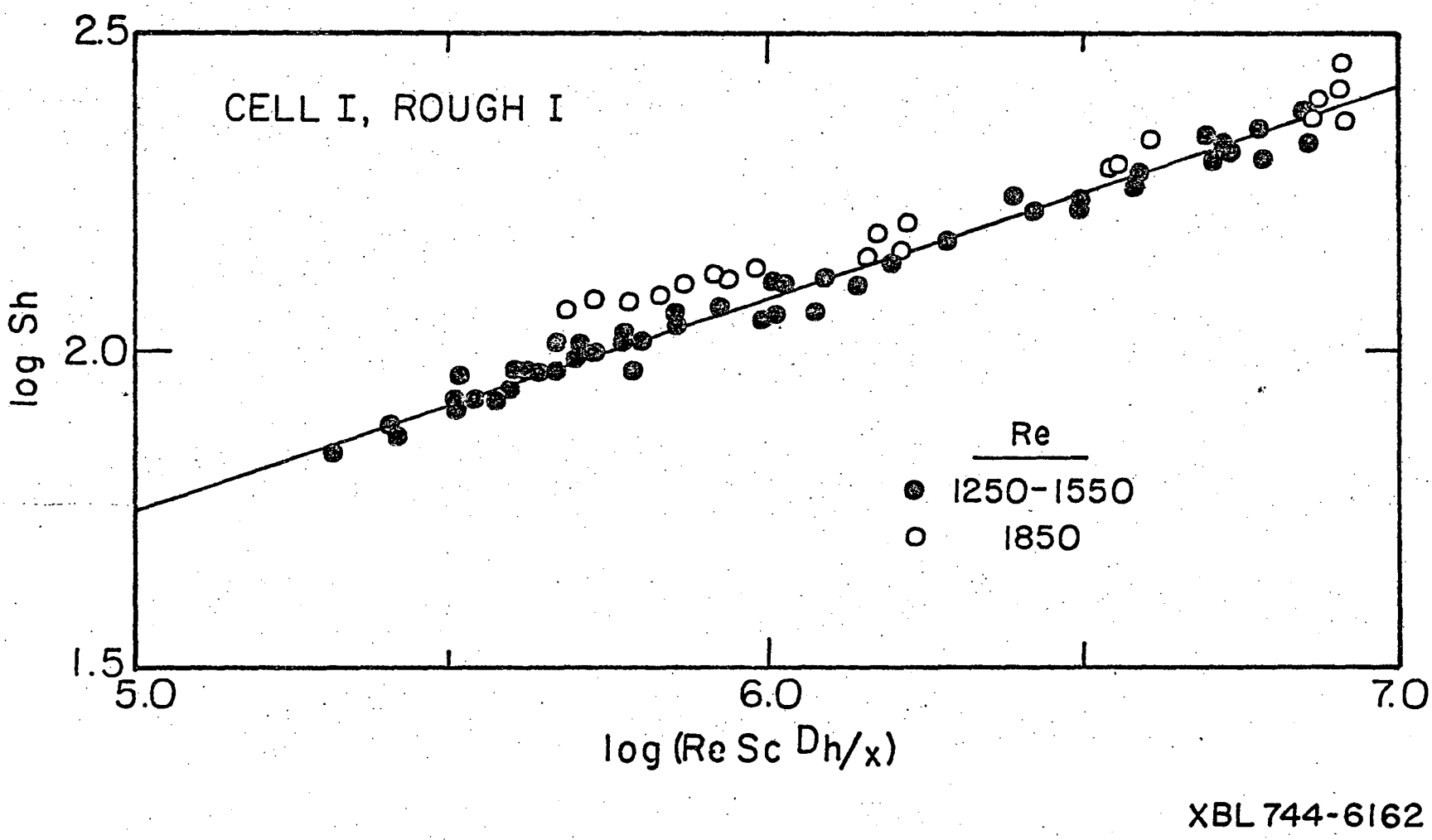

XBL 744-6162

Fig. V-5a. Cell I, Rough I. Comparison of experimental local Sherwood Number with the extension to the Graetz-Levêque solution given in Reference 31. Sc = 3,000.

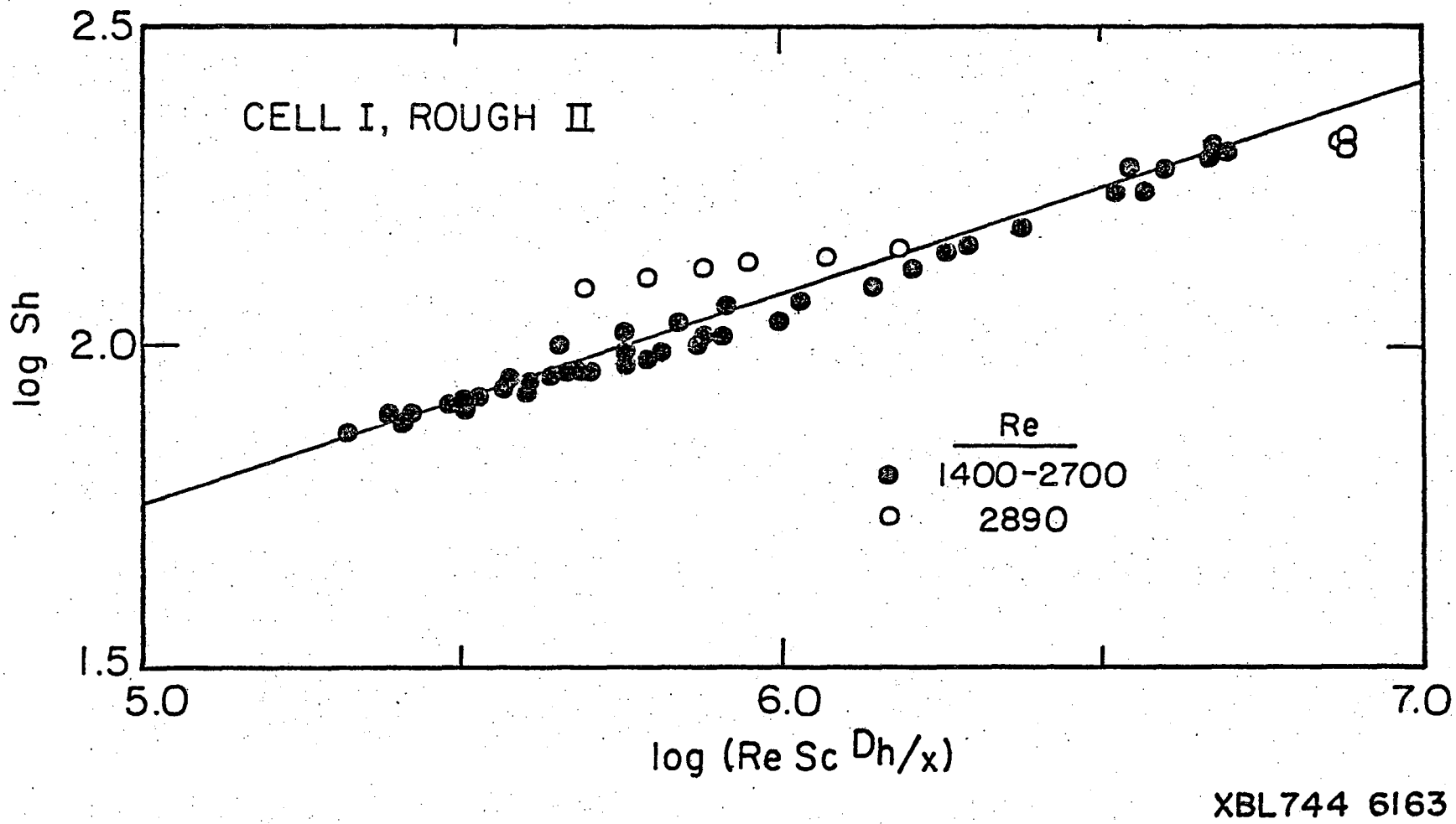

Fig. V-5b. Cell I, Rough II. Comparison of experimental local Sherwood Number with the extension to the Graetz-Levêque solution given in Reference 31. Sc = 3,100.

XBL 744-6163

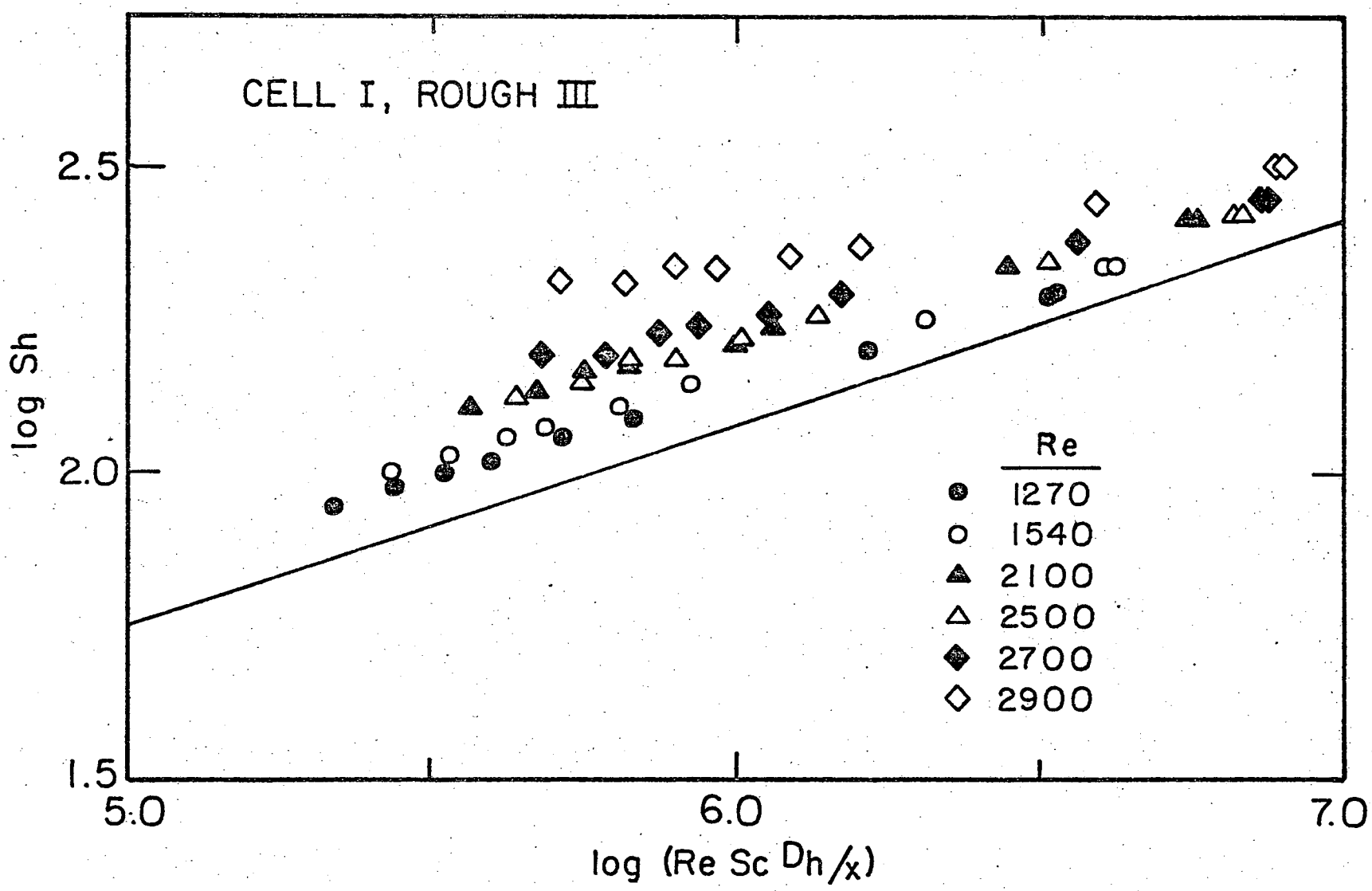

XBL 744-6164

Fig. V-5c. Cell I, Rough III. Comparison of experimental local Sherwood Number with the extension to the Graetz-Levêque solution given in Reference 31. Sc = 3,200.

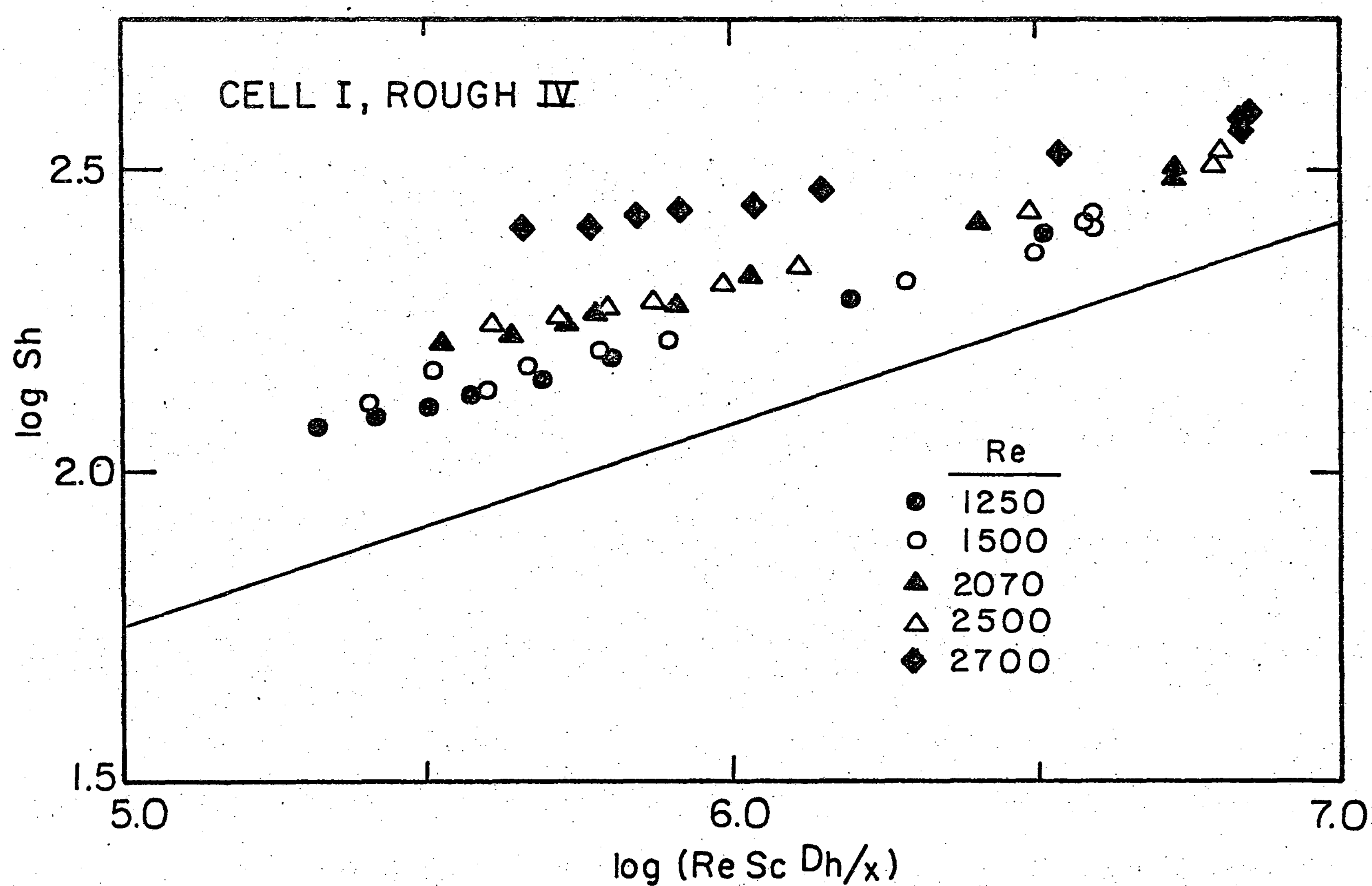

XBL744 6165

Fig. V-5d. Cell I, Rough IV. Comparison of experimental local Sherwood number with the extension to the Graetz-Levêque solution given in Reference 31. Sc = 3,050.

0 0 0 0 4 0 0 5 8 8 6

rough surfaces in the present study is the almost absolute lack of information on the subject.

The results for $2,700 \leqslant Re \leqslant 22,000$ are plotted in Fig. V-6 in the form of the Colburn coefficient j_D vs Re for the four roughnesses employed.

In each case, two regions are distinguishable: a transition regime followed by a fully turbulent region. The transition region, characterized by a more or less sharp increase in the value of j_D with Re varies in width depending on the roughness. For roughness I and III (the two sand-blasted surfaces) the transition region occupies the Reynolds number region $2,700 \leqslant Re \leqslant 5,400$, roughly the same interval occupied by the transition region for the smooth channel. Roughness II presents a slightly shorter transition region $2,700 \leqslant Re \leqslant 4,700$, while roughness IV presents an even shorter one, $2,500 \leqslant Re \leqslant 3,400$, that begins at a smaller Reynolds number.

In the turbulent regime the value of j_D decreases with increasing Reynolds number. In the case of Roughness III and IV, this decrease is sharper than for smaller values of the roughness.

Using the friction factor values determined for the same experimental channel (see below), the group $Sh/Sc^{1/3}$ is plotted against the abscissa Re f and $Re\sqrt{f}$ in Figs. V-7 and V-8, respectively.

5. Friction Factors

The friction factors calculated for the entire Reynolds number range are presented in Fig. V-9 in the form f vs Re.

At low Reynolds number (in the laminar regine) the value of the friction factor for the two smaller roughnesses coincides with that for

0 0 0 0 4 0 0 5 8 7

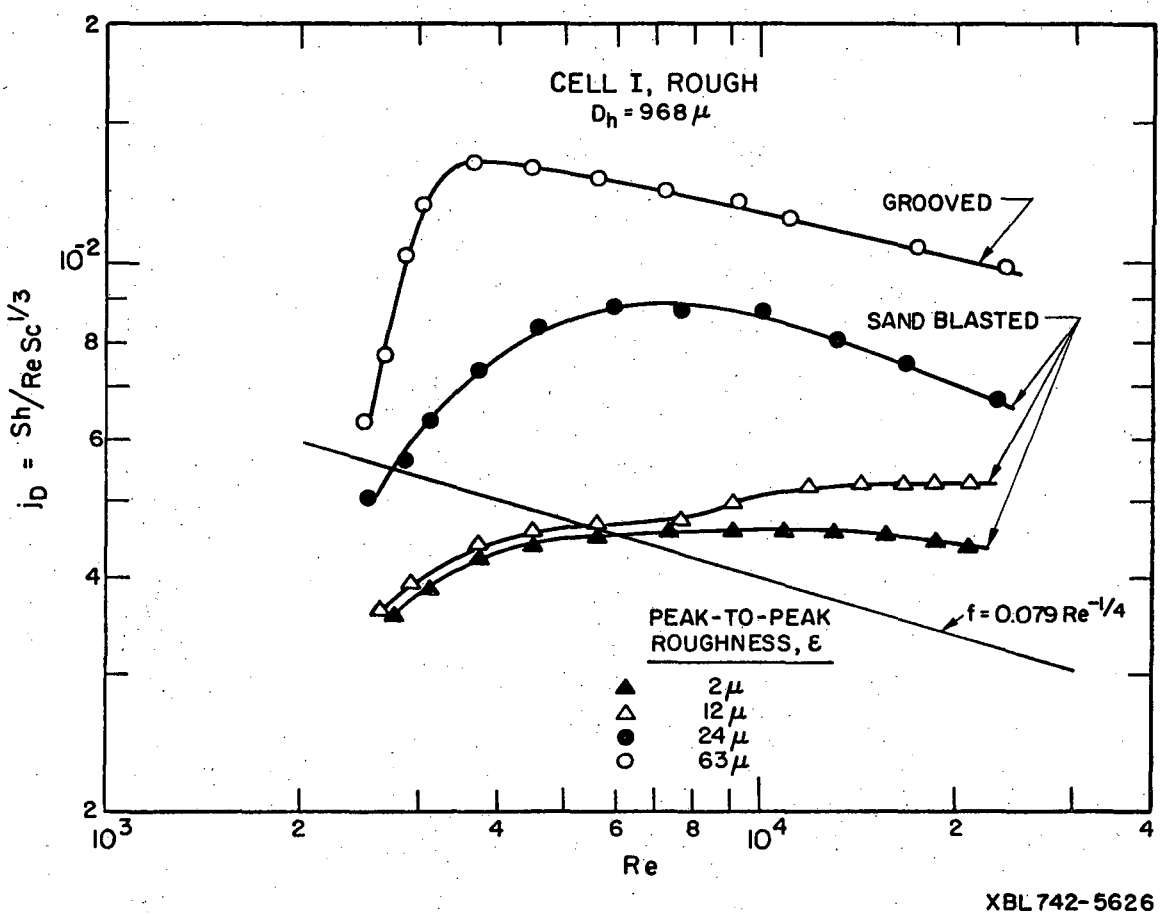

Fig. 6. j_D factor for Cell I, Rough. Sc = 3,000-3,500.

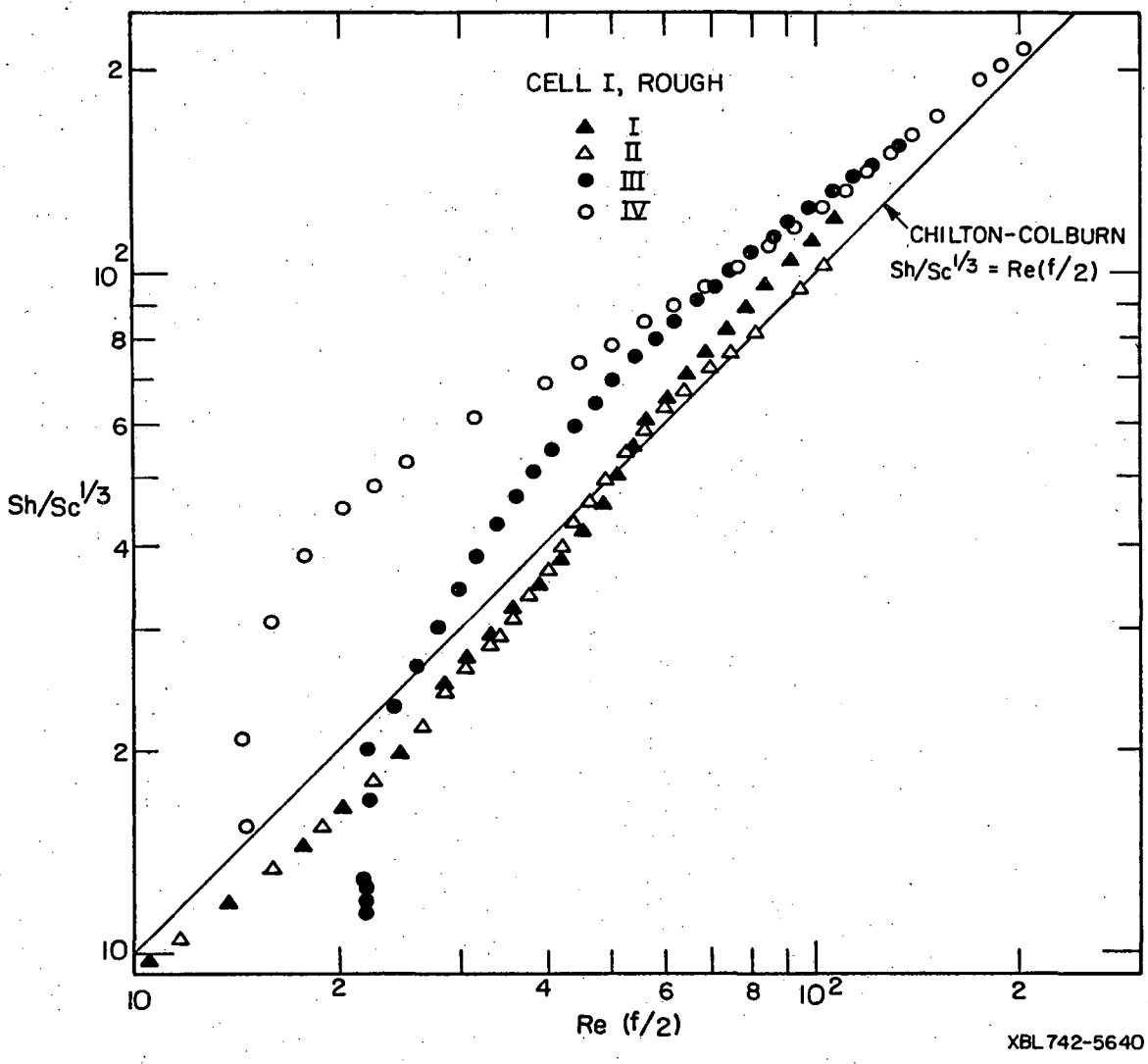

Fig. V-7. Comparison of the mass transfer coefficient and friction factors experimentally determined using Cell I, Rough, with the correlation of Chilton-Colburn.[6] Sc = 3,000-3,500.

0 0 0 0 4 0 0 5 8 6 8

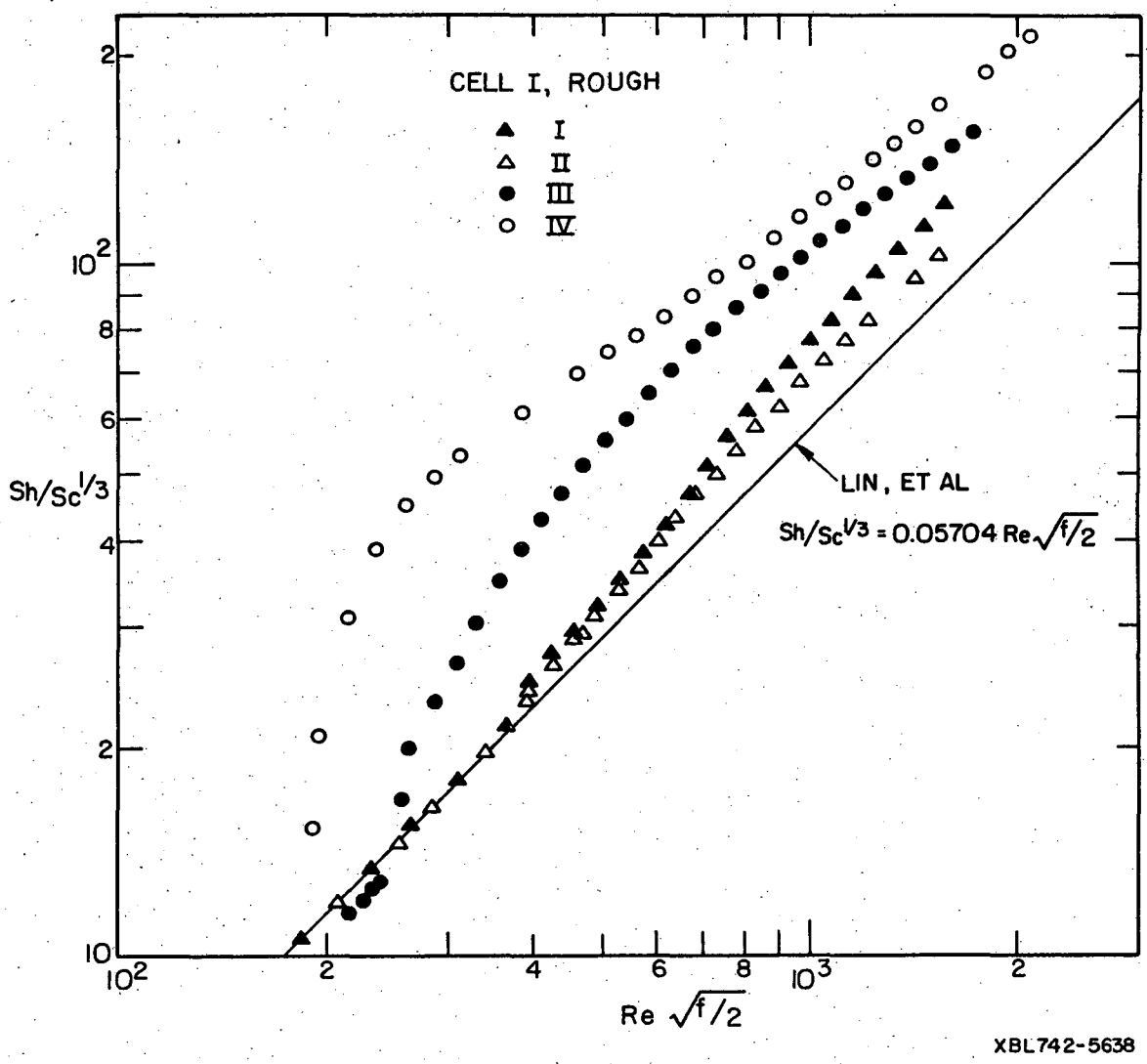

Fig. V-8. Comparison of the mass transfer coefficient and friction factors experimentally determined using Cell I, Rough, with the correlation of Lin et al.[29] Sc = 3,000-3,500.

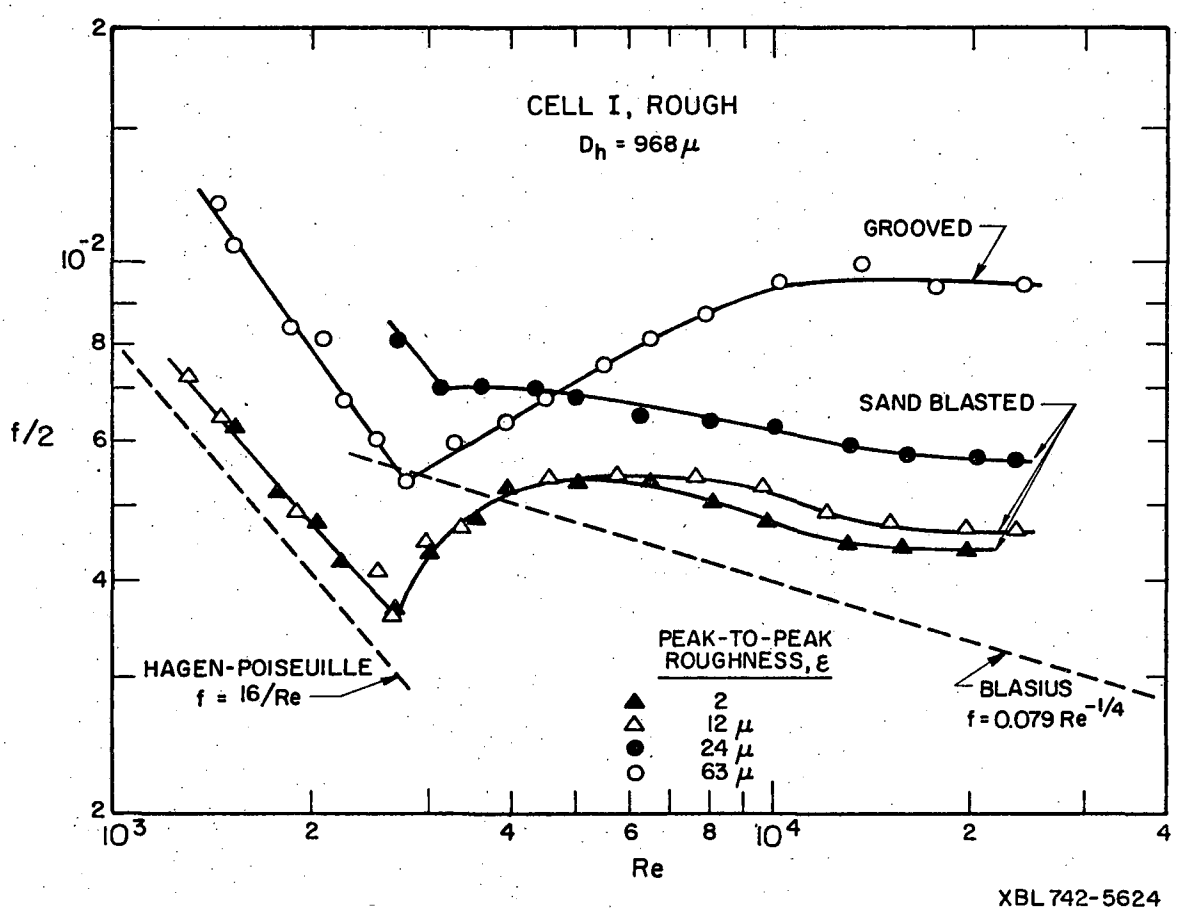

Fig. V-9. Experimental friction factors for Cell I, rough.

0 0 0 0 4 0 0 5 8 9

the smooth channel. For the channel roughness III and IV the friction factor also follows a fairly linear dependence on the Reynolds number, but the value of the slope is greater than -1, and the value of the coefficient is much larger than for the smooth channel (extrapolation of the results gives the equations $f = 23/Re$ and $f = 25/Re$ for roughness III and IV, respectively).

For the case of the grooved surface it is possible to calculate in a fairly accurate manner the increased surface of the channel walls and hence to correct the value of the true drag force on the walls. Recall that the friction factor f is defined[2] by

$$F_k = AKf$$

where F_k is the force exerted by the fluid on the surface of the duct by virtue of its movement, A is the wetted surface, and K a characteristic kinetic energy per unit volume. For flow without changes in potential energy through a channel with rectangular cross section w g, the friction factor is given by

$$f = \frac{\Delta P(w\ g)}{(1/2\rho v^2)\ A_{\text{wetted surface}}}$$

From the measured value of the grooves, the increase in wetted area is approximately 13.7%. This correction would bring the value of the friction factor for Rough Surface IV closer to the values of f for the smooth walled channel, but there still would exist a disagreement. One explanation for this discrepancy is the fact that the value corrected for the increased surface still fails to include the form drag caused by the shape of the grooves.

The transition regime for Roughness I and II extends through the same Reynolds number range as for the smooth channel, $2{,}400 \leqslant Re \leqslant 5{,}000$. As a matter of fact, the values of f for the smooth channel and Rough I and II are substantially indistinguishable in this range.

For Roughness IV the transition regime extends through a wider Reynolds number range, $2{,}400 \leqslant Re \leqslant 10{,}000$, before f becomes independent of the Reynolds number.

6. $j_D/(f/2)$ Ratio

Whether or not rough electrodes are adventageous for use in technology depends on the specific application contemplated. In general, however, the ratio $j_D/(f/2)$ is important, along with j_D, in considering the relative merit of mass transfer surfaces, this ratio being related to the mass transfer obtainable per unit of pumping power. Even though the Chilton-Colburn correlation ($j_D = f/2$) applies only at Reynolds numbers in the fully turbulent regime, and for the case of rough surfaces the friction factor includes the form drag, a departure from the value of 1 for this ratio can be used as an index of the effectiveness of a giving roughness in increasing the transfer coefficient.

Figure V-10 presents the values of $j_D/(f/2)$ vs Re. From this figure it is seen that for electrodes with a small roughness value this ratio becomes larger than 1 only for $Re > 10^4$. On the other hand, for a large roughness value the ratio reaches a maximum (greater than 1) in the transition region, and then quickly drops towards a value of 1. Limitations in the experimental system did not allow operation at higher Re to ascertain if asymptotic behavior is reached for this ratio. Similar results have been reported by Dipprey[10] for the ratio $j_H/(f/2)$. His

0 0 0 0 4 0 0 5 8 2 0

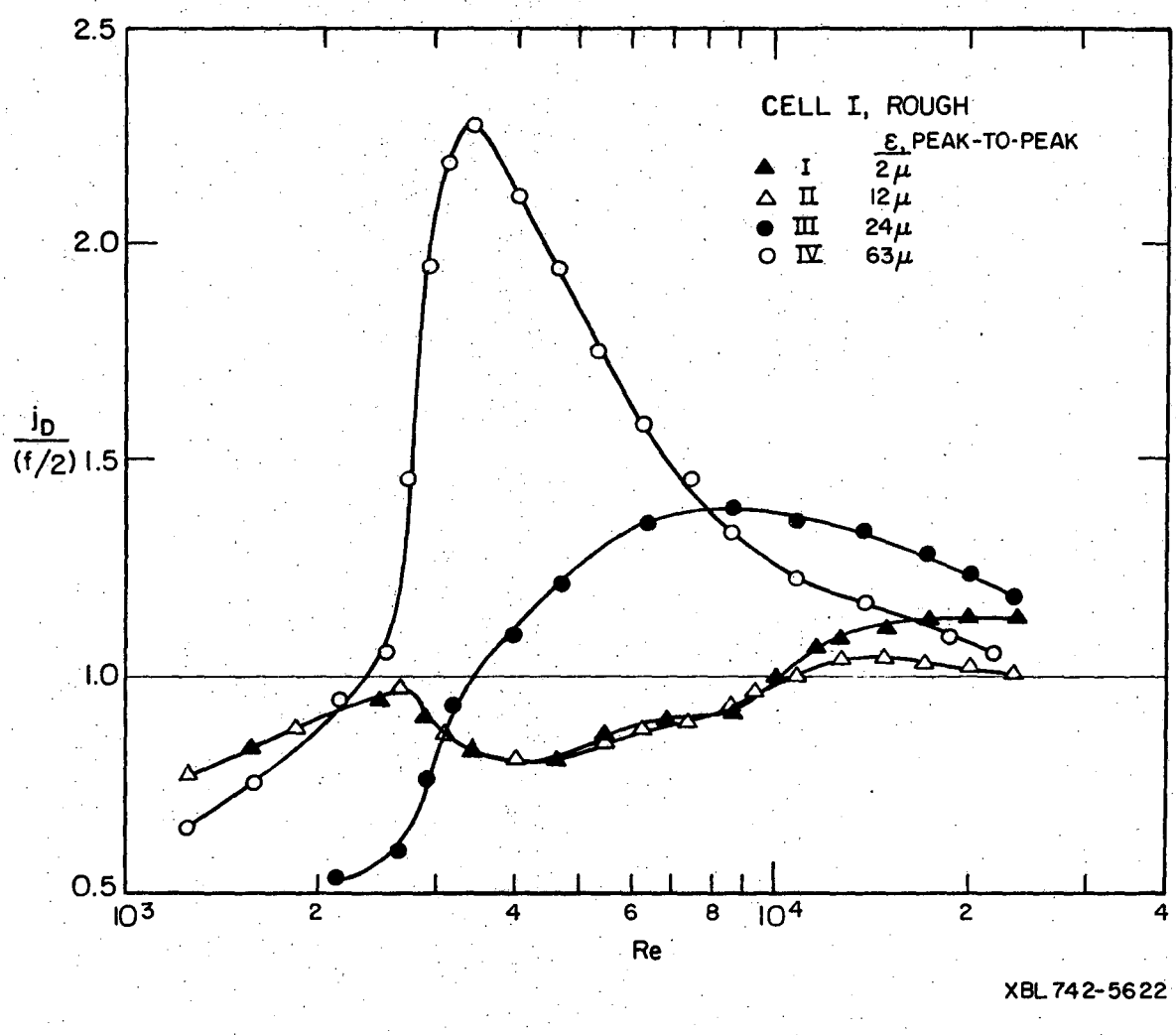

Fig. V-10. Ratio of mass to momentum transfer coefficient expressed as $j_D/(f/2)$ for Cell I, rough. Sc = 3,000-3,500.

experiments were conducted at higher Reynolds numbers ($14{,}000 \leq Re \leq 120{,}000$) and $1.20 \leq Pr \leq 5.94$. At the high values of Pr he found that the ratio $j_H/(f/2)$ reached a maximum at intermediate values of the Reynolds number, the position of this maximum depending on the value of the roughness. For the largest roughness that he employed ($\varepsilon/D = 0.048$) the maximum apparently fell below the lowest Reynolds number at which he operated.

B. Presentation of Results for Cell II, Rough

Figures V-11 to V-20 present the results for Cell II, rough, in the same order as used for the presentation of the results for Cell I, rough, in Section A above.

The remarks to the results for Cell I, rough, apply in general to the results for Cell II, rough. However, it must be kept in mind that the ratio ε/D_h for each of the roughness values employed was different for Cell I and Cell II.

In the Reynolds number range $2{,}500 \leq Re \leq 4{,}000$ (see Fig. V-19), the value of the friction factor present the same problem indicated for Cell II, smooth (refer to Section IV-B). Again, the mass transfer coefficient, measured on the opposite wall, did not show unusual behavior (Fig. V-16).

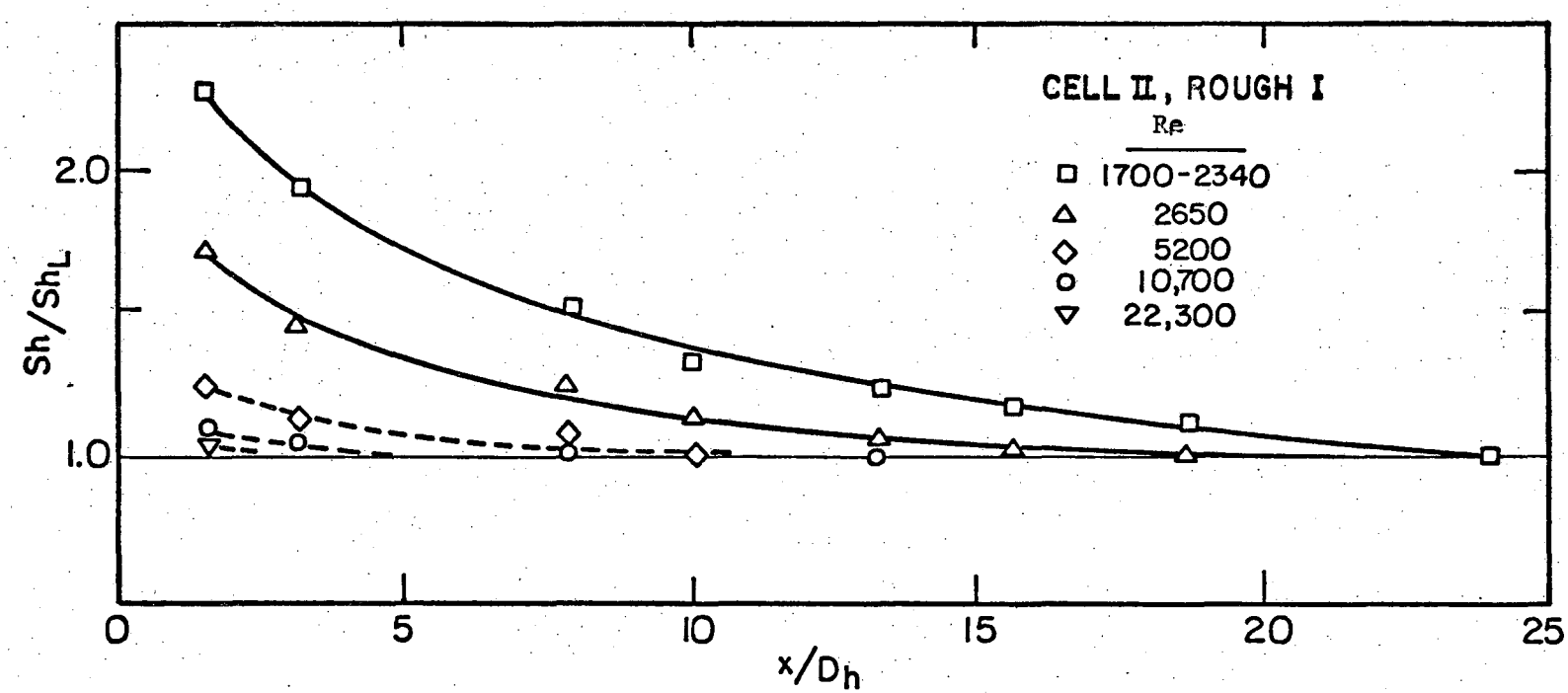

Fig. V-11. Dependence of the mass transfer coefficient on the distance from the mass transfer leading edge for Cell II, Rough I. Sh_L is the value calculated using the k value determined for electrode section IV when the four electrode sections were polarized.

0 0 0 0 4 0 5 8 1

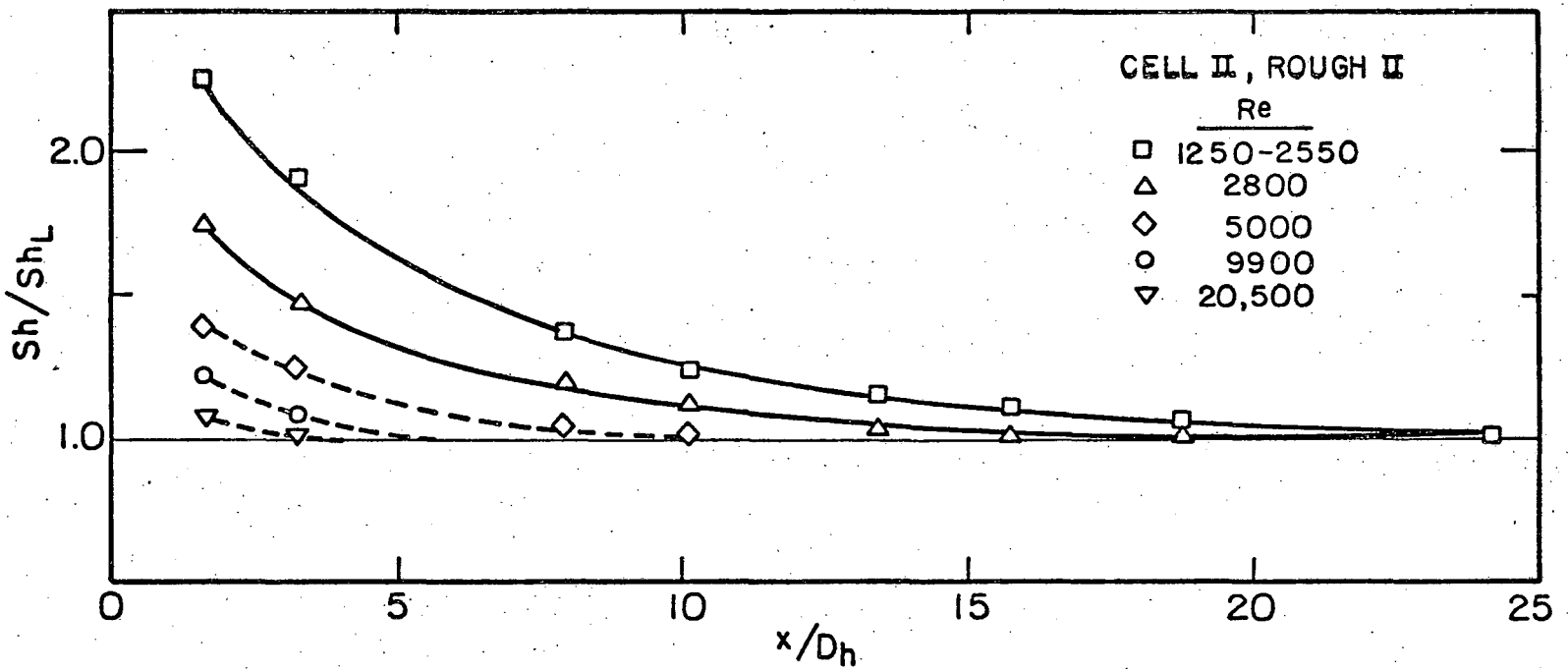

XBL744-6179

Fig. V-12. Dependence of the mass transfer coefficient on the distance from the mass transfer leading edge for Cell II, Rough II. Sh_L is the value calculated using the k value determined for electrode section IV when the four electrode sections were polarized.

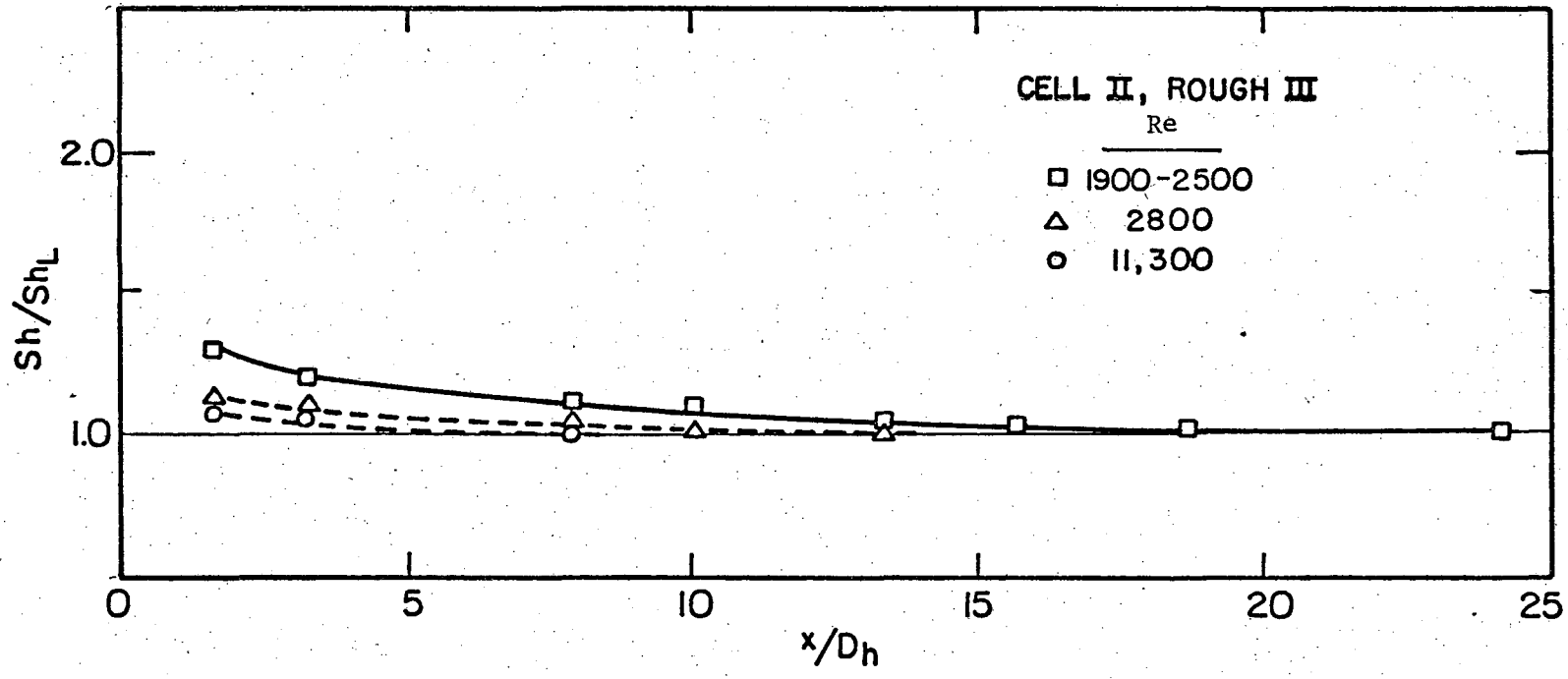

Fig. V-13. Dependence of the mass transfer coefficient on the distance from the mass transfer leading edge for Cell II, Rough III. Sh_L is the value calculated using the k value determined for electrode section IV when the four electrode sections were polarized.

0 0 0 0 5 8 1 2

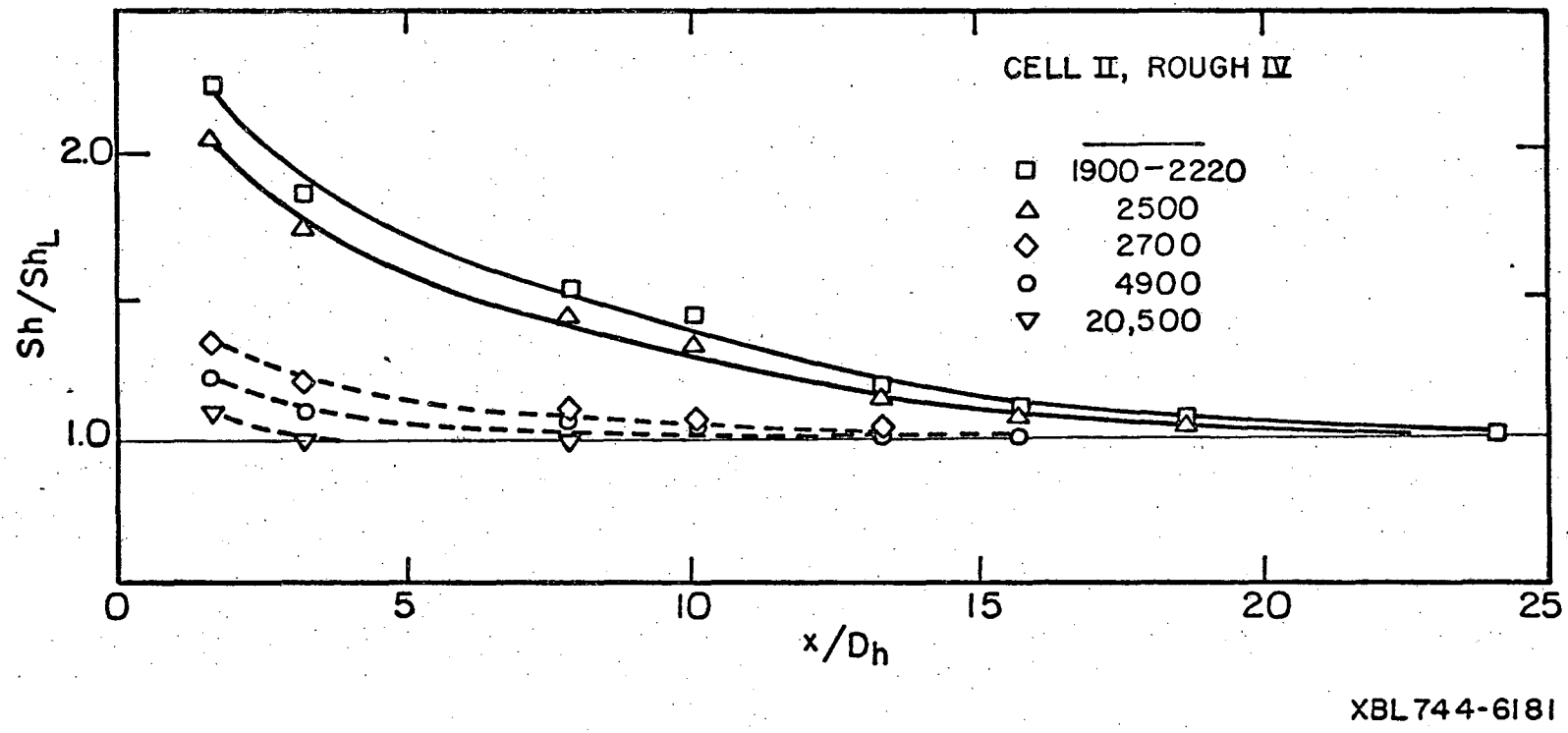

Fig. V-14. Dependence of the mass transfer coefficient on the distance from the mass transfer leading edge for Cell II, Rough IV. Sh_L is the value calculated using the k value determined for electrode section IV when the four electrode sections were polarized.

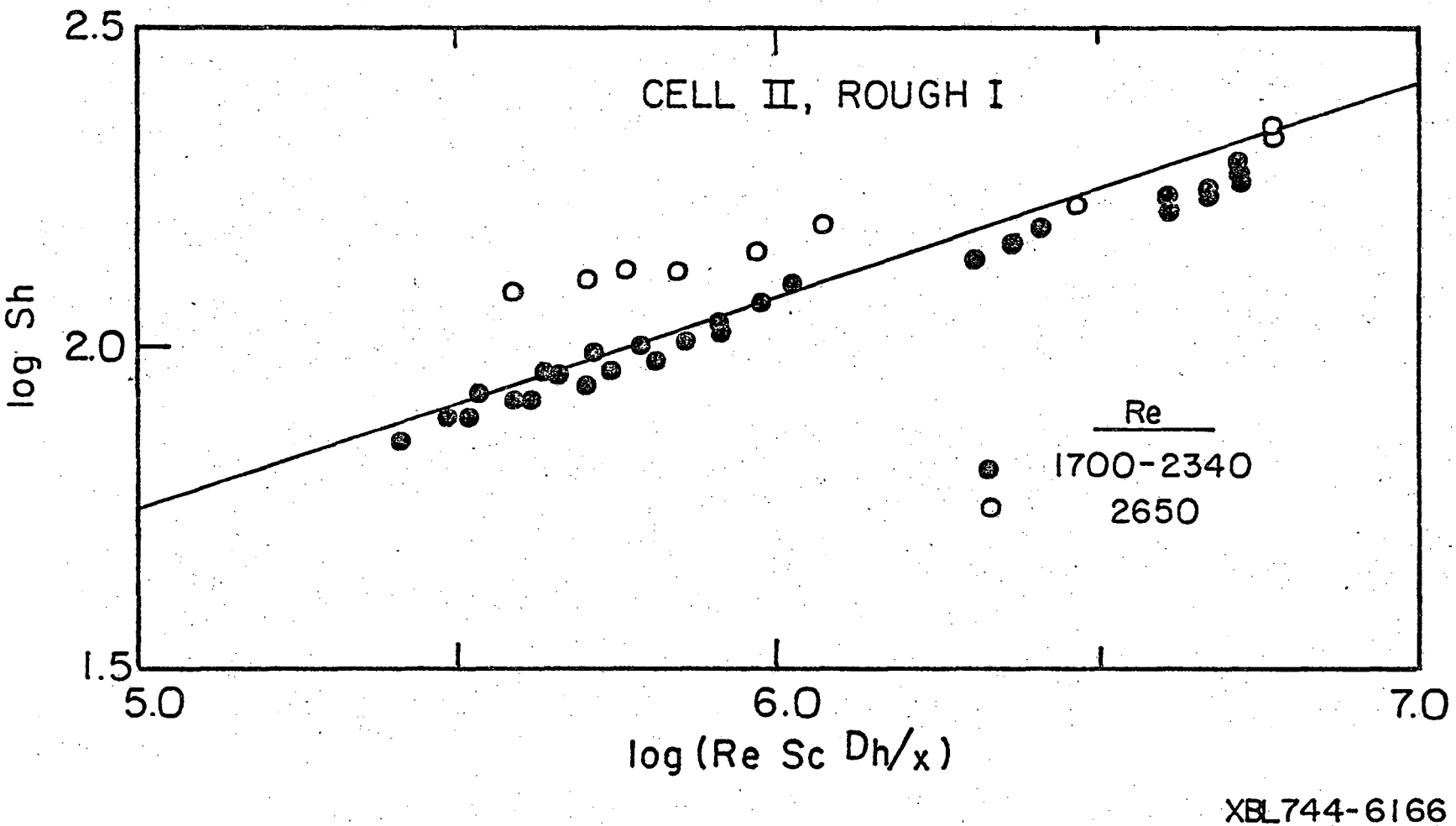

Fig. V-15a. Cell II, Rough I. Comparison of experimental local Sherwood Number with the extension to the Graetz-Levêque solution given in Reference 31. Sc = 3,500.

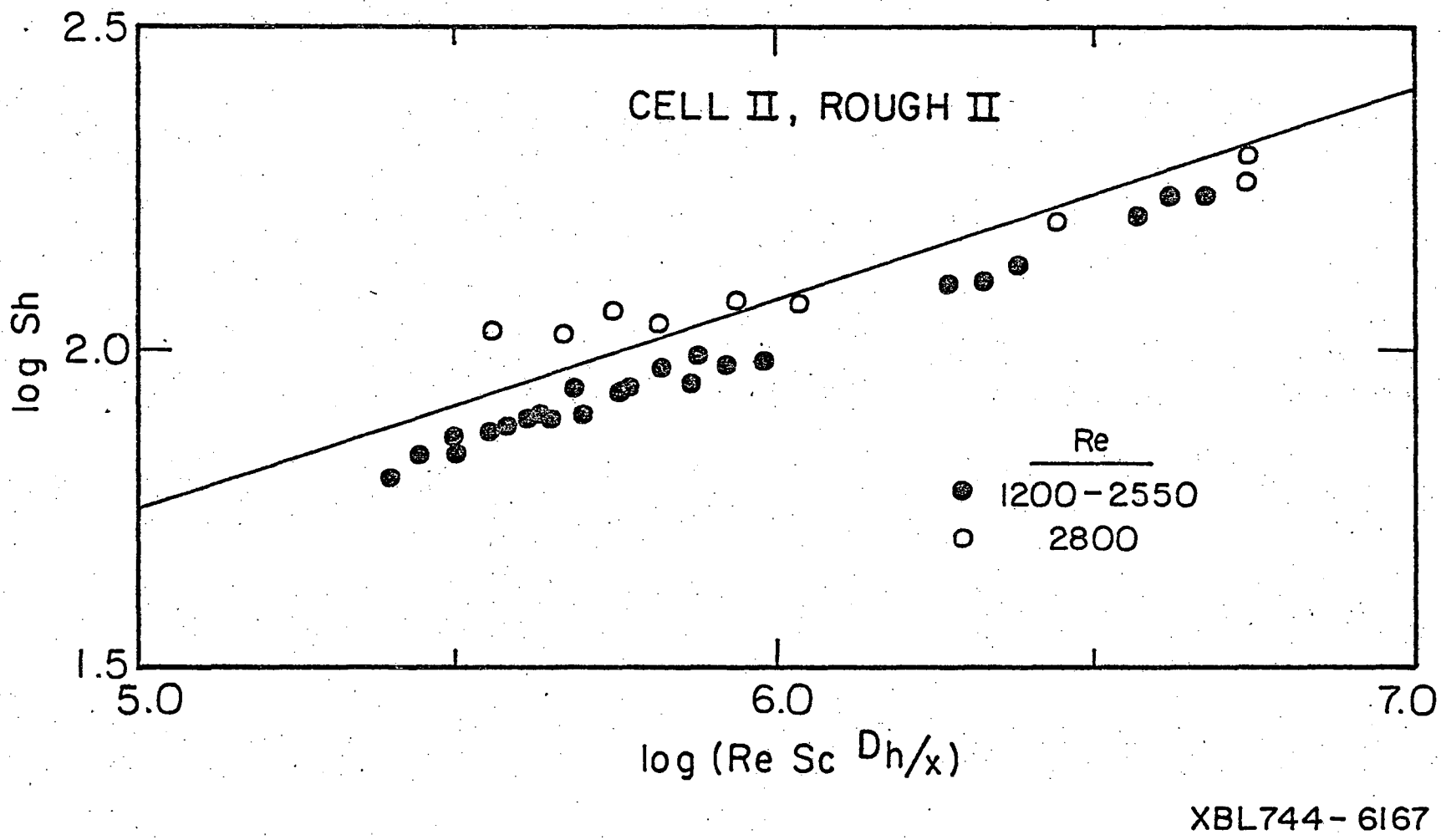

Fig. V-15b. Cell II, Rough II. Comparison of experimental local Sherwood Number with the extension to the Graetz-Levêque solution given in Reference 31. Sc = 3,000.

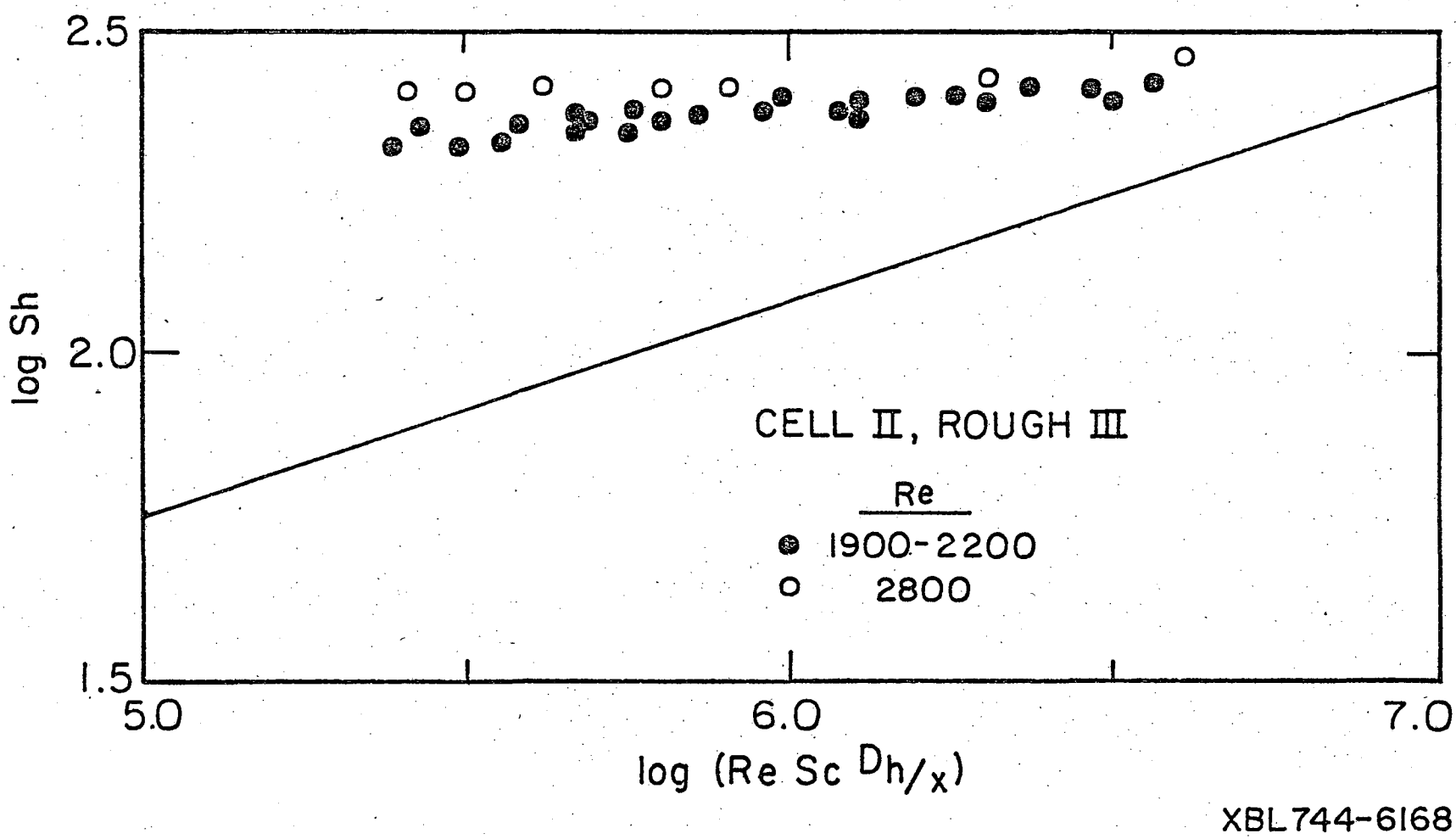

Fig. V-15c. Cell II, Rough III. Comparison of experimental local Sherwood Number with the extension to the Graetz-Levêque solution given in Reference 31. Sc = 3,000.

0 0 0 0 0 0 0 0 0 0 4

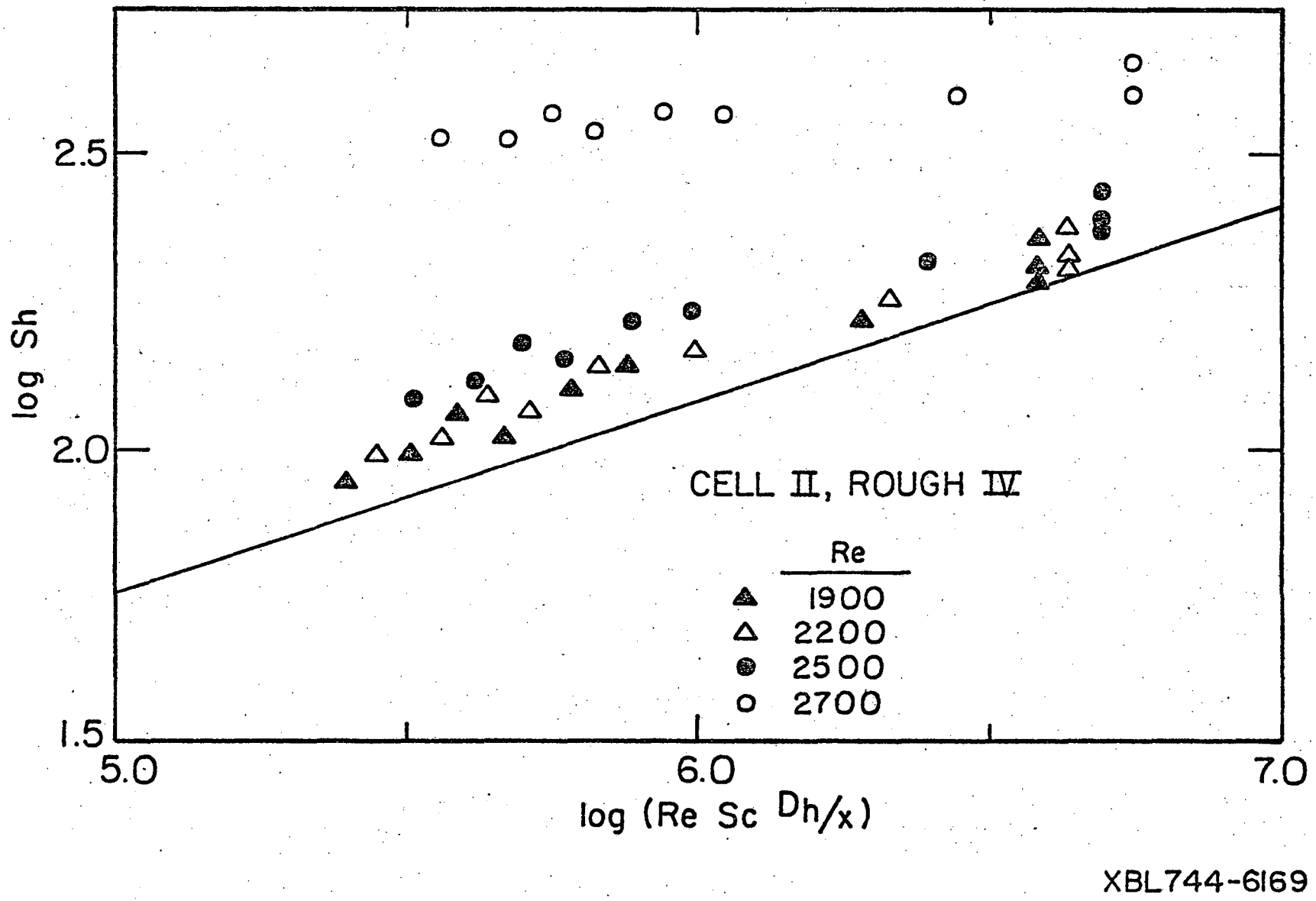

Fig. V-15d. Cell II, Rough IV. Comparison of experimental local Sherwood number with the extension to the Graetz-Levêque solution given in Reference 31. Sc = 3,150.

0 0 0 0 4 0 0 5 8 9 5

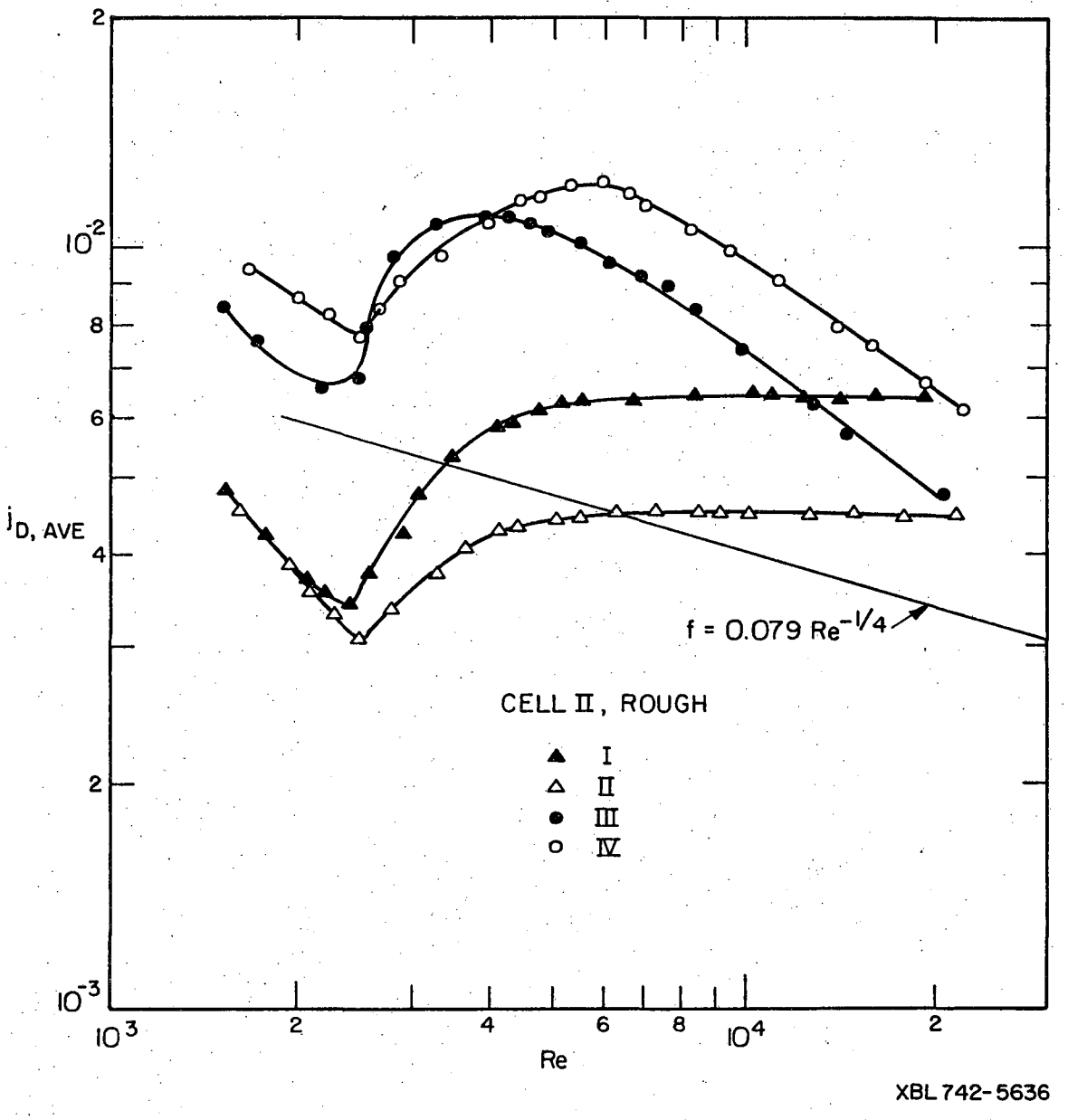

Fig. V-16. j_D factor for Cell II, rough. Sc = 2,700-3,800.

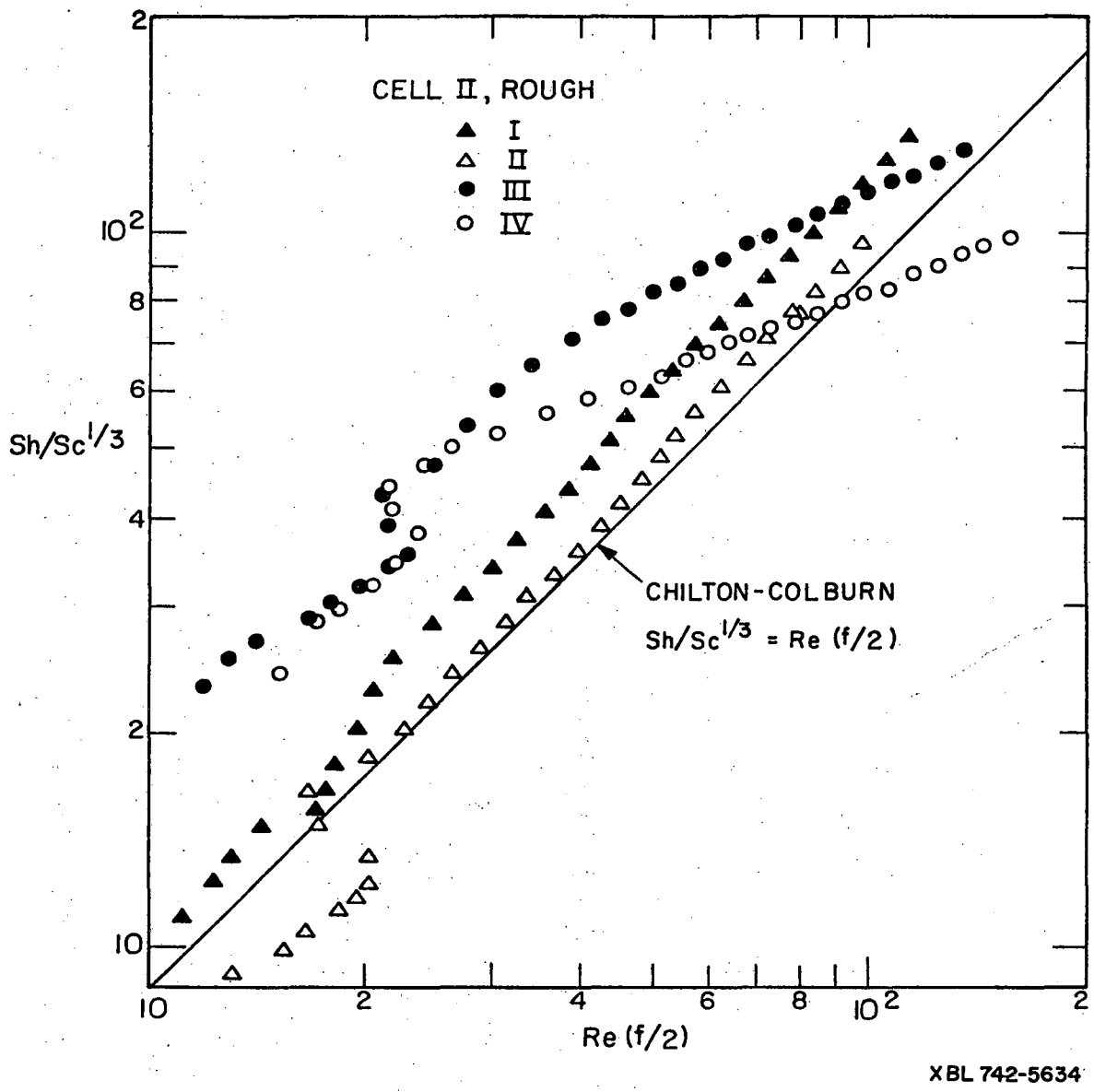

Fig. V-17. Comparison of the mass transfer coefficient and friction factors experimentally determined using Cell II, rough, with the correlation of Chilton-Colburn.[6] Sc = 2,700-3,800.

0 0 0 0 4 0 0 5 8 9 6

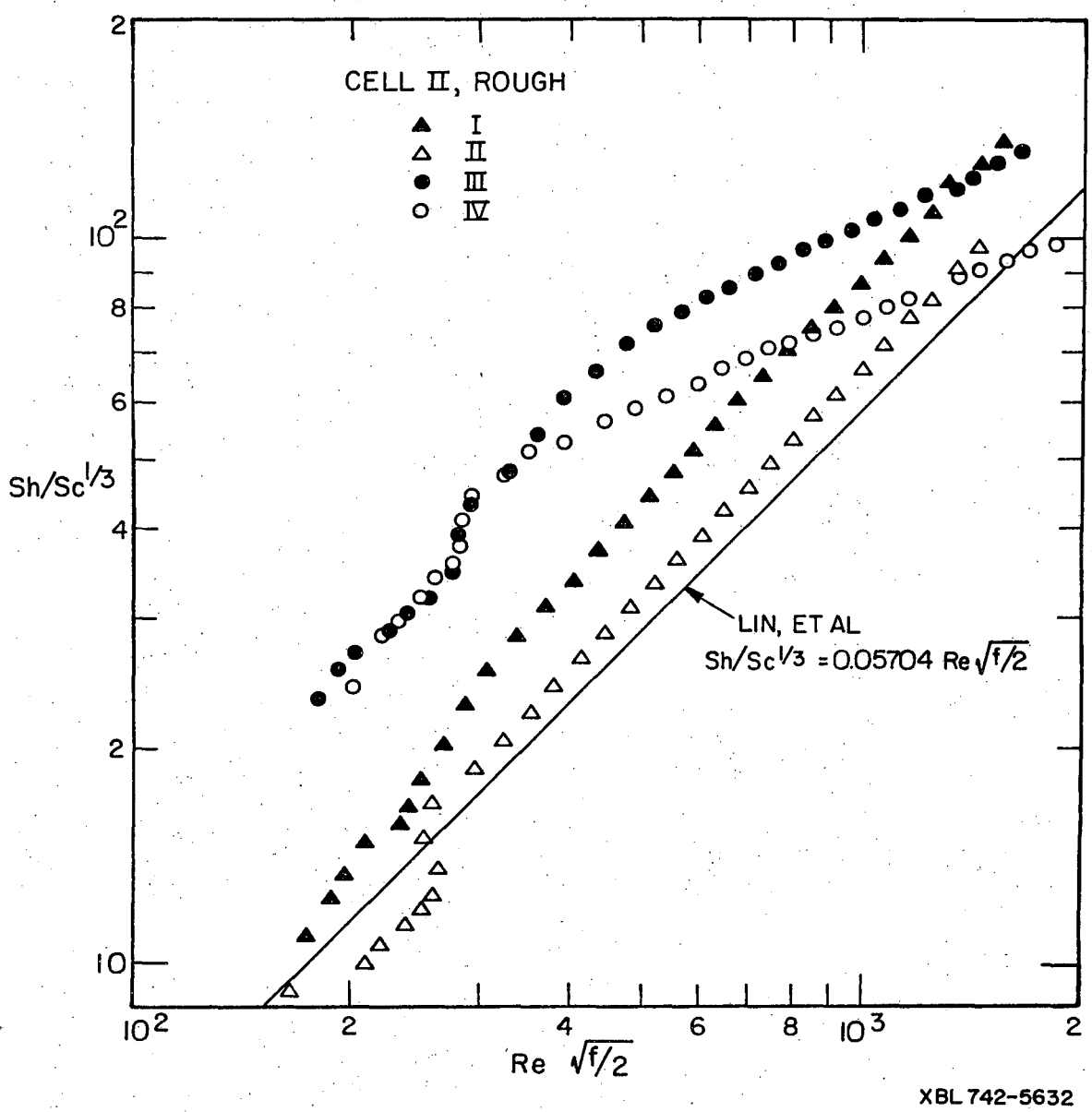

Fig. V-18. Comparison of the mass transfer coefficients and friction factors experimentally determined using Cell II, rough, with the correlation of Lin et al.[29] Sc = 2,700-3,800.

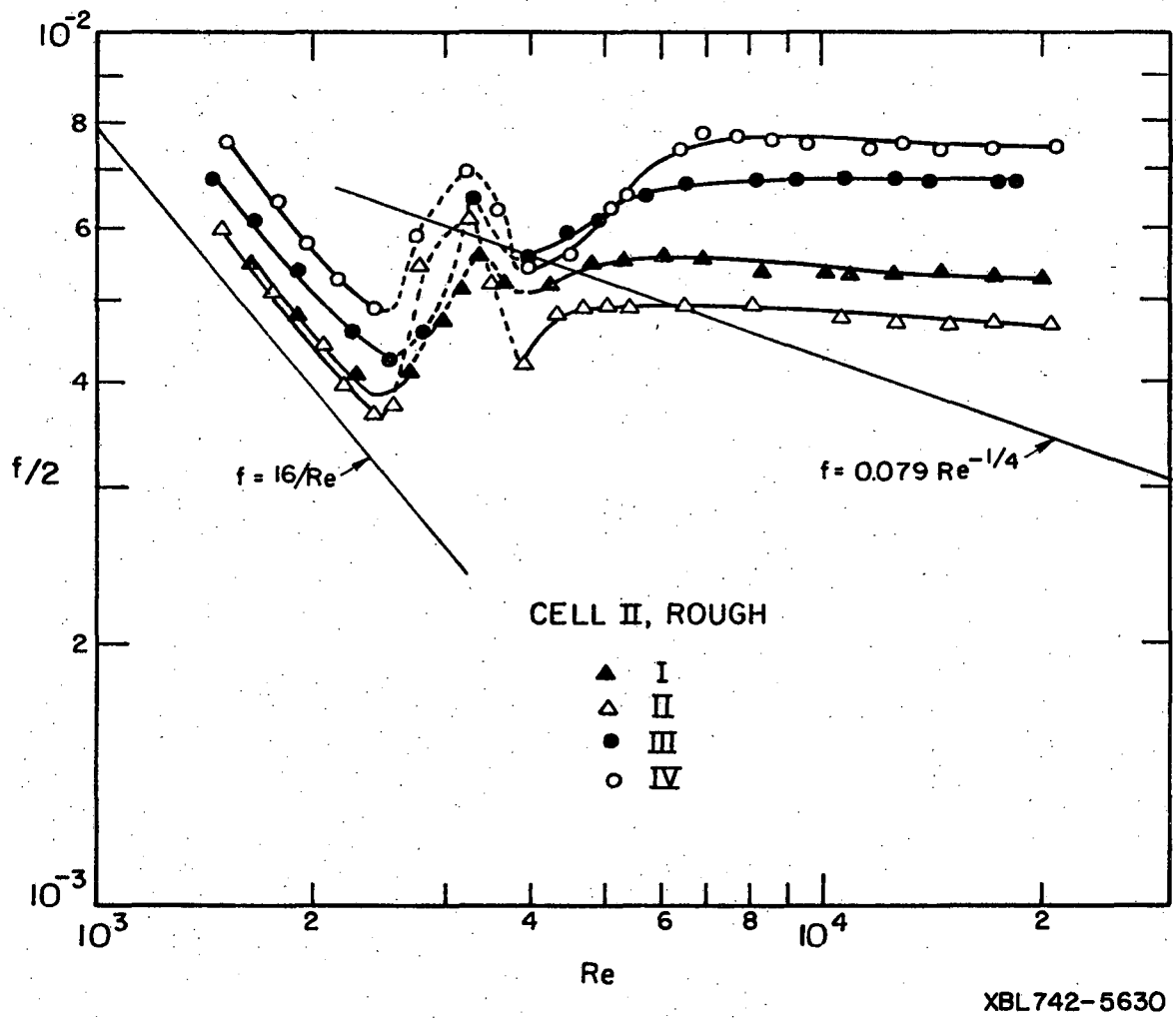

Fig. V-19. Experimental friction factors for Cell II, rough.

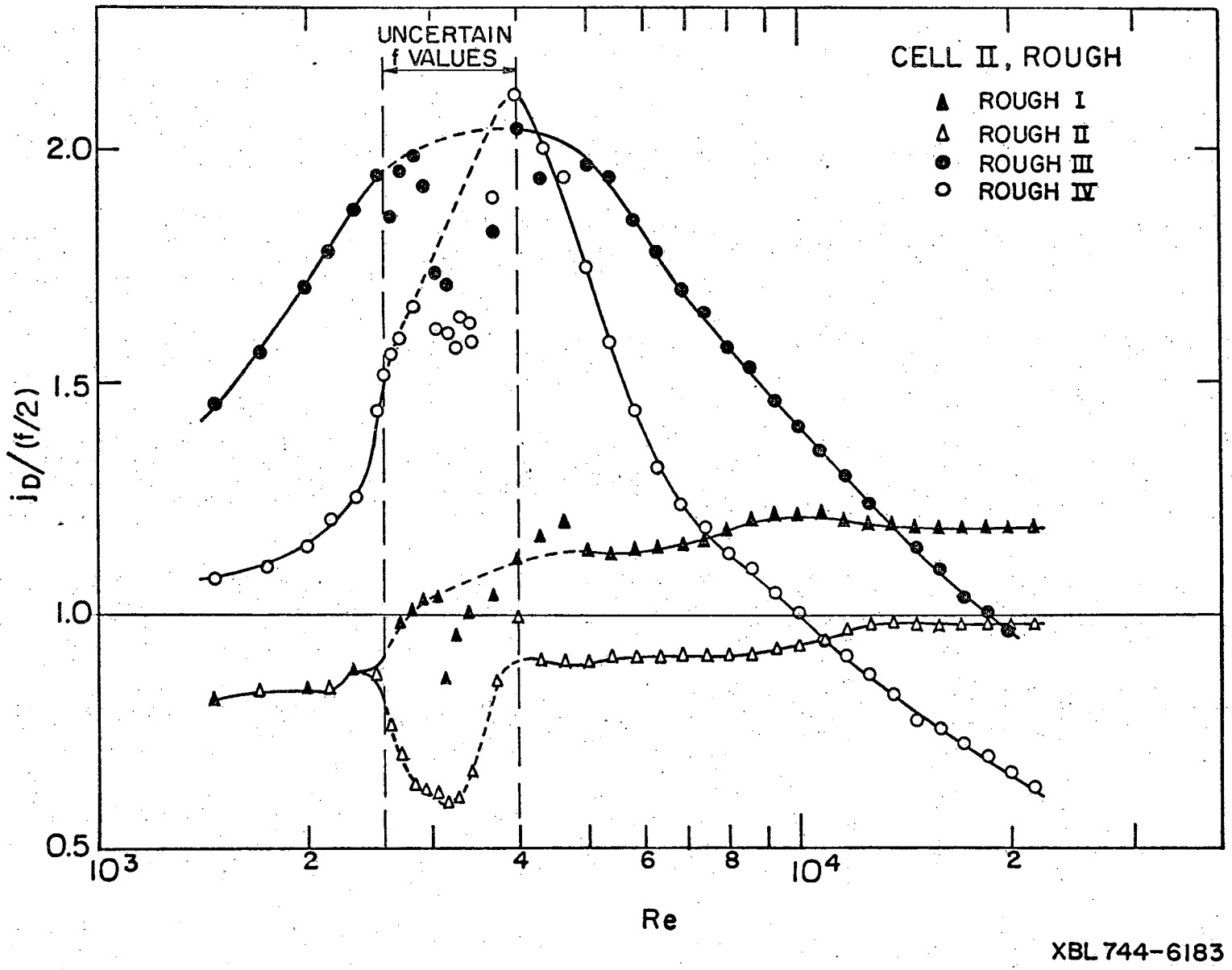

Fig. V-20. Ratio of mass to momentum transfer coefficient expressed as $j_D/(f/2)$ for Cell II, rough. Sc = 2,700-3,800.

0 0 0 5 6 8 7 7

VI. SUMMARY AND CONCLUSIONS

Coefficients for mass and momentum transport in rectangular cross-section channels with equivalent diameters of 0.096 and 0.038 cm have been successfully determined in the Reynolds Number range of 1,500 to 22,000. At the largest Reynolds numbers employed an equivalent mass transfer boundary layer thickness of 2.3×10^{-5} cm was obtained. To the author's knowledge mass transfer boundary layers as thin as this have not been previously reported.

The coefficients of mass and momentum transport in smooth rectangular channels with wall separations in the range of fractions of a millimeter can successfully be correlated by the equations that apply to smooth channels of much larger equivalent diameter. However, for thin channels to be considered "hydraulically smooth" at Re > 2,500, the walls must be polished to optical smoothness. Since this condition is rarely encountered in practical applications, care must be exercised in extrapolating results obtained with large equivalent diameters.

Under conditions where the Reynolds number falls in the laminar regine, only very gross surface roughness has an effect on the value of the transport coefficients. For smooth surfaces the mass transfer rate is given by the extension to the Graetz-Levêque solution:

$$Sh_{ave} = 1.85(ReSc\ D_h/x)^{1/3} \quad .$$

For smooth surfaces, the Chilton-Colburn correlation

$$Sh_{ave} = \frac{f}{2} ReSc^{1/3}$$

satisfactorily predicts the value of the mass transfer coefficient in

0 0 0 0 4 0 0 5 8 9 8

the turbulent regime, Re > 10,000.

When the surfaces are rough, the ratio of the mass transfer coefficient to the friction factor depends strongly on the type and degree of roughness of the surface. For the two largest roughness values employed in this study, this ratio had well defined maxima at 2,700 < Re < 10,000. A comprehensive study of roughness characterization would be necessary before a generally useful analogy between mass (heat) and momentum transfer can be developed for rough surfaces. Lacking this, the dependence of the $j_D/(f/2)$ ratio on Re for industrial electrolytic cells with very small D_h will have to be determined experimentally. This question is of great importance, since their operation is limited by the very large requirement of pumping power.

In the turbulent regime the mass transfer entrance length declined from 10 D_h at Re = 5×10^3 to 2.5 D_h at Re = 2×10^4. The present study did not attempt to provide a detailed analysis of entrance phenomena. Clearly more detailed studies are justified since previously reported values are not reliable.

The present results should be of help in clarifying the problems that appear in electrochemical machining. With a better understanding of the mass transfer effects in this process, elucidation of some surface and transient electrical effects in high rate anodic dissolution should be facilitated.

The conclusion that correlations developed for large D_h channels are applicable to thin channels--provided that careful attention is given to the effect of surface roughness--should be applicable to the problem

of heat transfer in very narrow slits (e.g., in nuclear reactors). It is not claimed here that an exact analogy exists between the two transfer process. However, it is known that in electrochemical mass transfer experiments a significantly higher degree of precision can be achieved than in heat transfer studies. Since departures from the behavior observed in systems involving large D_h would more likely occur when the boundary layer is thin (large Schmidt (Pradtl) number), one would expect that heat transfer correlations obtained for large D_h (and small Prandtl number) would also be applicable to heat transfer in thin channels.

Future work using very small equivalent diameters should extend the present results to much larger Reynolds numbers, to attain fully developed turbulence. The experimental difficulties involved in this type of endeavour will be significant because of the very large pressure drops associated with operation at high Reynolds numbers.

0 0 0 0 4 0 0 5 8 9 9

ACKNOWLEDGEMENTS

I would like to express my gratitude to Professor Charles W. Tobias for his advice and guidance during the course of this work. His enthusiasm and human warmth lightened what otherwise seemed an endless road.

I am also very grateful to Dr. Rolf H. Muller for his continued advice and insight into the many experimental difficulties involved in the project.

To Professor Donald R. Olander my thanks for reviewing this manuscript.

During the course of this work I had the invaluable support of many other individuals. I would like to thank the staff of the Inorganic Materials Research Division for their aid, particularly to Mr. Walter T. Giba, who was largely responsible for the construction of the experimental equipment; to Ms. Jean Wolslegel for graciously typing the manuscript, and to Ms. Gloria Pelatowski for her cooperation with the preparation of the drawings.

Financial support was provided by the U. S. Atomic Energy Commission through the Inorganic Materials Research Division of the Lawrence Berkeley Laboratory.

APPENDIX I. DESIGN OF THE EXPERIMENTAL CELLS

The minute dimension of the interelectrode gaps used in this study, together with the very high flow velocities necessary to achieve turbulent flow, give rise to rather exacting specifications in the design of the experimental cells.

The following characteristics were required of the cells:

i) Ease in cleaning the electrodes and in refinishing them when necessary. As explained in Chapter III, one of the disadvantages of the redox system employed in this study is the sensitivity of the nickel electrodes to poisoning. Also, it was necessary to be able to change the texture of the cell walls to study the effect of roughness on the momentum and mass transfer coefficients.

ii) Wall strength to withstand a differential pressure along the cell of the order of 2,500 psi. Due to the very large pressure drop that results at the highest Reynolds number studied, (up to 400 psi/cm) a very rigid structure was necessary to minimize distortions under the operating conditions.

iii) A precise separation between the electrodes. In order to ascertain the value of the hydraulic diameter to within 1%, the maximum variation in the interelectrode gap was not allowed to exceed 0.0004 cm (for D_h = 0.04 cm).

iv) Convenient changing of the aspect ratio of the cell. This feature was necessary in order to discriminate from the mass transfer results the effect of secondary flow at the corners of the channel.

v) Sectioned electrodes to allow measurement of the mass transfer coefficient as a function of distance downstream from the mass transfer leading edge.

0 0 0 0 4 0 0 5 9 0 0

vi) Pressure taps for measurement of the pressure variation in the flow direction.

vii) An entrance length before the mass transfer region (the electrodes) sufficient to allow for fully developed flow at that location.

viii) Minimum pressure drop.

The first feature was obtained using a sandwich type cell formed by bolting together two plates separated by an insulating shim, see Fig. AI-1 and Fig. AI-2. The two plates were made of 316 stainless steel to give the necessary wall strength (item ii above), and to make them resistant to attack by spills of the caustic electrolyte employed. The insulating shim was a piece of Mylar sheet.

Mylar was chosen as the material for the spacer since it is an insulating material with negligible compressibility and is available in thin sheets of uniform thickness. The latter was needed to insure a precise separation between the electrodes (item iii).

The channel for electrolyte flow was formed by cutting out a slot of the desired width in the Mylar spacer. When the two plates were bolted together with the Mylar sheet in between them, the edges of the slot in the Mylar formed the side (narrow) walls of the channel, while the bounding plates formed the wider walls, Fig. AI-3. Different aspect ratios were in this way easily attainable, by simply exchanging spacers.

The stainless steel plates forming the body of the cell were machined to the desired dimensions and a 3/8 in. deep cavity was milled on the two facing surface. This cavity was later filled with an oven-cure epoxy resin,* refer to Fig. AI-3. In this

*The epoxy resin formulation was: Resin 826 (Shell Chemical Co.) 76.5% by weight, Resin 736 (Dow Chemical Co.) 8.5% by weight, Catalyst D-40 (Furane Plastics, Inc.) 15.0% by weight.

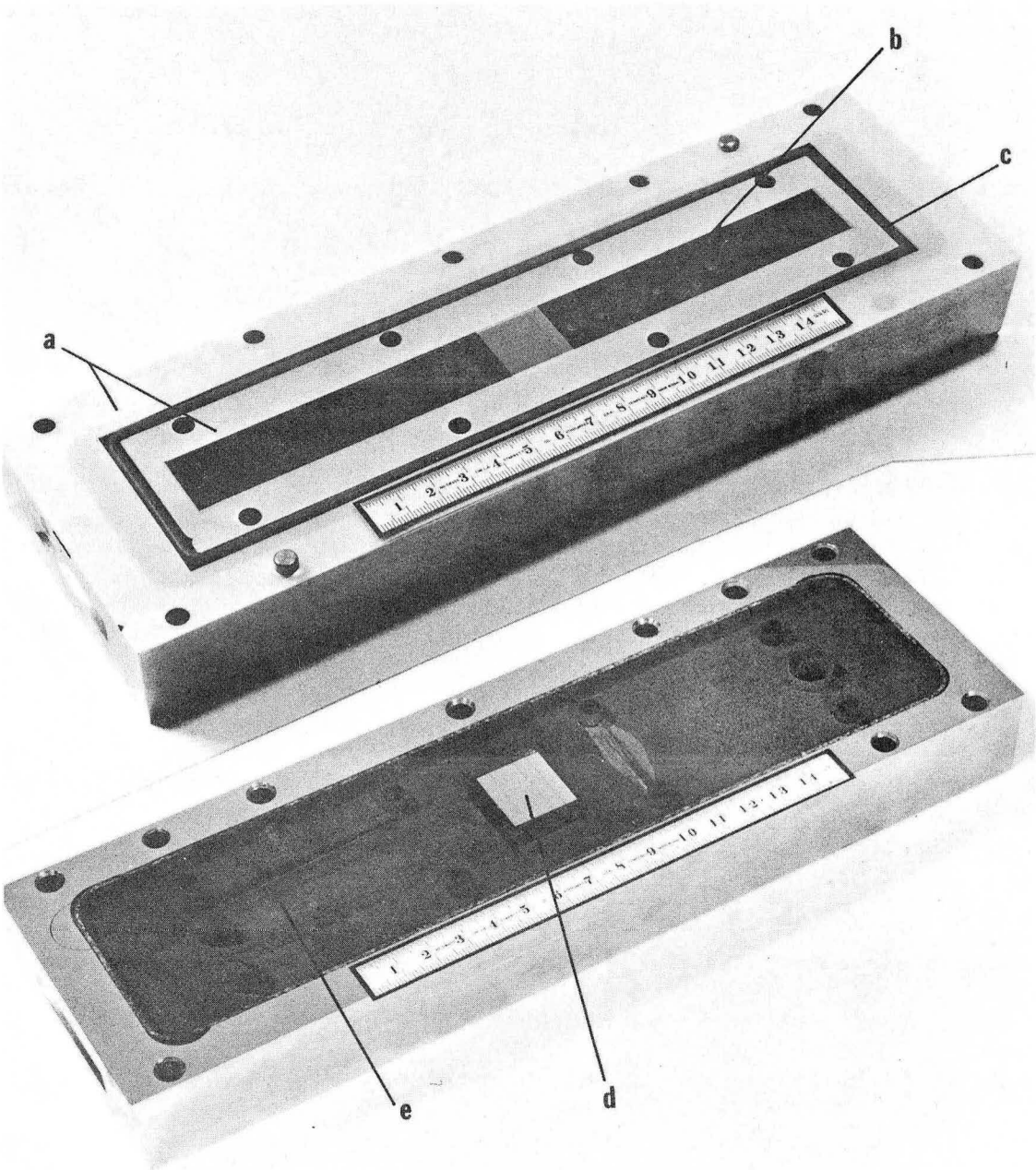

XBB 7112-6128

Fig. AI-1. Overall view of Cell I, opened. (a) Mylar spacer. (b) 7° effuser. (c) Silicone "O" ring. (d) Segmented electrode. (e) Capillary pressure tap holes.

0 0 0 0 4 0 0 5 9 0 1

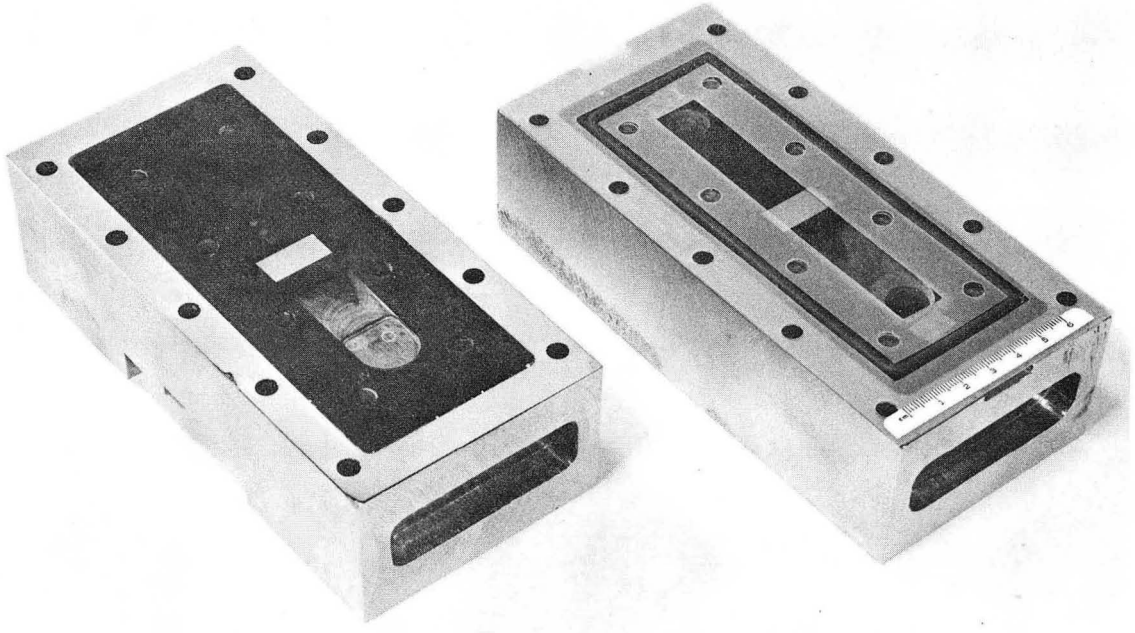

XBB 727-3726

Fig. AI-2. Overall view of Cell II, opened.

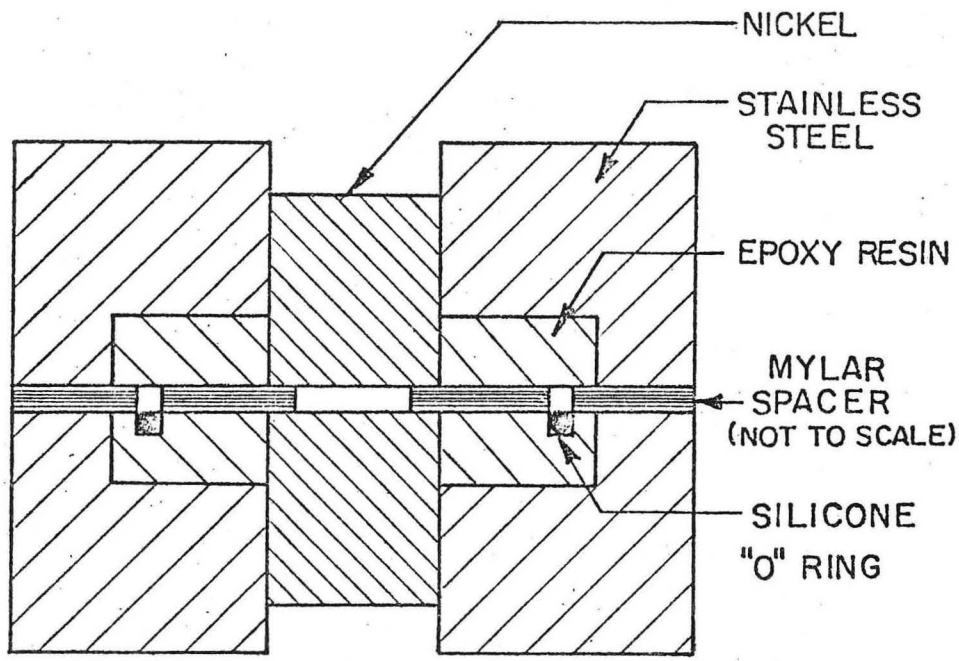

Fig. AI-3. Flow channel cross section.

0 0 0 0 4 0 0 5 9 2

manner the channel outside the mass transfer region was non-conducting, preventing stray currents. The epoxy surface was also found convenient when drilling the very small holes needed for the pressure taps (see below). A rectangular opening was milled through the center of the plate. This opening housed the sectioned electrode in the finished cell. For Cell I casting of the epoxy was made directly into the cavity with the electrode positioned in the rectangular opening. Since the epoxy resin was cured at 65°C, when the cell was removed from the oven contraction of the stainless steel plate caused the epoxy resin to crack, thereby ruining the cell. For this cell a solution to this problem was found by placing a thin layer of cork sheet around the edges of the cavity before the liquid epoxy was poured in. This prevented the epoxy layer from cracking upon cooling the cell, but left the epoxy layer in a state of unrelieved strain which made it susceptible to cracking. For Cell II, the epoxy facing was cast around the sectioned electrode in a separate tray made of aluminum foil. After curing the resin in the oven and allowing for a slow rate of cooling, the epoxy plates with the electrodes were machined to the dimensions of the cavity in the stainless steel plate and cemented in place using room temperature cure epoxy. In both cases, the final piece had to be milled and ground to make it flat previous to polishing. Grinding was performed using an aluminum oxide wheel. Polishing of the cell for the "smooth" experiments was done using a polishing wheel with velvet backing and diamond powder of 0.1μ size. The whole cell was polished until flat to within two wave lengths over its entire surface. Different formulations of epoxy resins were tried in order to find one giving the least differences in behavior upon

polishing between epoxy and nickel. However, since a compromise had to be made between hardness of the epoxy resin and its brittleness, the final formulation used did show some undesirable characteristics upon polishing. Namely, there was a "rounding" of the epoxy in the proximity of the nickel insert, the surface of the latter resulting 2-3 microns below the surface of the epoxy far from it. A profilogram trace obtained with the Surfanalyzer showing this problem is presented in Fig. AI-4. Several unsuccessful attempts were made to eliminate this effect. Considering that the change in hydraulic diameter due to the recessed electrode was only 2-3/1,000, and that this change in diameter occurred over a distance of 10 hydraulic diameters (the scale vertical/horizontal dimensions in Fig. AI-4 is 1:100) it was assumed that this effect would be negligible. One solution to this problem would be to cast a piece of nickel upstream from the electrode proper, electrically insulated from it, so that any disturbance of the flow would occur far from the electrode. This solution would also alleviate the problem of a crevice appearing in the junction epoxy-nickel, refer to Fig. AI-4, since it was found that in the very thin layers of epoxy insulating one electrode section from another this crevice was very small (in some cases undetectable either by microscope inspection or through the surfanalyzer).

The sections forming the electrodes were cut of 99.9% pure nickel plate, and machined to close specifications. The sides of these sections were sandblasted with a fine abrasive to assure adhesion of the epoxy resin. The electrode surface and a narrow region below it were masked for this operation, in order to preserve the straight electrode edges.

0 0 0 0 4 0 0 5 9 1 3

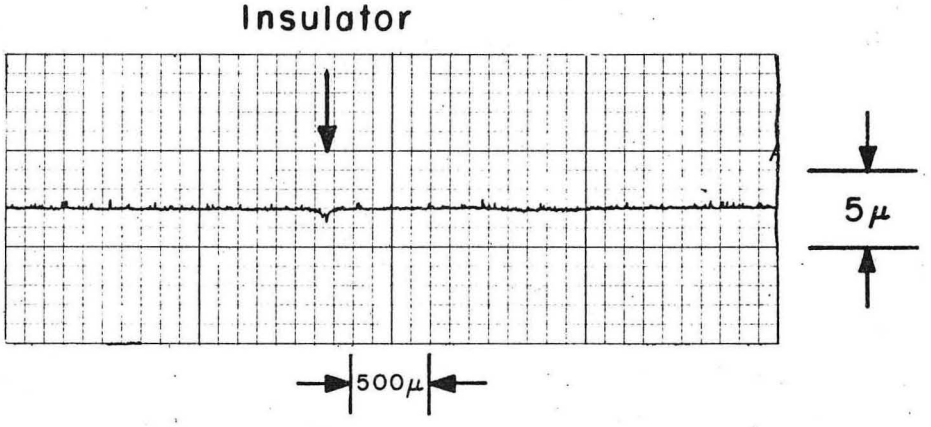

XBL 743-2478

Fig. AI-4. Profilogram trace of the smooth cathode.

Short strips of 0.001 in. thick Mylar sheet were glued to one of their sides and then all the pieces were clamped together (see Fig. AI-5). The clamped unit was immersed in warm oven-cure epoxy resin and vacuum was applied to the container. This succeeded in drawing the resin into the narrow crevice created between the electrode sections by the presence of the Mylar strips. The resin in the container, with the electrode still immersed, was put in an oven to cure. After the curing period, and allowing for a slow rate of cooling, the excess resin was mechined off the electrode. The resulting unit was then located in the center hole of the cell plate and cast in place simultaneously with the epoxy resin facing.

As Fig. AI-4 shows, the polished surface of the sectioned electrode was flat and the insulating strips were barely noticeable. However, when the cells were sandblasted for the rough surface experiments, the insulating strips tended to erode more rapidly than the nickel segments, giving a more noticeable discontinuity (Fig. AI-6). This imposes a limitation on the number of electrode segments employed since under ideal conditions (completely smooth junction epoxy-nickel) the velocity field over the electrode should be undisturbed. In any case, there will be a discontinuity in the mass transfer boundary layer since the transfer process is interrupted at the insulator (see Fig. AI-7). Under actual conditions both the flow field and the mass transfer boundary layer will be affected, and one will want to keep this disturbance to a minimum.

Pressure Taps. At the initiation of this project several means of measuring pressure drop in the flow channel were considered: hooked

0 0 0 0 4 0 0 5 9 4

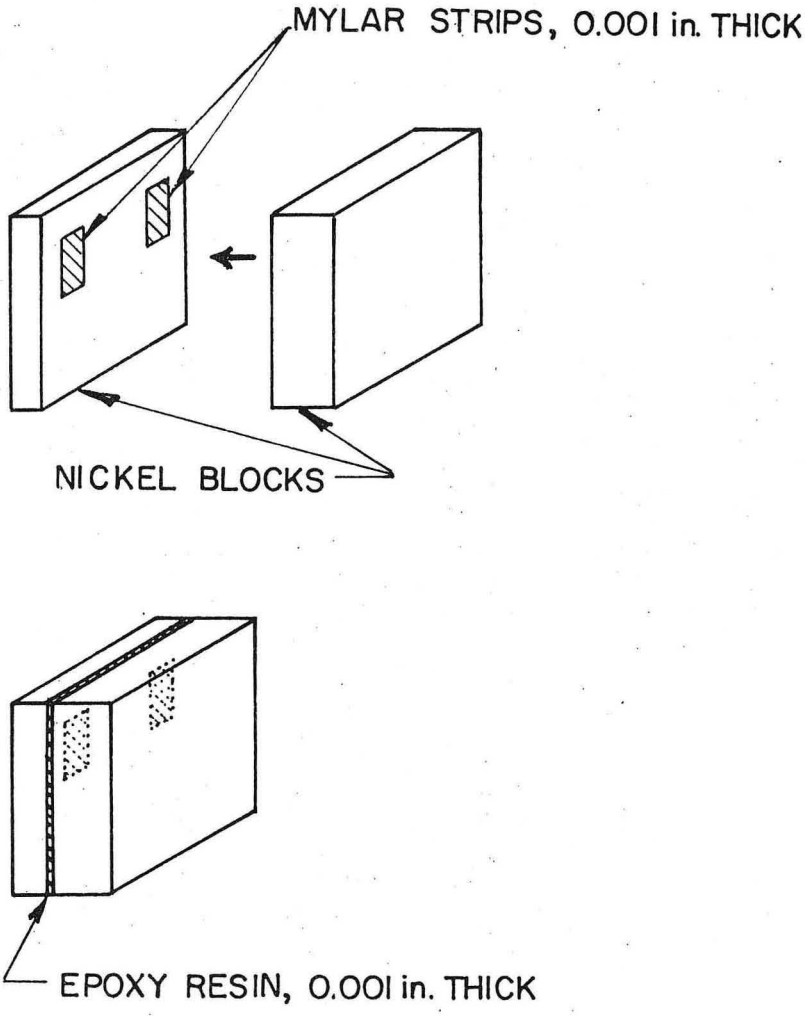

DETAIL, SECTIONED ELECTRODE
(NOT TO SCALE)

XBL742-5641

Fig. AI-5. Detail of the construction of the sectioned electrode.

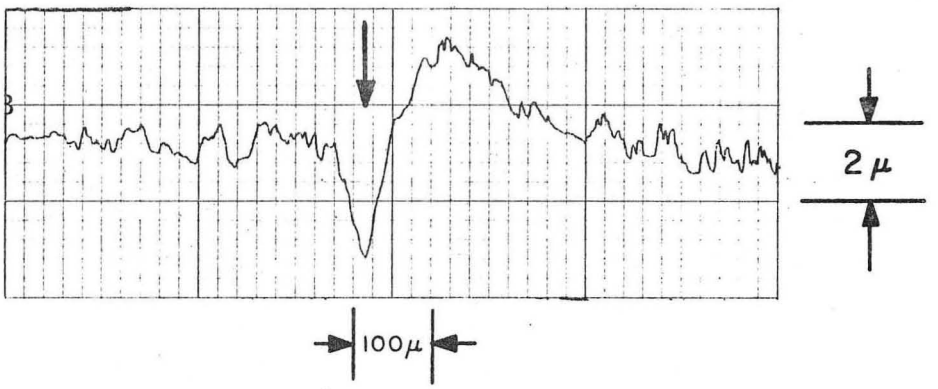

XBL 743-2478

Fig. AI-6. Profilogram trace of the sandblasted cathode.

0 0 0 0 4 0 0 5 9 3 5

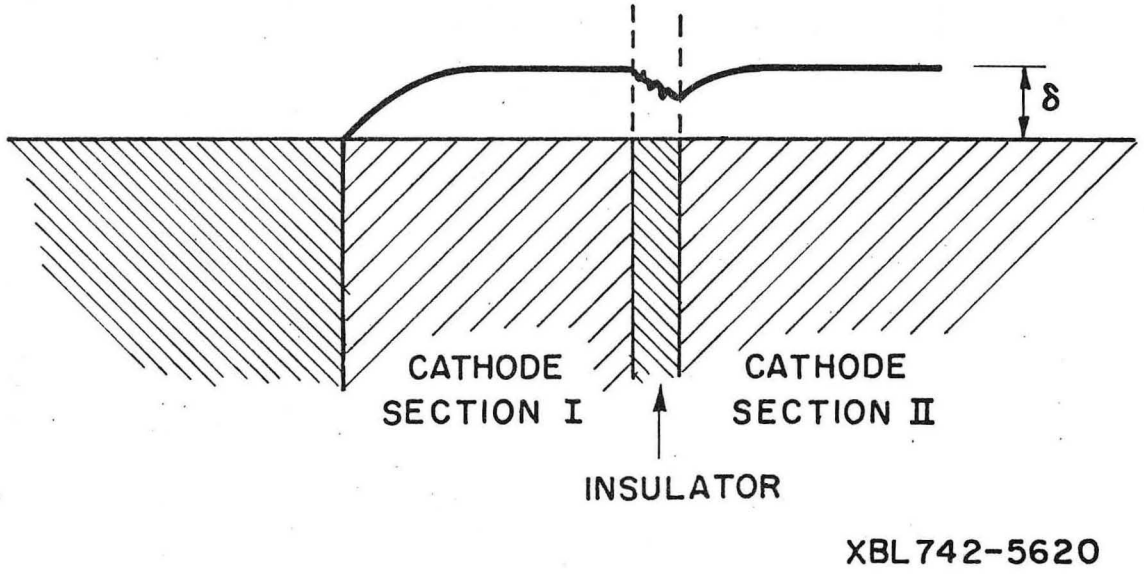

Fig. AI-7. Schematic diagram of the discontinuity in the mass transfer boundary layer created by the presence of the insulator in a sectioned electrode.

tubes inserted in the flow, direct installation of strain gauge pressure transducers in the walls, and piezometric holes on the walls. Hooked tubes are generally considered to give more accurate pressure values. However, in order for them to be rigid, the diameter for the tube would have to be several times the value of the channel gap. Direct installation of strain gauge pressure transducers in the walls presented a problem due to the large sensor surface, since for the smallest hydraulic diameter a pressure drop of the order of 25 atm/cm occurs at the larger Reynolds number. Difficulties would also have been encountered in trying to install the transducers flush with the wall surface, particularly when the exchange of transducers became necessary to cover the wide range of pressures that result from the range of flow rates.

In view of the above considerations recourse was taken to tap holes drilled in the wall of the channel. In order to affect the flow as little possible by the presence of the pressure tap openings, the diameter of the pressure tap hole had to be as small as possible. The pressure tap holes also had to be deep enough to allow repeated polishing and refinishing of the cell. The holes in the epoxy walls were drilled 6 mils in diameter, and 1/4 in. deep. It was found impracticable to drill holes with a smaller diameter. For the case of the pressure tap holes in the electrode proper, recourse had to be taken to drilling holes 0.040 in. in diameter, and to insert in them a short length of 0.004 in. ID tube that fitted snugly in the hole (see Fig. AI-8). This tube was manufactured from hypodermic stainless steel tube with a 0.008 in. OD to which nickel was electroplated until the necessary diameter was attained. After polishing it was found that the outline of the tube inserted

0 0 0 0 4 0 0 5 9 1 6

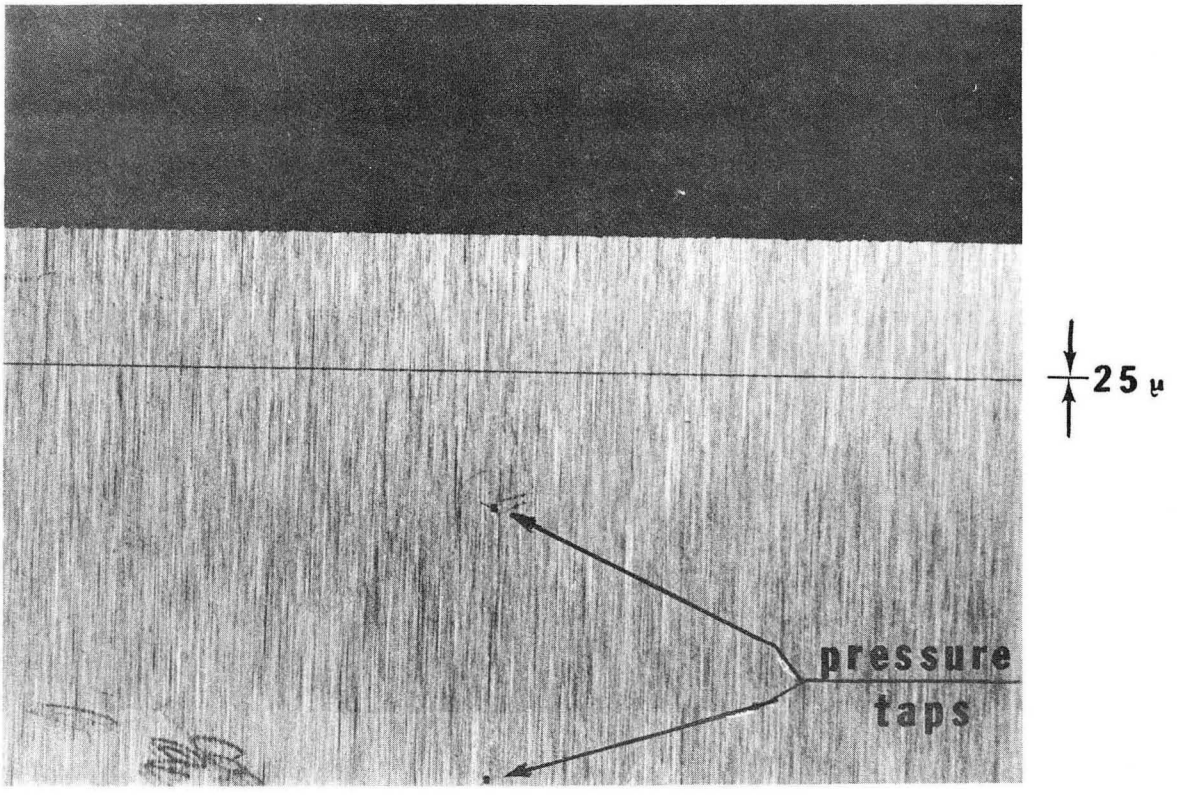

XBB 728-4051

Fig. AI-8. Pressure taps in the nickel electrode (anode).

was still visible (see Fig. AI-9). However, a profilometer trace over that section revealed an almost imperceptible crevice, which hopefully did not disturb the flow appreciably. Nevertheless, the effect of the hole itself on the value of the pressure measured may not be negligible; if we consider that the depth of the smallest channel was 7.5 mils, a hole in the wall with a diameter of 4 mils may produce a considerable disturbance in the hydrodynamic flow.

Hydrodynamic Entrance Length. A change in cross section, or direction, of the channel through which a fluid flows is accompanied by a disturbance of the velocity profile and a change in the pressure gradient of the flow. Whenever this occurs a certain distance, the entrance length, is required before the velocity profile and the pressure gradient regain their fully developed (i.e., constant) values. This distance is very long since the flow approaches the "fully developed" value in an asymptotic manner. Since the developed profile becomes established first near the walls, the fully developed profile growing inwards towards the axis of the flow, the pressure entrance length is somewhat shorter than the velocity entrance length.

In practice, the entrance length is reported as the "5%, or the 1%, entrance length", meaning that that is the length necessary for the velocity at all points, or the pressure gradient, to come to within 5%, or 1% respectively, of the fully developed value. This quantity is often less carefully defined in the literature on the subject.

Recent experimental work [5,7] fixes the 1% entrance length at 75 hydraulic diameters. A value of 80 D_h was employed in the design of the experimental cells.

0 0 0 0 4 0 0 5 9 7

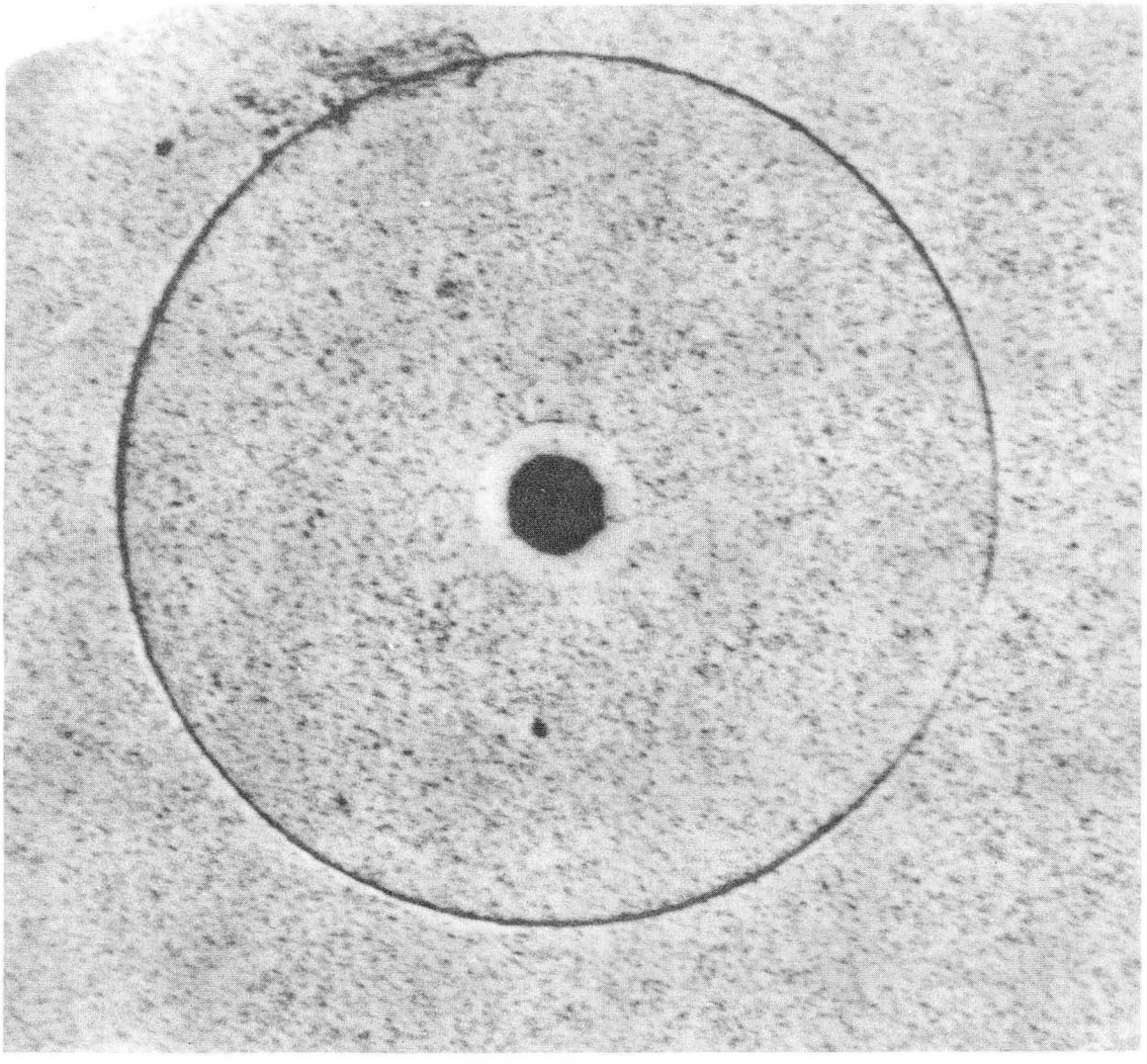

XBB 728-4050

Fig. AI-9. Close-up photograph of a pressure tap in the nickel electrode showing the outline of the hypodermic tubing insert.

Pressure Drop. One of the main concerns in the design of the present flow channels was to keep the pressure drop to a minimum. To this end, economy had to be exercised in the total length of the narrow gap forming the cell, and also measures had to be taken to minimize the pressure drop that occurs due to the change in cross section between the flow channel and the flow circuit.

The magnitude of the problem becomes clear from consideration of the following figures: Using the Blasius equation for the friction factor of a hydraulically smooth channel, $f = 0.079\ Re^{-1/4}$, the hydraulic diameter of 0.038 cm for Cell II (0.02 cm interelectrode gap), a kinematic viscosity $\nu = 1.38 \times 10^{-2}$ cm^2/sec, density $\rho = 1.13$ g/cm^3 and a Reynolds number of 25,000, the pressure drop in the cell is 31 atm/cm. For this hydraulic diameter an entrance length of 80 D_h equals 3.2 cm. Given a mass transfer section 1.0 cm long, and an exit length of 0.8 cm (20 D_h), the total length of the channel is 5 cm, with a resultant pressure drop of 155 atm.

A sudden expansion in the cross section of a channel has been empirically found to represent a major loss in pressure head. The equivalent length for pressure drop being given by[2]

$$\Delta P = \frac{1}{2} \frac{\rho}{g_c} v_1^2$$

where v_1 is the linear velocity before the expansion. For the channel under consideration, expansion of the cross section to a 1.0 cm diameter pipe would represent a pressure drop of 74 atm. Alternatively, for

0 0 0 0 4 0 0 5 9 0 8

ducts with a circular cross section, it has been found that a flared exit with 7° diverging walls gives a minimum loss in pressure head.[35a]

The minimum length of the channel was determined by the requirements of fully developed flow at the electrodes, the need for long electrodes to be able to determine several points in the Sh vs x/D_h curve, and enough exit length to prevent end effects. Since the total length of the channel was fixed, minimization of the pressure drop had to be achieved by using a suitable exit.

Lacking any other reliable criteria, it was decided to expand the cross section of the channel using a 7° angle of divergence between the two widest walls. At the initiation of this work the side walls of the channel, those formed by the cut-out in the Mylar spacer, were left parallel. However, when the experimental runs were conducted at the larger flow rates it was found that the Mylar spacer tended to break at the edges of the flaring walls. To solve this problem, first the cut-out in the spacer was widened at right angles at the point where the wider walls begin to flare, but this produced disturbances in the mass transfer at the last electrode section, see Appendix III. The final solution consisted in cutting the Mylar spacer also with a 7° flare beginning at the same point where the wider walls flare.

APPENDIX II. END EFFECTS

Even though the actual value of the entrance length is still a subject of argument, reliable estimates are available and one can confidently design a flow channel for mass transfer experiments where the flow velocity will have attained its fully developed profile at the point where the mass transfer begins.

On the other hand, the question of the length of channel over which exit effects are of importance has been neglected. On this subject there are no established criteria and one has to rely on an intuitive guess to prevent disturbances of the velocity profile from propagating upstream and distorting the results obtained in mass transfer experiments.

The dimensions of the present flow channels were kept constant downstream from the electrodes for a length equivalent to 4.5 and 24 D_h for cells I and II respectively (see Section III-D). These lengths were arbitrarily chosen. When cathode Section IV was the only active section of the electrode, the limiting current values obtained coincided with those obtained for cathode Section I. Hence, we were reassured that these exit lengths were sufficient to prevent small disturbances in the flow (caused by the smooth change in channel cross section) from propagating upstream to the mass transfer region.

However, there were some instances when small irregularities in the channel located at the end of the exit section resulted in disturbed rates of mass transfer at the electrodes. For instance, when the electrode spacer was cut in such a way that the channel widened at right angles at the beginning of the flaring sections, the mass transfer rates at the downstream electrodes was substantially increased, leading to the type

0 0 0 0 4 0 0 5 9 0 9

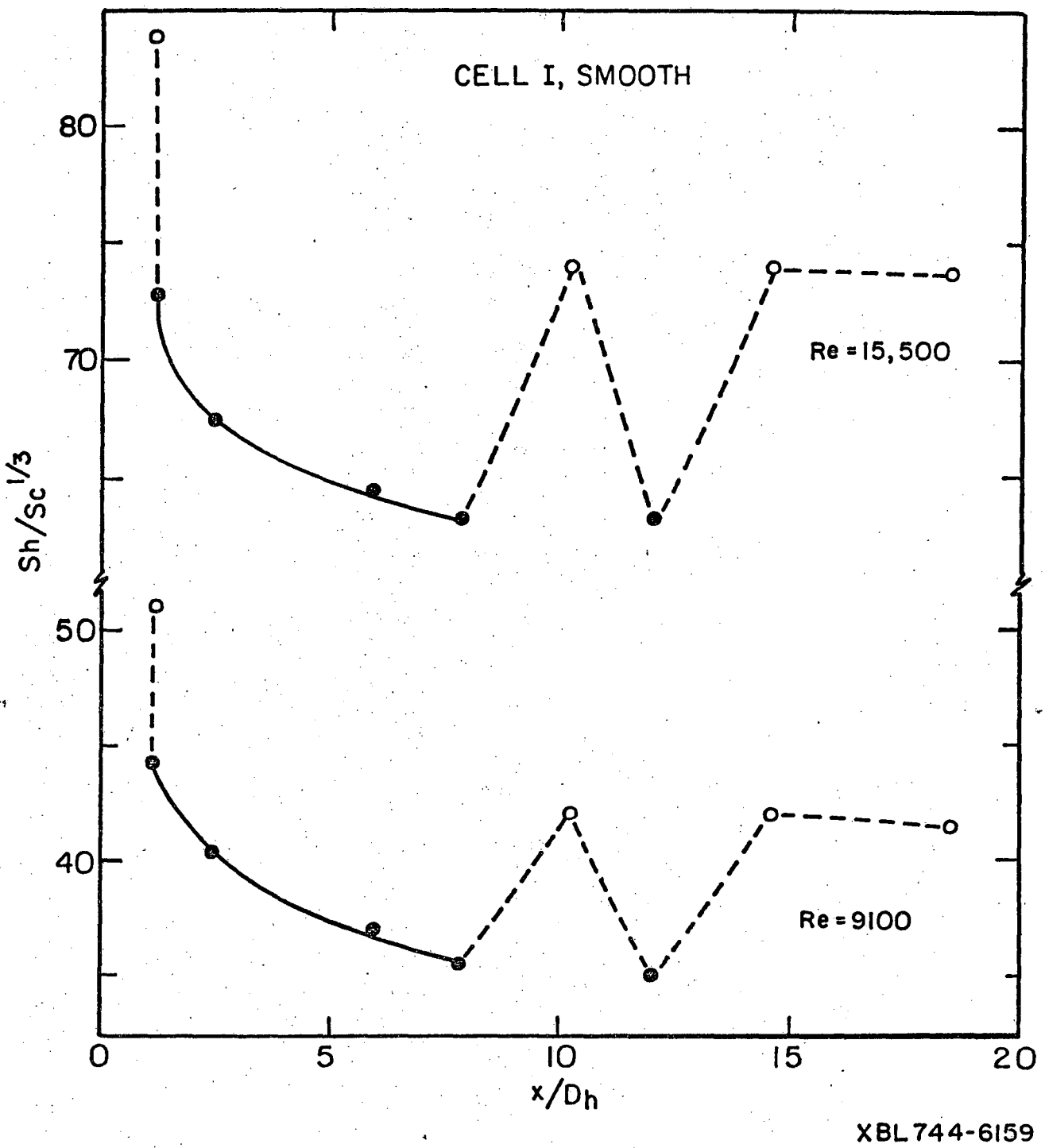

Fig. AII-1. Disturbance of the mass transfer rates caused by a spacer cut at right angles 4 D_h downstream from the mass transfer section.

of Sh vs x/D_h curves shown in Fig. AII-1 (refer to scheme of measurements in Section III-D). This condition was noticeable only at high Reynolds number, the departure from a smooth surve at small Re being very small and within the experimental scatter of the points. This irregularity in the Sherwood-distance curve disappeared when the spacer was cut with a 7° flare. The post-facto explanation for this effect is that the wake produced in the flow by the step created a narrowing in the central flow field (an effect similar to a vena contracta). One other possible explanation is that the edge of the step was not completely smooth, and this led to the formation of the wake upstream of the channel. This latter explanation is rather unlikely, since inspection of the spacer using a microscope did not reveal any protrusions at the corners.

A more dramatic effect was found when larger disturbances were present in the channel effuser. When the effect of the sharp step in the spacer described in the previous paragraph was first noticed, it was attributed to an insufficient exit length and an attempt was made to lengthen it. The effuser of Cell I was filled with room temperature cure epoxy resin, then it was milled leaving a longer (10 D_h) exit length, and the whole cell repolished. When experiments at high Reynolds number were run, the Sherwood-distance curves showed an even more startling irregularity, see Fig. AII-2. Upon disassembling the cell, it was found that the electrolyte solution had attacked the epoxy resin patch causing it to swell. This swelling was not large enough to make the effuser narrower than the 0.05 cm gap used in the mass transfer section, and was located approximately 2.5 cm (25 D_h) downstream from the electrode edge.

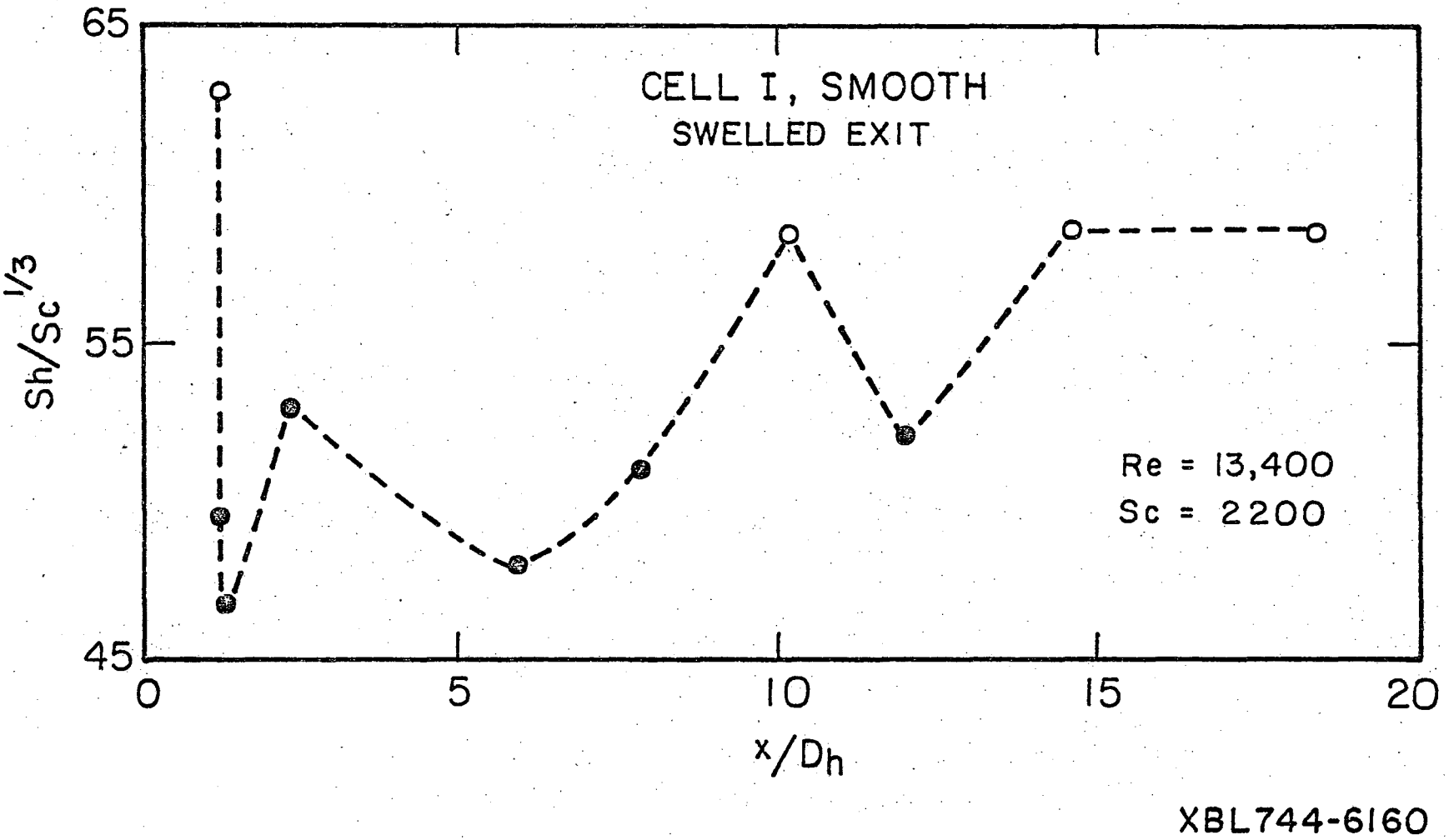

Fig. AII-2. Disturbed mass transfer rates caused by a constriction in the effuser located more than 15 D_h downstream from the mass transfer section.

0 0 0 0 0 0 9 1 6

All these effects point to the fact that the state of the flow channel downstream from the mass transfer section may be as important as that of the upstream, and that attention should be dedicated to this neglected aspect of channel flow properties.

0 0 0 0 4 0 0 5 9 1 1

APPENDIX III. FLUCTUATIONS IN THE HYDRODYNAMIC TRANSITION REGION

The region of transition from a purely laminar to a turbulent flow has been traditionally assigned to the regime $2{,}000 < Re < 10{,}000$. In this region the transport of mass and momentum is greatly increased above the values that one obtains in the purely laminar region. This effect is apparent by the hump in the friction factor vs Reynolds number curve.

In the present study an interesting phenomenon was observed: when experiments were run at Reynolds numbers corresponding to the beginning of the hydrodynamic transition flow, very marked fluctuations of the value of the current appeared superimposed on the limiting current plateaus. These fluctuations became less pronounced, and eventually disappeared, at higher Reynolds numbers, see Fig. AIII-1.

Since the present experiments were conducted using a chronopotentiostatic control there was the possibility that the fluctuating voltage was an artifact of the equipment: the finite capacitance due to the distance separating the reference electrode and the cathode could produce a time delay that was not being compensated for by the potentiostat. In order to test this possibility, a parallel set of experiments was done using chrono-galvanostatic control.* Again the current vs potential was traced and this time fluctuations approximately 1 volt wide in the cathode vs reference-electrode potential were obtained upon reaching the limiting current plateau, see Fig. AIII-2.

---

*Galvanostat Model C-618. Electronic Measurements, Eatontown, N. J.

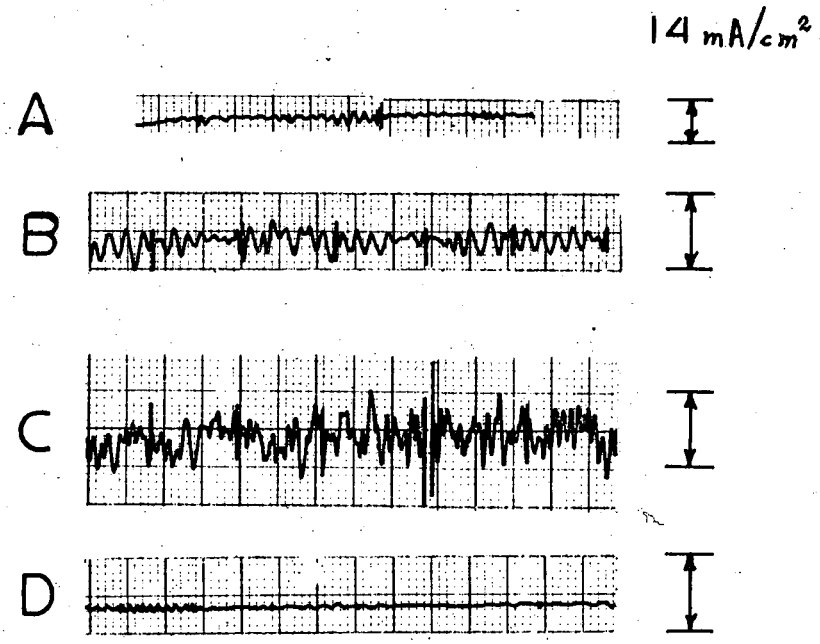

XBL 743-5712

Fig. AIII-1. Fluctuations in the value of the limiting current at various Reynolds Numbers in the hydrodynamic transition region. Chronopotentiostatic control.

0 0 0 0 4 0 0 5 9 1 2

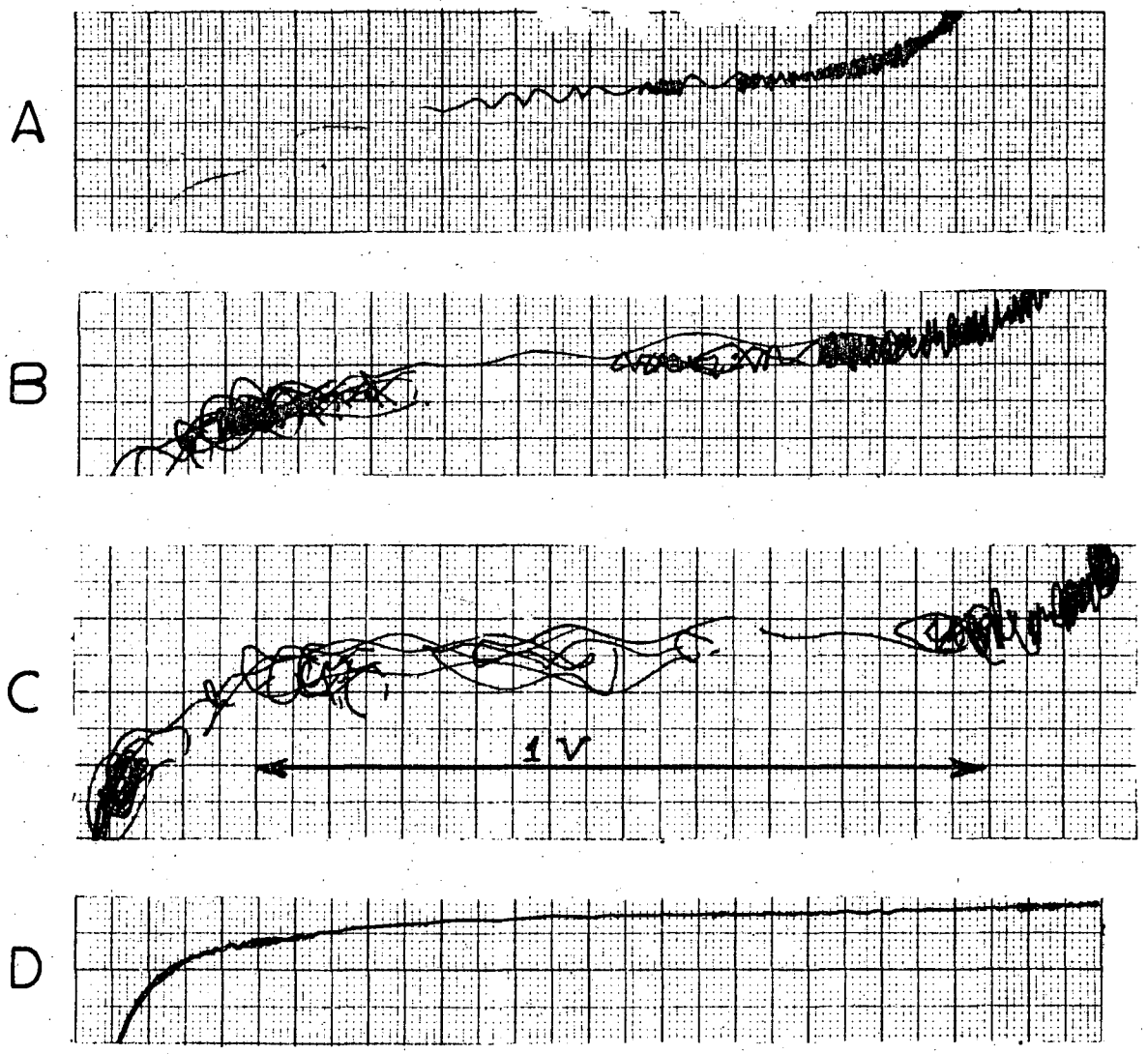

XBL 743-5711

Fig. AIII-2. Fluctuations in the value of the cathode voltage (vs Ni) upon reaching the limiting current value, when operating in the hydrodynamic transition region. Chronogalvanostatic control.

One possibility was that these fluctuations in potential were caused by fluctuations in the reference electrode potential--due to a varying concentration caused by back flow from the anode. To rule this out, a third set of experiments was run, this time also using chrono-galvanostatic control but simultaneously monitoring* the potential of the reference electrode against the upstream stainless steel pipe. Since the pipe is in contact with the solution, but in a position where there is no possibility of concentration fluctuations caused by the passage of current through the electrodes, any change in concentration at the reference electrode would have been reflected in a fluctuation of the reference electrode vs pipe potential. This potential remained practically undisturbed. The fluctuations observed were of the order of 3 to 5 mV, compared with cathode potential fluctuations 1 V in magnitude.

In summary, at the beginning of the hydrodynamic transition region fluctuations in the limiting current (for potentiostatic control), or of the potential at the limiting current (for galvanostatic control), are obtained while the potential of the reference electrode remains constant.

These current (potential) fluctuations are believed to be caused by the fluctuating concentration of the electrolyte next to the electrode surface. This explanation is at variance with the picture of the mass transfer occurring in a turbulent flow where the change in concentration occurs over a thin "mass transfer boundary layer" with a more or less

*Oscillograph Series 2300. Brush Instrument Division of Clevite Corporation, Cleveland, Ohio.

0 0 0 0 4 0 0 5 9 1 3

well defined thickness. Although this approach to turbulent mass transfer is of wide-spread use, and its pedagogical advantages are great, it can not be taken as a totally accurate picture of the turbulent transfer process.

One finds support for the conclusion that the observed phenomenon is due to concentration fluctuations in the vecinity of the cathode by comparing these results with those of Schraub and Kline.[43] Using hydrogen bubble evolution next to the wall of a flow channel they were able to observe "bursts of turbulent activity", the frequency of these bursts increasing with increasing Reynolds number. Along these lines one may postulate that at the beginning of the transition region the frequency of turbulent bursts is so small that the electrode surface is periodically swept alternatively by pockets of electrolyte with the bulk concentration and pockets with the concentration from the upstream region, giving rise to different values of the limiting current for a given potential. As the frequency of these bursts is increased, the electrode becomes unable to "see" the varying concentration field, and the limiting current that is obtained represents the average value for a mixed concentration field.

The fact that in turbulent flow the mass transfer rate in a region adjacent to the wall is not constant is of course inherent to the turbulent nature of the flow. Hanratty and his co-workers[47,48] have used point electrodes to study the fluctuation correlation in the axial and radial directions of a turbulent flow. What is remarkable is that this fluctuating nature of the flow could be detected when the

measurements are averaged over a fairly large surface. The limiting currents corresponding to Figs. III-1 were obtained over a surface measuring 5 hydraulic diam in the flow direction and 25 perpendicular to it. This type of fluctuations was reported by Ross and Badhwar [37a] but in their experiments it is not clear that the fluctuations were due to a hydrodynamic effect, and not to an artifact of the electrochemical system.

Even if one is to accept that in the very thin region next to the electrode the flow is never disturbed by the turbulence activity in the core of the flow, one still has to consider the possibility that the unstable nature of the core flow will periodically alter the thickness of that thin layer, and in this way lead to a fluctuating rate of transfer at the wall.

0 0 0 0 4 0 0 5 9 1 4

APPENDIX IV. GAS EVOLUTION

Of importance in ECM is the effect that the evolution of hydrogen at the cathode may have on the mass transfer process at the anode.

This Appendix is formed by the report "An Optical Study of Cathodic Hydrogen Evolution in High-Rate Electrolysis", published in the Journal of the Electrochemical Society 117(6), 839 (1970).

Most relevant to the present work are the following conclusions (Conclusions 4 and 5) of the above study:

"No plug phenomena seem to have been induced by the gas evolution under the conditions employed in the present study.

The influence of cathodic gas evolution on anodic processes such as mass transfer and current efficiency was usually very small."

UCRL-19064

AN OPTICAL STUDY OF CATHODIC HYDROGEN EVOLUTION IN HIGH RATE ELECTROLYSIS

Dieter Landolt[+], Raul Acosta, Rolf H. Muller and Charles W. Tobias

Inorganic Materials Research Division, Lawrence Radiation Laboratory and
Department of Chemical Engineering, University of California
Berkeley, California 94720

ABSTRACT

Hydrogen bubbles evolved cathodically under conditions encountered in electrochemical machining have been studied by stop-motion photography. Constant current densities up to 150 A/cm^2 and flow rates up to 2500 cm/sec have been employed with an experimental flow channel of 0.5 mm gap width. The observed bubble size decreased strongly with increasing flow rate and increased with increasing current density. At flow rates above 800 cm/sec, the bubble size was always below 20 μ, the smallest diameter resolved by the optical arrangement used. Less gas was evolved in nitrate than in chloride electrolytes under otherwise identical conditions. The hydrogen bubbles were usually confined to a region near the cathode. Voltage oscillations and electric breakdown coincided with the appearance of a new type of bubble.

[+]Present Address: University of California
Department of Engineering
Los Angeles, California 90024

0 0 0 0 4 0 0 5 9 1 5

UCRL-19064

INTRODUCTION

In electrochemical machining, metals are dissolved anodically at current densities in the order of 100 A/cm^2 or higher. Hydrogen gas is formed cathodically and must be transported away from the reaction zone by the electrolyte stream. This hydrogen may affect the electrolytic process in several ways: It may increase the ohmic resistance of the electrolyte, resulting in higher cell voltage and different local current distribution. It may be oxidized at the anode and thus, decrease the current efficiency of the metal dissolution process. It may form a continuous gas blanket at the cathode and thus, lead to sparking. It may accumulate in large bubbles, which extend over the entire inter-electrode gap, and thus, drastically affect mass transfer conditions at the anode. In order to obtain a better understanding of the relative importance of such phenomena, a photographic study of cathodically generated gas bubbles was initiated. During the course of this pursuit, somewhat related work has appeared in the literature.[1,2] In the present investigation, a more sophisticated optical arrangement has been employed and a better control and wider range of critical variables, such as current density and flow velocity have been employed in addition to the use of a well-defined flow system.

EXPERIMENTAL TECHNIQUE

The apparatus used has been described before.[3] It consisted of a rectangular flow channel cell of 8 mm width and 0.5 mm height. Its sidewalls were made of flat glass plates, which provided for the optical observation of the inter-electrode gap. The total channel length was 8.5 cm, the center of the electrodes was positioned 1 cm from the downstream end. The design of the flow cell provided for fully developed

velocity profiles at the electrodes. Flow rates up to 2500 cm/sec were employed, corresponding to inlet pressures in the order of 10 atm. Since most of the pressure drop occurs in the entrance length of the flow channel, the absolute pressure at the electrodes, even at the highest flow rate employed, was only about 2 atm. Although, under these conditions, the effect of pressure on the gas volume has to be taken into account, at flow rates up to 1000 cm/sec, where most observations were made, the absolute pressure at the electrodes was only 1 to 1.3 atm, and its effect on bubble size was negligible within the accuracy of the present measurements. The copper electrodes were 3.17 mm long in the flow direction and 0.53 mm wide. Before experiments, the electrode surfaces were mechanically polished with 1 μ diamond paste, cleaned with aqueous detergent and acetone and degreased by hydrogen evolution in aqueous caustic.

The optical arrangement is shown schematically in Fig. 1*: A commercial flash light source (A) of 0.5 μ sec flash duration** was used for illumination of the gas bubbles generated in the flow cell (B) in transmitted light mode. A camera (H) with open shutter and high speed film*** was attached to a microscope tube containing a 2x objective (C) (f = 48 mm, N.A. = 0.08) and a 10x eyepiece (E). A small circular

---

* Design considerations of the optical system will be discussed elsewhere in more detail.

** EG & G 594 microflash

*** Kodak SO 340

0 0 0 0 4 0 0 5 9 1 6

aperture (D) of 1.6 mm diameter, located in the rear focal plane of the objective (C) served as a telecentric stop.[4] The purpose of this device is to avoid variations in the apparent size of bubbles due to differing distances from the objective and to increase the depth of field. Unfortunately, the telecentric stop also reduces the speed and resolution of the objective, the latter being about 20 μ. In order to obtain a photographic distinction between the electrode surface and an adjacent, dense layer of gas bubbles, a pre-exposure in the absence of bubbles was made at reduced light intensity. In a typical experimental run, constant current was applied to the cell for a short period of time by switching the output of a constant current supply* from a dummy circuit to the cell circuit. A mercury relay, actuated by a pulse generator, was used for the switching. The circuit also served to trigger the flash light source after a pre-set time, which was chosen to correspond to the passage of 12 coulomb/cm^2. The current was switched back to the dummy load automatically after the total passage of 15 coulomb/cm^2. The charge passed between the start of an experiment and the moment the picture was taken, resulted in the evolution of about 1.5 cm^3 hydrogen (1 atm, 298°K) per cm^2 electrode. This was considered sufficient to establish steady state conditions with respect to gas evolution. During the experiments, current and potentials were recorded by means of a light beam oscillograph.

---

* Electronic measurements C-618

EXPERIMENTAL RESULTS

Bubble Size

Typical photographs obtained in 2 N KCl solution at different flow rates and current densities are given in Figs. 2 to 4. Figure 2 illustrates the influence of flow rate and cathode orientation on bubble size for a current density of 50 A/cm^2. An estimate of the size distribution of the bubbles for the same experiments is given in Fig. 5. These distributions were obtained by measuring the diameter of all the bubbles which were individually discernible in the whole inter-electrode gap, and determining the fraction in each size bracket of 25 microns width. The quantitative validity of the distributions given in Fig. 5 is limited for several reasons: (1) The number of measured gas bubbles (27-60) represent only part of the total gas volume and the differentiation between discernible and not discernible bubbles is subject to personal interpretation. (2) The variability of results in successive experiments probably requires a more sophisticated statistical evaluation. (3) Bubbles close to the cathode surface were usually not individually discernible and could, therefore, not be included in the count. (4) Bubbles smaller than 20 μ in diameter were below the optical resolution. Qualitatively, however, Fig. 5 illustrates not only the order of magnitude of cathodically generated bubbles, but it also shows the decrease in size with increasing flow rates: the median bubble diameters are 99, 69, and 35 μ for flow rates of 100, 200 and 400 cm/sec, respectively. It should also be noted that at the lower flow rates (below 400 cm/sec), a few large bubbles often existed in addition to a large number of smaller ones. It was observed during the experiments that these large bubbles were sticking to the cathode surface for prolonged periods of time while the smaller bubbles detached from areas in between. Figure 5 also

0 0 0 0 4 0 0 5 9 1 7

shows that the orientation of the cathode, i.e. whether it is facing up or down, has no systematic effect on size distribution, except at the lowest flow rate.

Figure 3 illustrates gas evolution at high flow rates. The size of the generated bubbles decreases rapidly with increasing velocity in this range and the size distribution becomes narrower, so that the previously observed co-existence of few large bubbles with smaller ones disappears. At flow rates of 800 cm/sec or higher, all individual bubbles were too small (below 20 μ) to be resolved photographically.

The effect of current density on bubble size is illustrated in Figs. 4 and 6. A clear increase in bubble size is observed with increasing current density under otherwise identical conditions: the median bubble diameters are 56, 78 and 99 μ for current densities of 5, 20 and 50 A/cm^2, respectively. These observations are in marked contrast to findings reported by Venczel,[5] who studied gas evolution at vertical electrodes in stagnant solutions and reported a decrease in bubble size with increasing current density. The discrepancy might possibly be explained by the different modes of convection. A bubble may be assumed to detach from the surface when external forces, such as gravity or friction with the moving liquid, become larger than the normal conponent of the surface tension. Since in a stagnant solution, the rate of stirring is increased when more gas is generated, higher current densities may lead to an earlier detachment of gas bubbles. In our experiments, on the other hand, local stirring was mainly due to the hydrodynamic flow and was, therefore, almost independent of current density. A decrease, rather than an increase, in bubble size with increasing current density would also be expected from the work of Kabanov and Frumkin.[6] They showed that the contact angle, which

determines the normal component of surface tension, depends on electrode potential. For very slow hydrogen evolution on mercury, smaller contact angles and, hence, smaller bubbles were observed at increasingly negative potentials.

Force balances have been applied to the prediction of bubble size in forced convection boiling.[7] Such a force balance for an individual bubble may be formulated as

$$F_\sigma = F_i + F_b \qquad (1)$$

where F_σ is the surface tension force which holds the bubble on the electrode, F_i is the inertia force of the electrolyte acting on the bubble and F_b is the buoyancy force of the bubble. The latter can be neglected at high flow velocities. According to Tong[7] a model of this kind predicts a decrease in bubble size with the square of the flow velocity. Such a dependence is at least qualitatively consistent with the present results. Relation (1) does, however, not account for the influence of current density and the wide distribution of bubble diameters observed at low flow rates. This distribution is at least partly due to the fact that the presence of other bubbles on the surface leads to locally varying flow conditions. Considering the fact that not even the dynamics of a single bubble, growing in a laminar velocity field, has been analyzed, no attempt has been made here to give a more detailed account of the vastly more complex case of multiple bubble dynamics in turbulent flow. Additional experimental studies should include the time-dependence of bubble growth for a more detailed description of gas evolution under the present conditions in turbulent flow. Glas and Westwater[8] have investigated electrochemical gas evolution in stagnant solutions by high speed cinematography. They found two growth stages; an early rapid growth period, associated with bubble diameters of up to

about 50μ, followed by a slow period. Theoretical aspects of growth mechanisms have been discussed by Cheh,[9] who applied mass transfer considerations to predict growth rates in the slow (asymptotic) growth period. No theoretical models exist at present which predict growth rate in the rapid growth period. Since, in our study, the bubble size was often smaller than 50μ, growth rate and residence time on the cathode surface could not be estimated on theoretical grounds.

Thickness of Two Phase Region

Figs. 2 to 4 illustrate the observation that the gas bubbles are not dispersed uniformly throughout the gap, but usually occupy a region near the cathode. At flow rates above 100 cm/sec, the thickness of this two-phase region is the same whether the cathode faces up or down. This behavior is to be expected, since at higher flow rates a gas bubble, unless it is very large, is swept away from the inter-electrode gap too fast to be affected by buoyancy. From Stoke's law, which may be applied to bubbles of less than 1 mm diameter,[10] the steady state velocity due to buoyancy can be described by eq. (2).

$$v = \frac{g \rho d^2}{18\eta} \qquad (2)$$

where g = gravitational constant, ρ = difference in density of gas and liquid, d = bubble diameter, η = viscosity of liquid. Assuming an electrolyte flow velocity of 400 cm/sec and a bubble diameter of 50μ, the vertical distance traveled by the bubble due to gravity during the time needed to pass over a 3 mm long electrode is only 1.2μ.

In order to account for the observed thickness of the two-phase region, unusually high velocities perpendicular to the flow direction are required. In Fig. 3c for example (100 A/cm^2, 1000 cm/sec), bubbles are found up to a distance of approximately 0.3 mm from the cathode surface. A bubble moving steadily outward from the leading edge of the electrode would need an average velocity perpendicular to the cathode of 100 cm/sec to reach this position at the downstream end of the electrode. This motion away from the cathode surface is aided by the turbulence in the liquid. Such an effect is suggested by the irregular shape of the two-phase region, which can show large variations in local thickness (Fig. 3). It is interesting to note, however, that the average thickness seems to increase little downstream from the middle of the cathode. If turbulent mixing were the only mechanism determining the spreading of the two-phase region, we would rather expect a steady increase of its average thickness in the flow direction. It is, therefore, possible that other mechanisms contribute to the dispersion of gas bubbles. An example is the "rapid fire mechanism" mentioned by Glas and Westwater,[8] who observed that in stagnant solution, bubbles were frequently ejected from the electrode at a high velocity. This phenomenon is, at present, not well understood. The relatively smaller increase of the two-phase region in the downstream part might also be ascribed to a lower current density in this region, caused by the higher gas fraction and the associated higher ohmic resistance in the electrolyte. Dissolution of gas in the electrolyte furnishes another possible explanation for the same phenomenon. Indeed, a simple estimation shows that, under most conditions, all the gas generated could be dissolved in

0 0 0 0 4 0 0 5 9 1 9

the total electrolyte volume passing through the gap. For example, assuming a current density of 100 A/cm^2, 8 x 10^{-6} moles of hydrogen are produced per second in our cell, while, at a flow rate of 1000 cm/sec, 40 cm^3 of electrolyte are flowing through it. A homogeneous dissolution of all the generated hydrogen would result in a concentration of 2 x 10^{-4} mole/liter, which is of the same order as the saturation concentration of hydrogen in potassium chloride solutions.[11] However, the direct dissolution of all cathodically generated gas without the formation of bubbles is, in general, not possible because the concentration gradients available under typical flow conditions are too small to account for the transport of dissolved hydrogen by convective diffusion. This is the case even under the assumption of a 1000 fold supersaturation at the electrode surface.

A rapid dissolution of initially formed gas bubbles could provide an alternate route to a homogeneous solution. This process would also affect the measured gas bubble diameters. Such a re-dissolution of gas bubbles would be similar to the behavior of vapor bubbles generated in a supercooled liquid under forced convection. Gunther[12] has shown that such bubbles became smaller and eventually disappeared upon moving downstream. The time required to dissolve 50% of the volume of a bubble of 50μ diameter can be estimated as follows: If we assume saturation concentration of the gas at the gas-liquid interface under constant pressure, and zero gas concentration in the bulk solution, the concentration difference driving force will be given by the saturation concentration, say 5 x 10^{-4} mole/liter. For a constant mass flux per unit area of a spherical bubble, the decrease in volume may then be expressed by eq. (3)

$$\frac{dV}{dt} = - A\ k\ C_{sat}\ V^{2/3} \qquad (3)$$

with $A = \frac{RT}{P}\ 4\pi\ (\frac{3}{4\pi})^{2/3}$, C_{sat} = saturation concentration, k = mass transfer coefficient (cm/sec), V = bubble volume. Integration leads to eq. (4)

$$3(V^{1/3} - V_o^{1/3}) = A\ k\ C_{sat}\ t \qquad (4)$$

where V_o = initial bubble volume. The time $t_{1/2}$ in which the volume is reduced to 1/2 V_o is

$$t_{1/2} = \frac{2.38\ V_o^{1/3}}{A\ k\ C_{sat}} \qquad (5)$$

With an arbitrarily assumed mass transfer coefficient of 10^{-1} cm/sec* one obtains $t_{1/2} \approx 1$ sec for 1 atm, 298°K. This time is almost four orders of magnitude larger than the residence time of a bubble moving at 1000 cm/sec between the electrodes (3×10^{-4} sec). The redissolution of gas is, therefore, too slow to produce a homogeneous gas solution between the electrodes or even to measurably affect the diameter of bubbles in our photographs.

---

* Since the relative motion between bubble and solution is not known, the mass transfer coefficient k has to be assumed arbitrarily. The value chosen is a maximum guess. It corresponds to the figure estimated for the electrode-solution interface at the highest flow rates employed.[3]

0 0 0 0 4 0 0 5 9 2 0

Influence of Electrolyte

Fig. 7 illustrates the surprising observation that less gas was produced at the cathode in KNO_3 than in KCl solutions, under otherwise identical conditions. The relative volume of the two-phase region in the interelectrode gap, shown in Fig. 8, has been obtained by planimetry of the areas occupied by the dispersed gas in the photographs. Since the solubility of hydrogen is about the same in both electrolytes,[11] the observed difference must be due to other than differences in solubility. For example, the same amount of hydrogen could appear to be smaller in nitrate solutions due to a more finely dispersed form. A more likely explanation is that, due to the reduction of nitrate at the cathode, only part of the current is used for hydrogen evolution. In the present flow apparatus, the total amount of evolved hydrogen could not be determined, but some experiments were performed in stagnant solutions of KNO_3 and KCl at 5 A/cm^2. They confirmed that a much smaller volume of hydrogen was produced in nitrate than in chloride solution. A more quantitative investigation of cathodic reactions in nitrate solutions has been initiated. The effect of different electrolytes on the amount of cathodically formed gas was further investigated by use of chlorate and sulfate solutions. Both, photographs taken in the flow system and volumetric measurements in stagnant solutions, indicated that, within the experimental accuracy, the same amount of gas was generated in these electrolytes as in the chloride solution.

Potential measurements under high current density conditions are dominated by large ohmic drops in the electrolyte between the working electrode and the tip of the reference electrode capillary.[3] The apparent cathode potentials, thus determined at constant current density,

provide an indirect measure of electrolyte conductivity and, consequently, gas volume fraction. Apparent cathode potential measurements are given in Fig. 9. It can be seen that a rapid increase of potential with decreasing flow rate, indicating the presence of a substantial volume fraction of gas in the electrode gap, occurs at a higher flow rate in chloride than in nitrate solutions. This shift is consistent with the evolution of a larger gas volume in the first electrolyte.

DISCUSSION

Ohmic Resistance

Since one of the purposes of this study was to define the effect of cathodically generated gas on the electrolyte resistance, the question remains, under which conditions this effect is significant. For the controlled current operation of these experiments, an increase in the ohmic resistance of the electrolyte results in an increase in overall cell voltage. A marked increase in cell voltage, which is observed with decreasing flow rate in 2N KCl (Fig. 10), can be attributed primarily to cathodic phenomena, since anode potentials did not vary by more than 1 to 4 volts for different flow rates. This increase in cell voltage occurs at flow rates which rise with increasing current density and parallels the onset of voltage fluctuations. Although the qualitative influence of gas bubbles on cell voltage is thus strongly indicated, it has not been possible to derive a simple quantitative relation between the gas volume fraction and the cell voltage, which would hold for different current densities. The difficulty may, in part, be due to the fact that the gas was not homogeneously dispersed, neither in the direction normal nor parallel to the electrodes. The bubbles which have been observed to stick to the cathode

0 0 0 0 4 0 0 5 9 2 1

surface at flow rates below 400 cm/sec further complicate the situation. Cole and Hopenfeld[1] have also investigated the influence of gas bubbles on cell voltage under ECM conditions. They accounted for the effect of the dispersed gas on the ohmic resistance of the electrolyte by using a relation given by De La Rue and Tobias.[13] By making certain simplifying assumptions about the two phase region and by adjusting one empirical parameter, they obtained agreement between theoretical and experimental results. The present study suggests, however, that such a simple treatment is not valid for the range of conditions employed here.

Sparking

The formation of continuous gas blankets on vertical wire electrodes in sulfuric acid, at current densities of 6-8 A/cm^2, has been described by Kellogg.[14] The formation of his gas blanket coincided with a drastic increase in surface temperature and a sharp drop in current. A similar phenomenon also is known to occur in heat transfer under forced convection conditions, where formation of vapor films leads to a sharp reduction in heat flux (burn out, critical heat flux).[15] It was, therefore, of interest to see whether, under ECM conditions, similar gas films are formed and whether they may lead to sparking and electrical breakdown. As long as a sufficiently high flow rate was maintained no such phenomena were observed in the present experiments, even at current densities much higher than those employed by Kellogg. Upon decreasing the flow rate, however, large voltage fluctuations and eventual sparking occurred. These fluctuations, indicated by the broken line in Fig. 10, soom became so large as to impede any measurement upon further reduction of flow rate. A close parallelism between oscillations in cathode potential and cell voltage confirmed the

cathodic origin of the oscillations. The onset of these fluctuations coincided with the appearance of a different type of gas bubble characterized by a large size and odd shape. Picture (a) in Fig. 3 is typical for this situation. It appears that, under these conditions, small individual bubbles are no longer generated and continuous gas pockets may cover a sizeable fraction of the cathode surface. Although an actual sparking event could not be photographed, it is possible that such a breakdown coincides with an instantaneous complete coverage of the cathode. The gas volume fraction, at which uncontrolled fluctuations set in, has been estimated on the basis of current density and flow rate (neglecting gas dissolution) to be approximately 0.4 at 100 and 150 A/cm^2.

Anode Reactions

Voltage oscillations in constant current electrolysis may also originate at the anode. While a detailed discussion of such phenomena is beyond the scope of the present report, it is interesting to note that the anodic oscillations have been observed under certain conditions with several electrolytes, most notably sodium chlorate. Figs. 12a to c illustrate how the anodic contribution to fluctuations in overall cell voltage U increases in the electrolyte series, chloride, nitrate, chlorate, while the cathodic contribution remains about the same (except for a slight reduction in nitrate, due to the smaller gas volume). Of particular interest are the usually well behaved periodic oscillations which originate at the anode (as indicated by the apparent anode potential e_A in Fig. 12c) in chlorate solution. The frequency of these oscillations depended primarily on current density and was only slightly affected by changes in flow rate. Typical frequencies were 130 and 300 cps at 50 and 100 A/cm^2, respectively. The voltage fluctuations which originate at the cathode were irregular. Their

0 0 0 0 4 0 0 5 9 2 2

frequency was much higher (mostly over 2000 cps) and the amplitude depended strongly on flow rate as well as current density. Periodic phenomena at the anode can be related to the formation of solid films,[3,16] and Fig. 11 shows indeed how solid dissolution products are being removed from the anode surface, (together with a small amount of gas). Similar, but less pronounced shedding of solid reaction products has been observed in sulfate and nitrate solutions.

The photographic pictures obtained in this study also demonstrate that, under the conditions of a previous investigation of anodic phenomena,[3] gas bubbles were usually confined to the vicinity of the cathode. In view of the low solubility of hydrogen gas, it can be concluded that any fraction of the total anodic current possibly used for the oxidation of hydrogen has been negligible. The distribution of gas bubbles in the inter-electrode gap gave no indication of the occurrence of plug flow phenomena, which could drastically affect mass transfer at the anode.

SUMMARY AND CONCLUSIONS

The present study was aimed at providing visual information on cathodic gas evolution during high rate metal dissolution, in order to determine the importance of cathodic phenomena on ohmic electrolyte resistance, anode reactions and sparking. Qualitative rather than quantitative conclusions can be drawn from the results:

1. The size of cathodically generated gas bubbles depends on current density as well as flow rate. At flow rates above 400 cm/sec, only very small bubbles (few microns diameter) were generated and immediately removed by the electrolyte stream.
2. A substantially smaller gas evolution in nitrate than in

chloride solutions has been observed. It indicates the occurrence of cathodic reactions other than hydrogen evolution in the former solution.

3. The influence of cathodically generated gas bubbles on the ohmic cell resistance was very small at flow rates above approximately 1000 cm/sec, for all current densities employed (up to 150 A/cm^2). At lower flow rates, this influence can be substantial. Models which are based on a uniformly distributed two phase region and, among other simplifications, neglect the residence time of gas bubbles on the cathode surface, did not predict valid electrolyte resistances.
4. No plug flow phenomena seem to have been induced by the gas evolution under the conditions employed in the present study.
5. The influence of cathodic gas evolution on anodic processes such as mass transfer and current efficiency was usually very small.
6. At insufficient flow rates, strong fluctuations in cell voltages were observed, which coincided with the formation of gas patches at the cathode and which eventually led to electric breakdown. The effect was more pronounced in chloride than in nitrate solutions, in agreement with the fact that less gas was generated in the latter solutions under otherwise identical conditions.
7. In the absence of a theoretical model describing even the most simple single bubble dynamics in a flow field, additional experimental observations are needed to gain even a qualitative

0 0 0 0 4 0 0 5 9 2 3

insight into the factors which determine growth, detachment and dispersion of gas bubbles generated at high current densities and electrolyte flow rates in narrow gaps.

ACKNOWLEDGEMENT

This work was conducted under the auspices of the U.S. Atomic Energy Commission.

REFERENCES

1. J. Hopenfeld and R. R. Cole, J. Eng. Ind. 88, 455 (1966).
2. J. Hopenfeld and R. R. Cole, J. Eng. Ind. 91, 755 (1969).
3. D. Landolt, R. H. Muller, and C. W. Tobias, J. Electrochem. Soc. 116, 1384 (1969).
4. G. H. Cook in: Applied Optics and Optical Engineering, R. Kingslake, ed., Vol. 3, p. 118, John Wiley and Sons, New York, 1965.
5. J. Venzcel, Ph.D. Thesis no. 3019, ETH, Zurich, 1961.
6. B. Kabanov and A. Frumkin, Z. Phys. Chem. A 165, 433 (1933).
7. L. S. Tong, Boiling Heat Transfer and Two Phase Flow, p. 138, John Wiley and Sons, New York, N. Y., 1965.
8. J. P. Glas and J. W. Westwater, Int. J. Heat Mass Transfer 7, 1427 (1964).
9. H. Y. Cheh, Ph.D. Thesis, University of California, Berkeley; UCRL-17324 (1967).
10. F. H. H. Valentin, Absorption in Gas Liquid Dispersions, E. F. N. Spon, Ltd., London 1967.
11. International Critical Tables, 3, 272 (1929).
12. F. C. Gunther, Trans. ASME 73, 115 (1961).
13. R. E. De La Rue and C. W. Tobias, J. Electrochem. Soc. 106, 827 (1959).
14. H. H. Kellogg, J. Electrochem. Soc. 97, 133 (1930).
15. S. Levy, in Lecture Series on Boiling and Two Phase Flow for Heat Transfer Engineers, H. A. Johnson, Ed., University of California Extension, Berkeley and Los Angeles, 1965; p. 81.
16. K. Kinoshita, Ph.D. Thesis, University of California, Berkeley, UCRL-19051, Sept. 1969.

0 0 0 0 4 0 0 5 9 2 4

FIGURE CAPTIONS

Fig. 1. Optical Arrangement for high speed photography of gas bubbles

A. Light source (flash)

B. Flow channel cell

C. Microscope objective

D. Telecentric stop

E. Microscope eyepiece

F. Beam splitting prism

G. Magnifier for visual observation

H. Camera film plane

Fig. 2. Influence of flow rate and cathode orientation on gas evolution in 2 N KCl. Current density 50 A/cm^2, electrode gap 0.5 mm.

a. flow rate 100 cm/sec cathode facing down

b. flow rate 200 cm/sec cathode facing down

c. flow rate 400 cm/sec cathode facing down

d. flow rate 100 cm/sec cathode facing up

e. flow rate 200 cm/sec cathode facing up

f. flow rate 400 cm/sec cathode facing up

Fig. 3. Influence of flow rate on cathodic gas evolution in 2 N KCl. Current density 100 A/cm^2, cathode facing up.

a. flow rate 400 cm/sec

b. flow rate 600 cm/sec

c. flow rate 1000 cm/sec

d. flow rate 2500 cm/sec

Fig. 4. Influence of current density on cathodic gas evolution in 2 N KCl. Flow rate 100 cm/sec, cathode facing down.

Fig. 4., cont.

a. Current density = 5 A/cm^2

b. Current density = 20 A/cm^2

c. Current density = 50 A/cm^2

Fig. 5. Distribution of cathodic gas bubble diameters in 2 N KCl. 50 A/cm^2, 100, 200 and 400 cm/sec. Total number of bubbles measured 31, 43 and 50 respectively, for cathode facing up (---) and 27, 32, 60 respectively, for cathode facing down (——). (Counts incomplete in range 0-25μ, due to lack of resolution below 20μ).

Fig. 6. Distribution of cathodic gas bubble diameters in 2 N KCl. Flow rate 100 cm/sec, current density 5, 20 and 50 A/cm^2. Total number of bubbles measured 47, 47 and 31, respectively for cathode facing up (---) and 37, 42 and 27, respectively, for cathode facing down (——). (Counts incomplete in range 0-25μ, due to lack of resolution below 20μ).

Fig. 7. Cathodic gas evolution at 100 A/cm^2 in 2 N KNO_3 and 2 N KCl, cathode facing down.

a. KCl, flow rate 400 cm/sec

b. KCl, flow rate 800 cm/sec

c. KNO_3, flow rate 400 cm/sec

d. KNO_3, flow rate 800 cm/sec

Fig. 8. Apparent volume fraction of interelectrode gap occupied by two phase region (gas-electrolyte mixture).

○ 2 N KCl, 400 cm/sec

● 2 N KCl, 800 cm/sec

Δ 2 N KNO_3, 400 cm/sec

▲ 2 N KNO_3, 800 cm/sec

Fig. 9 Effect of gas evolution in different electrolytes on apparent cathode potentials, measured vs. sat. calomel with capillary upstream from the electrode. Current density 100 A/cm^2, cathode facing up.

Δ 2 N KCl

□ 2 N KNO_3

--- amplitude range of voltage fluctuations

Fig. 10. Effect of gas evolution in 2 N KCl at different current densities on cell voltage.

● cathode facing down

O cathode facing up

--- amplitude range of voltage fluctuations

Fig. 11. Anodic dissolution products generated in 2 N $NaClO_3$ at 50 A/cm^2 and 100 cm/sec. Cathode facing up.

Fig. 12. Typical recorder traces of cell voltage U, current I, apparent anode potential e_A and apparent cathode potential e_C. 50 A/cm^2, 400 cm/sec.

a. 2 N KCl

b. 2 N KNO_3

c. 2 N Na ClO_3

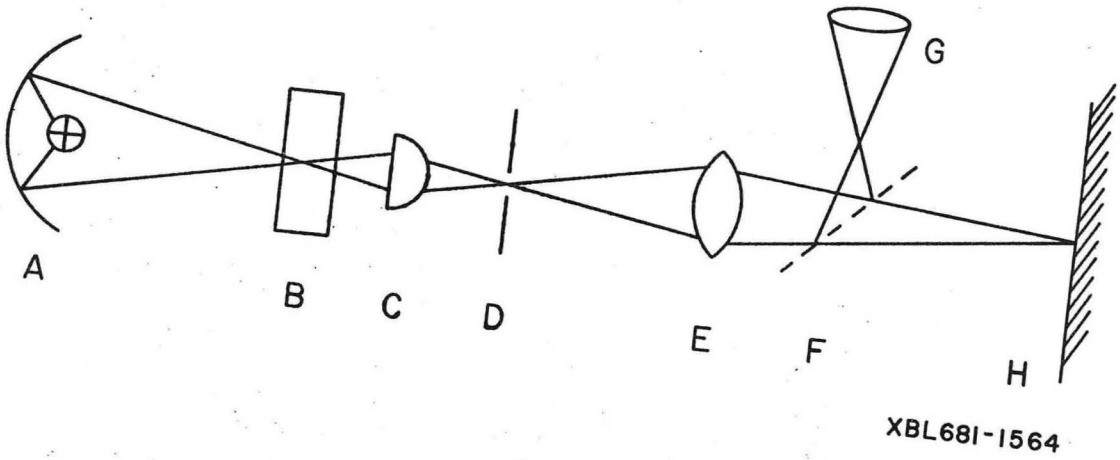

Fig. 1

0 0 0 0 4 0 0 5 9 2 5

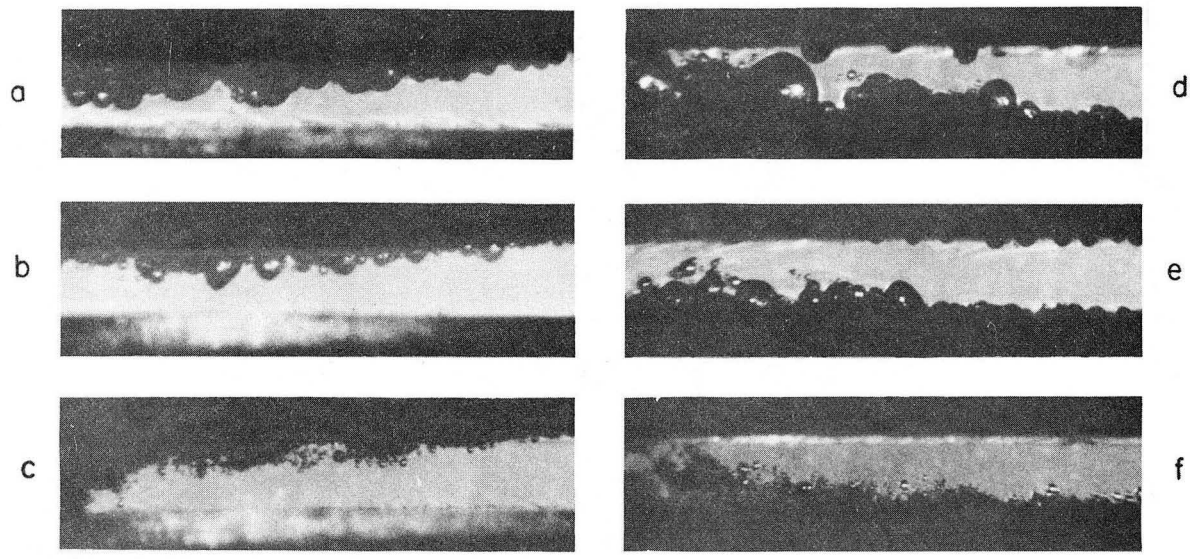

XBB 699-5795

← Flow

Fig. 2

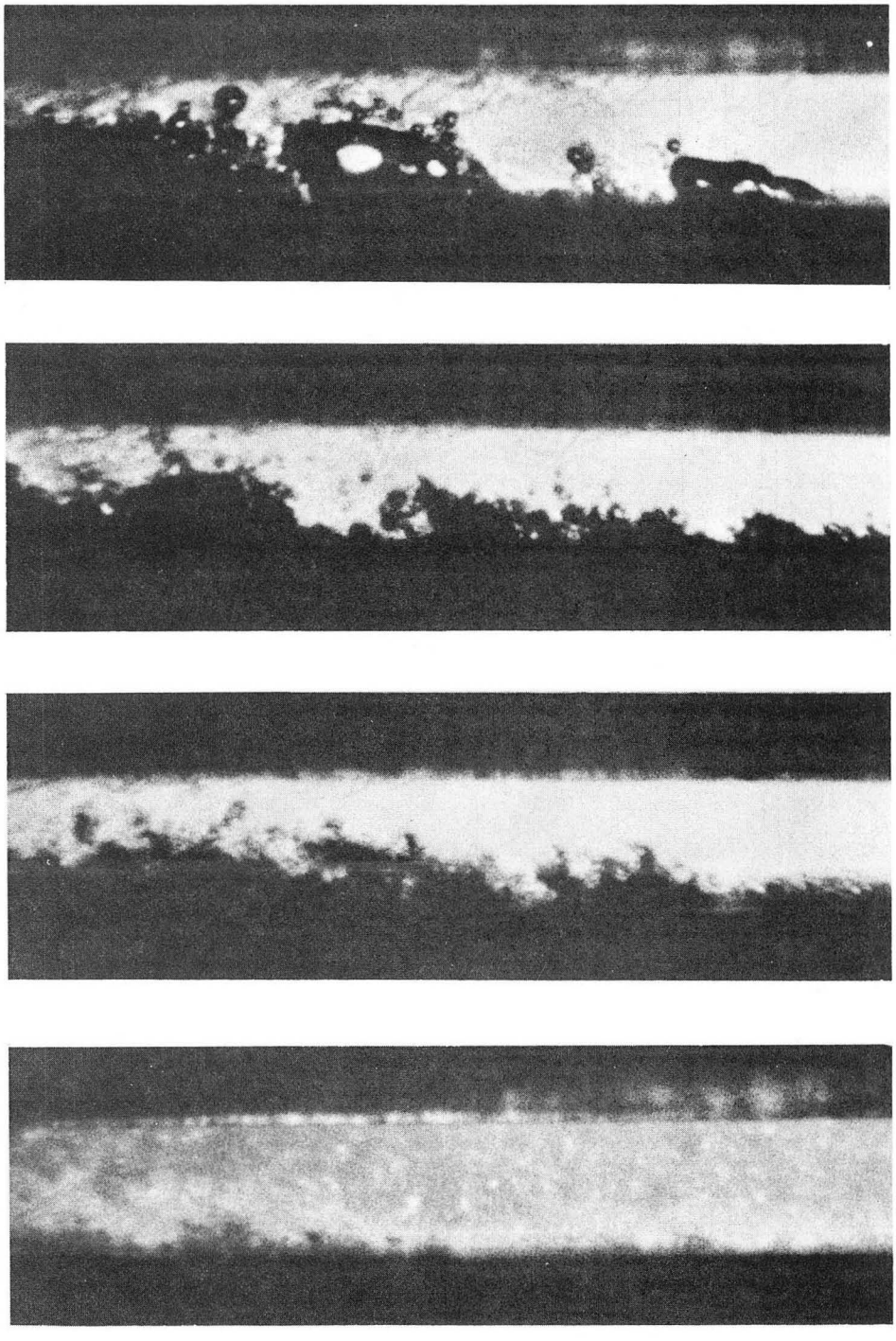

Fig. 3

0 0 0 0 4 0 0 5 9 2 6

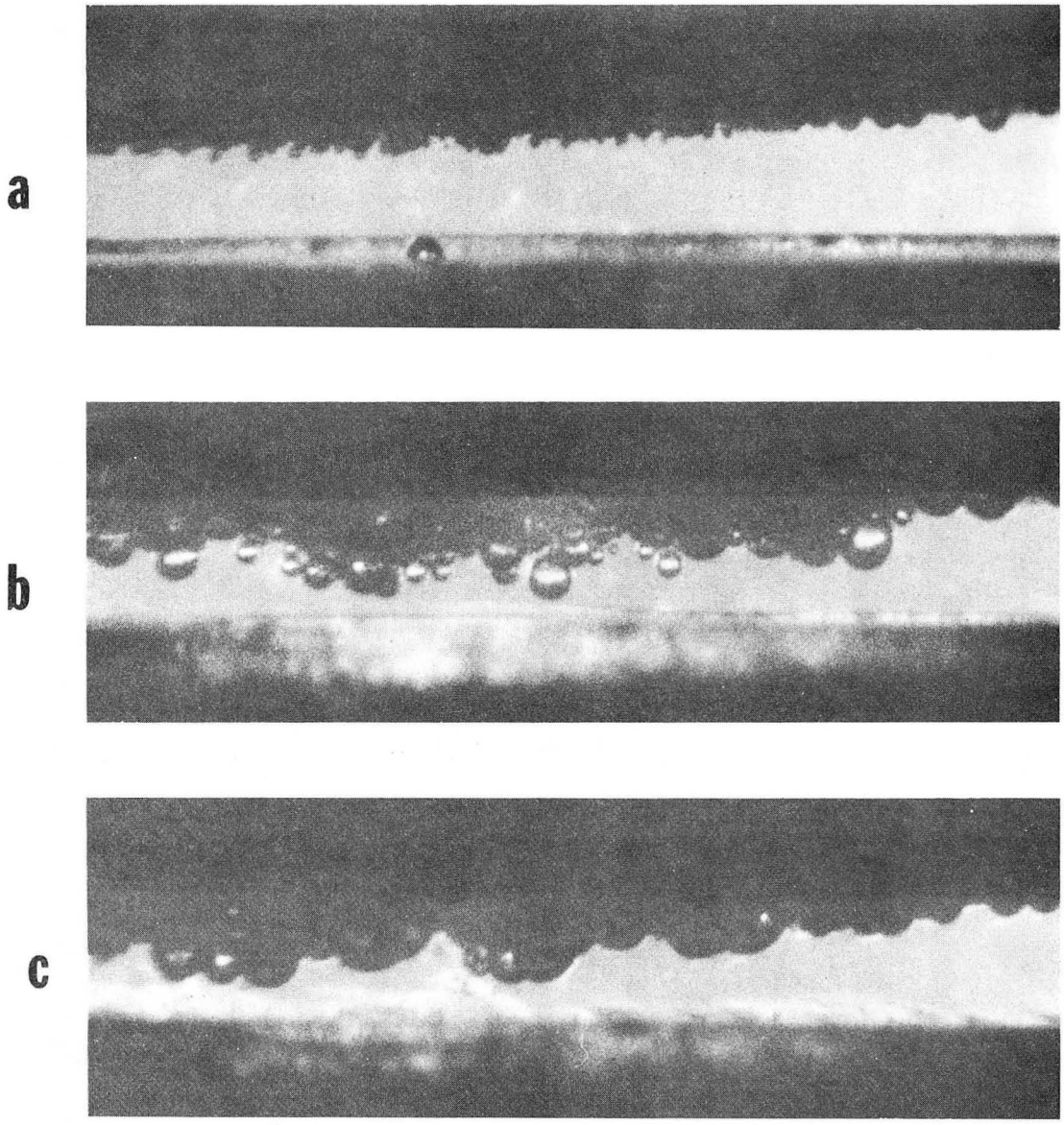

XBB 6912-7685

Fig. 4

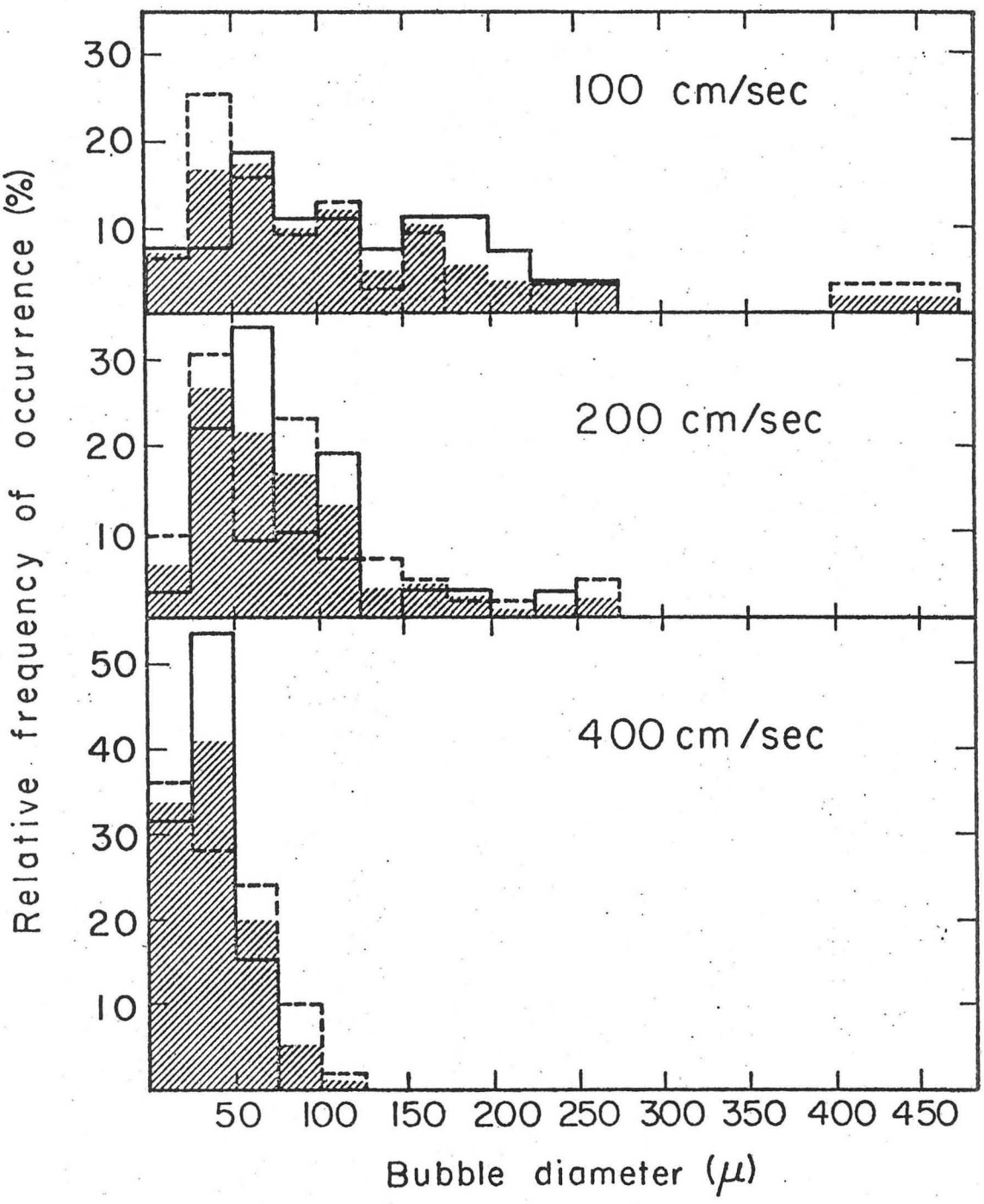

XBL698-3569

Fig. 5

0 0 0 0 4 0 0 5 9 2 7

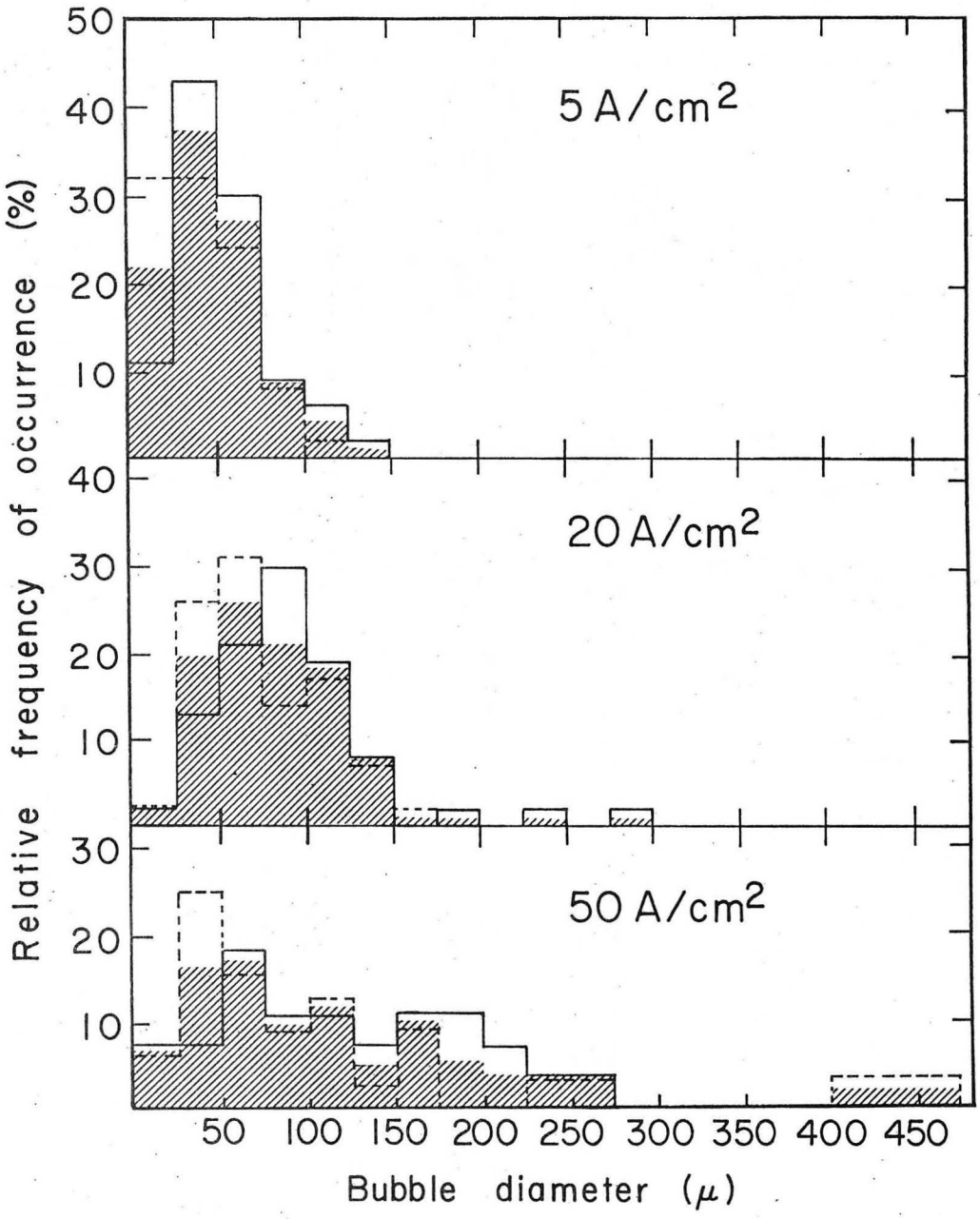

XBL6911-6205

Fig. 6

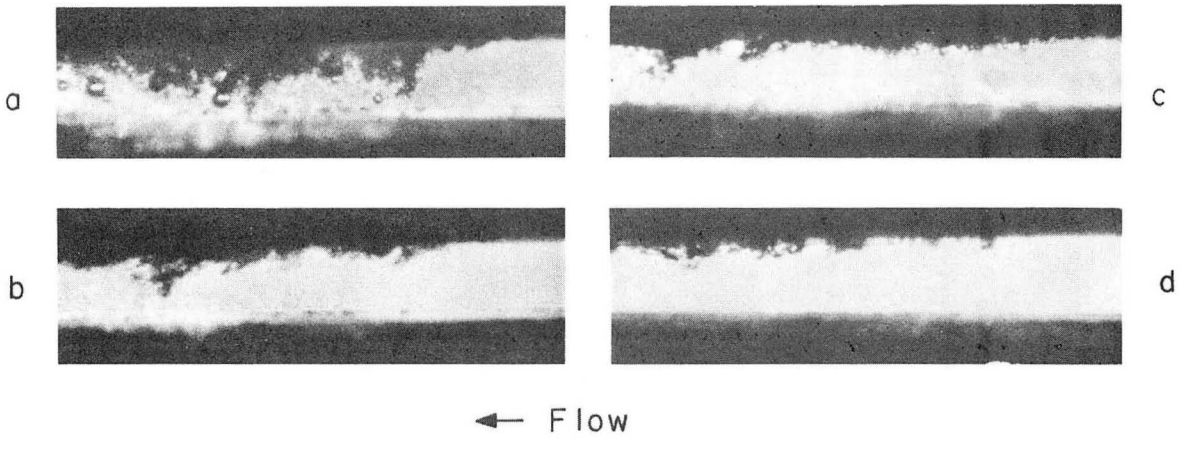

Fig. 7

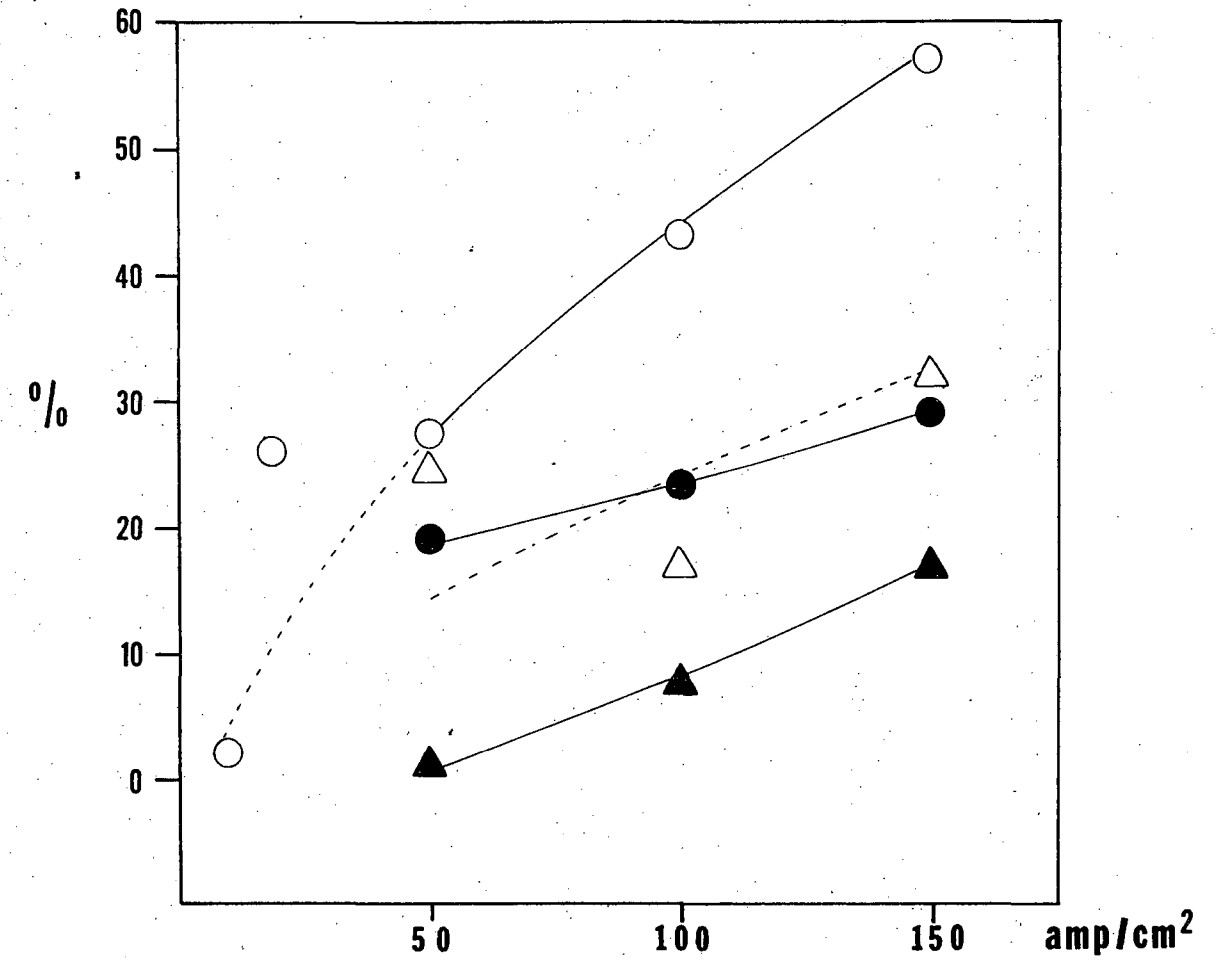

XBL 6911-6512

Fig. 8

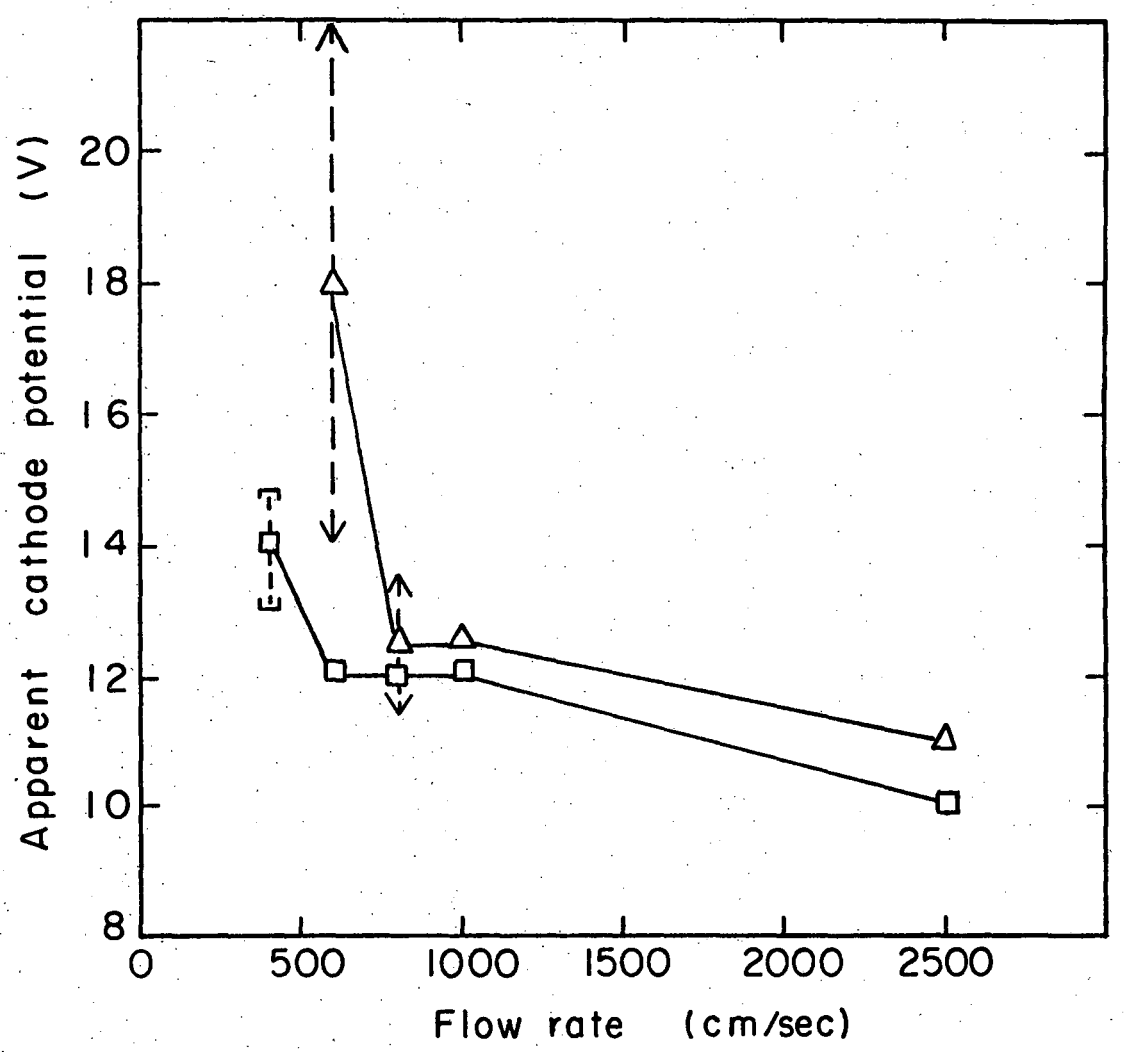

XBL 698-3570-A

Fig. 9

0 0 0 0 4 0 0 5 9 2 9

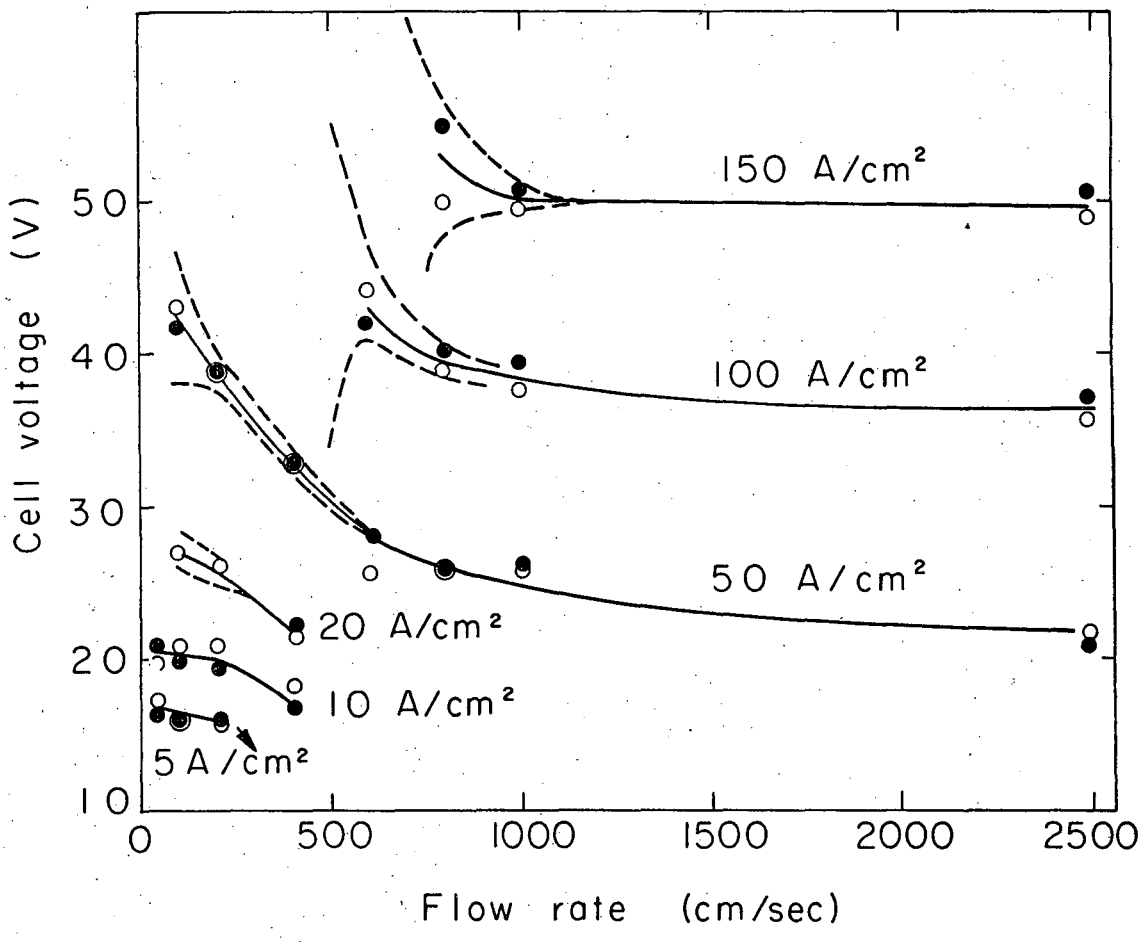

XBL 698 - 3571

Fig. 10

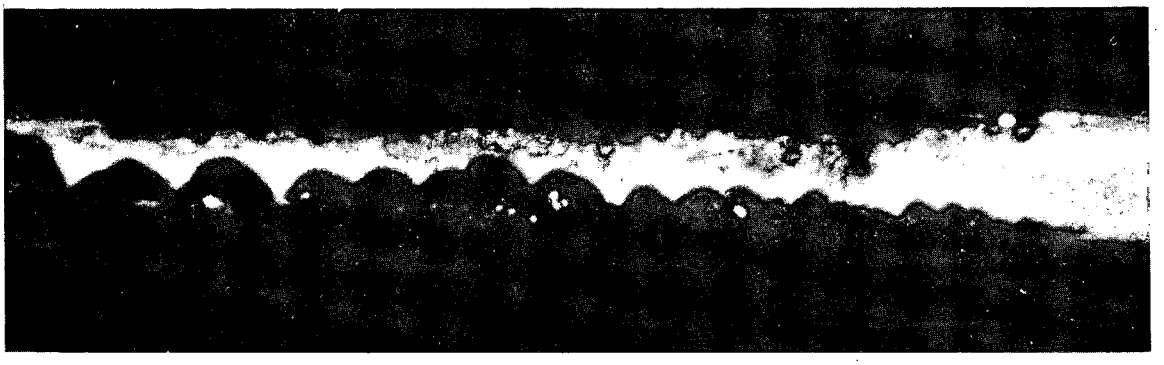

XBB 699-5798

← Flow

Fig. 11

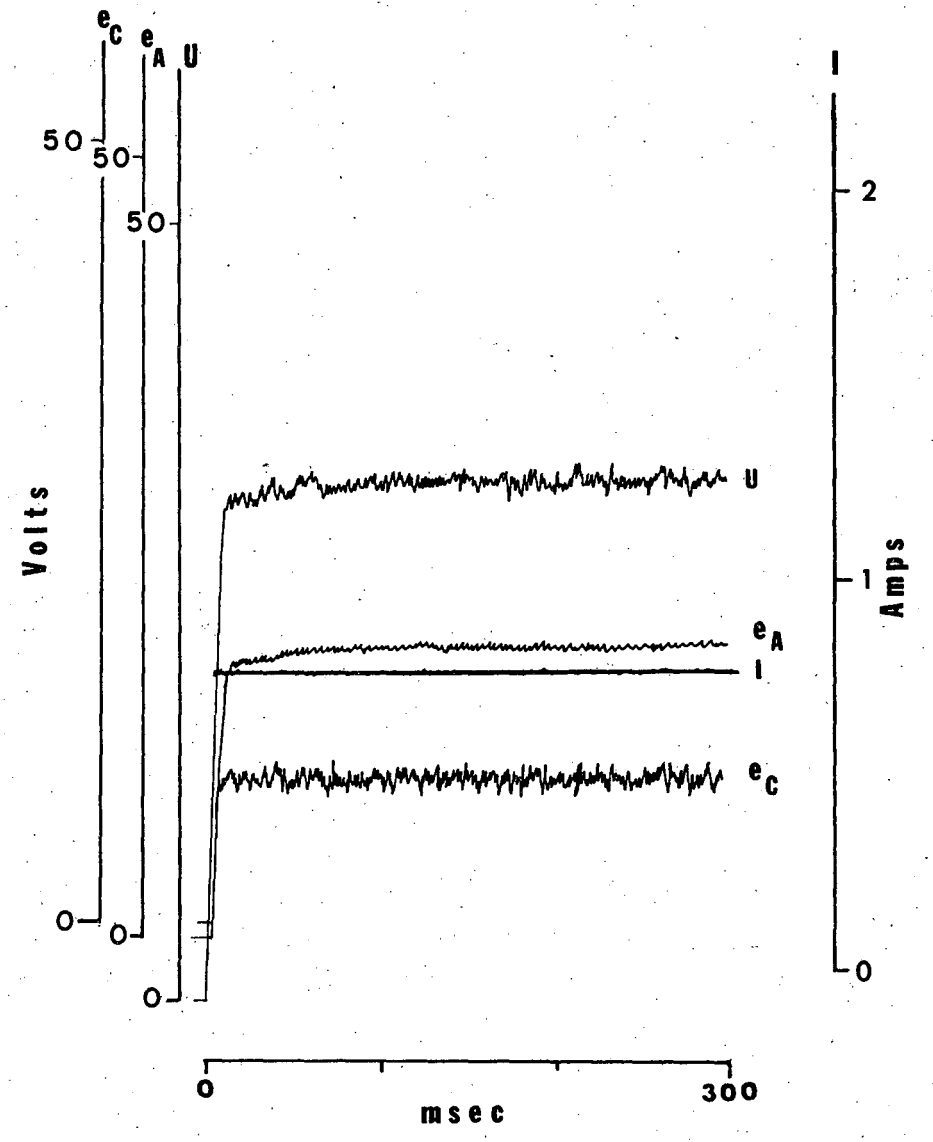
e_C
e_A
U
I
50
50
50
2
Volts
U
1
Amps
e_A
I
e_C
0
0
0
0
0
300
msec
XBL698-3565

Fig. 12 a

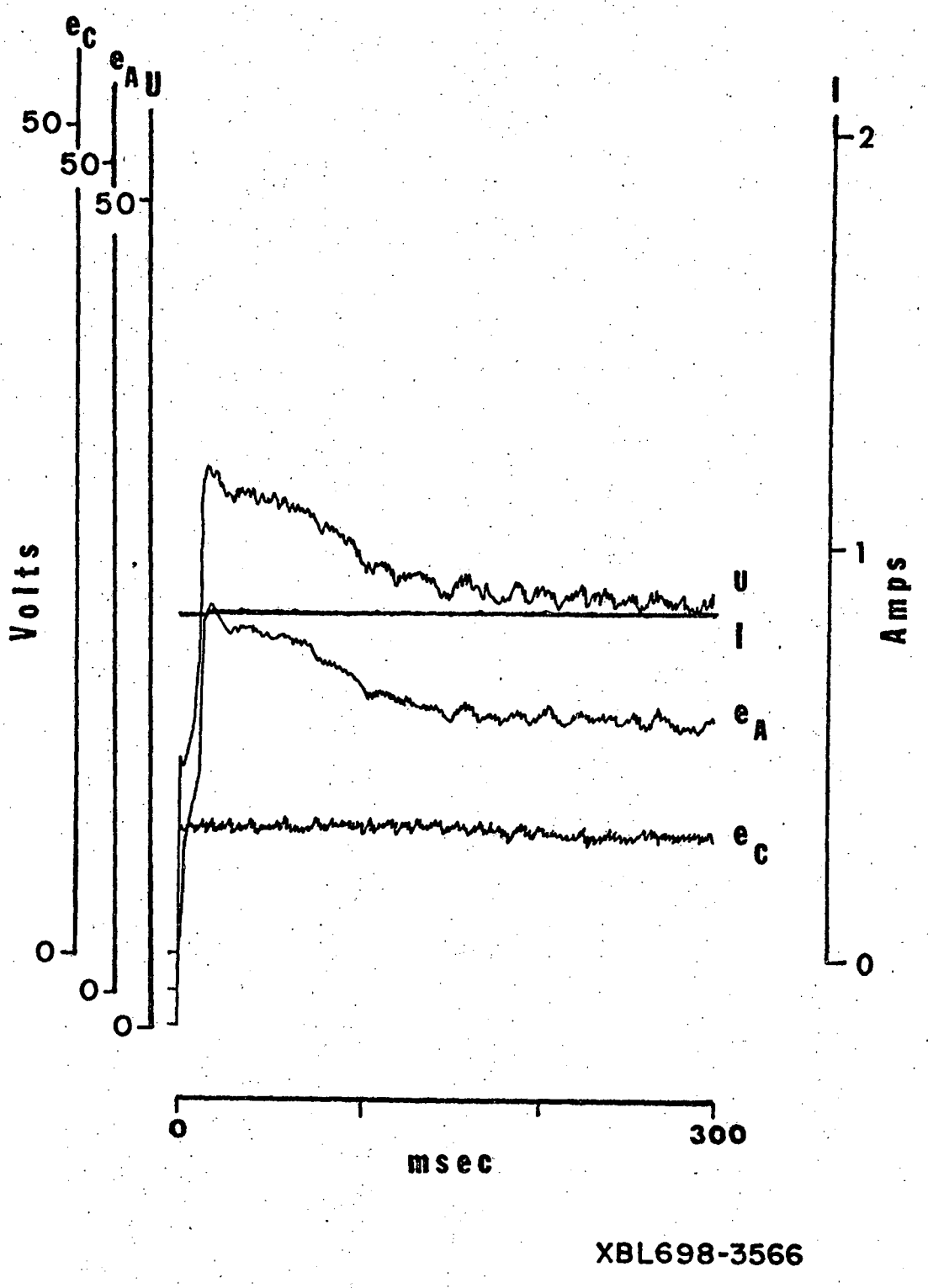
e_C
e_A
U
50
50
50
Volts
0
0
0
I
2
1
0
Amps
U
I
e_A
e_C
0
300
msec
XBL698-3566

Fig. 12b

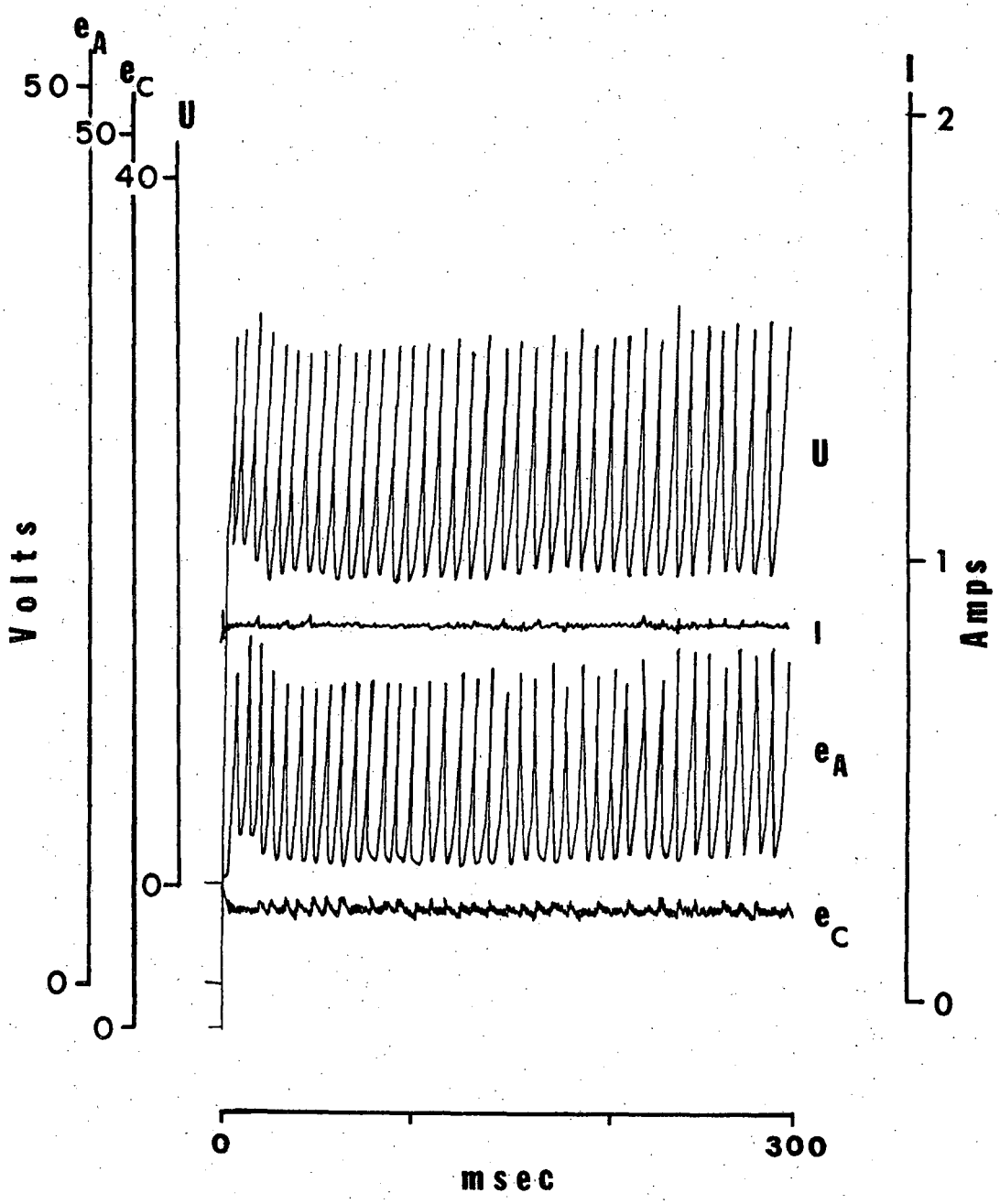
e_A
50
e_C
50
U
40
0
0
Volts
U
I
e_A
e_C
I
2
1
0
Amps
0
300
msec
XBL698-3567

Fig. 12c

REFERENCES

1. E. Battista and H. C. Perkins, Intl. J. Heat and Mass Transfer 13, 1063 (1970).

2. R. B. Bird, W. E. Stewart and E. N. Lightfoot, Transport Phenomena (Wiley and Sons, Inc, 1960).

3. A. J. L. P. M. Boeffard, Ionic Mass Transport by Free Convection in a Redox System, M. S. Thesis, University of California, Berkeley (1966).

4. W. C. Brennan, Mass Transfer in Turbulent Pipe Flow. The Effect of Surface Roughness, M. A. Sc. Thesis, Department of Chemical Engineering, University of Toronto (1963).

5. F. S. Bromfeld, The Hydrodynamic Entry Length in Rectangular Channels, Ph. D. Thesis, University of Washington (1964).

6. C. H. Chilton and A. P. Colburn, Ind. Eng. Chem. 26, 1183 (1934)

7. G. Comte-Bellot, Contribution to Turbulence Studies in a Channel, Thesis, University of Grenoble, France (1963).

8. D. A. Dawson and O. Trass, Intl. J. Heat and Mass Transfer 15, 1317 (1972).

9. R. G. Deissler, Analysis of Rurbulent Heat Transfer, Mass Transfer and Friction in Smooth Tubes at High Prandtl and Schmidt Numbers, NACA Report 1210 (1955).

10. D. F. Dipprey and R. H. Sabersky, Intl. J. Heat and Mass Transfer 6, 329 (1963).

11. H. G. Elrod, J. Aeronaut. Sci. 24, 468 (1957).

12. M. Eisenberg, C. W. Tobias and C. R. Wilke, J. Electrochem. Soc. 101(1), 306 (1954).

13. S. L. Gordon, J. S. Newman and C. W. Tobias, Berichte der Bunsengesellschaft fur physikalische Chemie 70(4), 414 (1966).

13a. J. Happel and H. Brenner, Low Reynolds Number Hydrodynamics (Prentice Hall, Inc., N. J., 1965), p. 38.

14. J. P. Hartnett, J. C. Y. Koh and S. T. McComas, J. Heat Transfer (Trans. ASME Ser. C) 84, 82 (1962).

15. J. O. Hinze, The Physics of Fluids Supplement, S122-S125 (1967).

16. D. W. Hubbard, E. N. Lightfoot, Ind. Eng. Chem. Fundamentals 5(3), 370 (1966).

17. W. R. Gambill and R. D. Bundy, Nuclear Sci. and Eng. 18, 69 (1964).

18. ICT, International Critical Tables.

19. M. H. Ibragimov, V. S. Petrishchev and G. I. Sabelev, Intl. J. Heat and Mass Transfer 14, 1033 (1971).

20. D. D. James, B. W. Martin and D. G. Martin, Forced Convection Heat Transfer in Asymmetrically Heated Ducts of Rectangular Cross Section, Intl. Heat Transfer Conference Proceedings, Chicago (USA), 1966. Vol. 1, pp. 85.

21. M. Jergel, K. Hechler and R. Stevenson, Cryogenics 10(5), 413 (1970).

22. A. Kitamoto and Y. Takashima, J. Chem. Eng. Japan 3(2), 182 (1970).

23. I. M. Kolthoff, Quantitative Inorganic Analysis, p. 371.

23a. S. J. Kline, W. C. Reynolds, F. A. Schraub and P. W. Runstadler, J. Fluid Mechanics 30(4), 741 (1967).

24. I. M. Kolthoff, and N. H. Furman, Volumetric Analysis (John Wiley and Sons, New York, 1928), Vol. I, p. 231.

25. I. M. Kolthoff and E. A. Pearson, Ind. Eng. Chem., Anal. Ed. 3, 381 (1931).

26. U. Landau, Ph. D. Thesis, University of California, Berkeley, California, LBL-2702.

27. V. Levich, Physicochemical Hydrodynamics (Prentice Hall, Inc., N. J., 1962).

28. C. S. Lin, E. B. Denton, N. S. Gaskill and G. L. Putnam, Ind. Eng. Chem. 43, 2136 (1951).

29. C. S. Lin, R. W. Moulton and G. L. Putnam, Ind. Eng. Chem. 45, 636 (1953).

30. T. Mizushina, F. Ogino, Y. Oka and H. Fukuda, Intl. J. Heat and Mass Transfer 14, 1705 (1971).

31. J. S. Newman, Ind. Eng. Chem. 60(4), 12 (1968).

32. J. Newman, Electrochemical Systems (Prentice Hall, Inc., N. J., 1973).

33. Nikuradse, VDI Forschungsheft 281, Berlin (1926) Cit. Hinze

34. V. S. Patel and M. R. Head, J. Fluid Mech. 38, part 1, 181 (1969).

35. Paul Perroud and Jean Rebiere, Convection Forcee de l'Hydrogene Liquide, Centre d'Etudes Nucleaires de Grenoble, Report CEA-R 2796, July 1965.

35a. Perry's Handbook, Perry, ed. (McGraw-Hill Co., NY, 19).

36. D. J. Picket and B. R. Stanmore, J. Appl. Electrochem. 2, 151 (1972).

37. W. D. Rannie, J. Aeronaut. Sci. 23, 485 (1956).

37a. T. K. Ross and R. K. Badhwar, Corrosion Science 5, 29 (1965).

38. H. Z. Reichardt, angew. Math. Mech. 31, 208 (1951).

39. H. Reichardt, Translation from German, NACA Tech. Memo 1408 (1957).

40. R. Ricque and R. Siboul, Intl. J. Heat and Mass Transfer 15, 579 (1972).

41. I. Rousar, J. Hostomský and V. Cezner, J. Electrochem. Soc. 118(6), 881 (1971).

42. H. Schlichting, Boundary Layer Theory (McGraw-Hill Co., NY, 1955).

43. F. A. Schraub and S. J. Kline, A Study of the Structure of the Turbulent Boundary Layer with and without Longitudinal Pressure Gradients, Report MD-12. Thermosciences Division, Department of Mechanical Eng., Stanford University (1965).

44. J. R. Selman, Measurement and Interpretation of Limiting Currents (Ph. D. Thesis), UCRL-20557, June 1971.

45. T. K. Sherwood, Chem. Eng. Progress Symp. Series 55(25), 71 (1959).

46. T. K. Sherwood and R. L. Pigford, Absorption and Extraction (McGraw-Hill Co., NY, 1952).

47. K. K. Sirkar and T. J. Hanratty, Ind. Eng. Chem. Fundamentals 8, 189 (1969).

48. J. S. Son and T. J. Hanratty, A.I.Ch.E.J. 13, 689 (1967).

49. D. B. Spalding, J. Appl. Mech. (Trans. ASME Ser. E) 83, 455 (1961).

50. D. B. Spalding, Intl. J. Heat and Mass Transfer 7, 743 (1964).

51. C. W. Tobias and R. G. Hickman, Zeitschr. fur physikalische Chemie 229, 145 (1965).

51a. H. W. Townes, J. L. Gow, R. E. Powe and N. Weber (Trans. ASME ser. D.) J. Basic Eng. 94(2), 353 (1972).

52. E. R. van Driest, J. Aeronaut. Sci. 23, 1007 (1956).

53. P. van Shaw, L. P. Reiss and T. J. Hanratty, A.I.Ch.E. J. 9, 362 (1963).

54. W. R. Vieth, J. H. Porter and T. K. Sherwood, Ind. Eng. Chem. Fundamentals 2, 1 (1963).

54a. T. von Kármán, Trans. ASME 61, 705 (1939).

55. D. T. Wasan, W. O. Jones and G. L. von Behren, A.I.Ch.E. J. 17(2), 300 (1971).

56. C. R. Wilke, M. Eisenberg and C. W. Tobias, J. Electrochem. Soc. 100(11), 513 (1953).

57. G. A. Whan, Characteristics of Transition Flow Between Parallel Plates, Ph. D. Thesis, Charnegie Inst. of Tech. (1956).

58. H. D. Young, Statistical Treatment of Experimental Data (McGraw-Hill, NY, 1962).

LEGAL NOTICE

This report was prepared as an account of work sponsored by the United States Government. Neither the United States nor the United States Atomic Energy Commission, nor any of their employees, nor any of their contractors, subcontractors, or their employees, makes any warranty, express or implied, or assumes any legal liability or responsibility for the accuracy, completeness or usefulness of any information, apparatus, product or process disclosed, or represents that its use would not infringe privately owned rights.

TECHNICAL INFORMATION DIVISION
LAWRENCE BERKELEY LABORATORY
UNIVERSITY OF CALIFORNIA
BERKELEY, CALIFORNIA 94720